

STUDY OF DRUG-DNA INTERACTIONS BY NMR SPECTROSCOPY

A THESIS

*Submitted in fulfilment of the
requirements for the award of the degree*

of
DOCTOR OF PHILOSOPHY
in
BIOTECHNOLOGY

By

MONICA

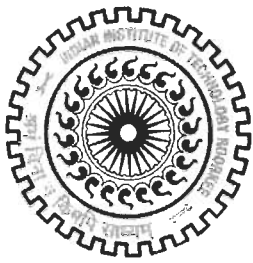


DEPARTMENT OF BIOTECHNOLOGY
INDIAN INSTITUTE OF TECHNOLOGY ROORKEE
ROORKEE-247 667 (INDIA)

DECEMBER, 2004



©INDIAN INSTITUTE OF TECHNOLOGY ROORKEE,
ROORKEE, 2004
ALL RIGHTS RESERVED



CANDIDATE'S DECLARATION

I hereby certify that the work which is being presented in the thesis entitled, **“STUDY OF DRUG-DNA INTERACTIONS BY NMR SPECTROSCOPY”** in fulfillment for requirement for the award of the **Degree of Doctor of Philosophy** and submitted in the **Department of Biotechnology** of the Institute is an authentic record of my own work carried out during a period from **January 2000 to December 2004** under the supervision of **Prof. Ritu Barthwal, Department of Biotechnology, Indian Institute of Technology Roorkee, Roorkee,**

The matter presented in this thesis has not been submitted by me for the award of any other degree of this or any other University/Institute.

Dated: 30.12.2004

Monica
(Monica)

This is to certify that the above statement made by the candidate is correct to the best of my knowledge.

Date: 31-12-04

Ritu Barthwal
(Dr. Ritu Barthwal)
Professor
Department of Biotechnology
Indian Institute of Technology,
Roorkee – 247 667 (India)

The Ph.D. viva-voce examination of Ms. Monica, Research Scholar has been held on 08.6.05

Ritu Barthwal
Signature of Supervisor

A.S. Shrivastava
Signature of H.O.D.
Act. Head

N. R. Jaiswal
Signature of External Examiner

Department of Biotechnology
Indian Institute of Technology Roorkee
Roorkee 247 667, India

CONTENTS

CANDIDATES'S DECLARATION

ABSTRACT

ACKNOWLEDGEMENTS

LIST OF PUBLICATIONS

	Page No.
CHAPTER 1	
INTRODUCTION	
1. 1 General	1
1. 2 Mode of Action of Anticancer Drugs	3
1. 3 Anthracyclines	8
1. 4 General Phenomenon of Intercalation in DNA	10
1. 5 Forces Between Intercalators and DNA	12
1. 6 Structure of Nucleic Acids	15
1. 7 Scope of Thesis	26
1. 8 Literature Review	27
CHAPTER 2	
MATERIALS AND METHODS	
2. 1 Materials	59
2. 2 Sample Preparation	61
2. 3 Methodology	62
2. 4 Two Dimensional NMR Techniques	70
2. 5 Experimental Parameters	75
2. 6 Determination of Three-Dimensional Structure	76
2. 7 Estimation of Interproton Distances	81
2. 8 Restrained Molecular Dynamics and Simulated Annealing	84
2. 9 Defining DNA Structure	89
CHAPTER 3	
STRUCTURE OF d-(CGATCG)₂ BY RESTRAINED MOLECULAR DYNAMICS	
3. 1 Strategy Followed	93
3. 2 Results and Discussion	98
3. 3 Trajectory Analysis	114
3. 4 Conclusions	117
CHAPTER 4	
STRUCTURE OF d-(TGATCA)₂ BY RESTRAINED MOLECULAR DYNAMICS	
4. 1 Strategy Followed	118
4. 2 Results and Discussion	123
4. 3 Structural Features of TpG/CpA Base Pair Step	135

CHAPTER 5		
	RESTRAINED MOLECULAR DYNAMICS STUDY ON DRUG DNA COMPLEX: d-(CGATCG)₂ WITH ADRIAMYCIN	
5. 1	Strategy Followed	148
5. 2	Results and Discussion	149
5. 3	Conclusions	187
CHAPTER 6		
	RESTRAINED MOLECULAR DYNAMICS STUDY ON DRUG DNA COMPLEX: d-(TGATCA)₂ WITH DAUNOMYCIN	
6. 1	Strategy Followed	
6. 2	Results and Discussion	
6. 3	Conclusions	
CHAPTER 7		
	STRUCTURAL INVESTIGATION OF HEXAMER d-(CGATCG)₂ COMPLEXED WITH DAUNOMYCIN	
7. 1	Sequential Assignment	236
7. 2	Titration Studies	241
7. 3	Changes with the Temperature	244
7. 4	Structural Features of Drug–DNA Complex	246
7. 5	Restrained Molecular Dynamics	254
CONCLUSIONS		277
REFERENCES		282

ABSTRACT

Nature has evolved a diverse set of antibiotics that bind to DNA in a variety of ways, but with the common ability to act as potent inhibitors of DNA transcription and replication. As a consequence, these natural products have been of considerable interest as potential anti cancer agents. Many synthetic compounds have been added to this list in the search for more potent drugs for use in chemotherapy. While it is appreciated that DNA is a primary target for many potent antitumor agents, data that pinpoint the exact mechanism of action are generally unavailable. A substantial body of research has been directed towards understanding the molecular basis for DNA sequence specificity for binding, by identifying the preferred binding sequences of many key drugs with DNA. Structural tools such as X-ray crystallography and NMR spectroscopy, coupled with molecular modeling techniques have had considerable impact in advancing our understanding of the microscopic structural homogeneity of DNA and the molecular basis for drug-DNA interactions. The present study is a significant step towards understanding the molecular basis of action of these drugs enabled by solution studies using nuclear magnetic resonance spectroscopy.

Chapter 1 contains introduction of the subject as well as highlights the work carried out in literature. Chapter 2 deals with the materials and methods being used. In chapter 3 structural refinement of d-(CGATCG)₂ has been carried out using a total of 10 spin-spin coupling constants and 112 NOE intensities by restrained Molecular Dynamics (rMD) with different starting structures, potential functions and rMD protocols. Refinement using different methods resulted in essentially the same structure, indicating that the structure obtained is defined by experimental restraints. The structural details have been analyzed with respect to torsional angles, base pair

geometries and helicoidal parameters. The final structure, representing a time-averaged structure, shows base-sequence dependent variations and hence strong local structural heterogeneity. In chapter 4, the structural features of duplex d-TGATCA has been investigated by restrained molecular dynamics up to 100 ps using a total of 12 torsional angles and 121 distance constraints. The structure is characterized by a large positive roll at TpG/CpA base pair step and large negative propeller twist for AT and TA base pairs. There is evidence of significant flexibility of the sugar-phosphate backbone with rapid inter conversion between two different conformers at TpG/CpA base pair step. The base sequence dependent variations and local structural heterogeneity have important implications in specific recognition of DNA by ligands. Chapters 5, 6 and 7 deals with the restrained molecular dynamics simulations of three complexes, that is, adriamycin-d-(CGATCG)₂, daunomycin-d-(TGATCA)₂ and daunomycin-d-(CGATCG)₂, respectively. The restraint data set consists of several intramolecular and intermolecular nuclear Overhauser enhancement cross peaks obtained from two-dimensional nuclear magnetic resonance spectroscopy data. The drug is found to intercalate between CG and GC base pairs at two d-CpG sites in adriamycin-d-(CGATCG)₂ and daunomycin-d-(CGATCG)₂ complexes. In daunomycin-d-(TGATCA)₂ complex the drug intercalates at T1pG2 and C5pA6 sites. The drug-DNA complex is stabilized via specific hydrogen bonding and van der waal's interactions involving 4OCH₃, O5, O13, 6OH, NH₃⁺ moiety of daunosamine sugar and ring A protons. The glycosidic bond C7-O7-C1'-C2' lies in the range 138°-160° during the course of simulations. The role of various functional groups leading to molecular basis of drug action is discussed. A comparison of structural features of the complexes shows that some of the related interactions are similar and may be related to a common mode of binding. Several other interactions are either DNA

sequence specific or drug specific. These may be attributed to difference in biological action of adriamycin and daunomycin.



ACKNOWLEDGEMENTS

This thesis is a result of more than four years of research, at the Indian Institute of Technology Roorkee (formerly University of Roorkee). It would not have been possible to complete this thesis without the help and guidance of numerous people and herein I would like to thank them all.

I would like to start thanking my supervisor, Professor Ritu Barthwal, for her guidance. This thesis grew out of a series of dialogues with her. Through her Socratic questioning, she brought me closer to the reality I had initially perceived, eventually enabling me to grasp its rich complexity. Her comments on chapter drafts are themselves a course in critical thought upon which I will always draw. I would also like to thank her for giving me the opportunity to discuss with so many famous NMR experts like Prof. G. Govil, Prof. R. V. Hosur and Prof. C. L. Khetrpal and not at least for the very pleasant time I have had visiting TIFR, Bombay.

I am most grateful to all the members of FT-NMR National Facility at TIFR for extending their cooperation and providing friendly atmosphere during my stay. I am thankful to the faculty of the department for help and valuable discussions during my stay.

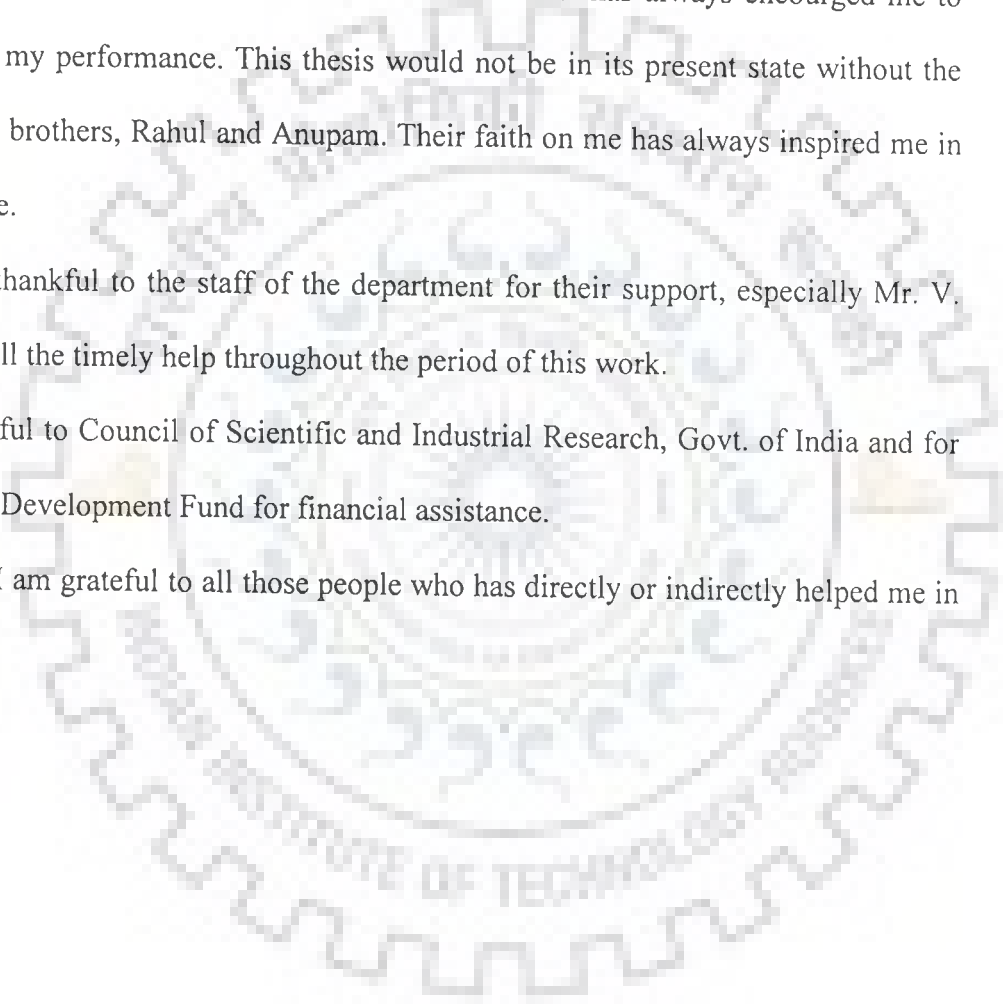
Special thanks to Manpreet, for being such a good colleague and friend. She always stood beside me through thin and thick. I wish her a happy and successful life. I am also indebted to all the other people who had contributed in this thesis. Today I recall all the names: Prashansa, Durai, Santosh, Amit, Lata, Kushuma, Prateek, Ambrish, Ruchi Singh, Pulkita, Anju, Chandan, Anvita, Anju and Indira. Timely help and suggestions of Dr. Soma, Dr. Arshi and Dr. Tarun will always be remembered.

I am forever grateful to my parents and in-laws, whose foresight and values paved the way for a privileged education, and to my husband Himanshu for supporting me with his gentle counsel and unconditional support at each turn of the road and tolerating all my moods. I am very grateful to my sister-in-law and brother-in-law for all they have done for me. I take this opportunity to thank my sister and jijaji for their encouraging words whenever I was tensed. Smile of little '*nammu*' has always encouraged me to ameliorate my performance. This thesis would not be in its present state without the help of my brothers, Rahul and Anupam. Their faith on me has always inspired me in this venture.

I am also thankful to the staff of the department for their support, especially Mr. V. Saini, for all the timely help throughout the period of this work.

I am thankful to Council of Scientific and Industrial Research, Govt. of India and for University Development Fund for financial assistance.

In the last I am grateful to all those people who has directly or indirectly helped me in my thesis.



LIST OF PUBLICATIONS

1. Ritu Barthwal, Pamita Awasthi, **Monica**, Manpreet Kaur, Nandana Srivastava, Sudhir Kumar Barthwal and Girjesh Govil. Structure of DNA sequence d-TGATCA by two-dimensional Nuclear Magnetic Resonance Spectroscopy and Restrained Molecular Dynamics. Journal of Structural Biology, Vol.148, 2004, pp34 -50.
2. Ritu Barthwal, **Monica**, Pamita Awasthi, Nandana Srivastava, Uma Sharma, Manpreet Kaur and Girjesh Govil. Structure of DNA hexamer sequence d-CGATCG by two-dimensional Nuclear Magnetic Resonance Spectroscopy and Restrained Molecular Dynamics. Journal of Biomolecular Structure and Dynamics, Vol. 21, 2003, pp 407 - 423.
3. Ritu Barthwal, Nandana Srivastava, Uma Sharma, **Monica**, Pamita Awasthi, Manpreet Kaur, Sudhir Kumar Barthwal and Girjesh Govil. Structure of adriamycin complexed to d-CGATCG by two-dimensional Nuclear Magnetic Resonance Spectroscopy.
Communicated to Journal of Magnetic Resonance, 2005.
4. Ritu Barthwal, Uma Sharma, Nandana Srivastava, **Monica**, Pamita Awasthi, Manpreet Kaur, Sudhir Kumar Barthwal and Girjesh Govil. Structure of daunomycin complexed to d-TGATCA by two-dimensional Nuclear Magnetic Resonance Spectroscopy.
Communicated to European Journal of Medicinal Chemistry, 2005.

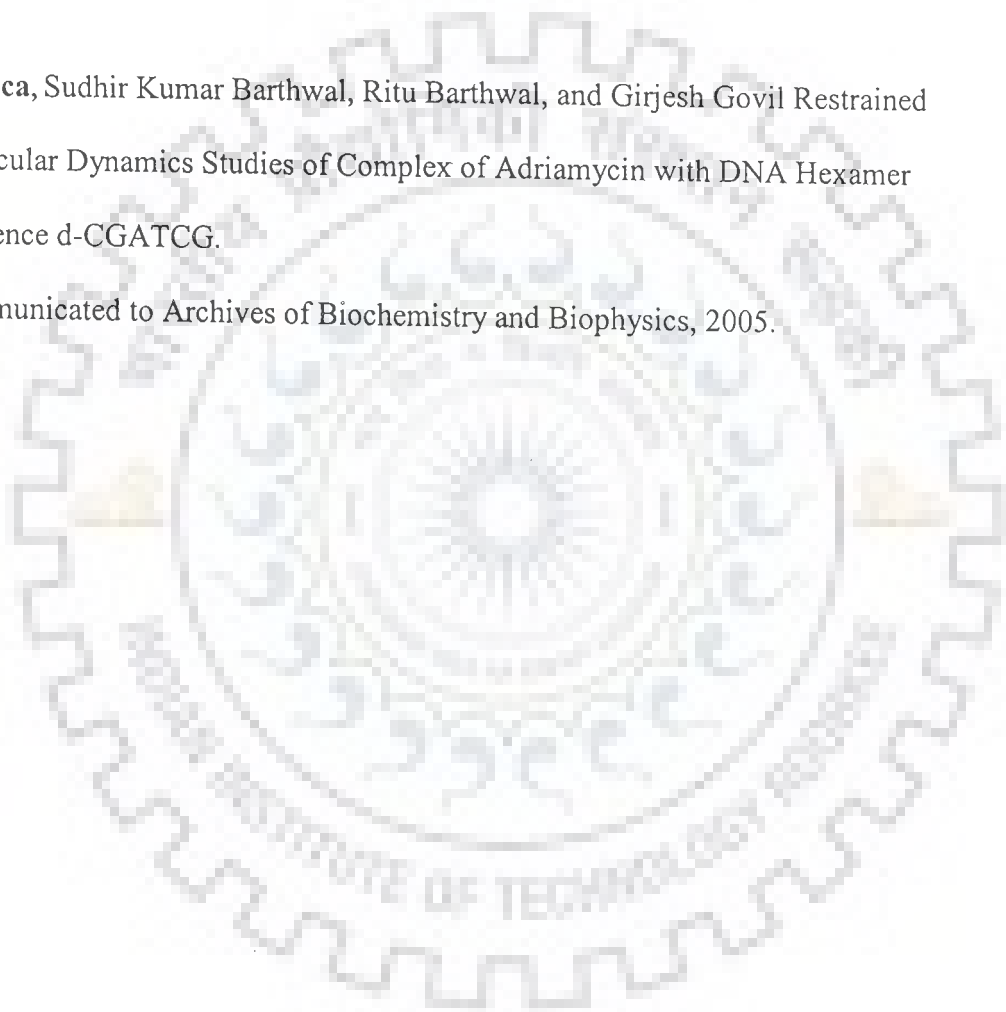
5. **Monica**, Sudhir Kumar Barthwal, Ritu Barthwal, and Girjesh Govil.

Restrained Molecular Dynamics Studies of Complex of Adriamycin with
DNA Hexamer Sequence d-TGATCA.

Communicated to *Biophysica Biochimica Acta*, 2005.

6. **Monica**, Sudhir Kumar Barthwal, Ritu Barthwal, and Girjesh Govil Restrained
Molecular Dynamics Studies of Complex of Adriamycin with DNA Hexamer
Sequence d-CGATCG.

Communicated to *Archives of Biochemistry and Biophysics*, 2005.



INTRODUCTION

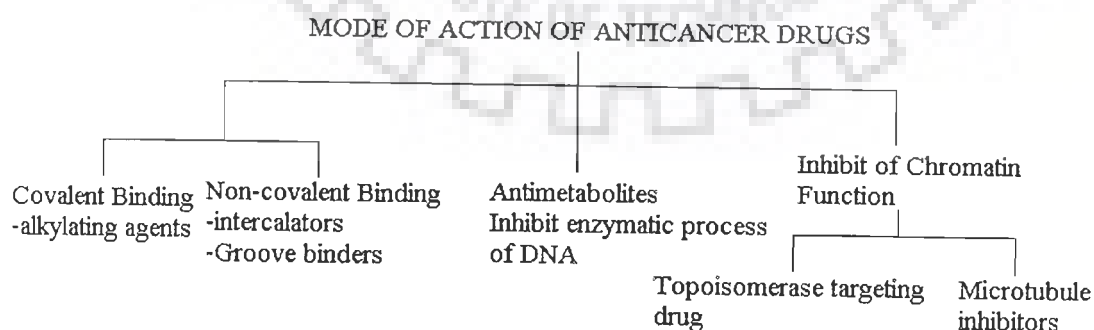
1.1 GENERAL

DNA, carrier of genetic information is a major target for drug interaction because of the ability of drug to interfere with transcription (gene expression and protein synthesis) and DNA replication, a major step in cell growth and division. Cancer is defined as the uncontrolled growth of cells, with loss of differentiation and commonly, with metastasis, spread of the cancer to other tissues and organs. Although there are many new ideas and treatments being studied every day, chemotherapy and radiation are still the most widely used treatments for the majority of cancers. Anticancer, or antineoplastic, drugs are used to treat malignancies and cancerous growths. There are many types of naturally occurring and synthetic chemical agents employed in treatment of cancer. The three principally different ways of drug binding to DNA are : first, through control of transcription factors and polymerases. Here, the drugs interact with the proteins that bind to DNA. Second, through RNA binding to DNA double helices to form nucleic acid triple helical structures or RNA hybridization (sequence specific binding) to exposed DNA single strand regions forming DNA-RNA hybrids that may interfere with transcriptional activity. Third, small aromatic ligand molecules that bind to DNA double helical structures by (i) intercalating between stacked base pairs thereby distorting the DNA backbone conformation and interfering with DNA-protein interaction or (ii) the minor groove binders. The latter cause little distortion of the DNA backbone. Both work

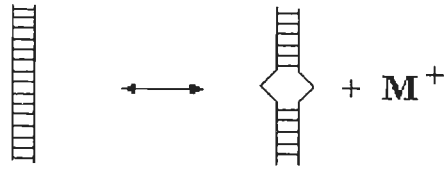
through non-covalent interactions (Fig. 1.1 a-c). Critical to the understanding of the function of such molecules is the characterization of their binding modes, which are usually investigated through ensemble measurements. Understanding how complex formation affects both the structural and mechanical properties of DNA is an important step towards understanding the functional mechanism of binding agents, and may also provide a key to more rational drug design.

1.2 MODE OF ACTION OF ANTICANCER DRUGS

In a broad sense, DNA and DNA topoisomerases are primary targets for numerous antitumor drugs. Drug can directly damage DNA by binding covalently or non covalently. They can alkylate the DNA or intercalate between the base pairs as well as bind to the major or minor groove of DNA. The inhibitors may exert their effect at three levels and can be divided into three groups accordingly. First group drugs act by alkylation of DNA and thereby forming reactive intermediates which crosslink the DNA or intercalate or binds to groove non-covalently. Second group comprises of many small molecules that mimic or block enzymatic process of DNA offer potential therapeutic agents. Third class of drugs may inhibit the DNA proliferation at the chromatin level itself.



Conformational Change ($\Delta G > 0$)



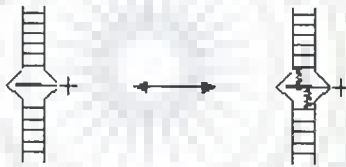
(a)

Hydrophobic Transfer ($\Delta G < 0$)



(b)

Molecular Anchoring ($\Delta G < 0$)



(c)

Figure 1.1: A conceptual model for intercalation (a) DNA conformation changes to form the intercalation cavity with the release of condensed counterions (b) Hydrophobic transfer of the intercalator into the interaction cavity with concomitant counterion release (c) Formation of molecular interactions (hydrogen bonds, van der waal's etc.) between intercalator and nearby DNA base pairs

1.2.1 Covalent DNA binding drugs

These drugs damage DNA.

1.2.1.1 Polyfunctional alkylating agents

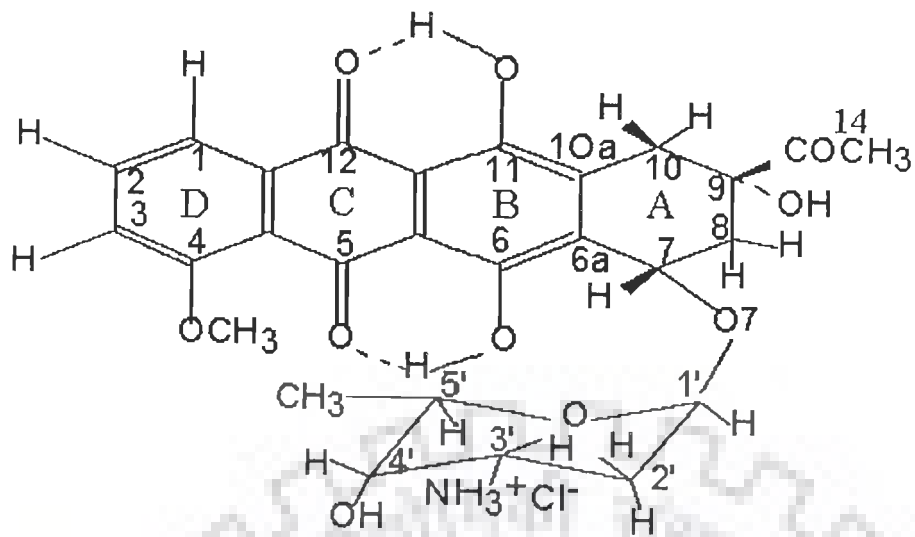
There are two types of alkylating agents: monofunctional (one reactive group) which cause single-strand breaks in DNA or damage bases and bifunctional (two reactive groups) which forms cross-links. A large number of 'first generation of anti cancer drugs' were designed to combine a simple alkylating function. Their common feature is that they form an initial physical complex with DNA before covalently bonding to it. The vital purpose is to kill bacteria by disrupting the synthesis of DNA and RNA. Many of them have also shown selective anti tumour activity, which must arise from selected toxicity. This can be attributed to DNA binding specificity or to preferential metabolic activation by tumour cells. The mechanism of action of these anticancer agents is by alkyl group transfer and they cause alkylation of DNA at N7 or O6 position of guanine (other sites as well) interaction may involve single strands or both strands. Other interactions involve the reaction of these drugs with amino, hydroxyl, and phosphate groups of other cellular constituents. These drugs usually form a reactive intermediate ethyleneimmonium ion. Polyfunctional alkylating drugs offer resistance against cancer by increased ability to repair DNA defects, decreased cellular permeability to the drug, increased glutathione synthesis, which inactivates alkylating agents through conjugation reactions. Mitomycin C requires enzymatic reduction of its quinone to initiate the processes that cause it to alkylate DNA.

1.2.2 Noncovalent DNA binding drugs

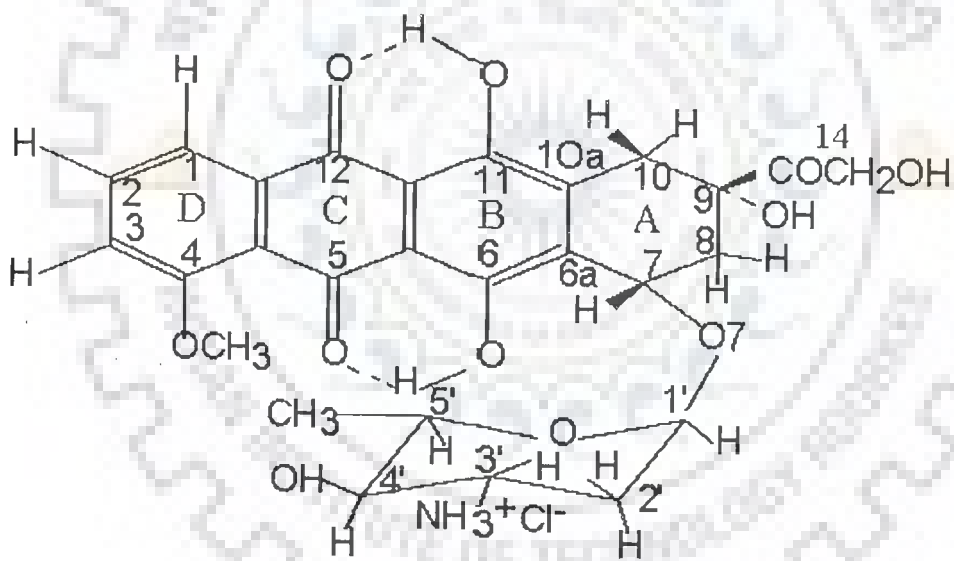
1.2.2.1 Anticancer Drugs, which intercalate in DNA

In the early 1960, Lerman conducted a number of physical studies on the interaction

of DNA with planar aromatic cations and concluded that planar aromatic molecules could bind to DNA by process, which he termed as intercalation. These are clinically useful anticancer antibiotics, which are primarily derived from *Streptomyces peucetius*. These antibiotics act by intercalating between base pairs of DNA causing lengthening of the double helix and a decrease in the helical twist on unwinding, inducing topoisomerase II mediated strand scission. These drugs prevent the religation of cleaved DNA thereby making the ternary complex stable either by increasing the rate of forward reaction i.e, more rate of DNA cleavage or by decreasing the rate of backward reaction i.e, slow rate of religation. Thus synthesis of DNA and RNA is blocked. They also alter membrane fluidity and ion transport. One potential mechanism is based on the ability of these agents to participate in electron-transfer processes, with the subsequent generation of free radicals. The property results from the presence of two very different types of redox-active groups, namely the quinone and hydroquinone moieties on rings B and C of daunomycin and adriamycin, respectively (Fig. 1.2 a, b). Quinone moiety of either daunomycin or adriamycin can undergo one-electron reduction to a semiquinone radical, which in the presence of oxygen gives rise to superoxide and other reactive oxygen species (ROS). The first crystal structure with a monointercalator and oligonucleotide was obtained by Wang and co-workers (Wang et al, 1987) for a complex of antibiotic daunomycin and d(CGTACG)₂. Synthetic bisintercalators have two covalently linked intercalated ring systems with connecting chains of variable length. The synthesis of these multiple ring compounds was partially stimulated by the idea that the medicinal activity of intercalating drugs could be enhanced by the significantly higher DNA binding



(a)



(b)

Fig. 1.2: Molecular structure of (a) daunomycin (b) adriamycin

constant and slower dissociation rates from DNA expected for bisintercalators relative to monointercalators. Ditercalinium is an important bisintercalator with partial rigidity in the linker chain that has been studied by X-ray and NMR methods. Natural bisintercalators includes quinoxaline antitumour antibiotics like echinomycin and triostin A. All intercalators explained above are classical intercalators. Non-classical intercalators have substituents on opposite sides of the intercalating aromatic system. These intercalators thread one of the substituents between the base pairs at the intercalation site in the binding mechanism. Nogalamycin is an example of non-classical intercalator.

1.2.2.2 Groove binding molecules

The major and minor groove differs significantly in electrostatic potential, hydrogen bonding characteristics, steric effects and hydration. Typically minor groove binding molecules have several simple aromatic rings connected by bond with torsional freedom. This creates compounds, which with the appropriate twist, can fit into the helical curve of the minor groove with displacement of water from the groove and forming van der waal's contacts with the helical chains which define the walls of the groove. Additional specificity in the binding comes from contacts between the bound molecule and the edges of the base pairs on the 'floor' of the groove. Thus, the aromatic rings of many groove binding molecules form close contact with AH2 protons in the minor grooves of DNA. Pullman and coworkers have shown that the negative electrostatic potential is greater in the A.T minor groove than G.C rich regions, and this provides an additional important source for A.T specific minor groove binding of cations. Examples of minor groove binding drugs are netropsin and distamycin.

1.2.3 Antimetabolites

1.2.3.1 Inhibit enzymatic process in nucleic acid synthesis

Purine antagonists like mercaptopurine (purinethol) act by hypoxanthine-guanine phosphoribosyl transferase (HGPRT) to form 6-thioinosinic acid, which inhibits enzymes involved in purine metabolism. Thioguanine acts as inhibitor of purine nucleotide pathway enzyme which decreases intracellular concentration of guanine nucleotides and inhibit glycoprotein synthesis, finally blocking DNA/RNA synthesis.

1.2.4 Inhibition of chromatin function

1.2.4.1 Topoisomerase targeting drugs

Chromosomal DNA is extensively twisted and topoisomerases permit selected regions of DNA to untangle so as to allow transcription and replication. These enzymes temporarily break DNA, allowing for topological changes, and then reseal the breaks. Topoisomerase targeting drugs like etoposide (VP-16) stabilizes the topoisomerase II-DNA complex preventing it from making a topological change. This result in an irreversible double strand break which is lethal to cells in S and G2 phases.

1.2.4.2 Microtubule Inhibitors

Microtubules are protein polymers involved in cellular movement and morphology. Microtubules occur in equilibrium between polymerized and free tubulin dimmers. Inhibitor drugs disrupt this equilibrium. Vinca alkaloids (vinblastine, vincristine) are examples of this type of drugs.

1.3 ANTHRACYCLINES

The anthracyclines are a fermentation product of *Streptomyces peucetius* var. *caesius* and were originally described as antitumour antibiotics. These drugs are

characterised by a tetrahydrotetracene quinone chromophore, which contains three flat, coplanar six-membered rings. Adriamycin and daunomycin (Fig. 1.2 a, b) has one additional non-planar six membered ring and daunosamine sugar moiety. Ring A of adriamycin (doxorubicin) differs from that of daunomycin. The 9COC14H_3 group at position nine in daunomycin is replaced by the $9\text{COC14H}_2\text{OH}$ group in adriamycin. Daunomycin and doxorubicin were first shown to have antitumor activity in the 1960. The daunosamine sugar moiety is attached to ring A at C1' position through a glycosyl linkage. The two torsion angles defined as $\text{H1}'\text{-C1}'\text{-O7-C7}$ and $\text{C1}'\text{-O7-C7-H7}$, respectively describe the orientation of sugar moiety with respect to non-planar ring A (Fig. 1.2 a, b). These angles play an important role in three-dimensional structure of the drug.

1.3.1 Structure activity relationships

The structures of the clinically used anthracyclines are shown in Fig. 1.2 (a, b). These drugs are positively charged at physiological pH, favoring intercalation into DNA. In addition, the anthracyclines possess quinone moieties on adjacent rings that allow them to participate in electron transfer reactions and generate oxygen free radicals. Daunomycin and doxorubicin differ only by a single hydroxyl at position C14, yet have distinct spectra of antitumor activity. A liposome-encapsulated formulation of doxorubicin (Doxil) has recently been approved for use in AIDS-related Kaposi's sarcoma.

1.3.2 Mechanism of action

The anthracyclines are highly reactive in solution and create panoply of effects on biological systems. A major component of their cytotoxicity is due to poisoning of topoisomerase II. Anthracyclines also intercalate into double-stranded DNA and

produce structural changes that interfere with DNA and RNA synthesis. Before the effect of the anthracyclines on topoisomerase II were fully appreciated, it was their ability to participate in oxidation-reduction reactions that was believed to produce cytotoxicity.

1.3.3 Activity

Doxorubicin has the broadest spectrum of activity and is one of the most active agents in the treatment of breast cancer. Doxorubicin has limited but demonstrable activity against thyroid cancer, ovarian cancer, and small cell lung cancer. Finally, it also has demonstrated activity against endometrial carcinoma, cancer of the testis, prostate, cervix, and head and neck, and multiple myeloma. Daunomycin is used mostly for the treatment of acute lymphocytic and myelogenous leukemias. Although it has some activity against pediatric solid tumors, it has little activity against adult solid malignancies. All anthracyclines produce cardiac damage that can result in serious and even life-threatening complications.

1.4 GENERAL PHENOMENON OF INTERCALATION IN DNA

1.4.1 Intercalation changes the physical properties of a double helix

Intercalation changes the physical properties of a double helix of DNA because base pairs must separate (unstack) vertically to allow the drug entry, the sugar phosphate bone is distorted and the regular helical structure is destroyed. According to such a model, the DNA must lengthen with increasing amount of added drug. This is indeed observed by enhanced viscosity and the diminution of the sedimentation coefficient, effects which also suggest overall stiffening of the DNA duplex (Gabbay et al, 1976). A two stage, anticooperative process was established from non-linear scatchard plot and from the kinetics which is the characteristic of intercalating agents..

1.4.2 The Nearest-neighbor exclusion principle

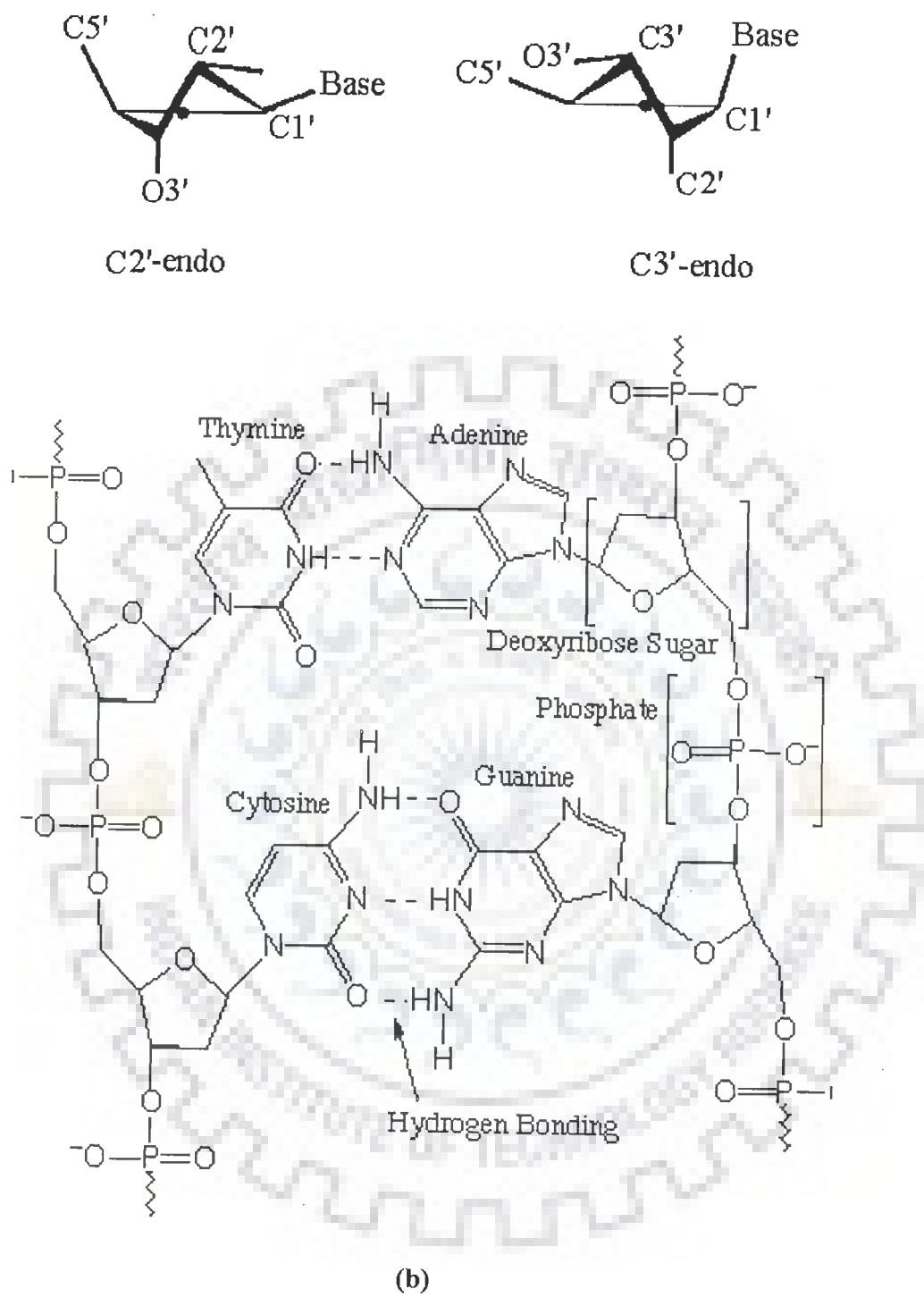
This principle states that intercalators can at most bind at alternate possible base pair sites on DNA, giving a maximum one intercalator between every second site. The exclusion principle states that when an intercalator binds at one particular site, binding of another intercalator at adjacent site is inhibited probably because nucleotides flanking the intercalator are geometrically distorted. All spaces between base pairs are potential binding sites for a non-specific intercalator.

1.4.3 Intercalation causes DNA unwinding

The separation of base pairs makes room for the intercalator. This can be visualized as a combination of pulling along the B-DNA double helix axis and left handed unwinding in order to prevent breakage of sugar-phosphate backbone. Intercalation into the pyrimidine 3'-5' purine sequence is 7-13 Kcal/mole more favourable than purine 3'-5' pyrimidine intercalation because base overlap is more pronounced in former than latter. The intermolecular interaction is supported by intramolecular electrostatic forces rendering pyrimidine 3'-5' purine sequences more prone to intercalation.

1.4.4 Sugar pucker

Usually all complexes have purine sugar at the 5' position in C3'-endo pucker. In most of them, the pyrimidine sugar at the 3' end is C2'-endo with only few cases of C3'-endo are found (Fig. 1.3 a). Upon intercalation both χ and β increase by over 50°, χ being pushed into high anti range. Model building studies suggested that the unwinding angle is dependent on a combination of small variations in the backbone torsion angles and base-pair geometry expressed as bend and twist, and not just on sugar pucker. It is clear that a correlation exists between unwinding angle and



(b)

Figure 1.3: (a) Preferred conformations C2'-endo and C3'-endo of sugar pucker
 (b) Watson and Crick base pairs showing the hydrogen bonding arrangements in the double helical DNA

shape of intercalator agent.

1.5 FORCES BETWEEN INTERCALATORS AND DNA

1.5.1 Hydrogen bonding

The phosphate group, sugar, bases in nucleic acids and hydrophilic groups in anthracycline drug participate in hydrogen bonding with water. Since all linear hydrogen bonds have similar free energies, they make little net contribution to the favourable free energy change when drug and nucleic acid interact in solution. By contrast, formation of poorly aligned hydrogen bonds, or absence of some of them on the complex formation, carries a free energy penalty of about 4 KJ mol^{-1} . Thus hydrogen bonds are one of the most important means of making sequence specific interaction of nucleic acid with drug. For example in adriamycin complex with DNA, two hydrogen bonds $9\text{OH}\dots\text{N}3$ and $9\text{O}\dots\text{N}2\text{H}$ between adriamycin and the base G2 stabilize the conformation of ring A (Chen et al, 1986; Frederick et al, 1990; Moore et al, 1989; Nunn et al, 1991; Wang et al, 1987). The $9\text{OH}\dots\text{N}3$ hydrogen bond has been found to be necessary for the *in vivo* anti tumour activity of adriamycin. There are additional hydrogen bonding interactions linking the C-14 hydroxyl of adriamycin to DNA, which further stabilizes the complex (Frederick et al, 1990). The daunomycin complex with $d\text{-(CGTACG)}_2$ (Wang et al, 1987) is stabilized by hydrogen bonding interactions involving hydroxyl and carbonyl groups at C9 of the daunomycin chromophore, the hydroxyl group being essential for activity.

1.5.2 Electrostatic forces: salt bridges

Salt bridges are electrostatic interactions between groups of opposite charge. They typically provide about 40 KJ mol^{-1} of stabilization per salt bridge. In drug-DNA complex they occur between the ionized phosphates of nucleic acid and positively

charged groups of drug. Salt bridges are influenced by the concentration of salt in the solution. Strength of salt bridge decreases with the increase in concentration of the salt. They are much stronger when there are no water molecules between the ionized groups because water has a high dielectric constant. These are relatively long-range forces.

1.5.3 Entropic forces: the hydrophobic effect

The hydrophobic effect is due to the behaviour of water at an interface. Any molecule in water creates a sharply curved interface and so orders a layer of water molecules around itself. When molecules aggregate, the ordered water molecules at the interface are released and become part of the disordered bulk water, thus stabilizing the aggregate by increasing the entropy of the system. Polar surfaces, where the enthalpy loss tends to offset the entropy gain or desolvation are less likely to aggregate than non-polar ones. Molecules of water left at the interface between the drug and the nucleic acid obviously decrease the entropy of the system. Therefore the surface of the non-planar aromatic chromophore of drug tends to be exactly complementary so that no unnecessary water molecules remain when the complex forms.

1.5.4 Base stacking: dispersion forces

Base stacking is caused by two kinds of interaction: the hydrophobic effect mentioned above and dispersion forces. Molecules with no net dipole moment can attract each other by a transient dipole-induced dipole interaction. Such dispersion forces decreases with the inverse sixth power of the distance separating the two dipoles, and so are very sensitive to the thermal motion of the molecules involved. Despite their extreme distance dependence, dispersion forces are clearly important in maintaining the structure of double stranded nucleic acids because they help to cause base

stacking. Besides they allow aromatic ring of the drug to intercalate between bases and stabilize it by base stacking.

1.6 STRUCTURE OF NUCLEIC ACIDS

Nucleic acids are very long thread like polymers made up of a linear array of monomers called nucleotides. The critical feature of DNA is its linear order of the four nucleotides, which are the storehouse of all the encoded information of DNA. DNA is composed of aromatic bases (a purine or pyrimidine ring), ribose sugars and phosphate groups. The hydrogen-bonding surface of the individual bases is on the inside, at the center of the double helix. The phosphate backbone is on the outside of the helix.

1.6.1 Bases

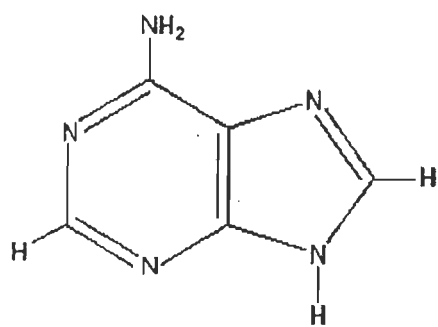
The purine and pyrimidine bases can undergo keto enol tautomerism.

1.6.1.1 Purines: Adenine and Guanine

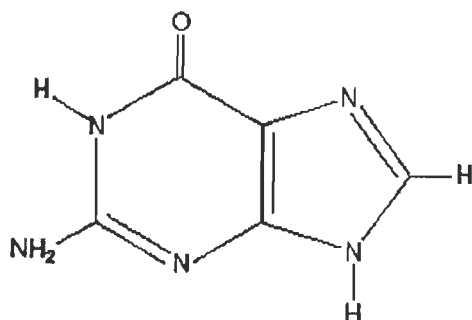
Two different heterocyclic aromatic bases with a purine ring (composed of carbon and nitrogen) are found in DNA (**Fig 1.4 a**). Adenine has an amino group ($-NH_2$) on the C6 position of the purine ring. Guanine has an amino group at the C2 position and a carbonyl group at the C6 position. Besides these, minor bases like inosine, 7-methyl guanosine, etc. are also found as components of nucleic acids.

1.6.1.2 Pyrimidines: Thymine, cytosine and uracil

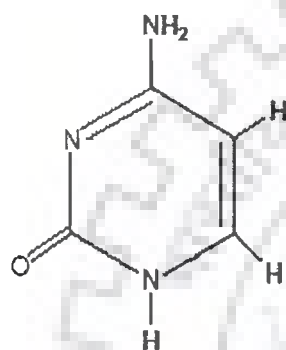
Thymine contains a methyl group at the C5 position with the carbonyl group at C4 and C2 positions. Cytosine contains a hydrogen atom at the C5 position and an amino group at C4 (**Fig 1.4 a**). In RNA thymine is replaced by uracil.



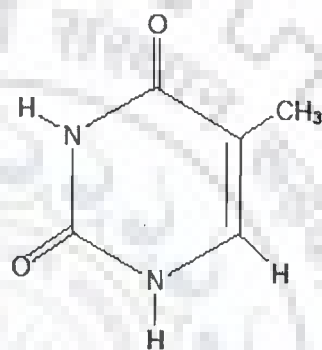
Adenine



Guanine

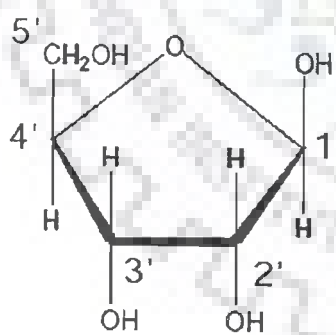


Cytosine

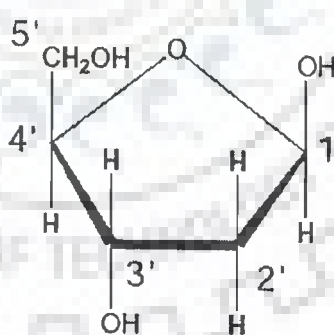


Thymine

(a)



Ribose (RNA)



2-Deoxyribose (DNA)

(b)

Figure 1.4: (a) Structural formulas of purines and pyrimidines (b) Five membered furanose ring of deoxyribose and ribose sugar

1.6.2 Sugar

Ribose sugar is found in all RNA molecules while a slightly different sugar, β -D-2-deoxyribose is found in DNA. This is a derivative of β -D-ribose in which the hydroxyl (-OH) at the 2' position is replaced by hydrogen (-H) (Fig. 1.4 b). The sugar moiety of DNA is one of the more flexible and dynamic parts of the molecule. The sugar base combination is called nucleoside unit. A nucleotide is a nucleoside phosphorylated at one of the free sugar hydroxyls.

1.6.3 The phosphodiester bond

In DNA and RNA the individual nucleotides are joined by a 3'-5' phosphodiester bond. The nucleotides are joined from the 3' sugar carbon of one nucleotide, through the phosphate to the 5' sugar carbon of adjacent nucleotide. This is termed as 3'-5' phosphodiester bond (Fig. 1.5). The primary sequence of nucleic acids is determined by the sequence of bases along the nucleotide chain and the function of acids namely replication, transcription and translation are governed by this sequence. The three dimensional conformation of nucleic acids is governed by a number of torsion angles seen in Fig.1.5. Considering that the purine and pyrimidines rings are planer one has three groups of torsion angles:

1.6.4 Glycosyl torsion angle (χ)

The glycosyl torsion (χ) angle define the orientation of the purine and pyrimidine bases relative to sugar ring. For pyrimidine nucleoside, χ is defined as torsion angle O4'-C1'-N1-C2 and for purines χ is O4'-C1'-N9-C4. Relative to the sugar moiety the base can adopt two main orientations about the glycosyl C1'-N link, called *syn* and *anti* (Fig 1.6 a). Rotamers with *chi* values between -90° and $+90^\circ$ are called *syn* whereas *anti* refers to *chi* values from $+90^\circ$ to $+270^\circ$. In Watson-Crick double helices

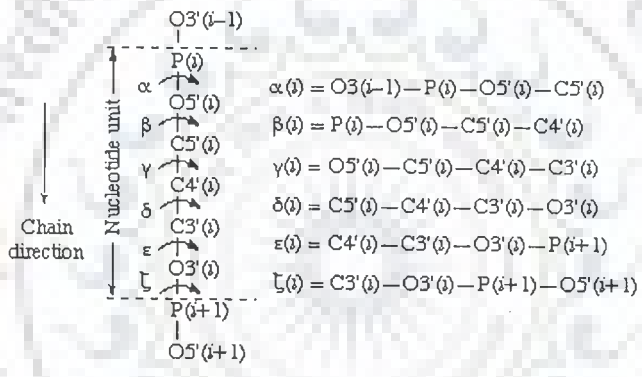
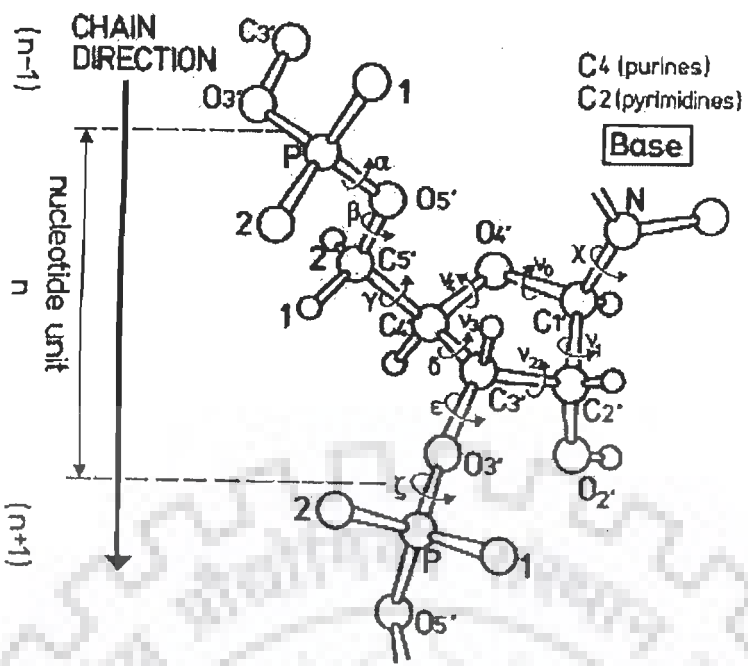
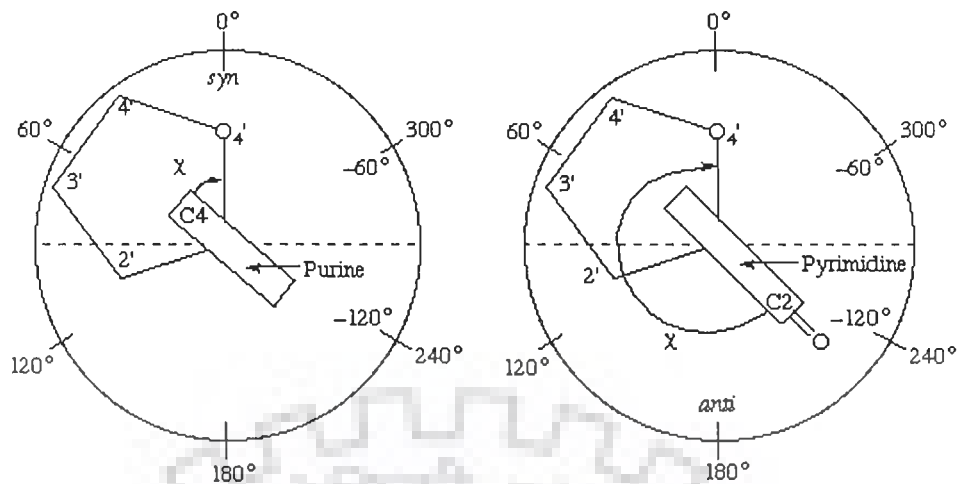
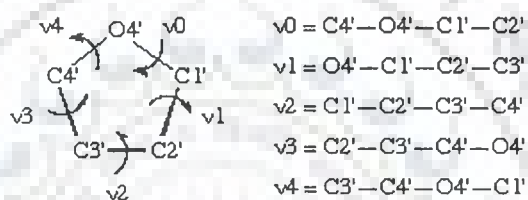


Figure 1.5: A nucleotide unit showing atomic numbering and definition of torsion angles



(a)



(b)

Figure 1.6: (a) Diagrammatic representation of the N-glycosidic bond torsion angle χ and the syn and anti regions for purine and pyrimidine derivatives. The purine derivative (left) is viewed down the N9-C1' bond and is shown in the +sc conformation. The pyrimidine derivative (right) is viewed down the N1-C1' bond and is shown in the -ac conformation. The sugar ring is shown as a regular pentagon (b) A ribose unit showing atomic numbering and definition of torsion angles

both bases of a base pairs are in *anti* conformation. Bases in *syn* conformation indicate a distortion of the double helix due to base pair opening or mismatched base pairs. The *syn* conformation is also found with guanines in left-handed Z-DNA (zig-zag helix). In *anti*, the bulk of heterocyclic atoms i.e., the six-membered pyrimidine ring in purines and O2 in pyrimidines is pointing away from the sugar, and in *syn*, pyrimidine is over and toward the sugar. An *anti* conformation is located near $\chi = 0^\circ$, whereas in *syn* domain is around 210° . There is also a high *anti* which denotes a torsion angle lower than *anti*.

1.6.5 Sugar ring torsion angles: Pseudorotation

The conformation of the ribose ring can be described by only two quantities, sugar pucker phase angle and sugar pucker amplitude. Pucker phase angle and pucker amplitude are calculated from the torsion angles about the five bonds in the ribose ring (Fig. 1.6 b). Conformations of cyclic systems introduce some constraints due to ring closure. In sugar, there are five atoms in the ring and we need $N-3 = 2$ torsion angles (Fig. 1.6 b) to define its three dimensional geometry. The torsion angles in a closed ring are highly correlated. Thus, out of five torsion angles τ_0 - τ_4 two are enough to define the geometry of the ring. C3' endo or 3E conformation is when C3' is on the same side of the plane described by the C5' atom (Fig. 1.3 a). When C3' is 0.6 Å below the plane, the conformation is called C3' exo or ${}_3E$. The most prominent conformations are C2'-endo in B-helices and C3'-endo in A-helices (Fig. 1.3 a). At room temperature both conformers are in a dynamic equilibrium. Transitions occur via the O4'-endo state. Intermediates between C2'-endo and C3'-endo are found in several (time-averaged) structures obtained from NMR and X-ray crystallography. When changing the pucker phase angle from 0° to 360° we step through all possible

conformations of the ribose ring. This pseudo-rotation cycle can be depicted as a conformational wheel (Fig. 1.7 a). The values of τ_1 corresponding to these conformations are $\pm 25.5^\circ$. The conformation of the sugar ring is described by two parameters P and δ (Altona and Sundaralingam, 1972). The five torsion angles τ_0 - τ_4 are related to these parameters by the equation:

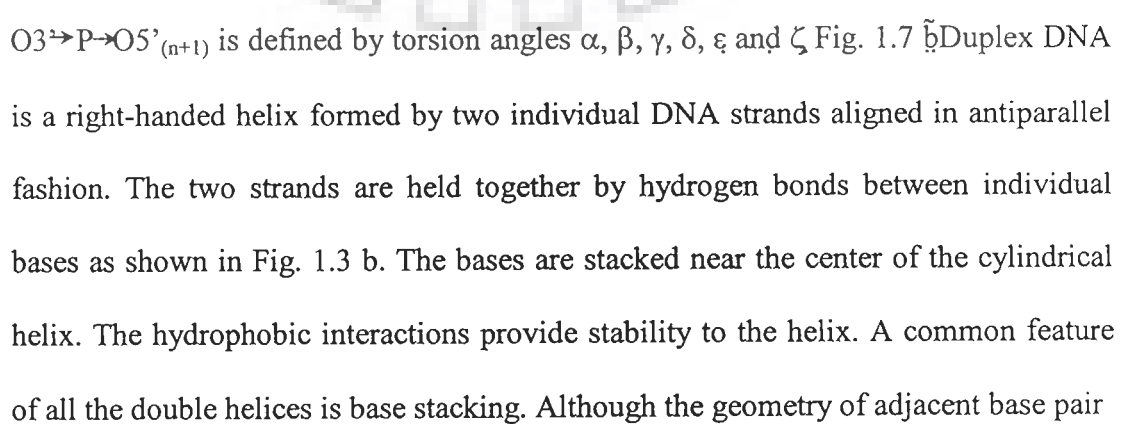
$$\tau_j = \tau_m \cos [P + (j-2)\delta]$$

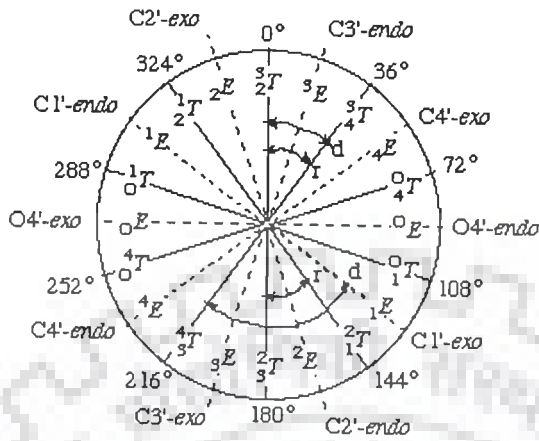
with

$$\tan P = \frac{(\tau_4 + \tau_1) - (\tau_3 + \tau_0)}{2(\tau_3 (\sin 36^\circ + \sin 72^\circ))}$$

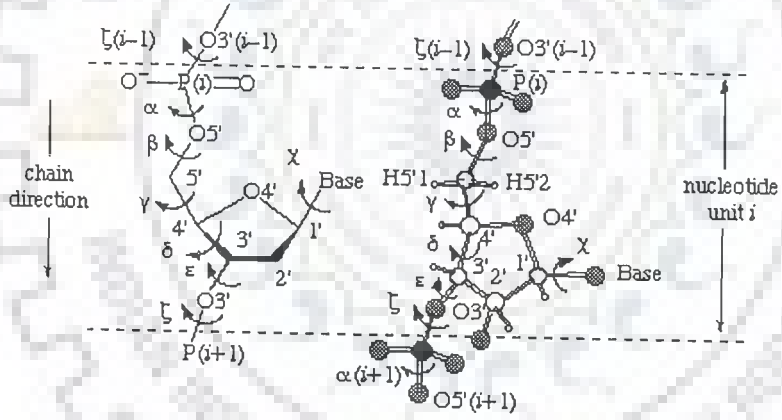
where $\tau_m = 38^\circ$, $\delta = 144^\circ$ respectively; $j = 0-4$. As P goes through the complete pseudorotation cycle (0° to 360°), values of τ_0 - τ_4 range from $-\tau_m$ to $+\tau_m$ through 0° . The conformational states that have a P value $0^\circ \pm 18^\circ$ and $180^\circ \pm 18^\circ$ corresponds to two isomeric states, denoted by N and S to indicate that they cover the north and south parts of the conformational wheel as shown in Fig 1.7. An energy barrier of about 4.0 Kcal/mol separates these two rotational states.

1.6.6 Backbone torsional angles

The sugar phosphate backbone conformation is fixed by the values of six conformational angles. The sequential numbering of atoms $(n-1)P \rightarrow O5' \rightarrow C5' \rightarrow C4' \rightarrow C3' \rightarrow O3' \rightarrow P \rightarrow O5'_{(n+1)}$ is defined by torsion angles α , β , γ , δ , ϵ and ζ Fig. 1.7  Duplex DNA is a right-handed helix formed by two individual DNA strands aligned in antiparallel fashion. The two strands are held together by hydrogen bonds between individual bases as shown in Fig. 1.3 b. The bases are stacked near the center of the cylindrical helix. The hydrophobic interactions provide stability to the helix. A common feature of all the double helices is base stacking. Although the geometry of adjacent base pair



(a)



(b)

Figure 1.7: (a) Pseudorotation cycle of furanose ring in sugar pucker (b) Section of a polynucleotide backbone showing the atom numbering and the notation for torsion angles

varies, in each case the distance between neighbouring base pair plane is about 3.4 Å. This is equal to van der waal's radius of planar aromatic compound. It was shown that purines cause large upfield chemical shift due to stacking as compared to pyrimidines. The sugar and phosphate groups are at the outer side of the helix and forms a backbone of the helix. In a double helix, the two polynucleotide chains are connected by complementary base pairing. Adenine always forms base pair with thymine and cytosine forms base pair with guanine according to Watson and Crick base pairing scheme (Fig. 1.3 b). Although right handed DNA is presumed to be the predominant conformation in vivo but under different conditions of salt and humidity DNA shows structural polymorphism i.e. it exists in alternative conformations like A and Z DNA. The main features of A, B and Z DNA are listed in Table 1.1. The structure of DNA can be described by number of helicoidal parameters like rise, pitch, tilt, roll, twist, no of bases per turn, etc. These different types of DNA differ from each other in their helicoidal parameters, which define the helix of DNA. At high temperature, the secondary structure of DNA is lost and random coils are generated.

Knowledge of the bound conformation of a ligand, and particularly of the key functionalities involved in binding are crucial to the rational design of more potent and specific drugs. Two-dimensional NMR methods has made it possible to assign the signals arising from the bound ligands and to use intramolecular NOEs to determine conformations of bound DNA. In addition, NOEs from the ligand to the target molecule may be used to determine the regions of the two species, which are directly involved in the intermolecular interactions. Restrained Molecular Dynamics (rMD) is a step further by NMR data obtained in the form of interproton distances and torsional angles are continually being improved. As greater accuracy is attained, greater

confidence can be placed in the precision of the structures, which are solved. Obviously refinement and model building is an integral part of biomolecular NMR structure determination. Whether employed alone or in combinatorial treatment regimen, anthracycline antitumor agents such as doxorubicin (adriamycin), the prototypical agent, remain amongst the most effective drugs for certain malignancies. Unfortunately, the original anthracycline antitumor agents suffer from a number of well known and significant drawbacks including their being substrates for the p-glycoprotein (P-gp) drug efflux mechanism associated with cellular drug resistance and the unfortunate ability to produce dose-dependent cumulative cardiotoxicity. Thus, considerations of toxicity and efficacy have, over the past three decades, driven the worldwide efforts at the development of new anthracycline antitumor agents.

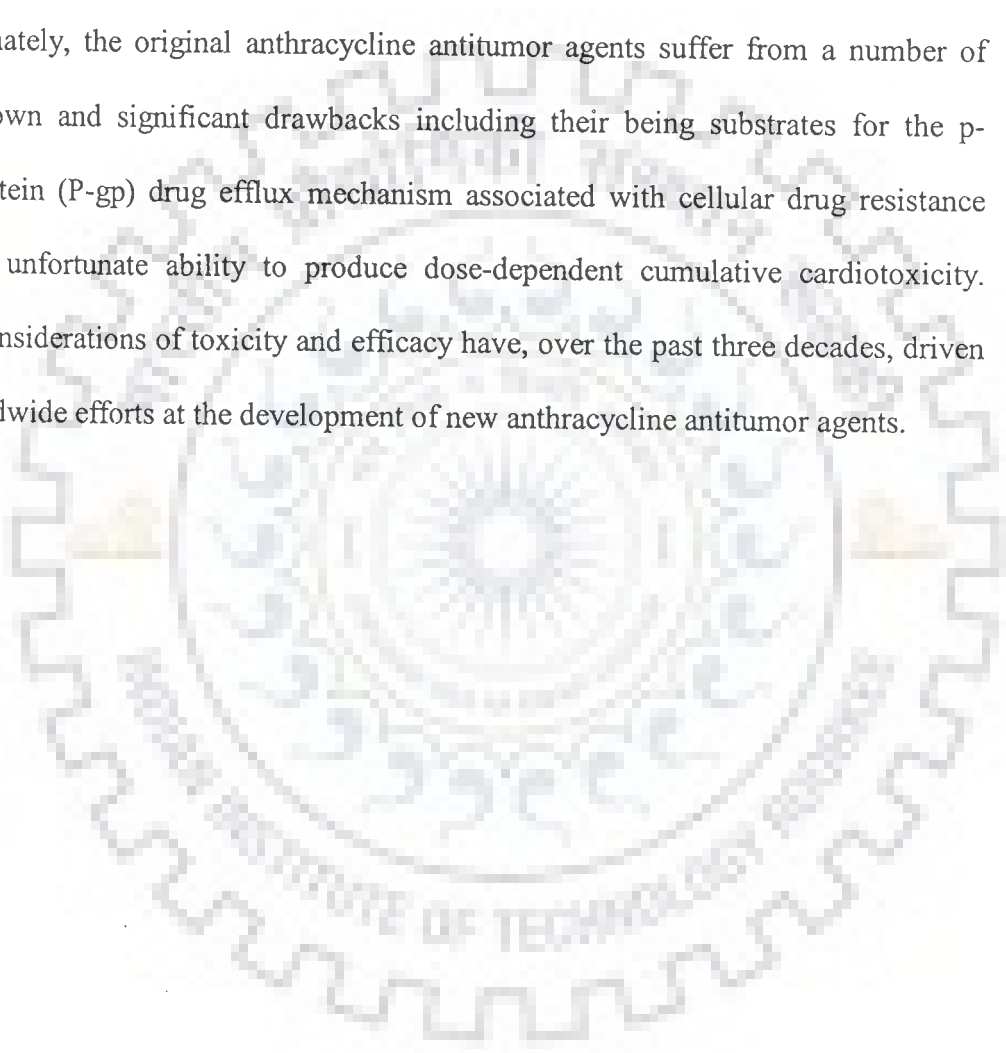


Table 1.1: Structural characteristics of A, B and Z type of double helices

	B DNA	Z DNA	A DNA
Helix sense	Right-handed	Left handed	Right handed
Repeating unit	1bp	2 bp	1 bp
Rotation/bp	35.9°	60°/2	33.6°
Mean bp/turn	10.0	12	10.7
Inclination of bp to axis	-1.2°	-9°	+19°
Rise/bp along axis	3.32Å	3.8 Å	2.3 Å
Pitch/turn of helix	33.2Å	45.6 Å	24.6 Å
Mean propeller twist	+16°	0°	+18°
Glycosyl angle	anti	C: anti, G: syn	anti
Sugar pucker	C2'-endo	C: C2'-endo, G: C2'-exo	C3'-endo
Diameter	20 Å	18 Å	26 Å

1.7 SCOPE OF THESIS

Interactions of small molecules with DNA have been studied for several decades in the hope of learning design principles for the targeting of specific DNA sequences in order to control gene expression. Many small molecules that bind to DNA are clinically proven therapeutic agents although their exact mode of action remains incompletely defined. There is a renewed focus on the use of small molecules as therapeutic agents in the biotechnology industry. This renewed interest arises, in part, as a result of several advantages of small molecules as potential drugs, including the economics of their synthesis and their effective delivery to cells. The results of these studies are correlated with biological (antitumor) efficiency of the compounds tested with the aim to exploit these data for design of new cytostatics with better therapeutic properties as compared to the drugs already used in the clinic. Therefore, these studies are aimed in particular at the development of new anticancer drugs whose antitumor efficacy is associated with their interactions with DNA, i.e. for which DNA is the main target inside tumor cells. The facilities of this laboratory make it possible to acquire theoretical knowledge, which is needed for design and synthesis of new cytostatics and suggestions for structure-pharmacological activity. Understanding structure-function directed macromolecule-target interactions of anticancer drugs, and further rational design of improved anticancer agents are the long-term research goals of our laboratory. This thesis deals with (i) the typical procedure for obtaining the structures using different starting structures by restrained Molecular Dynamics approach (ii) structure elucidation of the anticancer drug complexed with hexanucleotide (iii) to investigate the relationship between the structure and biological activity of the drug (iv) suggesting the functional groups of drug which may be

modified to get the drug with better anticancer activity and less side effects. The Ph.D thesis work has been reported in the form of seven chapters. Chapter 1 contains introduction of the subject as well as highlights the work carried out in literature. Chapter 2 deals with the materials and methods used. In chapter 3, we have discussed the results of rMD studies of d-CGATCG using torsional angles and inter proton distances obtained from proton NMR experiments. The helical parameters and backbone torsional angles etc. have been analyzed using CURVES software version 5.1. Sequence dependent variations have been observed. Chapters 4, 5, 6 and 7 deal with similar studies on d-TGATCA, complex of adriamycin with d-CGATCG, complex of daunomycin with d-TGATCA and complex of daunomycin with d-CGATCG, respectively.

1.8 LITERATURE REVIEW

The first suggestion of the intercalation of planar aromatic molecules between and parallel to adjacent base pairs was made on the basis of hydrodynamic and X-ray fiber diffraction studies of DNA in presence of acridine dyes. (Lerman et al, 1961). Anthracycline antibiotics typically possess a tetracyclic aglycon chromophore and an amino sugar. The crystal structure of anthracyclines, among them daunomycin (Anguilli et al, 1971; Coursielle et al, 1979) carminomycin (von dreele et al, 1977), nogalamycin (Arora, 1983) and steffimycin B (Arora, 1985) all show similar features. In these structures, the semi saturated ring A is in half chair conformation with C8 farthest out of plane of the ring. Daunomycin is most effective in the treatment of leukemia (Paciucci et al, 1997) and the closely related adriamycin is more effective in treatment of solid tumours (Di Marco et al, 1974). The intercalation of anthracyclines between base pairs of DNA produces the elongation and distortion of

double helix, inducing the inhibition of topoisomerase II (Tewey et al, 1984). The positioning of the amino sugar in the minor groove and its additional substituent groups contributes to the inhibition of topoisomerase I (Pilch et al, 1997). Inactivation of both topoisomerase I and II prevents the replication and transcription of DNA. Calendi et al, 1965 suggested that daunomycin complexes with DNA through two bonds; the one at the chromophore and the other at the amino sugar. Kersten et al, 1974 noted that daunomycin and planar compounds such as the acridines have similar effect on DNA in solution and suggested that the chromophore of daunomycin intercalates between successive base pairs of DNA in the manner postulated by Lerman et al in 1961 for the DNA-proflavin complex. It has been demonstrated that to allow the intercalation, the size of cavity must be such that an intercalating molecule would fit in, that is, the distance between two base pairs along the helix axis within the cavity must be at least 6.8 Å.

1.8.1 Biochemical studies of drug -DNA complexes

High-resolution structural information is necessary, but by no means sufficient, for understanding how drugs bind specifically to DNA. Structural studies provide a static view of the final complex that forms, and inevitably focus attention on to the specific molecular interactions between the drug and the DNA. In order to completely understand the molecular forces that drive and stabilize complex formation, biochemical studies are needed to complement the structural studies.

The relation between the stereochemistry of anthracycline antibiotics and their ability to bind to DNA has been investigated (Zunino et al, 1972) using homologous series of derivatives of daunomycin. The quenching of fluorescence and high stability of DNA by 4-demethoxy daunomycin shows that 4-methoxy group does not interfere with

chromophore/base pair stacking. However inverted configuration at position 7 and 9 decreases the binding to DNA. Complexes of calf thymus DNA with daunomycin, nogalamycin and carminomycin were studied by circular dichroism over a range of drug/DNA ratios (Dalglish et al, 1974). The existence of intercalative complex is predicted for daunomycin along with presence of free drug and DNA. Comparing the results with that obtained for 9-aminoacridine, which is believed to intercalate in DNA, it was observed that none of these antibiotics appeared to behave exactly as intercalating molecules. This was attributed to difference in chromophoric group present in antibiotics giving rise to transition dipoles in different directions and due to the difference in position of intercalation. Zunino et al, 1976 carried out spectroscopy, viscometry and thermal denaturation studies to investigate the interaction of daunomycin, adriamycin and its other derivatives with calf thymus DNA. It was observed that binding of daunomycin to DNA involves more than one class of sites. Adriamycin binds to DNA as strongly as daunomycin itself. The amino sugar residue plays an important role in the stabilization of the complex. Interaction specificity of salmon sperm DNA with various derivatives of daunorubicin was looked into, using ¹H Nuclear Magnetic Resonance (NMR), flow dichroism, DNA template inhibition, rates of dissociation and circular dichroism techniques (Gabbay et al, 1976). Their studies indicated that daunorubicin, adriamycin, rubidazole form more intimate complexes with DNA and rate of dissociation of both daunomycin and adriamycin from DNA is same but greater than rubidazole. Peptide derivative substituted at the amino sugar function of daunorubicin lower the affinity of the drug to DNA. It presumably interferes with the full insertion of the anthracycline drugs between base pairs of DNA. Their results were found to be consistent with an intercalative mode of

binding of the anthracycline drugs. Their preliminary approach has been centered on the modification of the amino group of the sugar moiety of daunorubicin. The results are consistent with specific H-bonding of the amino group of the sugar moiety with DNA as has been suggested by Pigram et al in 1972.

The interaction of adriamycin with single stranded polydeoxyribonucleotides, double stranded DNA and double stranded ribonucleotide hybrids were investigated by Tsou et al, 1976. This work represented a model study about the period of stability of the complex in the circulatory system before it reaches the target tissue. The most important factor in determining the stability of the complex is the interaction of the complex with DNase I in serum. Adriamycin effectively inhibited DNase II more than DNase I. Change in fluorescence intensity accompanied by large increase in polarization was used as an indicator of intercalation. Poly(dT) and poly(U) have very little effect on fluorescence of adriamycin. Poly(A) and 5'd-GMP slightly quenched the fluorescence of adriamycin. Poly(dG) efficiently quenched the fluorescence of adriamycin suggesting interaction between Poly(dG) and adriamycin. It is the known fact that Poly(dG) forms multistrands itself through hydrogen bonding of guanine bases and comparative studies of association constant of this complex with other complexes suggested that Poly(dG)-adriamycin complex could be thermodynamically less stable. Double stranded Poly(dA). Poly(dT), Poly(dA-dT), Poly(A).poly(dT) quench the fluorescence of adriamycin. Double stranded poly(dG-dC) complex of adriamycin has higher association constants and better adriamycin incorporation than calf thymus DNA. The rate of hydrolysis decreased in order poly(dA-dT) > calf thymus DNA >> Poly(dG-dC) > Poly(dA).Poly(dT) > poly(dG).poly(dC) for DNase I and poly(dA).poly(dT) > calf thymus DNA > poly(dG-dC) > poly(dA).poly(dT) >>

poly(dG).poly(dC) for Dnase II. On the other hand, intercalation of adriamycin to homodeoxynucleotide duplex poly(dA).(dT) and poly(dG).poly(dC) enhanced the DNase I hydrolysis. The best adriamycin carrier suggested by this investigation could be poly(dA).poly(dT) and poly(dG.dC). Adriamycin, daunomycin and their reduced forms bind intercalatively and completely relax supercoiled DNA. The results provide a possible rationale for the degradation of DNA, which accompanies anthracycline administration (Lown et al, 1977). Plumbridge et al (1977) investigated the changes in the visible absorption spectrum and the degree of fluorescence polarization of daunomycin and mepacrine on binding to DNA. The results have been compared with those shown by archetypical intercalating agent ethidium bromide. Ethidium bromide shows a reduction in extinction coefficient and bathochromic shift on binding to both DNA and poly(I.C) but interacts less avidly with poly(I.C) than with DNA. For daunomycin similar results were obtained with DNA but no isobestic point was observed with poly(I-C). Further the shift of λ_{max} was less and extinction coefficient of bound daunomycin to poly(I-C) showed much smaller decrease with respect to free drug. When daunomycin binds to DNA, fluorescence was quenched but enhancement of fluorescence was observed with poly (I.C) therefore it was inferred that daunomycin does not intercalate into poly(I.C) and external ionic binding is the probable mode of intercalation. Mepacrine behaves similar to daunomycin and its fluorescence was also quenched on binding to DNA and the fluorescence polarization was increased significantly. Mepacrine is able to intercalate into DNA though it does not intercalate into poly(I.C) and electrostatic binding is the probable mechanism of its intercalation with poly(I.C). It was shown that the interaction of daunomycin with t-RNA is different from that of daunomycin with viral ds-RNA (Shafer et al, 1977).

By fluorescence, quenching, spectral titration and T_m studies, it was revealed that t-RNA interacts with daunomycin in a manner similar to DNA. At the low ionic strength, t-RNA is probably in an extended form, but still possessing hydrogen bond regions. These results are consistent with, but not proof of, intercalation of the drug in the double helical segments of t-RNA, as proposed for ethidium bromide.

Pachter et al, 1982 has published his results on the binding of anthracycline analogues - adriamycin, carminomycin, pyrromycin, Musettamycin, marcellomycin and aclacinomycin to calf thymus DNA and covalently closed circular PM-2 DNA. Quenching of the fluorescence of marcellomycin occurs by increasing concentration of native and heat denatured calf thymus DNA. The ratio of heat denatured to native apparent association constant (K_{app}) demonstrated that the binding affinities of all the anthracyclines studied for heat denatured DNA were only 35-62% of the corresponding binding affinities for native DNA. This suggests the dependence on double strandedness of the DNA for binding. The significant increase in affinity for DNA was observed for adriamycin, carminomycin and marcellomycin as the ionic strength of reaction buffer decrease. The apparent number of binding sites per nucleotide (n_{app}) was also higher in low ionic strength buffer and this shows the importance of electrostatic forces in the interaction of these anthracycline with DNA. Viscometric studies indicated that under high ionic strength conditions, which negated electrostatic effects, all of the anthracyclines induced an unwinding-rewinding process of the close superhelical PM-2 DNA typically observed for DNA intercalators. The anthracycline exhibited unwinding angles that were approximately half that of ethidium bromide; that is, compared to an unwinding angle of 26° observed in ethidium bromide, anthracycline indicated unwinding angle of approximately 13° .

Adriamycin and carminomycin induce greater extent of uncoiling while pyrromycin, musettamycin and marcellomycin exhibit lower unwinding angles. With decrease in ionic strength, unwinding angles of adriamycin did not change significantly while that of carminomycin and marcellomycin slightly decreases and increases, respectively relative to ethidium bromide. Since the present study has shown that non intercalative binding contributes to the DNA binding of several anthracycline and ethidium bromide to similar extends, it is more likely that the lower unwinding angle of the anthracycline results from some other mechanism, such as a difference in the drug-DNA intercalation complex. Among other possibilities, the anthracycline may achieve only partial insertion between base pairs upon intercalation into DNA or the mechanism of intercalation of anthracycline may differ fundamentally from that in ethidium bromide. Structural differences in the intercalation complexes have also been proposed to explain the low unwinding angles of quinoline derivatives relative to that of ethidium bromide (Jones et al, 1980). The lack of change in the unwinding angle of pyrromycin with additional 2-deoxyfucose residues on the glycosidic side chain at higher ionic strength demonstrate that the presence of second and third sugars on the anthracycline side chain does not effect the drug ability to distort DNA upon intercalation. Thus, it is likely that these sugars do not sterically hinder the intercalation of anthracycline into DNA duplexes.

Chaires et al, 1982 studied the interaction of daunomycin with DNA by equilibrium dialysis, fluorescence and absorption titration techniques. Binding of daunomycin to DNA results in red shift and isobestic point. Ionic strength has no apparent effect on the extinction coefficient of the free or bound drug. In the presence of DNA, the fluorescence emission of daunomycin was quenched. Daunomycin binds tightly to

DNA and shows negative cooperativity. Binding strength of daunomycin (intrinsic binding constant) drops as sodium ion concentration increases with the exclusion parameter, essentially constant at 3.25 ± 0.25 . Daunomycin binding is exothermic with vant Hoff enthalpy of -12.8 Kcal/mol. The G+C rich DNAs bind more strongly to daunomycin and preferentially alter the bouyant density of G+C rich DNAs in CsCl density gradient. Daunomyin dramatically stabilizes the DNA as it increases T_m by about 30° C. The biphasic thermal denaturation seen at low r (where r is the number of moles of bound daunomycin per mole of DNA) values are similar to those observed by Patel and Caunel, 1978. Daunomycin, a potent anthracycline antibiotic self-associates in aqueous solution at concentrations greater than $10 \mu\text{M}$ (Chaires et al, 1982a). In this study they have carried out visible absorbance, sedimentation equilibrium and NMR experiments that characterize the self-association. Sedimentation studies show that daunomycin aggregates beyond a dimer. NMR data shows that the aromatic protons of daunomycin are most effected by aggregation, probably due to stacking of the anthracycline rings. Knowledge of the applicable model for the self-association process has enabled them to assess quantatively the possible effects of drug aggregation on the interpretation of drug-DNA binding data. Mainfait et al, 1982 made an attempt to determine the nature of the interaction of the chromophore of adriamycin with nucleic acid by comparing of the resonance raman spectra of the free and bound drug in water solution at neutral pH. The spectral change shows that adriamycin is intercalated between GC sequences and hydrogen bonds are formed at intercalation site. Graves et al, 1983 studied the binding of antitumour agents by phase partition techniques. Both adriamycin and daunomycin exhibit positive cooperativity in their equilibrium binding to DNA as indicated by the

positive slopes in the initial region of the binding isotherms under conditions of simulating physiological ionic strengths. Adriamycin exhibits a greater degree of positive cooperativity than daunorubicin. The dependence of the equilibrium-binding constant upon the ionic strength has been well established for a variety of drugs (Chaires et al, 1982). Such studies have demonstrated that increasing the ionic strength of the buffer decreases the drug binding affinity for the DNA. However at ionic concentration of 0.01 M and 1M NaCl, both drugs have been shown to interact with DNA in a non-cooperative manner. In an effort to examine the effects of base composition or sequence on the binding of adriamycin and daunorubicin at low r (where r is the number of moles of bound daunorubicin per mole of DNA) values, the alternating copolymers poly(dA-dT).poly(dA-dT), poly(dG-dC).poly(dG-dC) and poly(dA-dC).poly(dG-dT) were examined. Adriamycin exhibits a much greater degree of cooperativity with poly(dA-dT).poly(dA-dT) than daunorubicin under identical conditions. Conversely the binding to poly(dG-dC).poly(dG-dC) showed a marked decrease in this cooperative binding effect. The correlation of base sequence with the cooperative binding could be associated with the thermodynamic property of helix as for example stability of poly(dG-dC).poly(dG-dC) as compared with poly(dA-dT).poly(dA-dT) or the relative enthalpy of base pair stacking in the three polynucleotides studied.

Chen et al, 1983 reported the effects of adriamycin on B to Z transition of poly(dGm⁵dC).poly(dGm⁵dC) by using CD and ³¹P NMR data. Addition of adriamycin to poly(dGm⁵dC) in Z form resulted in its conversion to B form in presence as well as in absence of MgCl₂. The transition between Z and B forms was found to be cooperative. Further, it was observed by CD spectroscopy that high concentration of

Mg^{2+} was required to induce B to Z transition in presence of adriamycin. Thus, it was inferred that adriamycin inhibits B to Z transition and binds preferentially to B-DNA. The interaction of daunomycin with calf thymus DNA over a wide range of temperature and NaCl concentration was studied (Chaires et al, 1985a). High NaCl concentration or temperature decreases binding affinity. Daunomycin binding is exothermic. Favourable free energy of binding of drug to DNA arises primarily from the large negative enthalpy. Both enthalpy and entropy of the binding reaction are strongly dependent on the ionic strength but free energy is less dependent due to compensating changes in the enthalpy or entropy. Hydrogen bonding at the intercalation site is the primary contributor to the observed thermodynamics parameters. The kinetics of the interaction of daunomycin with calf thymus DNA has been studied using (Chaires et al, 1985) stopped flow and temperature jump relaxation methods. A binding constant (K) = $7.0 \times 10^{-5} M^{-1}$ and exclusion parameter (n) of 3.6 was obtained. Three relaxation times were observed, all of which were concentration dependent; the two slower relaxation approaches constant value at high reactant concentrations. Relaxation time over a wide range of concentrations was gathered, and data were fitted by a minimal mechanism in which a rapid bimolecular association step is followed by two sequential isomerization step. The six rate constants for this mechanism were extracted by relaxation analysis. The values determined for the six rate constants may be combined to calculate an overall equilibrium constant that is in excellent agreement with that obtained by independent equilibrium measurements. Additional stopped flow experiments, using first sodium dodecyl sulphate to dissociate bound drug and second pseudo first order conditions to study the first bimolecular step, provides independent verification of three of the six

rate constants. The temperature dependence of four of the six rate constants was measured, allowing estimates of the activation energy of some of the steps to be made. They speculated that the three steps in the proposed mechanism may correspond to the rapid outside binding of daunomycin to DNA, followed by intercalation of the drug, followed by either conformational adjustment of the drug or DNA binding site or redistribution of bound drug at the preferred sites.

Foot printing and binding experiments (Chaires et al, 1987) have shown that the preferred daunomycin triplet binding site contains adjacent G.C base pairs flanked by A.T base pairs. Recent results from a high resolution DNase I foot printing titration procedure identified that the most strongly preferred daunomycin binding site is 5' A/TGC or 5' A/TCG, where notation A/T indicates that either A or T may occupy the position neighbouring the intercalation site. Most preferred site is 5'-ATCG (Chaires et al, 1990). Footprinting (Chaires et al 1987) and theoretical (Pullman et al, 1987) studies indicate that sequence specificity of the daunomycin-DNA interaction cannot be described in terms of the two base pairs comprising the intercalation site. A quantitative explanation can be obtained only by model in which a triplet of base pairs is regarded as the recognition sequence of the drug. The binding of adriamycin to DNA phosphate was investigated by infra-red spectroscopy and quantum chemical calculations (Pohle et al, 1987). The distinct absorption at 1070 cm^{-1} region corresponding to C14-OH of adriamycin was found to split in presence of DNA. The quantum chemical CNDO/2 calculations performed on those structural fragments of DNA and adriamycin involved in interaction, show diminution of both P---O bond index and O---P---O bond angle of phosphate groups on complexation. These results corroborate the speculation about involvement of C14-OH group of adriamycin in

binding to DNA phosphate during its interaction. Skorobogaty et al in 1988 investigated the DNA sequence specificity of daunomycin by DNase I footprinting and an E.Coli RNA polymerase transcription- inhibition assay. The 5'CA sequence was identified as being the highest affinity binding site although other modest affinity (5'GC, CG, CT, TC, AC) and poor affinity sites (5'AA, AT, TA) sites were also observed. The preference of daunomycin for 5'CA nucleotide sequence suggests that its biological activity may arise from association with the 5'CA containing sequences which are thought to be associated with genetic regulatory elements in eukaryotes. Xodo et al, 1988 explored the binding range of $r > 0.05$ (where r is ratio of bound drug to DNA base pairs). The intercalation of drug into the DNA proved to be anticooperative, as indicated by the pronounced upward curvature of all scatchard plots obtained. Extinction coefficient of the bound daunomycin does not markedly depend upon the polynucleotide base composition but level of fluorescence quenching showed marked dependence on base composition of the intercalation site. Presence of a guanine residue at the intercalation site completely quenched fluorescence while AT, AU or IC base pairs at intercalation site cause only a partial fluorescence quenching. Calf thymus DNA quenches the daunomycin fluorescence in a way intermediate between poly(d(G-C).poly(d(G-C) and poly(d(A-T).poly(d(A-T) at low DNA/drug (P/D) ratios, but it tends to promote a nearly total quenching at very high DNA/drug (P/D) ratios. Intercalation of daunomycin with polynucleotides shows anticooperativity, which can be entropic or energetic in origin due to the neighbour exclusion effects or due to polyelectrolyte effects or due to the interactions between ligands. Data is fitted by applying the formalism of Friedman and Manning considering both limiting cases: model 1 FM-I (site size =1 bp) and model FM-II (site

size = 2 bp). As number of binding site (n) is integer in FM-II and not in FM-I, it is suggested that probably FM-II better reflects the physical nature of the system. The anticooperativity, which accompanies an intercalation process, is essentially poly-electrolytic in origin. The binding affinity shown by the drug for the different sites decreases in the order $G_m^5C > AT > AC-GT > IC > GC > AU$, indicating a stabilizing effect of the $-CH_3$ group of pyrimidines. Total quenching at high DNA/drug ratio suggests a rather complicated sequence specificity of this drug involving at least base triplets. At low DNA/drug ratios the drug binds to both classes of sites (i.e. with and without the 2-NH₂ purine group), but at a very high DNA/drug ratios, it binds mainly to the sites which quenched the fluorescence totally i.e. G containing sites. The influence of both the temperature and the ionic strength on the free energy of drug intercalation into calf thymus DNA, poly[d(G-C):polyd(G-C)] and poly [d(A-C) poly d(G-T)] was examined and discussed. Infra red spectroscopy shows the formation of hydrogen bond between the intercalated drug molecule and the PO₂⁻ moiety of DNA via the following terminal hydroxyl groups; C14OH for adriamycin and daunomycin and C4OH for both aclacinomycin A and vidamycin BI and more tentatively the external side chain OH of mitoxantrone (Pohle et al, 1990). By transcriptional footprinting (Cullinane et al, 1990) showed that the physical size of the drug induced blocking moiety comprising of a maximum of two base pairs and the same was observed at all the three GpC elements probed by RNA polymerase from both directions. Fe(III) enhanced the amount of transcriptional blockages by 12-15 fold. Remeta et al, 1991 determined the binding enthalpies of daunomycin with 10 polymeric DNA duplexes. It was found that daunomycin binding enthalpies exhibited small but significant dependence on Drug/Phosphate ratio (r). Binding enthalpies

depend on the drug binding densities. Duplex dilution enthalpies in terms of influence of base composition sequence and conformation/hydration was also discussed.

Pindur et al, 1993 have discussed structure dependent models of intercalation with DNA as well as with that base paired oligonucleotide for some cytostatic agents of the anthraquinones, compounds of carbazole series, actinomycin D, triostin A, the bleomycins and amasacrine. The results described are based on molecular spectroscopic data in combination with molecular modeling. The combinations of experimental and theoretical methods have actively promoted the rational development of cytostatic agents of the intercalator type in the last few years. Molecular permutations can now be performed with greater reliability and potentially useful compounds can be developed rapidly. Roche et al, 1994 analyzed whether there was multiple binding site of daunomycin to oligonucleotide and the effect of having the A tracts at the end of the molecule. The information so obtained is used to determine whether daunomycin binds preferentially to any particular sequence. CD spectra showed the oligonucleotide conformation is the summation of the internal concentration which is presumed to be B form and the A tracts. Daunomycin exhibit affinity for CGATG core sequence by two fold. The exothermic binding enthalpy for daunomycin with CGATG core is twice as large as that for the TATATA sequence. Binding with dA₂₀.dT₂₀ is endothermic and for oligomers containing flanking A sequence less exothermic component can be detected in the binding curve. Affinity of daunomycin to CGATG core sequence is slightly larger than that for other sequences. Stopped flow data indicates that the AG sequence does not have a relatively strong site for the drug and is least comparable in kinetic stability to that of CG sequence. Hairpin sequence containing CG shows weak binding possibly due to structural

distortion. Relative binding of daunomycin and its analogs (differing in sugar moiety) was tested. Daunomycin has high affinity for each oligonucleotide tested relative to other analogs except for iodo substituent in the L-sugar. Iodo substituent binds with same affinity as daunomycin. In general L-form of sugar elicits a more favourable interaction than the D-form and is naturally occurring isomer. The intercalative binding of drugs daunomycin, ethidium bromide, nogalamycin etc. has been verified by observing changes in the supercoiling of closed circular DNA, as revealed by changes in the sedimentation coefficient (Waring, 1970). Daunomycin causes a definite decrease in the sedimentation coefficient S_{20} of ϕ X174 RF, as expected for intercalative binding. The apparent unwinding angle has been calculated for all intercalating drugs by taking the unwinding angle of ethidium $\approx 12^\circ$ as a reference.

1.8.2 Theoretical studies

Miller's technique AGNAS was used to determine possible intercalation site geometries in B-DNA (Miller et al, 1982). Nuss et al, 1979 carried out empirical potential function calculations on a base paired dinucleotide GpC and CpG and its complex with proflavin, ethidium bromide and 9-aminoacridine and their calculations were able to reproduce and rationalize the pyrimidine-3'-5'-purine specificity of these intercalators. Islam et al, 1985 deduced that the best intercalator was 1, 5 disubstituted compound while 1, 6 disubstituted was the weakest. The antiproliferative effects were in agreement with the ranking 1, 5 > 1, 4 > 1, 8 > 1-. The flexibility of daunomycin about the chromophore-sugar linkages, defined by $\phi_1 = \text{C8-C7-O7-C1}'$ and $\phi_2 = \text{C7-O7-C1}'\text{-O5}'$ have been explored using semi empirical energy calculations (Neidle and Taylor, 1979). The minimum energy conformation is close to the N-bromo acetyl derivative, which does not have intermolecular O7...O9 hydrogen bond. The

coformational analysis of both the neutral (NH_2) and charged (NH_3^+) forms of doxorubicin has been carried out by metric energy minimization method (Nakata and Hopfinger, 1980) Three energy minima were observed for the neutral molecule and the conformer having $\phi_1 = 250^\circ$, $\phi_2 = 260^\circ$ was the most stable one than the other two conformers. It was observed that the stable conformation for both doxorubicin and daunomycin were different from their crystal structure. The intercalation of doxorubicin with dinucleotide dimer sequences d-CpG and d-TpC has been modeled using molecular mechanics calculations (Nakata and Hopfinger, 1980a). Minor groove intercalation was preferred. The conformation was characterized by the anthraquinone ring aligned nearly perpendicular to the long axis of CpG base pairs having alternate C3'-endo 3'-5' C2'-endo sugar ring puckering. The energy preference for the minor groove intercalation decreased for the ionized form of doxorubicin. The conformational preference was not found for intercalation with TpC-ApG dimer. Miller and Newlin, 1982 results were used to form three and four fused ring systems that can bind in an optimum manner to form ideal intercalators. Chen et al, 1985 performed theoretical computations on the energy and the structural factors involved in sequence selective binding of daunomycin to six self-complementary hexanucleotides including d(CGTACG)₂ sequence. The analysis of interaction of individual constituents of daunomycin, namely daunosamine side chain, its two 9-hydroxyl substituents and 9-acetoxy substituent and the chromophore ring revealed that the overall sequence preference found was a result of intricate interplay of intrinsic sequence preferences. Theoretical computations were performed on the structural and energy factors involved in sequence binding of adriamycin to five self-complementary hexanucleotides (Chen et al, 1986).

The model adopted for computation was similar to the one used in a previous study on daunomycin (Chen et al, 1985). The analysis here revealed overall preference of adriamycin for mixed oligomeric sequence d(CGTACG)₂. The 14-OH of adriamycin participated in additional hydrogen bonding with O1' oxygen of deoxyribose linked to base on 3' strand. There was an overall parallelism in the sequence selectivity of adriamycin with that of daunomycin. Cieplak et al, 1990 has performed free energy perturbation studies showed the preferences of acridine and daunomycin to bind to a specific base sequence in the DNA. It was observed that daunomycin prefers GC as second base pair and TA as third base pair, which was consistent with studies done earlier (Chen et al, 1985; Wang et al, 1987). Structural properties and intercalater-DNA interactions were investigated in daunomycin bound to 14-mer DNA duplex using molecular modeling technique (Treib et al, 2004). They have revealed that at each site of intercalation the phosphorus in I strand is in the B_I and the phosphorus directly lying on the opposite strand is in B_{II} state which are not subject to fluctuations but stable during the course of simulations thus daunomycin induces and stabilizes a distinct pattern of the phosphates of the DNA backbone. It was suggested that daunomycin intercalation increases the population of B_{II} conformation of DNA. Amino sugar is flexible at glycosidic bond angle which allows the sugar to switch in different conformations and very important for anchoring the intercalator in the minor groove. Ammonium group of the drug imparts sequence specificity. For glycosidic angle of amino sugar 3 conformations were found, out of these two conformations i.e. 155° to 162° and 135° to 138° was also represented by X-ray. The third conformation shows a dihedral angle value of 57° to 61°. It was inferred that rise alone is not sufficient to accommodate daunomycin and an additional buckle of the concerned

base pair is also necessary coupled by high unwinding of DNA at intercalation step.

Intercalation also causes widening of major groove

1.8.3 Nuclear Magnetic Resonance studies

Interaction of iremycin (IM) and daunomycin (DM) with DNA was studied by electric dichroism (Fritzsche et al, 1982). The protonation of the sugar dimethylamino group of IM-HCl is expected to affect the NMR lines of the neighbouring nuclei with respect to the lines of the free base. The significant difference of the IM HCl ^1H NMR spectrum to the corresponding spectrum of the IM base dissolved in CDCl_3 is the strong downfield shift of the N-dimethyl signal, which may be attributed to the protonation of the nitrogen of the N-dimethyl group of IM HCl. The apparent increase in length of DNA by drug intercalation increases in the order $\text{DM} < \text{IM} < \text{IM-Cu(II)}$. The tilt (long axis) and twist (short axis) of the iremycin chromophore was $28 \pm 4^\circ$, whereas for daunomycin the long axis is perpendicular to the helix axis and the short axis is twisted by about 25° . Unwinding behaviour of iremycin and daunomycin is similar with respect to orientation of both drugs. It was observed that long axis of daunomycin was almost perpendicular to the helix axis whereas that of iremycin is 30° tipped away from perpendicularity. For the major short-axis transition both daunomycin and iremycin are nearly 25° tipped away from perpendicularity. It was inferred that cyclohexane ring and sugar residue must play an important role in the geometry of orientation. Patel et al, 1978 elucidated structural features of the intercalated complex of daunomycin and nucleic acids by high resolution NMR spectroscopy in aqueous solution. The proton NMR parameters for the nucleic acid and the antibiotic resonances for the daunomycin-poly(dA-dT) complex at various DNA/drug ratio was reported. Patel et al, 1979 studied the duplex to strand transition

of the self-complementary sequence dG-dC-dG-dC by monitoring the exchangeable and the nonexchangeable protons and backbone phosphates. The complex formed between the antitumour anthracycline daunomycin and the dG-dC-dG-dC duplex was probed by the nucleic acid and the antibiotic resonances as a function of temperature.

Nuss et al, 1980 proposed a model consistent with the intercalation of daunomycin with different dinucleotides. This model was consistent with (1) the aromatic and methoxy proton resonances being shifted upfield (2) small but significant upfield chemical shifts of the protons on the A ring and (3) down field shift of some of the daunosamine protons. Proton nuclear magnetic studies of the self complementary hexanucleotide d(TpA)₃ and its interaction with daunomycin was investigated by Philips and Roberts, 1980. Extensive fraying was observed at 5°C but the hexanucleotide duplex was stabilized on interaction with daunomycin at 21°C at a drug/nucleotide ratio of 0.063. Daunomycin was released cooperatively from d(TpA)₃-daunomycin complex on heating. The chemical shift of 5'CH₃ of dausoamine sugar was found to be independent of temperature. These results suggested that planar aromatic portion of drug (rings B and C) intercalates while ring D protrudes outside the helix and on opposite side of the sugar moiety.

Patel et al, 1981 have performed proton and ³¹P NMR investigations on complexes of daunomycin and its analogue 11-deoxydaunomycin with poly (dA-dT) respectively in H₂O. The 6-OH and 11-OH protons of ring B, C of daunomycin shift upfield by ≈ 1.6 ppm on complexation, which is characteristic of intercalation. One of the ³¹P signals presumably the one at intercalation site also shift downfield by ≈ 0.45 ppm on complexation. The 11H proton of 11-deoxydaunomycin was found to undergo large upfield shift of ≈ 1.42 ppm which shows that ring B, C intercalate between base pairs

while ring D protrudes out. Neumann et al, 1985 studied interaction of daunomycin with B and Z helices of a self complementary DNA fragment d(CGm⁵CGCG). It was observed that with increase in daunomycin concentration, proportion of both B and Z free duplexes decreases and only duplex-daunomycin complex was detected. No signal corresponding to Z duplex-daunomycin complex was observed. It was shown that daunomycin binds exclusively to the B form of d(CGm⁵CGCG). The interaction of daunomycin with self complementary DNA fragment d(CGATCG) was studied by ³¹P NMR. Two molecules of drug intercalate between d(CG) at both ends of the helix and evidence for deformation in backbone is given. Binding constants was calculated to be 2 ± 10^4 and $1.4 \pm 1.0 \times 10^4 \text{ M}^{-1}$ while dissociation constant is $1.5 \times 10^{-3} \text{ M}$ (Ragg et al, 1988). Gorenstein and Lai, 1989 studied ³¹P to monitor phosphate ester backbone conformational changes upon binding of the intercalating drugs ethidium, quinacrine and daunomycin to sonicated poly(A).poly(U), to calf thymus DNA and RNA. A new ³¹P signal arises from phosphates, which are in perturbed environments due to intercalation of the drug. Similar though smaller deshielding of the ³¹P signals was observed in sonicated poly(A).Poly(U)-quinacrine complexes as well as in daunomycin complexes. The effect of added ethidium ion, quinacrine and daunomycin on the ³¹P spectra of sonicated calf thymus DNA is consistent with earlier study by Wilson and Jones, 1982. In these drug-DNA complexes the drug produces a gradual downfield shift in the ³¹P signal without the appearance of a separate downfield peak. These differences are attributed to differences in the rate of chemical exchange of the drug between free and bound duplex states (Wilson and Jones, 1982). Searle et al, 1990 the conformation of dynamics of the deoxyribose rings of (nogalamycin)₂-d(GCATGC)₂ complex have been determined from one-

dimensional NMR spectra and from COSY and DQF-COSY. Structure of the 2:1 complex of antitumor drug 3'-(2-methoxy-4-morpholinyl) doxorubicin with d-CGATCG was solved (Odefey et al, 1992). The drug intercalates between CG base pairs. Eight intermolecular NOEs (nuclear Overhauser enhancement) were extracted from the spectra and were used in building a model of the complex. Their results show that insertion of the primary amino group of the daunosamine moiety of anthracycline into a morpholinyl ring increases the potency of the drug dramatically and can interact covalently with DNA to form adducts.

Barthwal et al, 1994 investigated interaction of daunomycin with dCpG by two dimensional proton magnetic resonance techniques. The non-exchangeable base protons of dCpG and the ring protons of the drug chromophore shift upfield upto 0.27 ppm on intercalation. Changes in chemical shift decreases with temperature and are attributed to stacking of drug chromophore between G.C and G.C base pairs. The sugar is predominantly in the S-conformation state for both cytosine and guanine residues in the right-handed helix of the d-CpG complex. The glycosyl angles are about $-120 \pm 20^\circ$ and $-90 \pm 20^\circ$ for C and G residues, respectively. In daunomycin, the spin-spin coupling- $J(1'H-2'eqH)$, $J(1'H-2'axH)$, $J(4'H-5CH_3)$, $J(7H-8axH)$ and $J(7H-8eqH)$ are altered on complexation with dCpG, further, the interproton distances- $1'H-2'axH$, $7H-8axH$, $7H-eqH$, $5'H-8axH$ and $5'H-8eqH$ are altered significantly on complexation. The observed intermolecular NOEs- CH_6-2H , $1H$; CH_6 , CH_5-4OCH_3 ; $CH_1'-2'axH$ and $CH_4'-9COCH_3$ demonstrate the existence of specific conformation of the complex. Solution structure of $d(CGTACG)_2$ with 9-Amino anthracycline (SM-5887) with drug to DNA ratio 2:1 was solved by Igarashi et al, 1995. The cytosine residues shows that their chemical shift is effected by ring

currents of drug, therefore it was inferred that the drug intercalates between two cytosine residues. Ring D of the anthracycline aglycon is sandwiched between C1 and C5 bases. In comparison to daunomycin and adriamycin, this model of the 2:1 d(CGTACG)₂-SM-5887 complex has its aglycon sliding toward the minor groove. The reported work establishes the feasibility and relevance of NMR studies of SM-5887 bound to DNA and has led to the development of an initial model for the complex. The intercalation geometry of SM-5887 is a hybrid between those of adriamycin and nogalamycin. Mazzini et al, 1998 made an attempt to study the interaction (2S)-2-methoxymorpholino doxorubicin and morpholino doxorubicin with hexanucleotide d(CGATCG)₂ and d(CGTACG)₂ by 2D ¹H NMR and ³¹P NMR coupled with molecular dynamics techniques. The results of above study were compared with doxorubicin and daunorubicin. On intercalation of drug, deformation was noticed in DNA as torsional angle α and ξ changes from value of gauche gauche (as found in B-DNA) to gauche trans values. The change is associated with downfield shift of phosphorus. Different nucleotide sequences do not affect the dissociation rate constants of the drug from the DNA. As a consequence it appears that structural modifications at a level of ring A and amino sugar in the anthracycline molecule are important and the methoxymorpholino moiety plays a significant role in stabilizing the complex. Many intermolecular NOEs indicates that aglycone moiety of drug is oriented in orthogonal position with respect to terminal base pairs. Ring D protrude out on a major groove and ring A is placed in front of G2 and G12 residues. Their work reports that during complex formation the B_{II} conformational state increases.

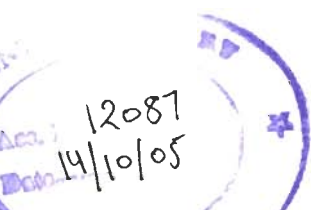
Robinson et al, 1997 has designed new class of bis intercalating drug with lower cytotoxicity, higher activity for resistant cancer cells. Two daunorubicins

symmetrically linked together via a p-xylenyl group, either at their N3' (WP631) or N4' sites (WP652). WP631 has high affinity towards DNA than WP652. In WP631-ACGTACGT complex, the aglycon chromophore has their D ring protruding into the major groove and two daunosamines plus the p-xylenyl tether moiety occupying the entire minor groove. WP652 binding is reminiscent that of the other bisintercalating antibiotics triostin A and echinomycin. The two aglycon rings of WP652 bracket two base pairs. Such drastically different binding models for WP631 and WP652 are due to the respective 3' and 4' sites of linkage for the tether. WP631 prefers CGTACG sequence while sequences like CGCG or more generally PyGCPu are required by WP652. Lam et al, 1997 studied the structure of eight self complementary DNA molecules $d(CGXX'CG)_2$ and $d(CAXX''TG)_2$ (where X=C, G, T or A and X' is complementary of X). Based on the structural data obtained in solution, a novel sequence dependent local structure function, Σ_{LS} , is composed of the sum of the contributions from the helix twist, Ω , base roll, ρ , base pair slide $\Delta\delta$ and propeller twist, ω is introduced to describe their sequence specific local structure. The results demonstrate that in addition to the interstrand purine-purine clashes, the base morphology of the nearest neighbour base pair is also important in defining the local geometry of the base pairs. Their results also forms the basis for using the trimer-tetramer model for the prediction of sequence specific local structures of deoxyribonucleic acid. Favier et al (2001) used 1D and 2D homonuclear NMR spectroscopy combined with simulated annealing/rMD to characterize the interaction of 2-(pyrido[1.2-e]-purin-4-yl) with $d-(CGATCG)_2$. Intercalation occurs at the C1pG2 step. Pyridopurine derivative rings were not exactly perpendicular to the helix. C1 was not involved in the intercalation process and does not stack with its upper base

G2. There was a weak, stacking interaction between the intercalated ligand and the DNA bases; however the drug/DNA affinity was enhanced by a hydrogen bond between the hydroxyl group at the end of the intercalant (drug) side chain and amide group of G6. The structure of the intercalated complex enabled insight into the structure activity relationship.

1.8.4 X-ray studies

Pigram et al, 1972 stated that an intercalation model can be built in which the amino sugar of the daunomycin is in the large groove of the DNA and the hydrophobic faces of the base pairs and the drug overlap extensively. The amino sugar is at the side of the groove close to a sugar phosphate chain enabling the ionised amino group to interact strongly with the second DNA phosphate away from the intercalation. A possible additional intercalation would be a hydrogen bond between the first phosphate and the hydroxyl attached to the saturated ring of the daunomycin chromophore. Molecular structure of daunomycin complexed to d-(CGTACG)₂ has been solved by Wang et al, 1987. In daunomycin the C9 atom is displaced by 0.59 Å in the same direction as the amino sugar relative to the plane of aglycon having O9 perpendicular or axial to the plane of the aglycone molecule. O7 is projected further away from A ring so that O7 and O9 atoms can no longer form an intramolecular hydrogen bond in contrast to those observed in other crystal structures of anthracycline antibiotics (Anguilli et al, 1971; Neidle and Taylor, 1977; von Dreele and Einck, 1977). DNA adopts a distorted right-handed double helical structure with modification in local area where it accommodates the drug molecule. The sugar pucker are mostly C2' endo while glycosyl for all other residues is high anti (-86°) except C1 which has a normal anti glycosyl torsion angle ($\chi = -154^\circ$). In overall conformation, daunomycin



molecule intercalate their aglycone chromophore between the CpG sites at both ends of the hexamer duplex with drug amino sugar filling the minor groove of the duplex and ring D protruding into the minor groove. O9 of daunomycin forms hydrogen bond with N3 and N2 of G2 residue. Two bridging water molecules between the drug and DNA stabilize the complex in the minor groove. In the major groove, a hydrated sodium ion is coordinated to N7 of the terminal guanine and with O4 and O5 of daunomycin with a distorted octahedral geometry. The intercalator allow to identify three principal functional component of anthracycline antibiotics: the intercalator (rings B-D), the anchoring functions of ring A and the amino sugar. The structure-function relationships of daunomycin binding to DNA as well as other related anticancer drugs are discussed.

Holbrook et al, 1988 studied the local mobility of nucleic acids. The directions and amplitude of the local motion indicate that changes in the mobility of DNA due to daunomycin binding and is primarily limited to the residues forming the intercalation site. The intercalated daunomycin ring system (aglycon) is rigidly fixed in the base stacks, apparently serving as an anchor for the amino sugar segment of the drug, which is one of the most mobile regions of the entire complex. This mobility implies that if the central AT base pair is switched to a CG base pair, there should be a low energy cost in avoiding the guanine amino group. The energy difference (for the sugar-binding preference) between $d(\text{CGTACG})_2$ and $d(\text{CGCGCG})_2$ could be considerably less than 20kcal/mol, a value proposed previously from computation. Moore et al, 1989 found out that the overall intercalation geometry in the daunomycin-d(CGATCG) complex is similar to that observed in the same complexes by other workers (Quigley et al, 1980; Wang et al, 1991). The larger differences in

backbone torsion angles, especially between those of the intercalation sites d(C1pG2) and d(C5pG6) indicate a somewhat more extreme asymmetric conformation adopted by d(CGATCG)₂ than by d(CGTACG)₂ on binding to daunomycin. The daunomycin aglycon chromophore is oriented at right angles to the long axis of the DNA base pairs. This head on intercalation is stabilized by hydrogen bonding interactions between the chromophore and its intercalation site base pairs. The cyclohexene ring and amino sugar substituent lie in the minor groove. The amino sugar N3' forms the hydrogen bond with O2 of the next neighbouring thymine. This electrostatic interaction helps to position the sugar in a way that results in extensive van der waal's contacts between the drug and the DNA. There is no interaction between daunosamine and the DNA sugar-phosphate backbone.

Structural comparison of anticancer drugs, adriamycin and daunomycin complexed with DNA sequence d(CGATCG)₂ was done by Frederick et al, 1990. In all the three complexes that is, daunomycin-d-(CGATCG)₂, daunomycin-d(CGTACG)₂ and adriamycin-d-(CGATCG), the aglycon moiety intercalates at the GC base pair on either end of the duplex. The orientation of the aglycon and conformation of ring A are highly conserved throughout the series. It appears that neither the addition of a hydroxyl group nor the change in DNA sequence adjacent to the intercalation site has an effect on the position of the aglycon. In all three complexes, the one end is anchored by two direct hydrogen and indirect hydrogen bond and the other end is anchored by coordination to a solvent molecule that appears to be a sodium ion. Due to presence of extra hydroxyl group in adriamycin containing complex there are bridging interactions to phosphate groups of the proximal DNA strand, while in daunomycin containing complexes there are several water molecules interacting with

a minor groove edges of the terminal base pair. Amino sugar extends into minor groove. In comparison with daunomycin-d(CGTACG)₂, the amino sugar in daunomycin-d(CGATCG)₂ and adriamycin-d(CGATCG)₂ form more favourable interactions with the DNA. Daunomycin and adriamycin complex with (dCGATCG)₂ has increased stability as N3' of amino sugar forms additional direct hydrogen bond and several van der waal's contact with the edges of base pair within the minor groove. The two hydrogen bonds from N3' to solvent molecules are conserved in all three complexes. In DNA at G2pA3 step and the C5pG6 steps, ξ values have been increased to trans conformation; while ϵ for C1 is reduced and χ adopts low anti conformation which causes base pair separation. The conformation and interactions in the complexes formed by 4'-epiadriamycin with d(CGATCG)₂ are consistent with the previously reported complex. A direct hydrogen bond from 4'OH group of amino sugar to N3 of A3 is formed due to inversion of stereochemistry of at the 4' position of 4'-epiadriamycin. This bond is not formed in other complexes. Hydrogen bond is formed between 9-OH with N2 of G2. Solvent molecules forms hydrogen bonds with O4, O5, N3 and O4' of drug chromophore and with N7 of G12, O2 of T4. A water mediated hydrogen bond is observed from the O13 of the A ring to the O2 of C1. Anthracycline sugar interacts more intimately with d(CGATCG)₂ than with d(CGTACG)₂ forming direct hydrogen bonds to d(CGATCG)₂ but not to d(CGTACG)₂. Spermine binds to major groove of the complex and its methylene and amino groups form van der waal's contact with both the DNA and drug. In daunomycin-CGATCG-spermine complex, the spermine molecule forms two direct hydrogen bonds and several indirect hydrogen bonds via mediating water molecule to the backbone of the DNA. Spermine molecule aligned roughly perpendicular to the

helical axis. In epiadriamycin-CGATCG-spermine ternary complex, terminal amino group of spermine forms two hydrogen bonds with the phosphate oxygen of DNA (Williams et al, 1990)

Nunn et al, 1991 studied the complexes of daunomycin with d(TGTACA) and d(TGATCA) referred to as TGT-daun and TGA-daun, respectively. Binding occurs via intercalation of the drug chromophore at d(TpG) step. Hydrogen bonding interactions involves the drug, DNA and solvent molecules. The torsion angles values for the oligonucleotide backbone and glycosyl bond for two complexes are similar to those observed in literature (Frederick et al, 1990; Moore et al, 1989; Wang et al, 1987). The TGT sugar puckering is close to that observed for d(CGTACG)-daunomycin complex (Frederick et al, 1990; Moore et al, 1989; Wang et al, 1987) Major deviations occur at intercalation site with significant buckling at T1.A12 base pair (10° for TGT-daun and 11° for TGA-daun). The G2.C11 at other side is buckled by 20° in opposite direction for both complexes. The position of chromophore is similar in both complexes but the orientation and conformation of sugar is however different. The daunomycin sugar is located in the minor groove of the DNA is stabilized by hydrogen bond between the amino and functional groups of the sugar. The amino sugar of the d(TGATCA)₂ duplex interacts directly with the DNA sequence, while in the d(TGTACA)₂ duplex, interaction is via solvent molecules. In all the complexes analyzed, the distance from O9 to N3 is shorter than to N2. In the four T/CGT/A-daunomycin complexes, a water molecule is bonded to the O13 of drug. This water further coordinates in all cases to O2 of T1 or C1 with the exception of TGATCA-daunomycin complex. Sodium or water mediated interaction with ring D is absent only in TGT-daunomycin. For the sequences T/CGA there is direct

hydrogen bonding with O2 (T10), O2 (C11), O4' (C11) and water. Their calculation predicts that an AT base pair at the center of the DNA is more stable than a GC base pair in this position. MAR 70, is a synthetic derivative of the anticancer drug daunorubicin containing an additional sugar, attached to O4' of daunosamine was crystallized with the DNA hexamer d(CGTⁿACG), where ⁿA is 2-aminoadenine. In both complexes two MAR 70 molecules are intercalated between the CpG steps and ring A-D penetrates the DNA with ring D protruding in major groove and disaccharide lie in the minor groove. O9 of drug forms two hydrogen bonds with N2 and N3 of guanine G2. C13 of drug is bridged to O2 of C1 by water molecule, O7 of glycosyl linkage forms weak hydrogen bonds with NH₂ of G2. High buckle (18.4° for TⁿA complex and 17.8° for TA complex) and low unbinding angle (-8.4° in TⁿA complex and 17.8° in TA complex) was observed. The cross-linking reaction by HCHO in the MAR 70 TⁿA complex appears quite effective. Both sugars are in chair conformation and torsion angles C5'-C4'-O4'-C1'F (τ_1) and C4'-O4'-C1'F-C2'F (τ_2) (F is fucose) between two sugars are 268°, 160° for TA complex and 276°, 151° for TⁿA complex, respectively. The combination of τ_1 and τ_2 makes both sugars nearly perpendicular to each other. It was suggested that attaching certain functional groups (e.g. alkylating) at the N3' amino position of daunomycin/doxorubicin molecule is useful as they may be able to alkylate the N3 position of adenine very effectively, thereby increasing the therapeutic index.

The structure of the complex between d(TGATCA) and the anthracycline 4'-epiadrimycin has been determined by Langlois d' Estaintot et al, 1992. The overall structure is similar to that observed in the series of hexamer anthracycline complexes (Frederick et al, 1990; Leonard et al, 1992; Moore et al, 1989; Nunn et al, 1991;

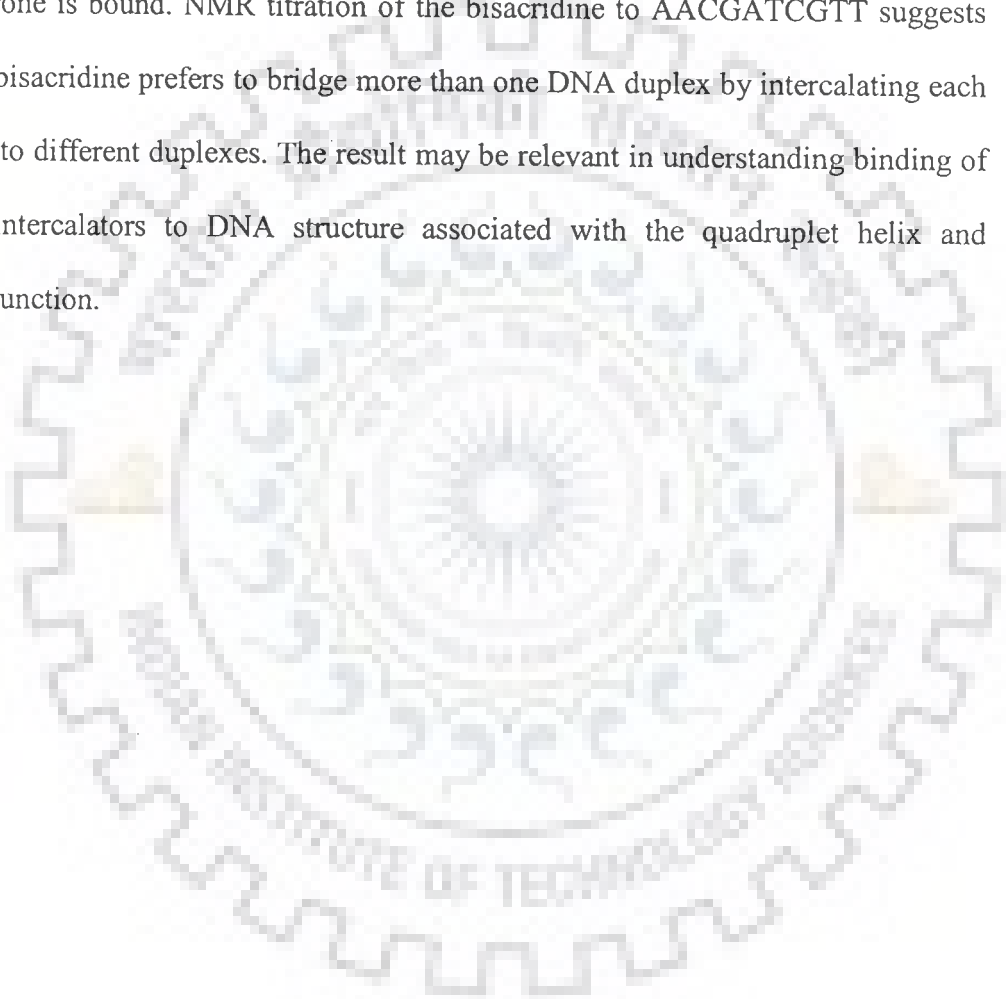
Williams et al 1990; Quigley et al, 1980). The crystal structure of morpholino derivative of adriamycin bound to d(CGTACG)₂ was studied by Cirilli et al, 1992. Chromophore ring interacts between CpG base pairs, with ring D in major groove and amino sugar in minor groove. Hydrogen bonds are formed between O9 of drug and N2, N3 of G2 and G8, respectively. Indirect hydrogen bond is formed from O13 of drug through water molecule to O2 of C1 and C7. On major groove side, the other end of aglycon is anchored by coordinating to a solvent molecule. This solvent forms direct hydrogen bonds to O4 and O5 of aglycon and N7 of G2 and G12. The binding site involves four base pairs and the absence of positive charge on the amino sugar appears to influence the hydration pattern on both grooves.

The structures of two hexanucleotide anthracycline complexes d(CGGCCG)/daunomycin and d(TGGCCA)/adriamycin have been determined using single crystal X-ray diffraction techniques (Leonard et al, 1993). In both cases the anthracycline molecule is bound to non-preferred d(YCG) base-pair triplet sites, daunomycin type anthracyclines lack affinity for d(YGG) and d(YGC) sites.

WP631, a bisintercalator in which 2 daunorubicins linked together via a p-xylene group at N3', intercalates between CG base pair at both ends of d-(CGATCG)₂. DNA conformation is most conserved at the intercalation site and most disparate in the center of the complexes. G2 is the most conserved residue in the complex. The central AT base pair show significant positive buckle which is in contrast to the daunomycin-d-(CGATCG)₂ complex (Hu et al, 1997). Hydrogen bonds from 9-OH of daunomycin to N2 and N3 of G2 are conserved in WP631 complex. Minor groove binding of amino sugar is observed. In the daunomycin complex, the 3' amino nitrogen forms three hydrogen bonds with the DNA and but these hydrogen bonds are lost in the

WP631 complex. WP631 complex is a near absence of stabilizing van der waal's interactions between the amino sugar/linker and the minor groove of the DNA. The unfavourable oxygen-oxygen interaction and deficit of stabilizing interactions of the linker/amino sugar with DNA are evidence of the linker strained. The DNA binding of WP631 is ultra tight. The study by Saminadin et al, 2000 was conducted on N-cyanomethyl-N-(2-methoxyethyl)-daunomycin (CMDA), a synthetic analogue of cyanomorpholino-daunomycin complexed with d-(CGATCG)₂. Crystal structure shows that the chromophore is intercalated at each extremity of the duplex. The amino sugar moiety is in the minor groove while the chromophore ring D protrudes in the major groove. The long axis of the chromophore is roughly perpendicular to the flanking base pairs. Numerous van der waal's interactions between the methoxy ethyl chain, A9 and T10 are observed. The observed densities indicate the formation of N-hydroxymethyl-N-(2- methoxyethyl)-daunomycin (HMDA) with the release of cyano moiety without DNA alkylation. The formation of this degradation compound is discussed in relation with other drugs modifications when they bind to DNA. Comparison with two other drug-DNA crystal structure suggests a correlation between a slight change in DNA conformation and nature of the amino sugar substituent at the N3' position located in the minor groove. The binding of macrocyclic bisacridine and ametantrone to CGATCG was studied (Yang at al, 2000). Only one acridine of the bisacridine drugs binds at C5pG6 step of DNA, with the other acridine plus both linkers completely disorderd. Surprisingly both terminal G.C base pairs are unreveted. The C1 nucleotide is disordered and the G2 base is bridged to its own phosphate through a hydrate Co⁺ ion, G2 swing towards the minor groove with its base stacked over the backbone. The C7 nucleotide is flipped away from the

duplex part and base paired to a two-fold symmetry related to G6. The central four base pairs adopt the B-DNA conformation. An unusual intercalator platform is formed by bridging four complexes together such that the intercalator cavity is flanked by two sets of G.C base pairs (i.e., C5G8 and G6C7) on each side, joined together by G6.G8 tertiary base pair interaction. In the bisacridine-CGATCG complex, only one acridine is bound. NMR titration of the bisacridine to AACGATCGTT suggests that the bisacridine prefers to bridge more than one DNA duplex by intercalating each acridine to different duplexes. The result may be relevant in understanding binding of certain intercalators to DNA structure associated with the quadruplet helix and holiday junction.



MATERIALS AND METHODS

2.1 MATERIALS

The deoxyribonucleic sequence d-(CGATCG)₂ was purchased from Microsynth, Switzerland. Deuterium Oxide (D₂O), Dimethyl Sulphoxide (DMSO) with isotopic purity 99.96%, daunomycin and adriamycin were purchased from Sigma Chemical Co., USA. Sodium 2, 2-dimethyl-2-silapentane-5-sulphonate (DSS), an internal NMR reference was purchased from Merck Sharp Dohme Ltd. All other chemicals like Na₂HPO₄ and NaH₂PO₄, etc. used for buffer preparation were purchased from Sigma, Ltd. All HPLC grade reagents like water, triethyl amine, acetonitrile, glacial acetic acid, etc. were from Qualigens, Ltd. Drug samples were used without further purification but nucleotide sample was purified by dialysis using benzoylated dialysis tubing from Sigma-Aldrich Co.

Further, d-(CGATCG)₂ and d-(TGATCA)₂ samples were also synthesized for routine 1D NMR experiments and absorption studies. Synthesis was carried out on 0.2 μM, 1 μM and 10 μM scale on Applied Biosystems DNA Synthesizer (model 392 A) using cyanoethyl phosphoramidite chemistry. The starting material was a solid support derivatized with a nucleoside, which will become the 3'-hydroxyl end of the oligonucleotide. The 5' hydroxyl end was blocked with a dimethoxytrityl (DMT) group. The steps of the DNA synthesis cycle are as follows:

- (i) The treatment of derivatized solid support with acid removes the DMT group and thus frees the 5'-hydroxyl for the coupling reaction. An activated intermediate is created simultaneously adding the monomer and

tetrazole, a weak acid, to the reaction column. The intermediate is so reactive that addition is complete within 30 seconds.

- (ii) The next step of capping terminates any chains, which did not undergo addition. Capping is done with acetic anhydride and 1-methylimidazole. Capping minimizes the length of the impurities and thus facilitates their separation from the final product.
- (iii) During the last step of oxidation, the internucleotide linkage is converted from the phosphite to the more stable phosphotriester. Iodine is used as an oxidizing agent and water as oxygen donor. The reaction gets completed in less than 30 seconds.

After oxidation, the DMT group was removed with trichloroacetic acid. The cycle was repeated until chain elongation was complete. Treatment with concentrated ammonium hydroxide for 1 hour removes β -cyanoethyl protecting groups and also cleaves the oligonucleotide from the support. The benzoyl and isobutyryl base protecting groups were removed by heating at room temperature in ammonia for 8-15 hours.

2.1.1 Purification by dialysis

The sample was further purified by dialysis using benzoylated dialysis tubing. The tube of 6 cm length was cut and activated by boiling it in large volume of 2% (w/v) sodium bicarbonate and 1 mM EDTA (pH = 8.0) for 10 minutes followed thorough rinsing in distilled water. Dialysis membrane was then again boiled for 10 minutes in 1 mM EDTA (pH = 8.0). The sample was then put into the tubing, sealed with holders and dialysed against 4 M NaCl for 12 hours followed by dialysis against distilled water for 12 hours twice. Sample was then taken out lyophilized and dissolved in

phosphate buffer. The purified oligonucleotide was annealed by heating it in a computer aided Cary 100 Biospectrophotometer equipped with a thermoelectric control unit (peltier unit) upto 80°C at the rate of 1°C per minute with hold time of 10 minutes and then slowly cooled it to the room temperature to get oligonucleotide in duplex state.

2.2 SAMPLE PREPARATION

Solution of daunomycin (30.2 mM) was prepared by dissolving a known quantity of sample in D₂O. It was lyophilized and redissolved in D₂O and the process was repeated twice. The final concentration was checked by absorbance measurements at wavelength of 480 nm using Cary 100 Biospectrophotometer. The extinction coefficient (ϵ) value used for adriamycin was $\epsilon = 11500 \text{ M}^{-1} \text{ cm}^{-1}$. Solution of deoxyoligonucleotide, d-(CGATCG)₂ (3.4 mM duplex concentration) was prepared by dissolving a known quantity of sample in deuterated phosphate buffer (16.25 mM) of pH = 7.0 having 15 mM Na salt. The sample was lyophilized and redissolved in D₂O and the process was repeated twice. Finally, d-(CGATCG)₂ was dissolved in 0.4 ml of D₂O and its concentration was determined by absorbance measurements at 260 nm using the extinction coefficient (ϵ) value = $59200 \text{ M}^{-1} \text{ cm}^{-1}$. Ethylene diamine tetra acetic acid (EDTA), 0.1 mM, was added to suppress paramagnetic impurity, which may cause line broadening during NMR measurements. Typically 1 μ l of 0.1 M solution of DSS was added to the complex of d-(CGATCG)₂ and adriamycin as an internal reference.

2.2.1 Preparation of complex

3.4 mM d-(CGATCG)₂ and 30.2 mM daunomycin samples were taken as a stock solution for preparation of complex. A complex of d-(CGATCG)₂ and daunomycin

was prepared by titration. 90 μl of 30.2 mM daunomycin was added in steps of 10 μl to 0.4 ml of 3.4 mM d-(CGATCG)₂ sample during titration in order to make 2:1 complex of daunomycin: d-(CGATCG)₂. The concentration of d-(CGATCG)₂ (N₁) in total volume of 0.41 ml is determined as follows:

$$N_1V_1 = N_2V_2$$

$$N_1 \times 0.41 = 3.4 \times 0.4$$

$$N_1 = 3.32 \text{ mM}$$

The concentration of daunomycin in this solution is determined as follows:

$$N_3V_3 = N_4V_4$$

$$N_3 \times 0.41 = 30.2 \text{ mM} \times 0.01$$

$$N_3 = 0.73 \text{ mM}$$

Like wise other daunomycin-d(CGATCG)₂ complexes of different drug/ nucleotide (D/N) ratios were prepared. The concentration of daunomycin (D), d-(CGATCG)₂ (N) and drug/ nucleotide (D/N) ratio are shown in Table 2.1

2.3 METHODOLOGY

2.3.1 NMR Spectroscopy- Technique for biological structure determination

Nuclear Magnetic Resonance (NMR) spectroscopy stand today as one of the most powerful physical methods to probe the biological systems and processes. It has proved to be a valuable tool in the determination of structure and dynamics of biological macromolecules in aqueous solution, under conditions similar to those in real systems.

Table 2.1: Various concentration ratios (D/N) for the complex formed between daunomycin and d-(CGATCG)₂

Nucleotide Concentration (mM) = N	Drug Concentration (mM) = D	D/N
3.40	0.00	-
3.31	0.73	0.21
3.23	1.43	0.43
3.16	2.10	0.65
3.09	2.74	0.86
3.02	3.35	1.08
2.95	3.93	1.30
2.89	4.49	1.52
2.83	5.03	1.74
2.77	5.54	1.95

NMR is a powerful spectroscopic technique that provides information about the structural and chemical properties of molecules. NMR exploits the behaviour of certain atoms when they are placed in a very strong magnetic field and many of the spectral parameters can be interpreted directly in terms of conformation or dynamics. As ^1H , ^{13}C , ^{15}N and ^{31}P are all present in nucleic acids, there are large number of signals present that can report on structure, dynamics and the effect of ligand binding.

2.3.1.1 *The phenomenon*

Subatomic particles (electrons, protons and neutrons) spin on their axis. A nucleus (of spin $1/2$) when placed in a static magnetic field behaves like a small magnet. This nucleus is in the lower energy level (i.e. its magnetic moment does not oppose the applied field). In the absence of an external magnetic field, these orientations are of equal energy. Each level is given a magnetic quantum number, m , characterizing Z component of spin, I . On interaction with magnetic field, nuclei with spin $I > 1/2$ distribute themselves among $2I + 1$ energy level with the separation by:

$$\Delta E = h \gamma B_0$$

The overall spin, I , is important. A nucleus with spin $1/2$ will have 2 possible orientations (Fig. 2.1a). These spins are capable of interacting with a beam of electromagnetic radiations. These energy levels correspond to the spins aligned along and against the applied magnetic field, B_0 . The spin oriented to oppose B_0 has higher energy. These spin do not align perfectly along B_0 and this give rise to a permanent torque. The nucleus also has the property of angular momentum because of its spin and thus as a result the nuclei precess (Fig. 2.1b), with frequency of precession given by:

$$\omega_0 = \gamma B_0$$

where, γ is proportionately constant, ω_0 is the resonant or Larmor frequency in radians/second and B_0 is the magnitude of the applied magnetic field. When the frequency of the beam is same as that of precessing spin then absorption of energy takes place, which causes the nuclei to flip from a lower energy state to a higher energy state by a process termed resonance (Fig 2.1c). In an NMR sample there are many molecules, each with its spin precessing about B_0 at same frequency and result in a net magnetization of M_z oriented along the Z-axis. On application of a rotation radio frequency field with frequency at or near $\omega_0 = \gamma B_0$, the spin resonate giving rise to net M_{xy} component which is phase coherent.

The following are the spectral parameters in NMR:

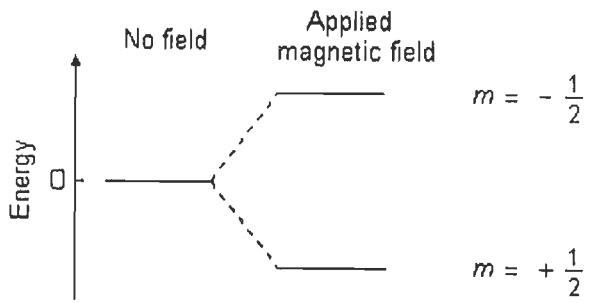
2.3.1.2 Chemical Shift

The magnetic field at the nucleus is not equal to the applied magnetic field, B_0 ; electrons around the nucleus shield it from the applied field. The difference between the applied magnetic field and the field at the nucleus is termed the nuclear shielding. The induced field is directly proportional to B_0 . This is represented by the equation:

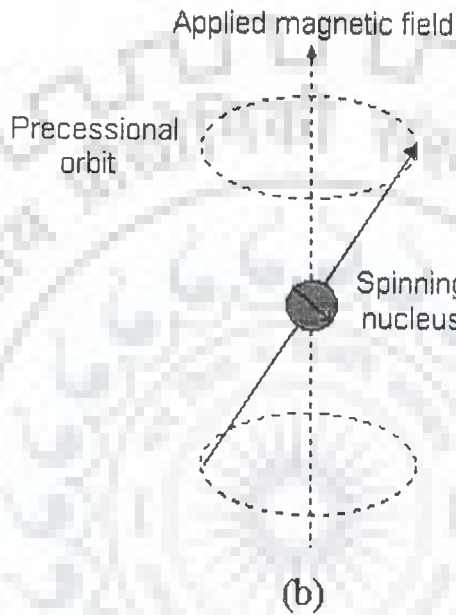
$$B_{\text{eff}} = B_0 (1 - \sigma)$$

where, σ is the shielding constant which depends on the nature of electrons around the nucleus. Chemical shift is a function of the nucleus and its environment. It is measured relative to a reference compound. For ^1H NMR, the reference is usually tetramethylsilane, $\text{Si}(\text{CH}_3)_4$. Chemical shift is expressed in parts per million (ppm) is given as:

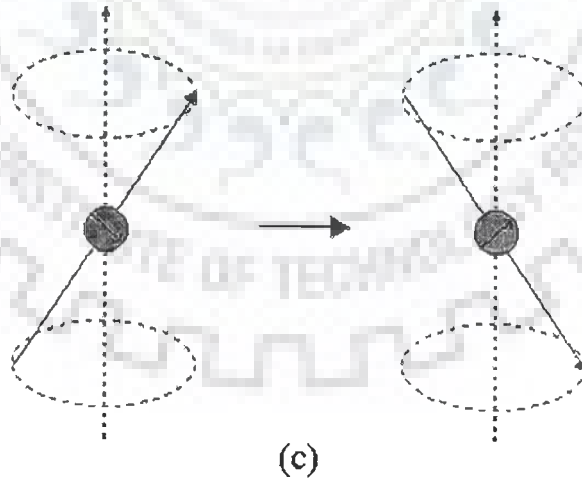
$$\delta = 10^6 \times \left(\frac{\delta_{\text{ref}} - \delta_{\text{obs}}}{\delta_{\text{ref}}} \right)$$



(a)



(b)



(c)

Figure 2.1: (a) Energy levels for a nucleus with spin quantum number $\frac{1}{2}$ (b) Precessional motion by the nucleus spinning on its axis in presence of the external magnetic field (c) Flipping of the magnetic moment on absorption of the radiations

where, δ_{ref} is the position observed for a reference compound and δ_{obs} is the position of the signal of interest. There are useful general conclusions that can be drawn from specific chemical shift value, or changes due to the binding of the ligand.

2.3.1.3 Spin-spin coupling constant (J)

Nuclei experiencing the same chemical environment or chemical shift are called equivalent. Those nuclei experiencing different environment or having different shifts are nonequivalent. Nuclei, which are close to one another, exert an influence on each other's effective magnetic field. This effect shows up in the NMR spectrum when the nuclei are nonequivalent. If the distance between non-equivalent nuclei is less than or equal to three bond lengths, this effect is observable. This effect is called spin-spin coupling or J coupling and is expressed in Hertz. This coupling causes splitting of lines. The appearance of multiplet patterns depends on relative magnitude of δ and J for coupled nuclei. Vicinal couplings (3J) display a characteristic dependence upon the involved dihedral angle (Fig. 2.2 a) according to the relation dihedral couplings;

$$^3J = 8.5 \cos^2\theta - 2.8$$

$$^3J = 9.5 \cos^2\theta - 2.8$$

This relationship is known as the Karplus relation. Fig. 2.2a and 2.2b shows the definition of dihedral angle and relationship between J couplings and dihedrals.

2.3.1.4 Relaxation process

The magnetization does not precess infinitely in the transverse plane but turns back to the equilibrium state. This process is called relaxation. Two different time-constants describe this behaviour. The importance of these phenomena is in the nuclear Overhauser effect (NOE), which can be used to probe internuclear distances in a molecule. There are two major relaxation processes namely, Spin-lattice

(longitudinal) relaxation (T_1) and spin-spin (transverse) relaxation (T_2). The relaxation time T_1 represents the "lifetime" of the first order rate process that returns the magnetization to the Boltzmann equilibrium along the +Z axis. The components of the lattice field can interact with nuclei in the higher energy state, and cause them to lose energy (returning to the lower state). The energy that a nucleus loses increases the amount of vibration and rotation within the lattice. The relaxation time, T_1 depends on the motion of the molecule. As mobility increases, the vibrational and rotational frequencies increase, making it more likely for a component of the lattice field to be able to interact with excited nuclei. T_1 spin-lattice relaxation rate is then measured by plotting M as a function of τ :

$$M(\tau) = M_0 (1 - 2\exp^{-\tau/T_1})$$

T_2 represents the lifetime of the signal in the transverse plane (XY plane) and it is this relaxation time that is responsible for the line width. In Solution NMR, very often T_2 and T_1 are equal. The very fast spin-spin relaxation time provides very broad signals. The transverse relaxation constant T_2 is related to the linewidth of the signals. The width of the signal at half height is given by:

$$(\Delta\omega)_{1/2} = 1 / \pi T_2$$

Fast decay leads to broad signals, slow decay to sharper lines. The transverse relaxation constant T_2 of spin $I=1/2$ nuclei is mainly governed by the homogeneity of the magnetic field and the strength of the dipolar interaction with other $I=1/2$ nuclei depending on the number and the distance of neighbouring nuclei the overall tumbling time of the molecule which is related to its size. Transverse relaxation (T_2) is faster than longitudinal relaxation. T_2 spin-spin relaxation rate is measured by plotting M as a function of τ :

$$M(\tau) = M_0 \exp(-\tau/T_2)$$

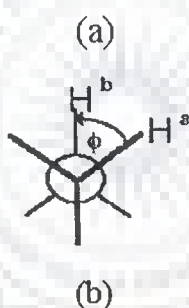
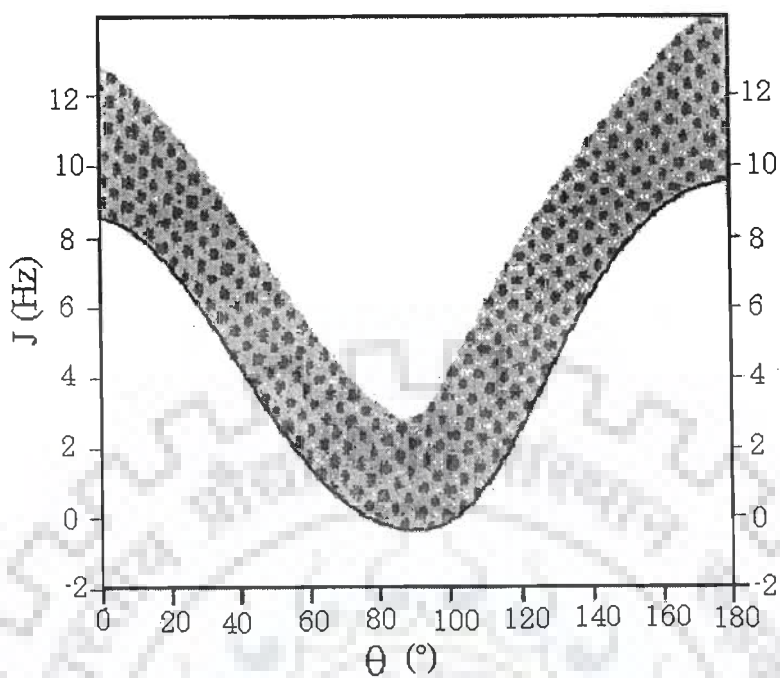


Figure 2.2: (a) Karplus Curve showing relationship between J couplings and dihedral angle (b) definition of the dihedral angle

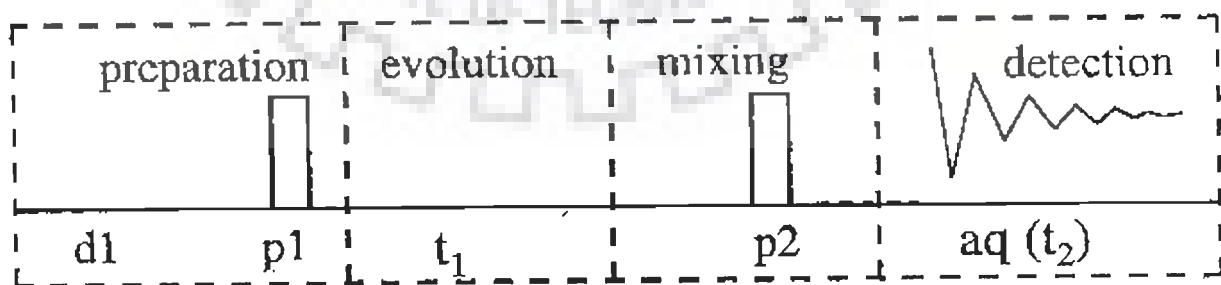


Figure 2.3: Four different time segments of a 2D NMR experiment namely (i) preparation period (ii) evolution period (t_1) (iii) mixing period (τ_m) (iv) detection period (t_2)

2.4 TWO-DIMENSIONAL (2D) NMR TECHNIQUES

In one-dimensional pulsed Fourier transform NMR the signal is recorded as a function of one time variable and then Fourier transformed to give a spectrum, which is a function of one frequency variable. In two-dimensional NMR the signal is recorded as a function of two time variables, t_1 and t_2 , and the resulting data Fourier transformed twice to yield a spectrum, which is a function of two frequency variables. The two-dimensional signal is recorded in the following way. First, t_1 is set to zero, the pulse sequence is executed and the resulting free induction decay recorded. Then the nuclear spins are allowed to return to equilibrium, t_1 is then set to Δt , the sampling interval in t_1 , the sequence is repeated and free induction decay is recorded and stored separately from the first. Again the spins are allowed to equilibrate, t_1 is set to $2\Delta t$, the pulse sequence repeated and a free induction decay recorded and stored. The whole process is repeated again for $t_1 = 3\Delta t$, $4\Delta t$ and so on until sufficient data is recorded, typically 50 to 500 increments of t_1 . Thus recording a two-dimensional data set involves repeating a pulse sequence for increasing values of t_1 and recording a free induction decay as a function of t_2 for each value of t_1 . The general scheme for two-dimensional spectroscopy is (Fig. 2.3):

Preparation time: The sample is excited by one or more pulse. This consists of a delay time or a sequence of pulses separated by fixed time intervals saturation sequences. Thermal equilibrium is attained during this period.

Evolution Period (t_1): The resulting magnetization is allowed to evolve for the first time period, t_1 . The evolution period is the pulse sequence element that enables frequency labelling in the indirect dimension. Further, one or several radiofrequency pulses may be applied to create coherence.

Mixing time (τ_m): During this period coherence is transferred between spins. Mixing sequences utilize two mechanisms for magnetization transfer: scalar coupling or dipolar interaction (NOE). After the mixing period the signal is recorded as a function of the second time variable, t_2 . This sequence of events is called a pulse sequence.

Detection Period: The signal is recorded during the time t_2 at the end of the sequence, detection, often called direct evolution time; during this time the magnetization is labelled with the chemical shift of the second nucleus. The data is recorded at regularly spaced intervals in both t_1 and t_2 .

2.4.1 Two-dimensional correlation spectroscopy (2D-COSY)

The COSY experiment is used in determining which atoms are connected through bonds. The basis of COSY experiment whose pulse sequence is shown in Fig. 2.5 is the classical Jeener sequence (Jeener, 1971). After the preparation period of 90° pulse constitutes brief mixing period whose effect is to mix single quantum coherence into a whole range of orders of coherence. However, only the single quantum coherence will give rise to any measurable signal during the detection period. The mixing process interchanges orders of coherence, mixes coherence among the transitions associated with a given spin and exchanges coherence between spins having a mutual scalar coupling. Thus a magnetization, initially associated with the A spin of an A-X spin system, may be transferred to spin X through the scalar coupling, J_{ax} . Therefore the A magnetization in the X-Y plane will also depend upon the Larmor frequency ω_x and the 2D COSY will show signals with frequency coordinates (ω_A, ω_X) and (ω_X, ω_A) as well as (ω_A, ω_A) . The former are the characteristic cross peaks of COSY spectrum and the latter, the diagonal peaks, which corresponds to 1D spectrum. COSY experiment can be carried out with special phase cycling and data processing to

change the 2D line shape into pure 2D absorption mode, allowing the use of phase-sensitive display. There are two different methods in use, the first requires the results of two complete COSY experiments with different phase cycling to be added (States et al, 1982) and the second known as TPPI (Time proportional phase incrementation) method uses a single experiment with phase cycling which changes with t1 increment (Bodhenhausen et al, 1977; Keeler and Neuhaus, 1985; Marion and Wuthrich, 1983; Redfield et al, 1975). The phase sensitive COSY spectra have cross peaks in anti phase. The antiphase multiplet structure of a cross peak only occurs in the active coupling giving rise to cross peak. Extra splittings present in multiplet but which do not give rise to cross peaks are called passive couplings and appear inphase. Thus, the advantage of phase sensitive COSY is that the phase relation between peaks can be used for accurate assignment and calculation of coupling constants.

2.4.2 Phase sensitive COSY: Double quantum filtered COSY (DQF-COSY)

The experiment uses a pulse sequence $90_{\phi}-t_1-90_{\varphi}-90_{\zeta}-t_2$ where ϕ , φ and ζ are the appropriate phase cycles (Piantini et al, 1982). In double quantum filter COSY experiment, (Fig. 2.4) the resonance from a COSY experiment is passed through a double quantum filter, thereby removing methyl and other singlets from the final spectrum. The short delays, Δ , immediately before and after the final pulse, are of order of microseconds. Twice as many transients are needed in these experiments to achieve the same signal to noise ratio than in conventional COSY. Another advantage of DQF COSY is that it converts the phase of COSY diagonal signals from dispersive antiphase to absorptive antiphase. These signals then do not interfere with the cross peaks. So, the cross peaks lying close to diagonal can be observed in double quantum filtered phase-sensitive COSY. Double filter COSY can be used to determine the coupling constants (Celda et al, 1989; Gochin et al, 1990).

2.4.3 Total Correlated Spectroscopy (TOCSY)

During this pulse sequence, after the evolution period t_1 , the magnetization is spin-locked. During this mixing time the magnetization exchange ^{occurs} through scalar coupling. During this spin-lock period, the magnetization behaves as a strongly coupled spin system and evolve under the influence of a "collective spin-mode". In that collective mode, coherence transfer is possible between all coupled nuclei in a spin system, (even if they are not directly coupled). This essentially gives the same information as that of COSY, except that COSY gives information only on the directly coupled spins, whereas TOCSY gives the complete spin-coupling network

2.4.4 Nuclear Overhauser Effect Spectroscopy (NOESY)

NOESY is one of the most useful techniques as it allows to correlate nuclei through space (distance smaller than 5Å). By measuring cross peak intensity, distance information can be extracted. The pulse sequence starts as usual with a 90° pulse followed by an evolution time t_1 (Fig. 2.4). This delay is varied systematically as usual to provide chemical shift information in the F1 domain. Then 90° pulse transmits some of the magnetization to the Z-axis and during the following mixing period, the non-equilibrium Z component will exchange magnetization through relaxation (dipole-dipole mechanism). This exchange of magnetization is known as NOE (Nuclear Overhauser Effect). After some time (shorter than the relaxation time T_1), the transverse magnetization is restored and detected. If relaxation exchange (or chemical exchange) have taken place during the mixing time, cross peaks will be observed in the spectra. The phase cycling ensures proper detection of NOESY signal.

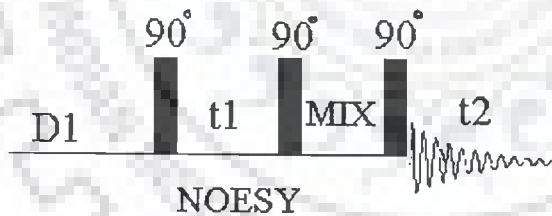
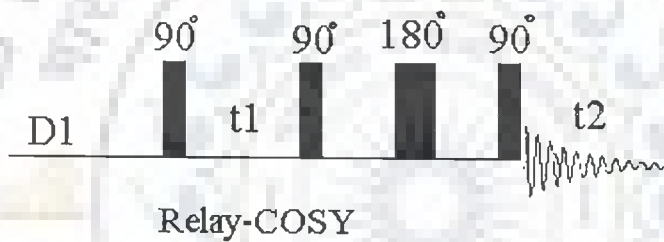
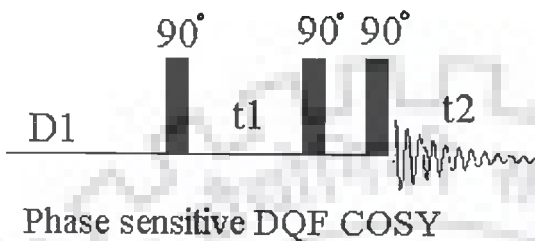
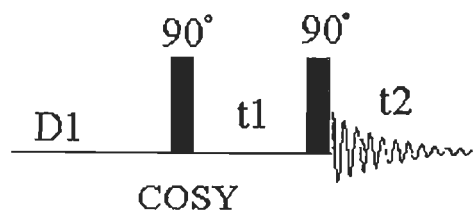


Figure 2.4: Pulse schemes of various 2D NMR techniques

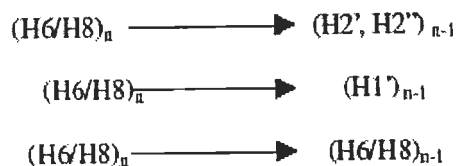
2.5 EXPERIMENTAL PARAMETERS

All proton NMR experiments were carried out at National FT-NMR Facility located at Tata Institute of Fundamental research (TIFR), Mumbai and were recorded on 500 MHz high resolution Bruker AMX 500 FT-NMR spectrometer equipped with aspect X32 computer and Varian Unity + 600 MHz FT-NMR spectrometer with SPARK station LX computer. Typical parameters for one-dimensional NMR experiments are pulse width = 10-12.5 μs (60° pulse); number of data points = 8-16 K; spectral width = 4000 Hz; number of scans = 64-128 and digital resolution = 0.25-0.5 Hz/point. Receiver gain was optimized in each instance to obtain the best signal to noise ratio. NMR parameters used for 600 MHz 1D NMR experiments are: pulse width = 8 μs (60° pulse); number of data points = 64 K; spectral width = 6499.8 Hz; number of scans = 32 and digital resolution = 0.1 Hz/point. Receiver gain was optimized in each instance to obtain the best signal to noise ratio. Homonuclear ^1H 2D phase-sensitive DQF-COSY and NOESY experiments on d-(CGATCG)₂ and its complex with daunomycin were carried out at 285 K in D₂O. However 2D NOESY experiments were recorded with variable mixing times (τ_m) 50, 75, 150, 250 ms at 500 MHz and τ_m 100, 150, 200, 250 ms at 600 MHz for daunomycin-d-(CGATCG)₂ complex. Typical parameters for 2D experiments at 500 MHz were: 1024-2048 data points along t_2 dimension; 512 free induction decays in t_1 dimension; pulse width \approx 9.5-12 μs (500 MHz) or 13.8 μs (600 MHz); spectral width \approx 4000 Hz (500 MHz) and 5400 Hz (600 MHz); no. of scans = 64-128 (500 MHz) and 32-48 (600 MHz); digital resolution 2.30 – 4.60 Hz/point and relaxation delay \approx 1.0 sec and ssb 2,2.

2.6 DETERMINATION OF THREE-DIMENSIONAL STRUCTURE

2.6.1 Resonance assignments in nucleic acids

Resonance assignment is the first endeavour in the structural determination of DNA. From the NMR point of view, the protons can be grouped into four categories; (i) exchangeable OH, NH and NH₂ protons of the bases and nonexchangeable base protons between 7-15 ppm (ii) nonexchangeable sugar protons between 2-6.5 ppm (iii) methyl protons of thymine between 0.5-2 ppm. In order to observe OH, NH and NH₂, protons, experiments have been carried out in water whereas the other protons were observed in D₂O solution. The strategy for resonance assignment consists of two steps. In the first stage, the J correlated spectra are used to identify network of coupled spins. In the second stage, the spin systems so identified are assigned to particular nucleotides along the sequence of the molecule by making use of the NOESY spectrum as described below. The sugar protons H1', H2', H2'', H3', H4', H5' and H5'' form a complex J correlated network (**Fig. 2.5**). The various cross peaks observed in the 2D J-correlated between these protons was used in identification of spin system within individual nucleotide units. The H1' proton shows a cross peak with H2', H2'' sugar protons. The H2' and H2'' protons are further coupled to H3' proton. We have used phase sensitive DQF-COSY spectra to identify the various J-coupled cross peaks. In the second phase sequential assignment is carried out using NOESY spectrum. Short internucleotide distances between adjacent nucleotide units are used as shown in **Figure 2.5**. In right handed DNA with sugars in C3'-endo/C2'-endo/O1'-endo pucker and glycosidic angle in anti domain, a convenient strategy for sequential assignment is



where, n stands for nth residue in 5'-3' oligonucleotide sequence.

In case of Z-DNA, where the repeating unit is a dinucleotide. The internucleotide pathway is Base (2n-1) H5' (2n-1) Base (2n) H1' (2n) H2' (2n) and H2'' (2n) Base (2n+1).

2.6.2 Pseudorotation

Because of the r^{-6} dependence of the pre-steady state NOE, the relative magnitude of the NOEs provide a sensitive probe which can be used to obtain a qualitative view of the solution structures of short oligonucleotides. The glycosidic and sugar pucker conformations can be assessed qualitatively on the basis of the relative magnitudes of the intranucleotide sugar-base NOEs. The flexible five-membered sugar ring plays a pivotal role in nucleic acid structure and dynamic behaviour. In B-DNA family sugar responds to its surroundings (e.g. base stacking pattern) by an appropriate adaptation of its geometry. X-ray studies have now shown that P values usually occur in two distinct ranges. In a conformational wheel (Fig. 1.7a of Chapter 1) one range of form occupies the "Northern" half of the circle (N-type, $P_N 0^\circ \pm 90^\circ$); the second range occupies the "Southern" hemisphere (S-type, $P_S 180 \pm 90^\circ$). To a good approximation (0.4-0.7°) the torsion angles can be reproduced by a two-parameter pseudorotation equation:

$$v_j = \phi_m \cos [P + 0.8\pi (j-2)]$$

for j equals 0-4 and ϕ_m is amplitude of pucker. In crystal structures nucleotides usually a single pure N- or S-type conformer is found, but not necessarily the one that

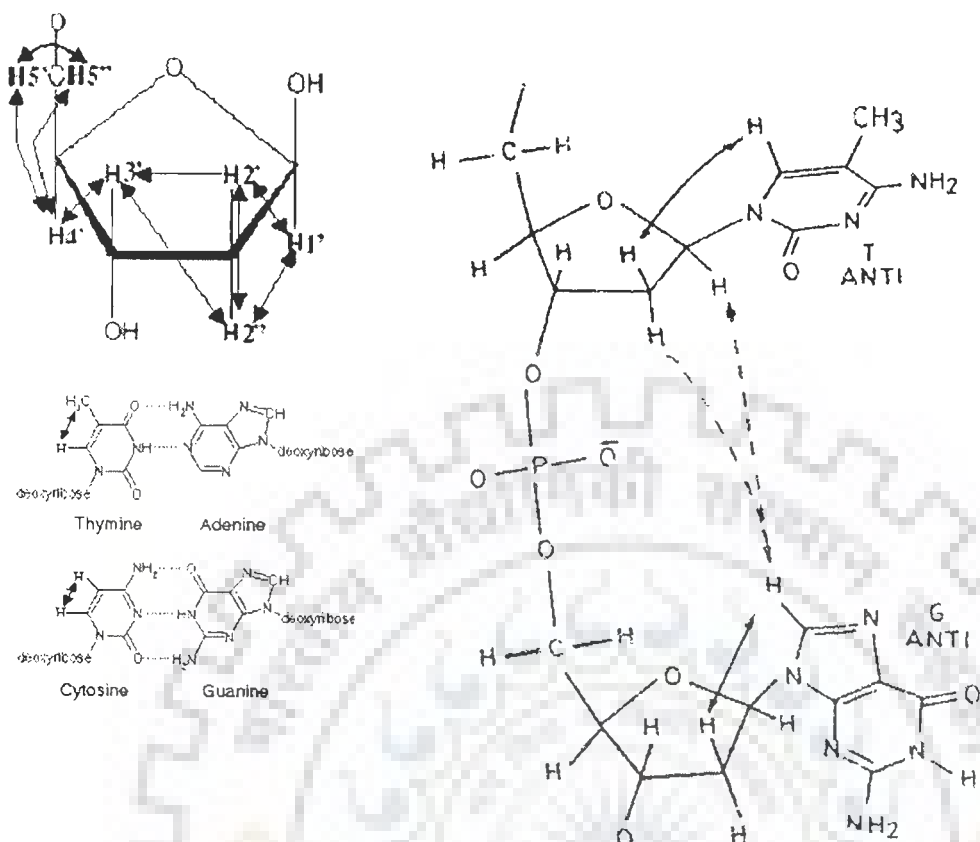


Figure 2.5: Schematic representation of through bond J connectivities (\longleftrightarrow) and short interproton distances between adjacent nucleotides units in right handed DNA bases

is predominant in aqueous solution. In some cases both N and S forms reside side by side in the same unit cell. Statistical analyses of X-ray data make it clear that details of sugar geometry of monomers are influenced by anisotropic crystal packing forces. The situation appears to be different in the helical oligomers, where stacking forces may play a more predominant role. NMR investigations in solution have demonstrated that N (C3'-endo) and S (C2'-endo) type conformations are in rapid equilibrium. If the interconversion rate between conformers is sufficiently rapid then observed couplings represent weighted average of couplings in individual conformers. Generally, in deoxyribose sugar, a trend to a larger proportions of C2'-endo pucker sugar is observed. A phase sensitive DQF-COSY spectrum allows J-coupling patterns to be delineated from the well-resolved crosspeaks. In general, the relation between 3J and φ takes the form of the semiempirical Karplus equation:

$${}^3J = A \cos^2(\varphi) + B \cos(\varphi) + C$$

The constants A, B and C have to be determined from 3J values measured for compounds for which the value of φ , in solution, is known. There are five 3J values in deoxyribose sugar, $H1'-H2'$, $H1'-H2''$, $H2'-H3'$, $H2''-H3'$ and $H3'-H4'$, which are related to the relevant H-C-C-H dihedral angle, φ , according to the relation:

$$J = 10.2 \cos^2\varphi - 0.8 \cos \varphi$$

The above dihedral angles are inter-dependent and their values can be calculated in terms of the two pseudorotation parameters, P and φ_m . φ_m is a constant for deoxyribose and thus various geometries can be expressed in terms of P. Fig 2.6 (Hosur et al, 1986) shows the plots of five coupling constants in a deoxyribose ring as a function of P, ($T_m = 38^\circ$). It is clear from the curves that the value of coupling constants ${}^3J(H1'-H2'')$ and ${}^3J(H2'-H3')$ vary within a narrow range of 6-10 Hz and are

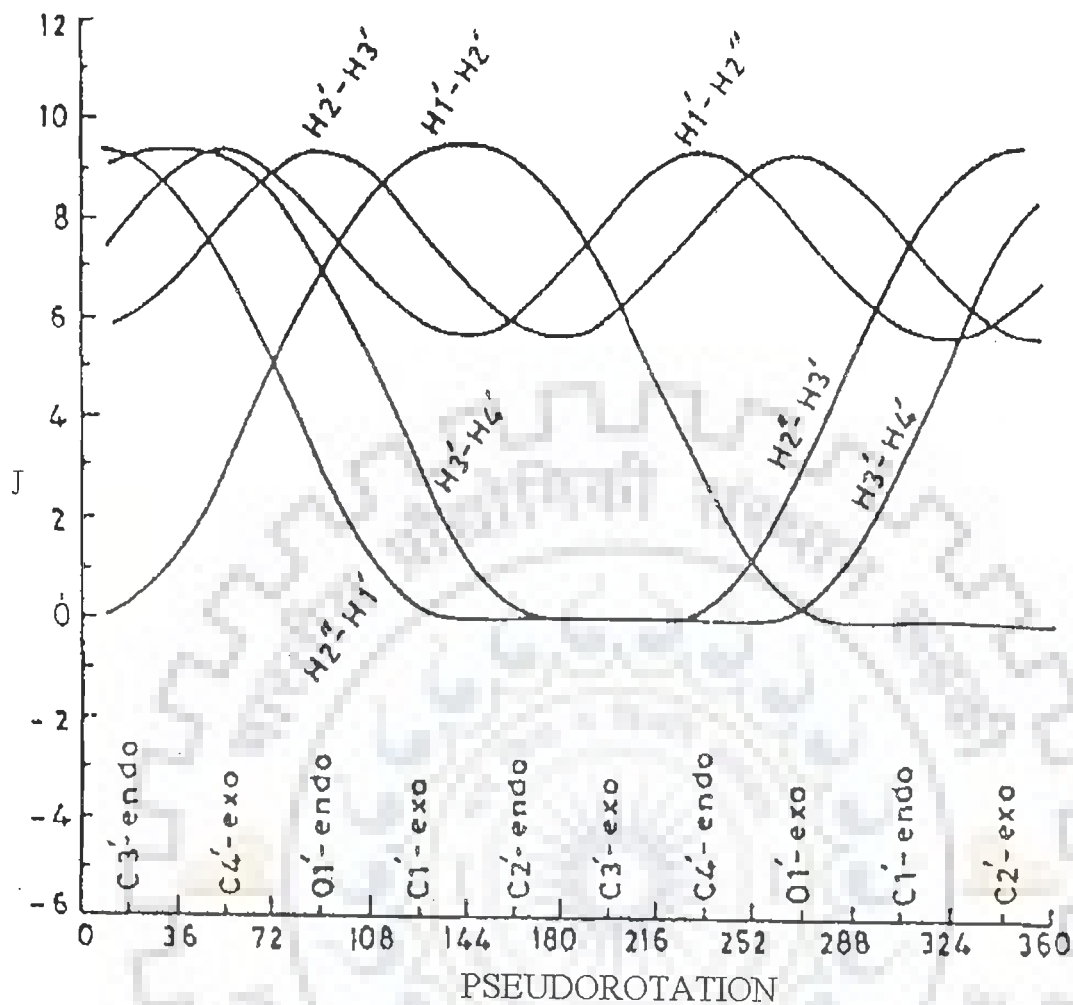


Figure 2.6: Variation of the vicinal coupling constants in the deoxyribose ring as a function of the ring geometry

comparatively insensitive to the sugar geometry. On the other hand, values of $^3J(\text{H2}''\text{-H3}')$, $^3J(\text{H3}'\text{-H4}')$ and $^3J(\text{H1}'\text{-H2}')$ coupling constants vary in the range 0-10 Hz and can be utilized with greater advantage in fixing the domains of sugar geometry. $^2J(\text{H2}'\text{-H2}'')$ is a geminal coupling which does not show significant conformational dependent variation. Rest five i.e. $^3J(\text{H1}'\text{-H2}')$, $^3J(\text{H1}'\text{-H2}'')$, $^3J(\text{H2}'\text{-H3}')$, $^3J(\text{H2}''\text{-H3}')$ and $^3J(\text{H3}'\text{-H4}')$ are vicinal coupling which show a strong dependence on the conformation of the deoxyribose ring (Hosur et al, 1986). The approach used for determination of sugar geometry is based on interpretation of intrasugar proton-proton distances.

2.6.3 Conformation about the glycosidic bond

A large body of crystallographic data for nucleotides and nucleosides clearly establishes that the torsional angle, χ_{CN} , defining the orientation of base ring falls into two relatively narrow ranges designated as syn and anti conformation (Sundaralignam, 1969).

$$\chi \begin{cases} \text{O4}'\text{-C1}'\text{-N9-C4 (Purines)} \\ \text{O4}'\text{-C1}'\text{-N1-C2 (Pyrimidines)} \end{cases}$$

The relative magnitudes of the intranucleotide and internucleotide (H8/H6)-H1' and (H8/H6)-(H2', H2'') cross peaks in NOESY spectra at different mixing times can be used to establish the domains of glycosidic dihedral angles of individual nucleotide unit (Hosur et al, 1985; Roche et al, 1994). Below the spin diffusion limit, the intensity patterns of the cross peak look similar at all mixing times although the absolute intensity may vary with the mixing time. The expected intensity patterns for the above mentioned cross peaks for different glycosidic dihedral angles are given below:

1. For the syn conformation, a strong NOE between base H8/H6 and H1' protons should be observed. At the same time, the NOEs from base to H2' and H2'' protons will be relatively weak and will have different intensities.
2. In the anti conformation, the NOE from base H8/H6 to H2' is stronger than the NOE from base H8/H6 to H2''. Also, for right handed structures the H2'' proton shows a stronger NOE to the base proton of the next nucleotide.
3. In the high anti conformation, the (H8/H6)-H2' and (H8/H6)-H2'' NOEs will have similar intensities for C2'-endo geometry.

The (H8/H6)-H1' distance depends only on χ while, other distances depend on both P and χ . Iso-distance contours have been calculated by Wuthrich (Wuthrich, 1986) in (P, χ) space for H8/H6-H2', H2'', H3', H4' and H5' distances.

2.7 ESTIMATION OF INTERPROTON DISTANCES

If one resonance A is irradiated, an increase (positive NOE) or decrease (negative NOE) of signal intensity of other resonances such as resonance C is observed when spin C is close in space to spin A. This phenomenon is called Nuclear Overhauser Effect or NOE. The NOE effect is the method for elucidation of 3D structural features and stereochemistry using NMR together with information from scalar spin-spin couplings. The most important quantity derived from NOE cross peaks is the cross-relaxation rate between protons i and j . The cross relaxation rate σ_{ij} between two proton spins i and j is related to the distance between protons i and j in the following way:

$$\sigma_{ij} = \langle d_{ij}^{-6} \rangle f(\tau_{ij}) \quad (1)$$

$\langle d_{ij}^{-6} \rangle$ denotes an ensemble average of molecular structures interconverting in thermal equilibrium where $f(\tau_{ij})$ is a function of correlation time τ_{ij} for the vector connecting

the two spins. This function accounts for the influence of motional averaging processes on the NOE. The cross relaxation rates can be measured from buildup rates of cross peaks in 2D NOE spectra at several mixing times. According to equation (1), the measured cross relaxation rates are a function of the ensemble average properties, which are dependent on the configurational space accessible to the molecular system at the temperature and time scale. If the interconversion between conformational equilibria in the oligonucleotide is fast on NMR time scale, NOEs from several equilibrium conformations will be observed simultaneously. This means the derived set of distance constraints does not necessarily represent the average structure, and there may be no single conformation that is consistent with the data set. Initially the intensity of the cross peak in equation (1) varies linearly with mixing time, and therefore this condition is referred to as “linear regime”, but on higher mixing times, this condition does not exist due to multispin relaxation. Interproton distances can be estimated by measuring the intensities of cross peaks in the “linear regime”. Two-spin approximation is used in NOE distance measurements in which only the rate of dipolar magnetization transfer between proximal spins i and j is monitored and all other spins are ignored. For two spin approximation, the intensity I_{ij} can be written as:

$$I_{ij} = \frac{\gamma^4 \hbar^2 \tau_c \tau_m}{10r_{ij}^{-6}} \quad \text{when } \omega \tau_c \gg 1$$

where γ is gyromagnetic ratio and \hbar , is Planck’s constant divided by 2π . In order to determine the accurate value of τ_m for estimation of interproton distances, NOE build up curves should be obtained as a function of τ_m for several cross peaks, since spin diffusion can be different for different protons. Correlation times, τ_c , can be obtained from T_2 and T_1 measurements, according to the equation:

$$\tau_c = 2\omega^{-1}(3T_2/T_1)^{-1/2}$$

which holds good for $\omega\tau_c \gg 1$

If protons i, j, k, l have similar τ_c values and if r_{ij} is a known distance, then the unknown distance r_{kl} can be calculated by comparing the intensities I_{ij} and I_{kl} in a single spectrum.

$$\frac{I_{ij}}{I_{kl}} = \frac{r_{kl}^6}{r_{ij}^6}$$

The choice of known distance is important in the light of the mobility associated with different atoms in the nucleic acid. Gronenborn et al (Gronenborn and Clore, 1985) have expressed the opinion of using different yardsticks for NOEs involving different group of protons. The $r(\text{CH5-CH6})$ and $r(\text{H2}'\text{-H2}'')$ have different effective correlation times and can be used as reference depending on the cross peak being compared. The thymidine (H6-CH_3) distance of 3.0 Å can be used as reference for all NOEs involving CH_3 protons, the sugar $\text{H2}'\text{-H2}''$ protons and for the rest, cytidine H5-H6 distance of 2.45 Å can be used. Reid et al (Reid et al, 1989) examined $\text{H2}'\text{-H2}''$ and H5-H6 cross relaxation at 15, 30, 60, 90 and 100 ms in dodecamer DNA duplexes. Results indicate that sugars and bases have the same correlation times, therefore all proton-proton distances in short DNA duplexes can be determined by scaling the initial NOE build up rate to the slope of cytosine H5-H6 cross peak, as $\text{H2}'\text{-H2}''$ NOE cross peak are close to diagonal and are usually unresolved.

The characteristics of NMR data can be summarized as below:

1. NOEs cannot be translated into the precise distances. In practice this means that NOEs give only a number of approximate upper limits (e.g., 3 Å, 4 Å and 5 Å for strong, medium and weak NOEs) Sometimes it is not possible to make

this division and only one single upper limit is used. For some proton pairs, corrections have to be applied to the upper limit value. This may arise due to stereospecific assignments (e.g., methyl group of thymine) or because of dynamic effects such as rotation of hydrogens in a methyl group and flipping of the aromatic rings.

2. Translating NOEs into reliable lower limit constraints is difficult, and it is preferable to take the sum of vander Waals radii as a lower limit to the distance. The absence of NOEs between two assigned protons may be translated into a minimum distance of proton pair.
3. NMR data contain contributions from different molecular conformations. Not all distance constraints need to be consistent with the single conformation.
4. NOE information is limited to short distance relative to the size of the drug-DNA complex. For some part of the molecule none or only a few NOEs are observed.

2.8 RESTRAINED MOLECULAR DYNAMICS AND SIMULATED ANNEALING

When restrained energy minimization methods are used, inevitable local energy minima are encountered which can lead to inaccurate structures. To circumvent this, restrained molecular dynamics (rMD) are usually employed. This involves including NMR restraints in one of the many molecular dynamics simulation programs.

Molecular dynamics solve Newton's equation of motion,

$$\mathbf{F}_i = m_i \mathbf{a}_i \quad (1)$$

Where F_i is the force, m_i is the mass and a_i is the acceleration of atom i . The force on atom i can be computed directly from the derivative of the potential energy V with

respect to the coordinates r_i . The energy can be expressed in an explicitly differentiable form:

$$dV/dr_i = m_i d^2 r_i / dt^2 \quad (2)$$

Therefore, with an adequate expression for the potential energy and the known masses, this differential equation can be solved for future positions in time t_i . In general, this can be solved only approximately, since V is usually a complex function of the coordinates of all (or many) of the atoms (i.e. $V = V(r_1, r_2, r_3, \dots, r_N)$). The temperature can be calculated from the atomic velocities

$$3N/2 k_B T = \sum_{i=1}^N 1/2 m_i v_i^2 \quad (3)$$

where, k_B is Boltzmann's constant, m_i and v_i are the mass and velocity of atom i , and N is the number of atoms (and $3N$ is the number of degrees of freedom). For a simulation at constant energy, the temperature fluctuates due to the interconversion of kinetic and potential energy. If the temperature is held constant then the atomic velocities can be adjusted accordingly. If the pressure is held constant, the volume is allowed to fluctuate by rescaling the interatomic distances.

The total potential energy V_{total} is usually defined as the sum of a number of terms:

$$V_{total} = V_{bond} + V_{angle} + V_{dihedr} + V_{vdw} + V_{coulomb} + V_{NMR} \quad (4)$$

where, V_{bond} , V_{angle} and V_{dihedr} keep bond lengths, angles, and dihedral angles at their equilibrium values. The first five terms are empirical energy terms describing the physical interactions between the atoms, whereas the last term is a means of including the NMR information, but does not correspond to any real physical force. They can be summarized as follows:

$$V_{\text{bond}} = \sum_{\text{bond}} 1/2 K_b (b - b_0)^2 \quad (5)$$

$$V_{\text{angle}} = \sum_{\text{angles}} 1/2 K_\theta (\theta - \theta_0)^2 \quad (6)$$

$$V_{\text{dihedr}} = \sum_{\text{dihedr}} K_\phi (1 + \cos(n\phi - \delta)) \quad (7)$$

These are pseudo-harmonic potentials that constrain bond lengths (b), bond angles (θ), and the rotamer angles (ϕ , δ) for staggered and eclipsed conformations, and K is a constant. The van der Waals and electrostatic interactions are described by V_{vdw} and V_{coulomb}

$$V_{\text{vdw}} = \sum_{\text{pairs } (ij)} [C_{12}/r_{ij}^{12} - C_6/r_{ij}^6] \quad (8)$$

$$V_{\text{coulomb}} = \sum_{\text{pairs } (ij)} q_i q_j / 4\pi \epsilon_0 \epsilon_r r_{ij} \quad (9)$$

where equation (8) is the Lennard-Jones potential, containing repulsive and attractive terms (C is a constant), and equation (9) describes the coulombic interactions between two charged particles (i , j) with partial charges q that are a distance r_{ij} apart in a dielectric medium described by $\epsilon_0 \epsilon_r$ term. The potential V_{NMR} contains the NMR restraints, and has the effect of pulling the protons that show an NOE interaction closer to the measured distance r_{ij} . Similarly, These potentials are also pseudo-harmonic functions of similar forms to equations (5)-(7). Distance constraints which can be reasonably accurately determined may therefore be defined as follows:

$$V_{\text{NOE}} = \begin{cases} K_1 (r_{ij} - r_{ij}^0)^2 & \text{if } r_{ij} > r_{ij}^0 \\ K_2 (r_{ij} - r_{ij}^0)^2 & \text{if } r_{ij} < r_{ij}^0 \end{cases} \quad (10)$$

where, r_{ij} and r_{ij}^0 are the calculated and experimental interproton distances, respectively, and K_1 and K_2 are force constants given by:

$$K_1 = k_B TS / [2(\Delta_{ij}^+)^2] \quad \text{and} \quad K_2 = k_B TS / [2(\Delta_{ij}^-)^2] \quad (11)$$

Where k_B is Boltzmann's constant, T , absolute temperature of the simulation, S a scale factor, and Δ_{ij}^+ and Δ_{ij}^- are the positive and negative error estimates, respectively, of r_{ij} . If, however, only ranges of distances can be specified, then the distance restraints are incorporated into a pseudo-square-well potential of the form:

$$V_{\text{NOE}} = \begin{cases} K_{\text{NOE}} (r_{ij} - r_{ij}^u)^2 & \text{if } r_{ij} > r_{ij}^u \\ 0 & \text{if } r_{ij} \leq r_{ij}^u \leq r_{ij}^l \\ K_{\text{NOE}} (r_{ij} - r_{ij}^l)^2 & \text{if } r_{ij} < r_{ij}^l \end{cases} \quad (12)$$

where r_{ij}^u and r_{ij}^l are the upper and lower limits, respectively, of the target distances obtained from the experimental, and K_{NOE} is the force constant, which is typically chosen to be the order of $1000 \text{ kJ mol}^{-1} \text{ nm}^{-1}$.

To ensure that the experimental restraints are the dominating factor in determining the conformation of the molecule, it is very important that the force constants for the restraints are set sufficiently high that the experimental data are satisfied within the precision of the measurements. At the same time, the contribution from the empirical energy function should be such that any individual RMD structure, the deviations from ideal geometry are small, and the non-bonded interactions are good (i.e. the Lennard-Jones potential is negative). Thus convergence on the structure is guided by the requirement to minimize NOE or other restraint violations. The number of distance restraint violations N_{viol} is counted when, for example, $r_{ij} \geq r_{ij}^0 + 1$, which would be for 1 Å fluctuations. Another parameter which can be minimized in addition to N_{viol} is the sum of the distances in excess of the constraints $\sum \Delta r_{\text{viol}}$, which is defined as:

$$\sum \Delta r_{\text{viol}} = N_{\text{viol}} \sum_{k=1} (r_{ij})_k - [(r_{ij})_k + 1] \quad (13)$$

where the sum runs over all those interproton (or pseudoatom) distances for which N_{viol} is defined. Although an arbitrary structure may be used for restrained molecular dynamics calculation, in practice a starting structure obtained from distance geometry and energy minimization is often used. The rMD approach requires a relatively large amount of computation time compared to distance geometry methods. This problem can be overcome by using a simplified potential energy function, where all non-bonded contact interactions are described by a single van der waals repulsion term. Also by using a cut off distance, in which non-bonded interactions for pairs of atoms that are separated by a distance greater than some reasonable value (e.g. 5-10 Å) are excluded, the number of non-bonded interactions is decreased considerably. Simulated annealing involves raising temperature of the system followed by slow cooling in order to overcome local minima and locate the global minimum region of the target function. It is computationally more efficient than RMD and yield structures of similar quality. The potentials are very similar to RMD and again Newton's laws of motion are solved as a function of time. However, in implementations found in commercial programs, the non-bonded interaction potential is modified so that there is a simple van der waals repulsion term with a variable force constant K_{rep} :

$$V_{\text{repel}} = \begin{cases} 0 & \text{if } r \geq s \cdot r_{\text{min}} \\ K_{\text{rep}} (s^2 r_{\text{min}}^2 - r^2)^2 & \text{if } r < s \cdot r_{\text{min}} \end{cases} \quad (14)$$

The values of r_{min} are given by the sum of the standard values of the van der Waals radii between two atoms as represented by the Lennard-Jones potential.

2.9 DEFINING DNA STRUCTURE

The structure of DNA can be described by a number of parameters (Fig. 2.7) that define the helix (Dickerson et al, 1989). Polynucleotides in helical arrangement display order which can be expressed in terms of Helical Parameters. The output from helix analysis program CURVES of Richard Lavery (Lavery and Sklenar, 1988), includes “global helical parameters” defined relative to a global helix axis and “local helical parameters” defined relative to local helix axis at each base pair. The helicoidal parameters are classified into three categories:

1. global base pair-axis parameters
2. intra-base pair or global base-base parameters
3. inter-base pair or base pair-step parameters

The global as well as the local inter base pair parameters are related to particular base pair steps. These parameters are vector quantities, which have a defined location in 3-dimensional space and with respect to the nucleic acid sequence. In contrast, the average inter base pair parameters are scalar values that are not related to any part of the structure. They characterize properties of the whole structure. Among global base pair-axis parameters, x- and y- displacement refers to the shift of bases in positive or negative x and y direction with respect to each other.

Intra-base pair or global base-base parameters comprises of the translational components as stagger, stretch and shear, and the rotational components are propeller twist, buckle, opening. Propeller twist refers to the angle between the planes of two paired bases. A base pair is rarely a perfect flat plane with each aromatic base in the same plane. Rather, each base has a slightly different roll angle with respect to

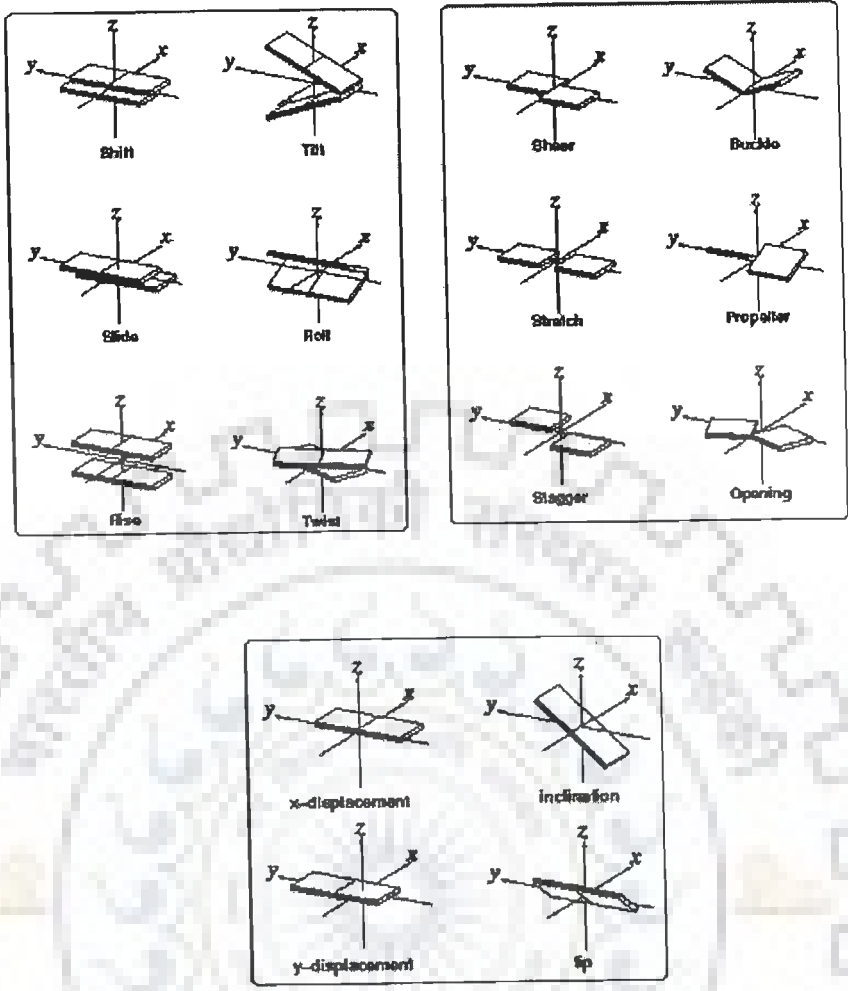


Figure 2.7: Pictorial representation of parameters that relate base pairs to its helical frame

the other base. This makes two bases look like an aeroplane propeller. Twist or rotation per residue refers to the angle between two adjacent base pairs. Each step from one plate to the next can be described as a combination of a translational and a rotational movement. The translational and the rotational displacements are three-dimensional vectors, which can be split into three orthogonal components. In inter-base pair or base pair-step parameters the three translational components are rise, shift and slide. Twist, roll and tilt are the three rotational components. Rise is the distance between adjacent planar bases in the DNA double helix i.e. it is a translation in the direction of the helical axis (z-axis), and shift is orthogonal to the helical axis and directs to the major groove side. Twist is a rotation about the helical axis (z-axis). Base pair roll refers to the angle of deflection of the base pair with respect to the helix axis along a line drawn between two adjacent base pairs relative to a line drawn perpendicular to the helix axis. A positive roll indicates that there is a cleft between two stacked base pairs, which opens towards the minor groove. A negative roll is related to an opening towards the major groove. Base pair tilt refers to the angle of the planar bases with respect to the helical axis. In the B-form DNA the bases are tilted by only -6° . In the A-form DNA the base pairs are significantly tilted at an angle of 20° . The sense of the base-pair tilt is associated with sugar puckering. In double helical polynucleotides, the normals to the base pair are not exactly parallel to the helix axis but inclined to it by up to 20° . The sense of tilt is positive in A-type and negative in B-type of helices, and hence is correlated with sugar puckering. Base tilt angle is correlated with rise per residue. If the bases in base pairs were coplanar and the base pairs exactly perpendicular to the helix axis, the axial rise per nucleotide should correspond to the van der waal's distance, 3.4 \AA .

STRUCTURE OF d-(CGATCG)₂ BY RESTRAINED MOLECULAR DYNAMICS

In this chapter, intensities at mixing time (τ_m) of 75 and 150 ms were translated to get intra and interproton distances in the complex from the NMR spectra for which the assignment was done previously. ^(Barthwal et al, 2003) The C1H5-C1H6 cross peak of cytosine was the reference distance = 2.46 Å; a range of ± 0.2 Å was provided to distance to account for any errors in integration. Figure 3.1 shows the portion of NOESY spectra of d-(CGATCG)₂ hexamer at $\tau_m = 200$ ms. Table 3.1 a-b lists all the interproton distances of d-(CGATCG)₂ within sugar moiety and those with base to ribose sugar. Table 3.2 lists the sequential peaks of the hexamer. Using these interproton distances and torsional angles as restraints restrained molecular dynamics of hexamer was carried out.

3.1 STRATEGY FOLLOWED

The model of d-CGATCG duplex was made using BIOPOLYMER module. Pseudoatom corrections were used for methyl and other equivalent protons. The NOEs were categorized as strong, medium, and weak within the corresponding distances in the range 1.8-2.4 Å, 2.5-2.9 Å, and 3.0-4.0 Å set for the respective protons. Force constants of 10, 5, and 2 Kcal mole⁻¹ Å⁻² were fixed for strong, medium, and weak peaks, respectively. The coupling constants J(H1'-H2') and J(H1'-H2'') were transformed to torsional angles using Karplus relationship. These were introduced as dihedral restraints allowing a range of $\pm 10^\circ$ on the calculated

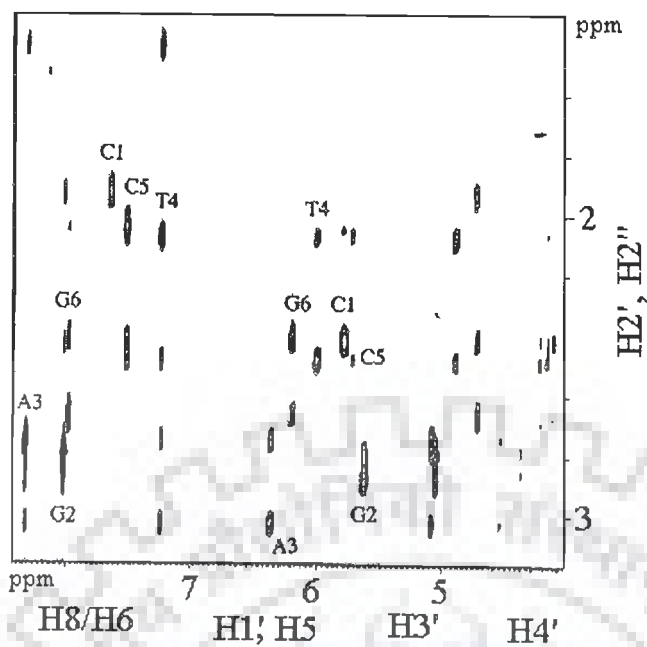


Figure 3.1: Expansions of selected portions of 500 MHz NOESY spectra of d-CGATCG showing specific through space correlations (a) H2' with H2'' protons at $\tau_m = 250$ ms (b) base H8/ H6, H1' H3' H4' with H2', H2'' protons at $\tau_m = 200$ ms (courtesy: Nandana Srivastava)

values with force constant of $20 \text{ Kcal mole}^{-1} \text{ rad}^{-2}$. The total number of dihedral and distance restraints used in the structure calculations using restrained molecular dynamics was 10 and 112, respectively. An initial model of double helical B-DNA structure was generated using INSIGHT II, version 97.0 (Molecular Simulations Inc., MSI, San Deigo.) on Silicon Graphics O2 workstation R5000. The force constants for hydrogen bonds were fixed as $40 \text{ Kcal mole}^{-1} \text{ \AA}^{-2}$ throughout the simulations. The energy of the molecule was minimized using 1000 steps each of Steepest Descent and Conjugate Gradient to remove any internal strain due to short contacts in starting structure using CFF91 force field (Maple et al, 1988; Maple et al, 1990) in DISCOVER software version 97.0 (MSI). Dielectric constant was fixed as $1.0 * r$ ($r =$ distance) for calculation of electrostatic interactions. Conformational search was performed by the following simulated annealing restrained molecular dynamics protocol. The molecule was heated to a temperature of 500 K in steps of 100 K and equilibrated at this temperature. Molecular dynamics was carried out for 24 ps (1000 iterations with time step of 1 fs) at 500 K during which 25 structures were saved at regular intervals of 1 fs. Each of them was then slowly cooled at 300 K in steps of 50 K. The force constants for NOEs for strong, medium, and weak peaks were held constant as 25, 15, and $10 \text{ Kcal mole}^{-1} \text{ \AA}^{-2}$, respectively while that for experimental dihedral restraints was fixed at $50 \text{ Kcal mole}^{-1} \text{ rad}^{-2}$. At the end of simulated annealing all the structures were minimized by 1000 steps of Steepest Descent until a predefined convergence limit of root mean square derivative of $< 0.001 \text{ Kcal mole}^{-1} \text{ \AA}^{-1}$ was reached. Each of the 25 structures thus obtained were examined in detail. That equilibrated for 19 ps at 500 K and cooled is referred to as rMD-B19SA structure and is described later in detail.

Table 3.1 a: Interproton distances (Å) obtained from intra nucleotide NOE connectivities (d_i) within sugar protons observed in NOESY spectra of d-CGATCG at 295 K.

Protons	C1	G2	A3	T4	C5	G6
H1'-H2'	2.8	2.8	2.8	2.8	2.9	2.9
H1'-H2''	2.2	2.2	2.2	2.2	2.2	2.2
H1'-H3'	-	3.6	3.5	-	-	-
H1'-H4'	-	3.1	2.9	2.8	3.2	3.3
H1'-H5'	-	-	-	3.8	-	-
H1'-H5''	-	-	-	3.4	-	-
H2'-H3'	2.3	2.3	2.3	2.3	2.3	2.3
H2''-H3'	2.6	2.6	2.6	2.6	-	2.6
H2'-H4'	-	3.6	3.5	3.5	3.6	-
H2''-H4'	-	-	3.5	3.4	3.4	-
H2'-H2''	1.8	1.8	1.8	1.8	1.8	1.8
H3'-H4'	2.6	2.6	2.6	2.7	2.6	2.6
H3'-H5'	3.3	3.0	2.6	-	-	2.8
H3'-H5''	-	3.2	2.7	-	-	-
H4'-H5'	2.3	2.3	2.3	2.3	2.3	2.3
H4'-H5''	2.5	2.4	2.4	2.4	2.4	2.4
H5'-H5''	1.8	1.8	1.8	1.8	1.8	1.8

Table 3.1 b: Interproton distances (Å) obtained from intra nucleotide NOE connectivities (d_i) within base to sugar protons observed in NOESY spectra of d-CGATCG at 295 K.

BASES	C1	G2	A3	T4	C5	G6
H8/H6-H1'	3.3	3.3	2.7	2.8	-	2.8
H8/H6-H2'	2.6	2.5	2.5	2.5	2.5	2.4
H8/H6-H2''	2.4	2.2	2.2	2.2	2.2	2.4
H8/H6-H3'	-	2.8	2.5	-	-	2.5

Table 3.2: Some of the inter proton distances (Å) from inter residue sequential connectivities observed in NOESY spectra of d-CGATCG at 295 K.

C1H2''-G2H8	2.5
G2H1'-A3H5''	3.2
G2H2''-A3H8	2.2
G2H2'-A3H8	3.6
A3H1'-T4H6	3.4
A3H2'-T4H6	3.2
A3H2''-T4H6	2.5
T4H2''-C5H6	2.5
T4H2''-C5H5	2.8
T4H2'-C5H5	3.3
C5H2'-G6H8	3.5
C5H2''-G6H8	2.5

3.2 RESULTS AND DISCUSSION

3.2.1 Restrained Molecular Dynamics Studies

Conformational space was searched via restrained molecular dynamics and restrained energy minimization for the conformation best defined by the experimental restraints. Simulations were carried out by starting with two different structures: (i) B-DNA using INSIGHT II software and (ii) the structure obtained by Lam and Au-Yeung available from the protein data bank (Identification no. 1UQD.pdb). Although the simulated annealing was carried out up to a temperature of 500 K, it is found that convergence to a final structure could be readily achieved even at 300 K. Several structures obtained after equilibration at different time intervals during the dynamics run at 500 K and 300 K as well as by using two different potential functions were examined. It was observed that they differ only marginally from each other in their overall feature irrespective of the rMD protocol followed (with and without simulated annealing), starting structure and the potential function used. Further no significant drift in either potential energy or restraint deviations was observed during the final equilibration. It can therefore be concluded that the system reached a minimum energy conformation (Mujeeb et al, 1993; Schmitz et al, 1992). A structure obtained without introducing NMR constraints and by following same steps of rMD protocols, was found to be quite different. This confirms that the structure is indeed defined by experimental restraints and not the refinement procedure or variables used. The root mean square deviation between any of the rMD structures and either of the starting structures is quite large but among various final structures was very low. This is generally acknowledged as an indication that convergence has been achieved.

Table 3.3 indicates an assessment of refined structures in terms of energetics

including restraint violations energies and root mean square derivative of energy with respect to atomic coordinates. The total potential energy of the rMD-B18 and rMD-19SA structures is $\sim 360 \text{ Kcal mole}^{-1}$ which is $\sim 328 \text{ Kcal mole}^{-1}$ lower than the initial B-DNA structure ($678 \text{ Kcal mole}^{-1}$). The forcing potential, which indicates contribution to potential energy due to violations of both experimental distance and torsional angle data, exhibits much lower values for all the four rMD structures ($154\text{-}162 \text{ Kcal mole}^{-1}$) in comparison to that in their corresponding starting structures ($422\text{-}526 \text{ Kcal mole}^{-1}$). The energy gradient with respect to atomic coordinates is lesser than $0.1 \text{ Kcal mole}^{-1} \text{ \AA}^{-1}$ (Table 3.3).

3.2.2 Conformational features of rMD structures

The stereoview of all rMD structures is shown in Fig. 3.2a-d. The rMD-B18 structure superimposed over the standard-BDNA structure is shown in Fig. 3.3a indicating the differences between the two structures. It may be noted that the one obtained by Lam and Au-Yeung, (Fig. 3.3b), is quite different from the standard B-DNA; it is observed that aromatic base pairs are not exactly planar in this structure. The stereoview of two rMD structures, rMD-B18 and rMD-B19SA, are shown superimposed in Fig. 3.4a; it may be noted that the two structures are quite similar. To gain more insight into structural details, all helical parameters, backbone torsional angles and sugar conformations of the resulting rMD structures were thoroughly analyzed with program CURVES, version 5.1 (Lavery and Sklenar, 1988; Lavery and Sklenar, 1989). The structural characteristics of various rMD structures are discussed further.

Table 3.3: Energy terms (Kcal mole⁻¹) and root mean square gradient of energy with respect to atomic coordinates (Kcal mole⁻¹ Å⁻¹) for starting models and structures obtained by restrained molecular dynamics (rMD)

Structure	Total	Bond	Angle	Dihedral	vdw	Repulsion	Dispersive	Electrostatic	Restraint*	RMS Derivative
B-DNA	678	96	456	103	345	1614	-269	-321	526	23.7
rMD-B18	358	93	450	111	6	966	-960	-305	162	0.19
rMD-B19SA	362	93	454	109	8	971	-963	-304	155	0.21
Lam & AuYeung	504	107	565	113	35	1018	-983	-318	422	18.20
rMD-Lam17	324	82	459	113	10	978	-968	-342	154	0.07
rMD-Lam16SA	311	81	460	114	18	996	-977	-364	156	0.08

*This contribution has been subtracted from the total energy

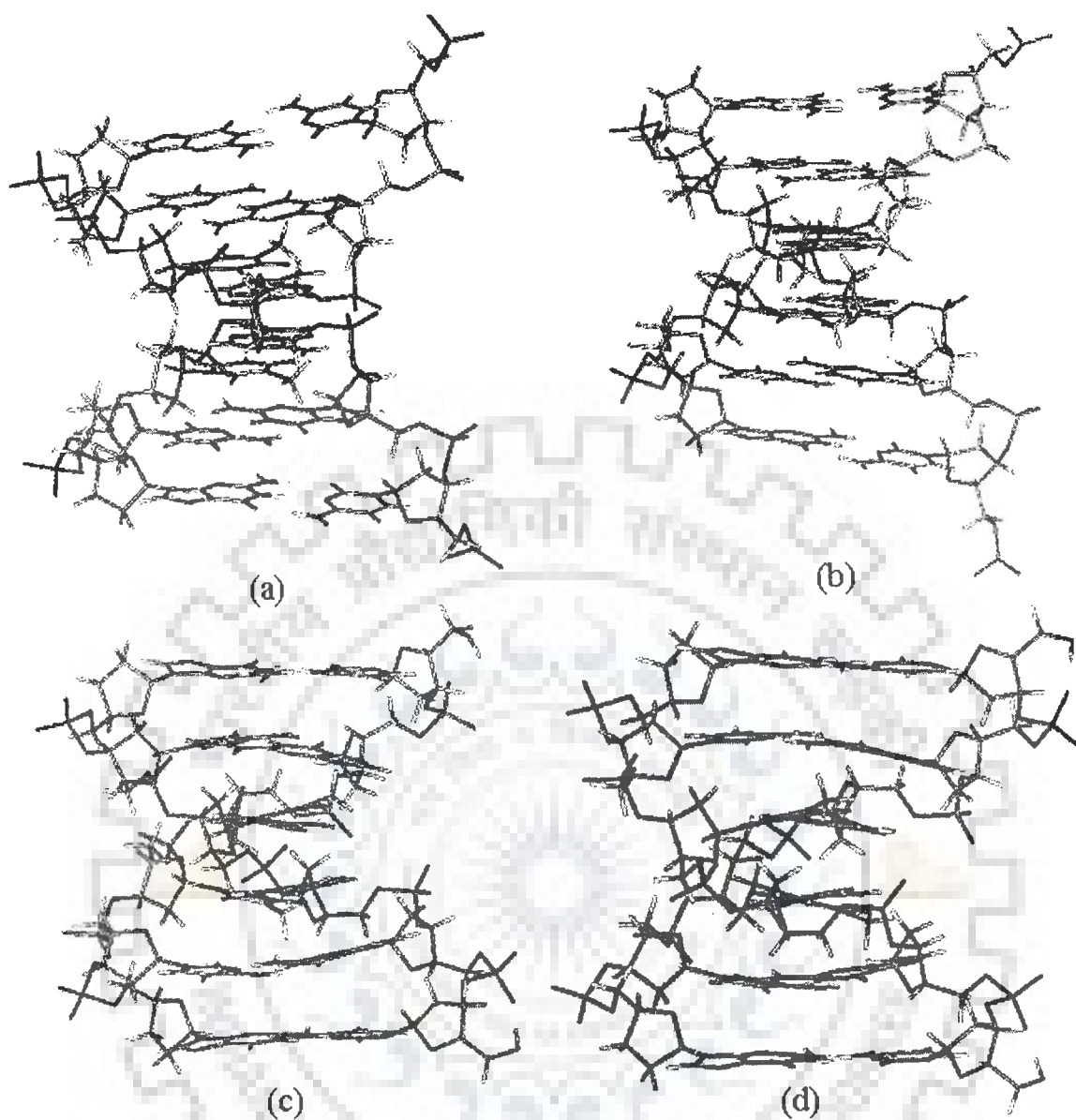


Figure 3.2: The stereoview of all rMD structures is shown (a) rMD-B18 (b) rMD-B19(SA) (c) rMD-Lam17 (d) rMD-Lam16SA

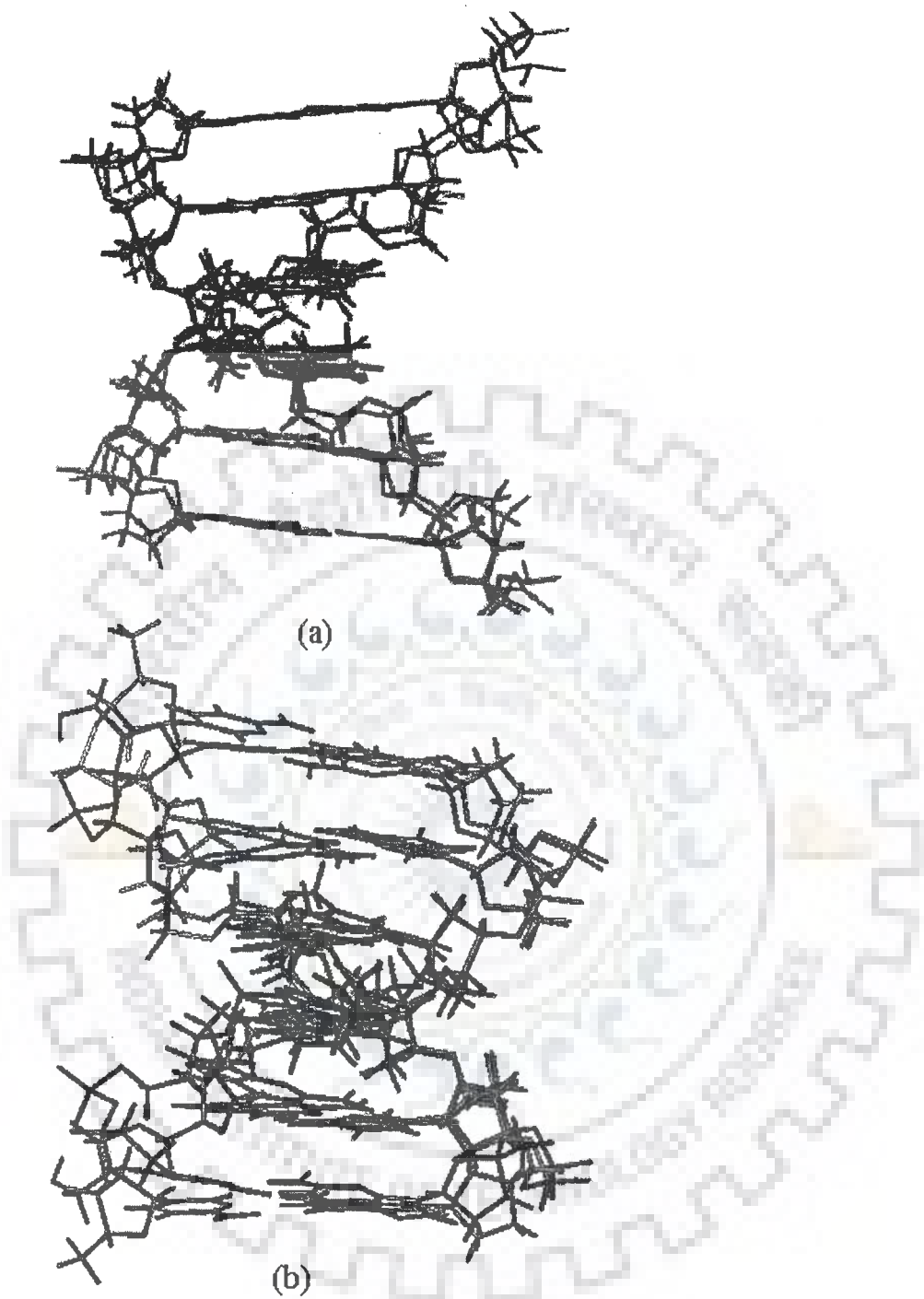


Figure 3.3: The difference between the final and initial structures (a) rMD-B18 structure superimposed with standard B-DNA (b) rMD-Lam17 structure superimposed with standard B-DNA

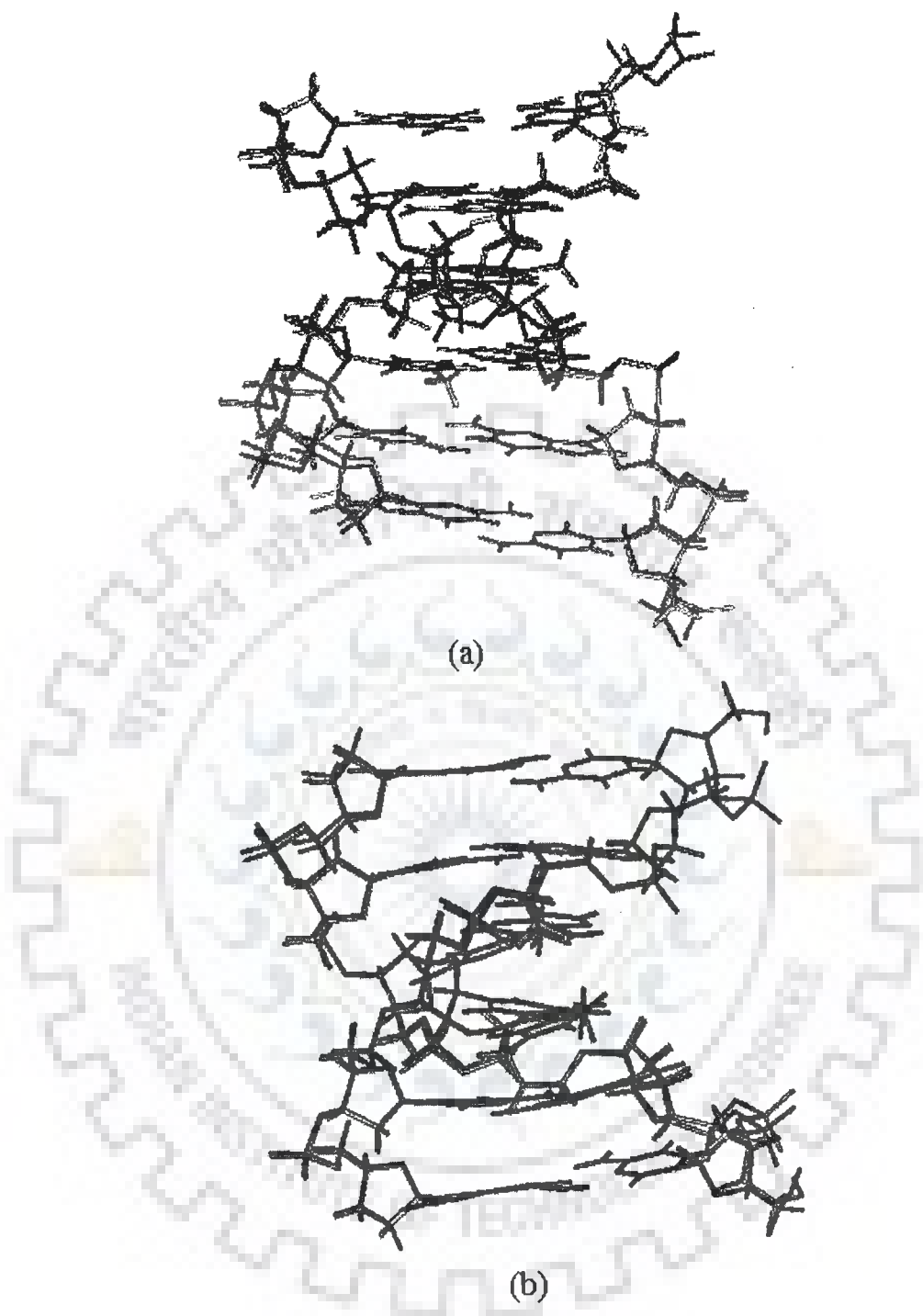


Figure 3.4: The similarity between the final structures obtained by different protocols
(a) rMD-B18 structure superimposed with rMD-B19SA (b) rMD-Lam17
structure superimposed with rMD-Lam16SA

3.2.2.1 Helicoidal Parameters

The output from CURVES includes “global helical parameters” defined relative to a global helix axis and “local helical parameters” defined relative to local helix axis at each base pair. Unless specified otherwise, we refer to the global helical parameters as calculated by CURVES. Plot of various helix axis parameters of d-CGATCG in rMD-B18 and rMD-B19SA structures as a function of residue position in the duplex is shown in Fig. 3.5. The structural parameters for two classical structures of A-DNA and B-DNA are also shown in Fig. 3.5. The helicoidal parameters are classified into three categories: global base pair-axis parameters, intra-base pair or global base-base parameters and the inter-base pair or base pair-step parameters (Bhattacharya and Bansal, 1992; Dickerson et al, 1992). It is evident from the figure that there are base sequence dependent variations in helicoidal parameters and the results on rMD structures are closer to that of B-DNA as compared to that of A-DNA.

Among the base pair-axis parameters, the x-displacements (dx) are ~ -1.1 Å for all the residues, which is close to a value of -0.7 Å seen in canonical B-DNA structures. The y-axis displacement (dy) is ~ 0.2 Å. Lam and Au-Yeung observed displacements of -0.2 to -0.6 Å and -0.3 to $+0.4$ Å along x and y-axis, respectively in the structure of d-CGATCG obtained by them. The base pair inclination is $\sim -6^\circ$ for regular B-DNA and $+19^\circ$ for regular A-DNA; the rMD structures display inclination values close to that of B-DNA structures, that is, -2° to -6° . The tip angle fluctuates within $\pm 6^\circ$ similar to canonical A-DNA and B-DNA forms. Fig. 3.6 shows a block representation of all base pairs in d-CGATCG in rMD-B18 structure obtained by using 3DNA software module (Olson and Lu, 2001). Among the intra base parameters, the shear (S_x) and stretch (S_y) values do not vary very much from their ideal values. The shear lies within the range ± 0.5 Å for different bases in all the rMD structures while the stretch varies in the range 0 to -0.2 Å.

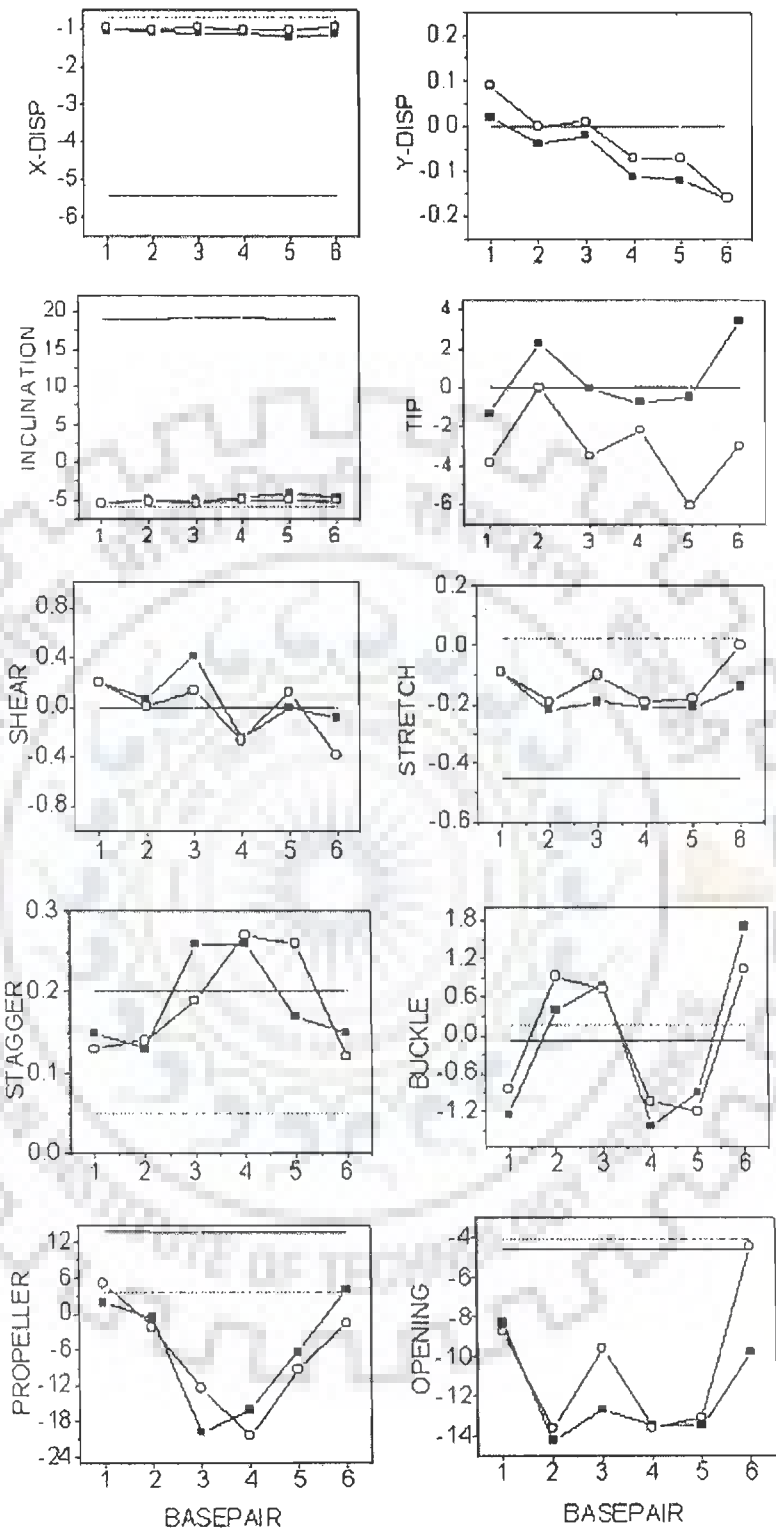
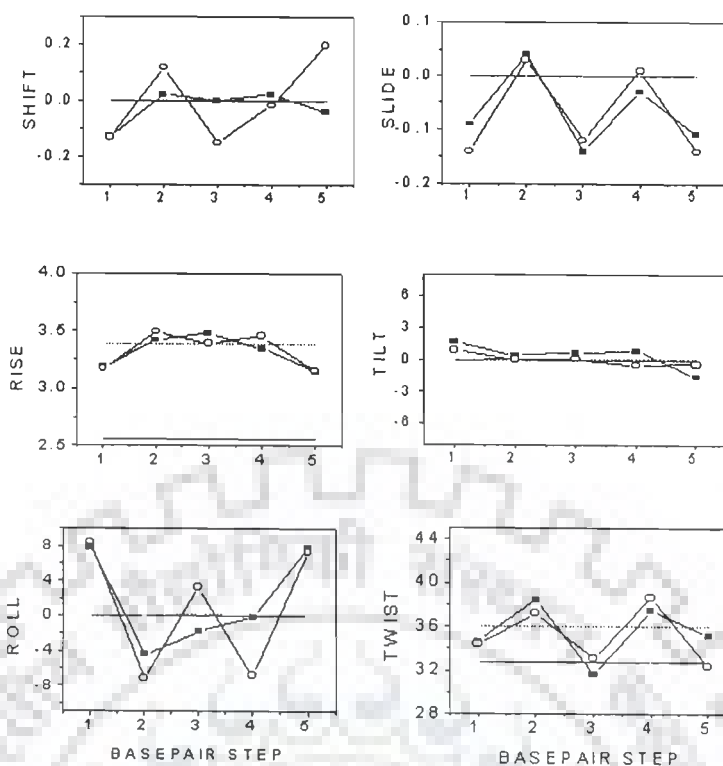


Figure 3.5(a)



(b)

Figure 3.5: (a) and (b) Helical parameters for d-CGATCG calculated for canonical A-DNA (—), B-DNA (---) and structure obtained by restrained molecular dynamics simulations : rMD-B18 (■) and rMD-B19SA (○) structures

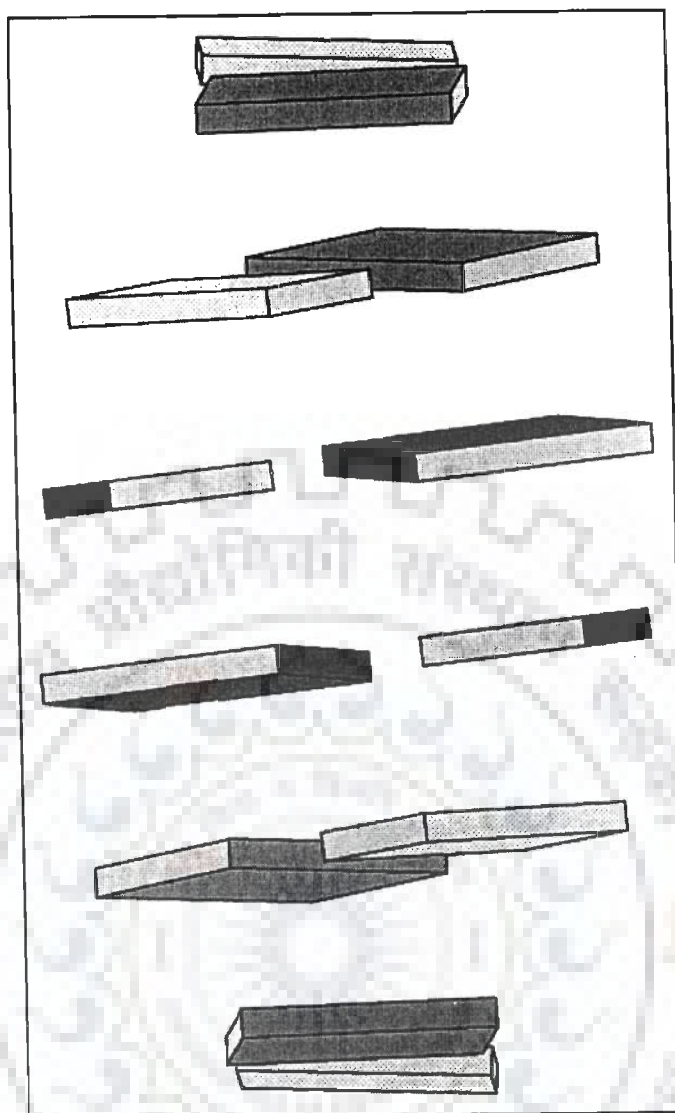


Figure 3.6: Block representation of base pairs in rMD-B18 structure of d-CGATCG obtained by 3DNA software

The stagger (S_z) values lie within ± 0.4 Å. It has large positive value for the two middle base pairs. The structure obtained by Lam and Au-Yeung (Lam and Au-Yeung, 1997) shows the same behavior. Buckle does not show much local variation in rMD-B18 and rMD-B19SA structures. The variations in the propeller twist are significantly large. For the two base pairs in the middle, that is, A3T4 and T4A3, large negative value in the range 12° - 20° are observed for rMD-B18 (Fig. 3.5) and rMD-B19SA structures. The two base pairs on either end show a much smaller propeller twist. The same behavior is seen in rMD-Lam17 and rMD-Lam16SA structures, although in these structures the magnitude of propeller twist is comparatively larger. Large negative values of propeller twist in A3T4 base pair have been reported in literature (Dornberger et al; 1998; Mujeeb et al, 1993; U. Schmitz et al, 1992) and may possibly occur to avoid steric clashes between the $-\text{CH}_3$ group of thymine and 5' neighbouring sugar in AX/XT base pair step (Hunter, 1993). The positive value of propeller twist for terminal base pairs may be attributed to fraying effects at both ends of oligonucleotides. Base pair opening lies in the range -8° to -14° for all base pairs; it being larger in magnitude for internal base pairs than the terminal base pairs in all rMD structures. In regular A-DNA and B-DNA geometries, global values of the inter base pair parameters - shift (D_x), slide (D_y), roll (ρ) and tilt (τ) are essentially zero. For rMD structures, the observed shift and slide values are small and do not show any significant variation with the base pair step. The rise per residue (D_z) lies within the range 3.0-3.5 Å, it is largest (Fig.3.5) in A3pT4 step (3.4-3.5 Å) and smaller at either ends of the helix (3.0-3.1 Å). The variation of tilt with base sequence is small in all cases. The roll angle lies within the range 7° - 9° for terminal base pairs steps. Positive roll opens the angle between base pair towards the minor groove; as a result, a wider minor groove and bending towards major groove causing a curvature in helix axis, occurs. The large positive roll value of

C1pG2 and C5pG6 steps also indicates reduced base stacking and hence emphasizes the flexibility at pyrimidine 3'-5'purine step (Dornberger et al, 1998). High flexibility and low stacking interaction at TpG step has been independently demonstrated by gel electrophoresis and other methods (Beutal and Gold, 1992; Donlan and Lu, 1992; Lyubchenko et al, 1993). The negative values of roll angle in non terminal 2 or 3 base pair steps indicates the widening of major groove and narrowing of minor groove at these steps, which is compensated by the decrease in propeller twist so as to prevent destacking of bases (Radha et al, 1995). The twist angle for all base pairs in rMD-B18 and rMD-B19SA structures lies in the range 32°-38° and is close to corresponding angle in B-DNA. The twist for rMD-Lam17 and rMD-Lam16SA structures, on the other hand, lie in the range 31°-45°. However the trend of variations of twist angle with base sequence is same in all the rMD structures. The angle is maximum at G2pA3 and T4pC5 step; it being 37°-38° in rMD-B18 and rMD-B19SA structures and 40°-45° in rMD-Lam17 and rMD-Lam16SA structures. It is minimum at A3pT4 step; being 31°-32° in all rMD structures). This effect is also reflected in sequential base H6/H8 to deoxyribose H2' inter proton distance observed in the NOESY spectra, where we observe the distance A3H2'-T4H6 = 3.3Å which is considerably smaller than that expected (Dornberger et al, 1998). The CURVES software reports both global and local helical parameters and therefore a correlation between them is expected (Lavery and Sklenar, 1989). The local helical parameters also show that the twist angle is large at G2pA3 and T4pC5 steps and smallest at A3pT4 step in each strand. It is observed that the helix axis bends by an angle of 4°-5° at each end and to a lesser extent at other steps. This is consistent with positive roll of ~ 8° observed at both ends of helix, that is, at the C1pG2 and C5pG6 steps leading to a bend in helix axis at these steps. The overall helix bend leading to a curvature is rather small ~ 4°.

3.2.2.2 Groove Width

The groove widths of the double helix are defined using the coordinates of the phosphate atoms. The smallest separation between the phosphate atoms in 2 antiparallel strands reduced by the sum of the van der waal's radii of the two phosphate atoms (5.8 Å) is used to define the minor groove width in B-DNA and major groove width in A-DNA. The minor groove generally occurs between the i and $(i-4)'$ phosphates for B-DNA and between i and $(i-3)'$ for the A-DNA (Bhattacharya and Bansal, 1992; Mujeeb et al, 1993). In the hexanucleotide only one major and one minor groove exists in the middle of helix. In the rMD-B18 structure, the width and depth of major groove is 12.3 Å and 3.0 Å while the corresponding values for minor groove are 5.8 Å and 5.0 Å, respectively. Thus the major groove is wider (by ~ 1 Å) and shallower (by ~ 1 Å) in our rMD structure. Similar results are seen in all rMD structures. This corroborates with the negative values of roll angle at A3pT4 step leading to widening of major groove which is compensated by large decrease in propeller twist observed at this step. The width and depth of minor groove, on the other hand, are closer to that seen in canonical B-DNA structure. This is contrary to B-DNA structure of d-CGATCG obtained by Lam and Au-Yeung in which a much narrower (~ 2.8 Å) minor groove was observed.

3.2.2.3 Base-base stacking

Presence of A3H8-T4CH₃ and T4H6-C5H5 sequential cross peaks (Table 3.2) is indicative of the good base to base stacking. Fig. 3.7 shows the stacking pattern in all basepairs of rMD-B18. It is clearly seen from the figure that overlapping of bases is minimum at C1pG2 and C5pG6 basepair steps while is maximum at G2pA3 and T4pC5 basepair steps. The same is corroborated by the values of the twist angles, it being minimum for C1pG2 and C5pG6 and maximum for G2pA3 and T4pC5 basepair steps.

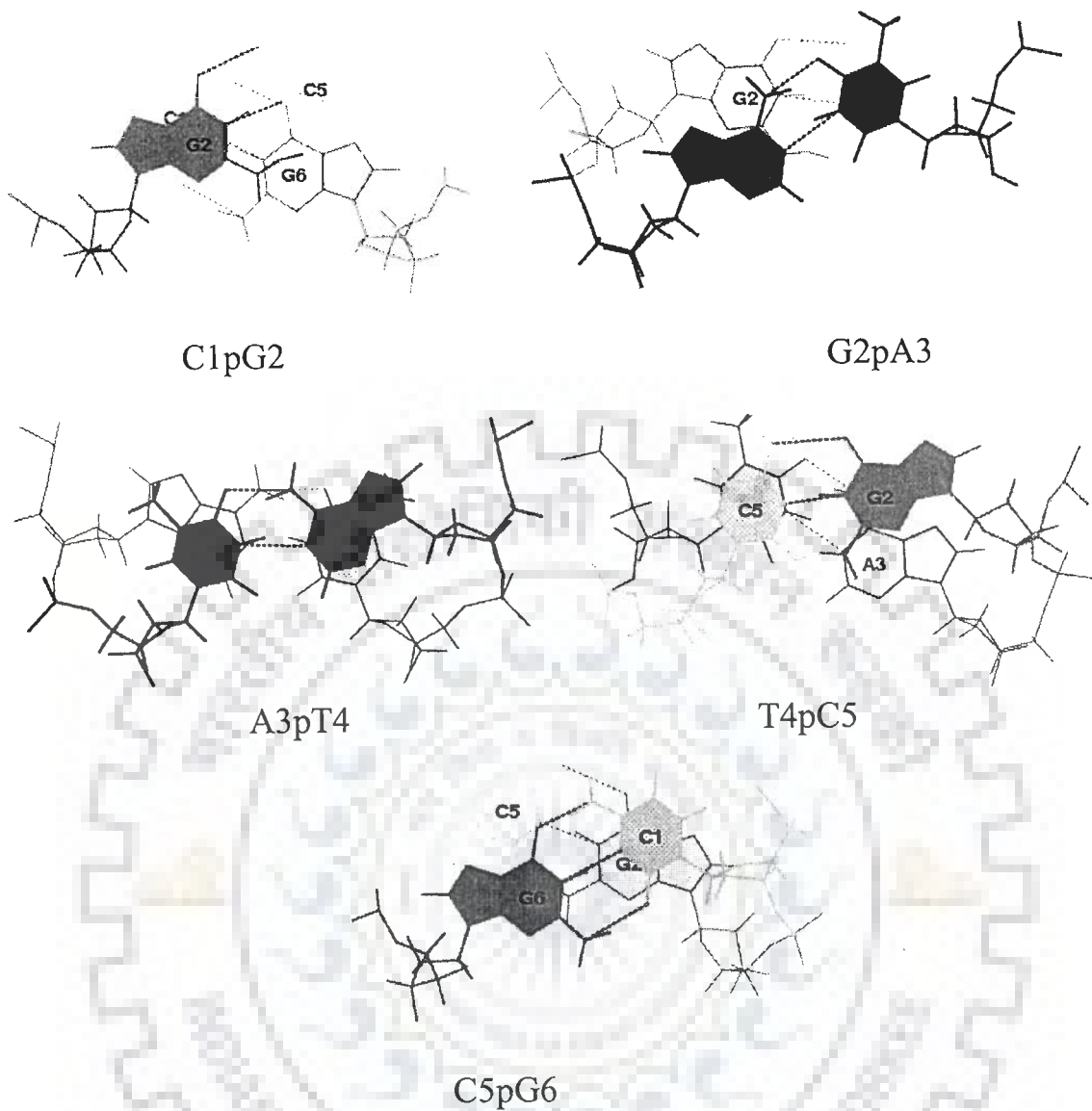


Figure 3.7: Base Stacking pattern at all the base pair steps in rMD-B18 structure

3.2.2.4 Torsional angles

Values of torsional angles for both the strands along with the values for canonical B-DNA and A-DNA are provided in Fig. 3.8. It is satisfying to see that all the torsional angles are practically equivalent in both the strands of the duplex; this is expected, as the DNA is self-complementary. It is further observed that although the difference in absolute values of torsional angles in the rMD-structures obtained with two different starting structures are slightly different ($\sim \pm 6^\circ$), the general features and trends with base sequence are strikingly identical. This further confirms that all rMD structures are uniquely defined by the restraints obtained by the NMR spectra. The backbone torsional angles (except δ) are not defined directly by NOE distance constraints. We have used a low force constant to permit a smooth search, which is conformationally compatible with other structural features. It is observed that the angles alpha through zeta show variations with base sequence but have values close to that of B-DNA for most residues rather than the corroborating A-DNA structure. The angle α varies between -53° and -77° and is maximum in magnitude in C5 bases. The angle β representing rotation about C5'-O5' ester bond does not vary appreciably with base sequence and adopts a trans conformation. The backbone torsional angle γ is slightly more positive (range 43° - 70°) than that for canonical B-DNA structure and is least β (43° - 48°) for C1 residue in all rMD structures.

The angle δ reflects the deoxyribose puckering and adopts a conformation between that of A-DNA and B-DNA. In several rMD structures observed A3 adopts a value of $\delta = 143^\circ$ - 148° (maximum value observed) while the T4 residue adopts lowest δ angle, It being in the range 109° - 120° . The torsional angle ϵ is representing rotation about C3'-O3' bond is in trans conformation for all residues while angle ζ is close to the corresponding value in B-DNA in rMD structures.

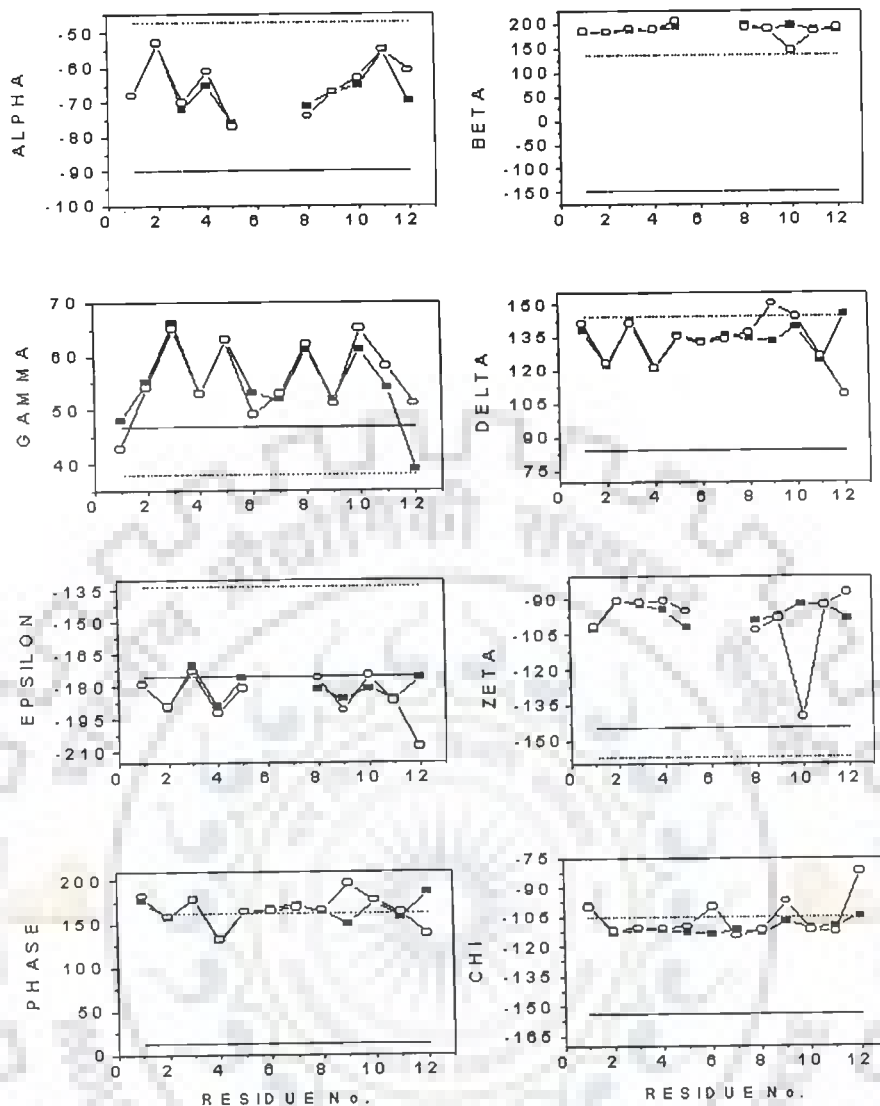


Figure 3.8: Backbone torsional angles calculated for canonical A-DNA (—), B-DNA (---) and structure obtained by restrained molecular dynamics : rMD-B18 (■) and rMD-B19SA (○) structures

The analysis of spin-spin coupling constants and inter proton distances revealed that deoxyribose rings are in dynamic equilibrium between two conformers and the dominant conformer possessed a pseudorotation angle P in the range 126° - 198° . The time-averaged structure resulting from our restrained rMD simulations is essentially consistent with that and shows that P values lie in the range 113° - 185° in all rMD structures. In several rMD structures, it was observed that P is fairly large (176° - 185°) for A3 residue and minimum for the adjoining T4 residue (113° - 130°). Sugar pucker and glycosidic torsional angle are typically the parameters best defined by NMR and define the geometry within a nucleotide. It is observed that all χ values lie in the range -92° to -128° , which is close to that observed in B-DNA. Further, at both the ends of helix, χ tends to adopt relatively a high anti conformation, particularly for C1 residue, with χ angle lying in the range -82° to -99° . As anticipated, a correlation between pseudorotation angle P and glycosidic torsional angle χ is observed. A large P value of $\sim 180^\circ$ is accompanied by high anti conformation of glycosidic bond rotation, with $\chi \sim -99^\circ$.

3.3 TRAJECTORY ANALYSIS

We have examined the trajectory of various intra- and inter-nucleotide vectors during the course of rMD simulations. It is observed that the amplitude and frequency of motions are different at the various sites chosen. Some of the results are shown in Fig. 3.9. It is observed that the intra sugar distances such as $H2''$ - $H4'$, $H2'$ - $H4'$, $H1'$ - $H4'$, etc. show minor variations with time, it being $\sim \pm 0.1 \text{ \AA}$ for C1, G2 and T4 residues and negligible for all A3, C5 and G6 residues. The intra nucleotide base H8/H6 to $H2''$, $H1'$, $H3'$ distances also show similar minor variations for all residues (except C1 residue) which stabilize after 12-15 ps (Fig. 3.9a). A relatively larger fluctuation ~ 0.1 - 0.4 \AA is observed in C1 residue, being the terminal residue at 5' end. The inter nucleotide or sequential distances e.g. base

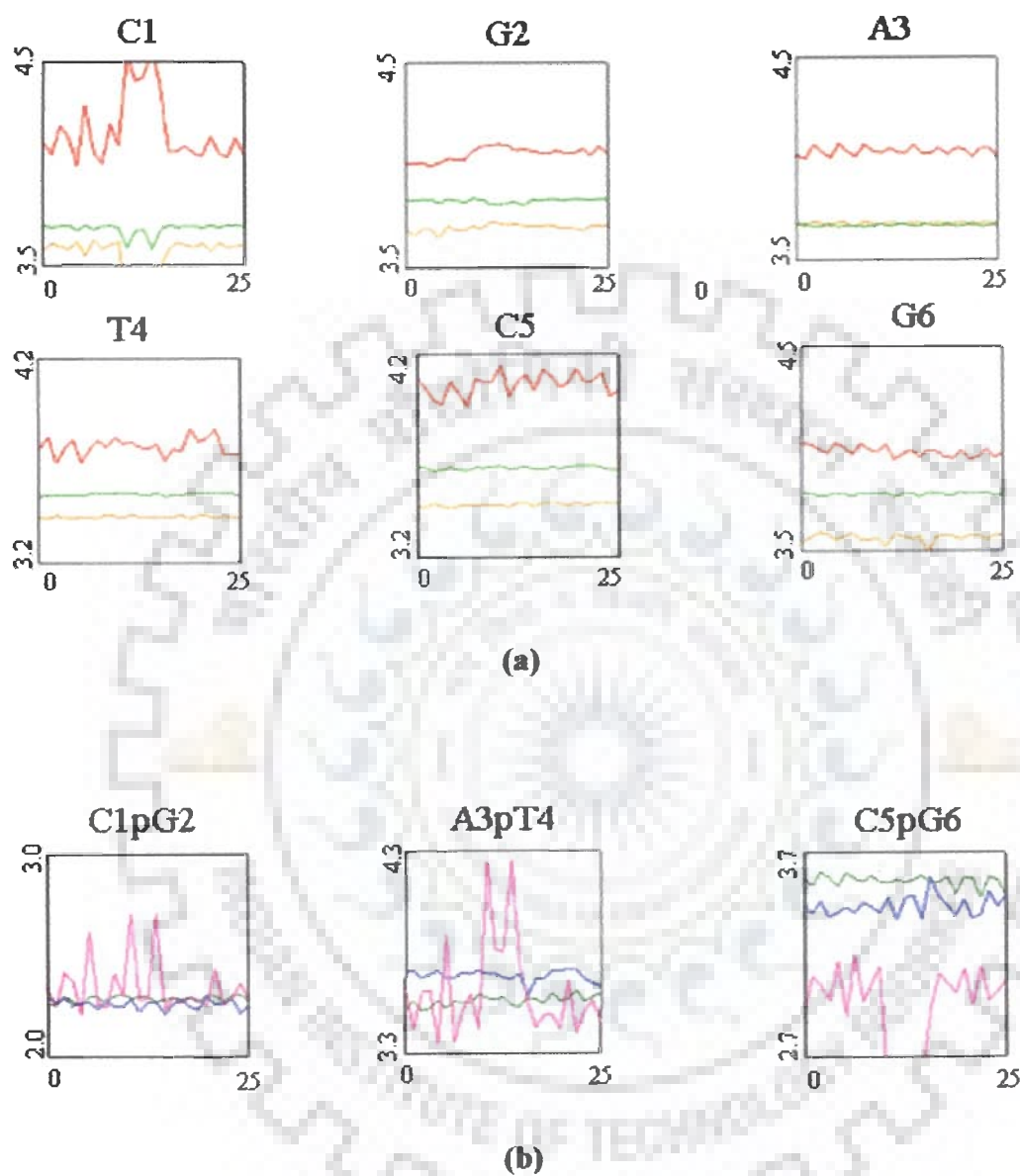


Figure 3.9: (a) Trajectory analysis of 0.024 ns restrained molecular dynamics simulations in rMD-B18 structure showing intra nucleotide inter proton distances H8/H6-H1' (green), H8/H6-H3' (red) and H8/H6-H2'' (orange) (b) some of the inter nucleotide base to sugar interproton distances (pink-C1pG2 step, green-A3pT4 step, blue-C5pG6 step)

H8/H6 to H1', H2', H2'' and H5''-H1' show minor variations for all the base pair steps except C1pG2 step (Fig. 3.9b). Large variations up to $\sim 0.8 \text{ \AA}$ are observed in C1pG2 step for all sequential base-sugar proton distances which stabilizes in about 15 ps. The variations in A3pT4 base pair step are particularly negligible. The intra nucleotide distances base-H2', base-H2'', base-H3' depend on both P and χ value while base-H1' depends on χ value only. The observed results therefore indicate that the orientation of bases with respect to the sugars (χ) and the sugar puckers (P) themselves do not show variability through the course of simulations except at 5' terminal of helix, that is for C1 residue. The large variations in intra nucleotide base-3', base-2'' and sequential distances base-sugar protons, show that the backbone is relatively more dynamic and significant fraying occurs at 5' terminal. Lam and Au-Yeung (Lam and Au-Yeung, 1997) have defined a local structure function, composed of the sum of the contributions from four of the helical parameters, that is, the helix twist, base roll, base pair slide and propeller twist. They have shown its correlation with the local stability of a base-pair step. It is also been emphasized that the nearest neighbour has effect on local geometry of base-pair so that the basic unit of trimer or tetramer should be used for analyzing base-pair and base-pair step structural parameters, respectively. This may be the reason for observed difference in dynamic behaviour of C1pG2 and C5pG6 base-pair steps (Fig. 3.9b). The observed results thus indicate the complexities and the variability in the motion in DNA, which contribute to the sequence dependent flexibility and deformability of the DNA. Some of these structure and dynamic aspects may have important implications in binding of ligands at specific sites of DNA. For instance it is shown that anticancer drugs, adriamycin and daunomycin, bind at C1pG2 and C5pG6 step (Frederick et al, 1990; Moore et al, 1989) wherein the roll, rise, twist and slide are similar. The binding at A3pT4

step in d-CGATCG is particularly not preferred perhaps due to rigidity or comparatively less deformability at this step.

3.4 CONCLUSIONS

Using a total of 10 spin-spin coupling constants and 112 NOE intensities, structural refinement has been carried out using Restrained Molecular Dynamics (rMD) with different starting structures, potential functions and rMD protocols. Refinement using different methods resulted in essentially the same structure, indicating that the structure obtained is defined by experimental restraints. The structural details have been analyzed with respect to torsional angles, base pair geometries and helicoidal parameters. It is observed that pseudorotation phase angle of deoxyribose sugar for A3 and T4 residues is $\sim 180^\circ$ and $\sim 120^\circ$, respectively while all other residues are close to C2'endo-conformation. A large propeller twist ($\sim -18^\circ$) and smallest twist angle ($\sim 31^\circ$) at A3pT4 step, in the middle of the sequence, a wider (12 Å) and shallower (3.0 Å) major groove with glycosidic bond rotation as high anti at both the ends of hexanucleotide are observed. The final structure, representing a time-averaged structure, shows base-sequence dependent variations and hence strong local structural heterogeneity.

STRUCTURE OF d-(TGATCA)₂ BY RESTRAINED MOLECULAR DYNAMICS

Cross peaks in the NOESY spectra were integrated and intensities at mixing times of 75, 150 and 200 ms were translated into inter proton distances using C5H5-C5H6 cross peaks of cytosine as the reference (2.45 Å). Figure 4.1 shows the NOESY spectra of d(TGATCA)₂ at $\tau_m = 250$ ms. Table 4.1a-b lists interproton distances within sugar, base protons with deoxyribose sugar and sequential d-(TGATCA)₂. Using these interproton distances and torsional angles as restraints restrained molecular dynamics of hexamer was carried out.

4.1 STRATEGY FOLLOWED

The model of d-TGATCA duplex was made using BIOPOLYMER module. Pseudoatom corrections were used for methyl and other equivalent protons. A range of ± 0.2 Å was provided to distance to account for any errors in integration. Pseudoatom corrections were used for methyl and other equivalent protons. The NOEs were categorized as strong, medium and weak with corresponding distance ranges 1.8-2.4 Å, 2.5-2.9 Å and 3.0-4.0 Å set for the respective intensities of cross peaks. Force constants of 10.0, 5.0, and 2.0 Kcal mol⁻¹ Å⁻² were fixed for strong, medium, and weak peaks, respectively. The coupling constants $J(\text{H1}'\text{-H2}')$ and $J(\text{H1}'\text{-H2}'')$ were transformed to torsional angles using Karplus relationship. These were introduced as dihedral restraints allowing a range of $\pm 10^\circ$ on the calculated values with force constant of 20.0 Kcal mole⁻¹ rad⁻². The total numbers of dihedral and

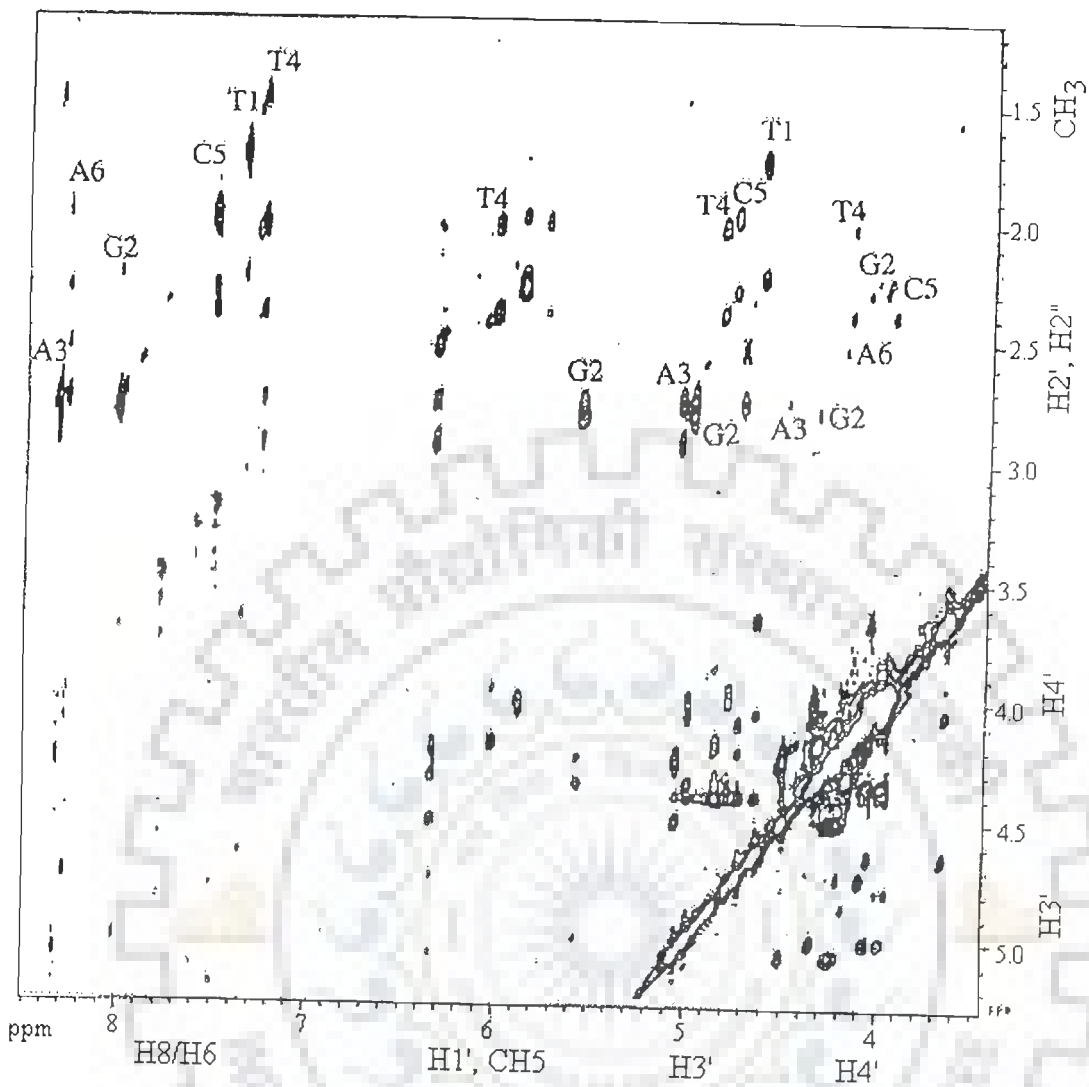


Figure 4.1: Expansions of a portion of 500 MHz NOESY spectra of d-TGATCA showing specific through space correlations at $\tau_m = 250$ ms (courtesy: Uma Sharma)

Table 4.1a: Some of the inter proton distances (Å) from intra residue connectivities observed in NOESY spectra of d-TGATCA at 295 K

	T1	G2	A3	T4	C5	A6
H1'-H2'	2.9	-	2.8	2.7	3.1	2.8
H1'-H2''	2.2	2.2	2.4	2.2	2.2	2.4
H1'-H3'	-	3.4	3.4	-	-	3.8
H1'-H4'	2.7	2.9	3.1	2.7	2.7	3.1
H2''-H3'	2.7	2.6	2.5	2.8	2.9	2.5
H2''-H4'	3.2	-	-	3.2	3.2	3.7
H8/H6-H1'	3.2	3.3	3.2	3.3	3.4	3.1
H8/H6-H2'	2.4	2.2	2.2	2.1	2.2	2.4
H8/H6-H2''	3.2	3.4 ^o	3.2	2.8	3.4	3.3
H8/H6-H3'	3.6	3.3	3.2	3.7	3.5	3.2
H8/H6-H4'	-	-	-	4.0	-	-
H8/H6-H5'	3.7	-	-	-	-	-
H8/H6-H5''	-	-	3.3	-	-	3.2

^o overlap of resonance

Table 4.1b: Some of the inter proton distances (Å) from inter residue sequential connectivities observed in NOESY spectra of d-TGATCA at 295 K

T1H1'-G2H5''	3.1	A3H8-T4CH ₃	2.9
T1H1'-G2H8	3.4	T4H1'-C5H5''	3.4
T1H2'-G2H8	> 4.2	T4H1'-C5H6	3.5
T1H2''-G2H8	3.6	T4H2'-C5H6	3.4
G2H1'-A3H5''	3.6	T4H3'-C5H6	4.0
G2H1'-A3H8	3.1	T4H2'-C5H6	2.4
G2H2'-A3H8	3.4	T4H2''-C5H5	3.1
G2H2''-A3H8	2.3	T4H2''-C5H5	4.0
A3H1'-T4H5''	3.1	T4H6-C5H5	3.7
A3H1'-T4H6	3.3	C5H1'-A6H5''	3.1 ^o
A3H2'-T4H6	3.2	C5H1'-A6H8	3.5
A3H2''-T4H6	2.9	C5H2'-A6H8	4.2
A3H2'-T4CH ₃	2.9	C5H2''-A6H8	3.7

^o overlap of resonance

distance restraints used in the structure calculations using Restrained Molecular Dynamics were 12 and 121, respectively. An initial model of double helical B-DNA structure was generated using INSIGHT II version 97.0, (Molecular Simulations Inc. MSI, San Diego) using Silicon Graphics O2 workstation R5000 and is referred to as B-DNA1. The force constant for hydrogen bonds was fixed as $40 \text{ Kcal mol}^{-1} \text{ \AA}^{-2}$ throughout the simulations. The energy of the molecule was minimized using 1000 steps each of Steepest Descent and Conjugate Gradient methods to remove any internal strain due to short contacts in starting structure using CFF91 force fields (Maple et al, 1988; Maple et al, 1990) in DISCOVER version 97.0 (MSI). Dielectric constant was fixed as $1.0 * r$ ($r = \text{distance}$) for calculation of electrostatic interactions. Conformational search was performed by the following simulated annealing restrained molecular dynamics protocol: The molecule was heated to a temperature of 500 K in steps of 100 K. Molecular Dynamics was carried out for 25 ps (1000 iterations steps of 1 fs each) at 500 K during which 25 structures were saved at regular intervals. Each of them was then slowly cooled to 300 K in steps of 50 K. The force constants for NOEs for strong, medium, and weak peaks were held constant as 25, 15, and $10 \text{ Kcal mol}^{-1} \text{ \AA}^{-2}$, respectively while that for experimental dihedral restraints was fixed at $50 \text{ Kcal mol}^{-1} \text{ rad}^{-2}$. At each step of cooling by 50 K the molecule was equilibrated for 25 ps (2500 iterations steps of 1 fs each). At the end of simulated annealing, 1000 steps of Steepest Descent minimized all the structures until a predefined convergence limit of root mean square derivative of energy with respect to atomic coordinates of $< 0.01 \text{ Kcal mol}^{-1} \text{ \AA}^{-1}$ was reached. The final structure thus obtained is referred to as rMD-B1SA. The complete protocol of rMD studies with simulated annealing at 500 K was repeated by taking another starting structure

(referred to as B-DNA2) built using AMBER 7.0 and is referred to as rMD-B2SA. Since the results obtained by NMR indicated existence of a structure within the B-family of DNA structures, we have also carried out studies using rather a mild rMD protocol with both the starting structures B-DNA1 and B-DNA2. In this protocol the temperature is maintained at 300 K throughout the process of restrained energy minimization and restrained molecular dynamics and the corresponding resulting structures are referred to as rMD-B1 and rMD-B2. Another rMD structure, obtained after 100 ps simulations with starting structure B-DNA1, is referred to as rMD-B1-100. All molecular dynamics calculations have been carried out in vacuum.

4.2 RESULTS AND DISCUSSION

4.2.1 Restrained Molecular Dynamics Studies

Restrained molecular dynamics permits the system to undergo conformational and momentum changes so that different parts of the phase space accessible to the molecule can be explored and stable conformations are identified by energy minimization. Simulations were carried out by starting with two different structures: B-DNA built using INSIGHT II and other built using AMBER 7.0 software package. Simulated annealing was carried out up to a temperature of 500 K but it was found that convergence to a final structure could be readily achieved even at 300 K. The stereo view of various rMD structures is shown in Fig. 4.2a. The rMD-B1SA structure superimposed over the standard B-DNA structure is shown in Fig. 4.2b indicating the difference between the two structures. Several structures obtained after equilibration at different time intervals during the dynamics run at 500 K and 300 K were examined. It was observed that they differ only marginally from each other in their overall feature irrespective of the rMD protocol followed and starting structure.

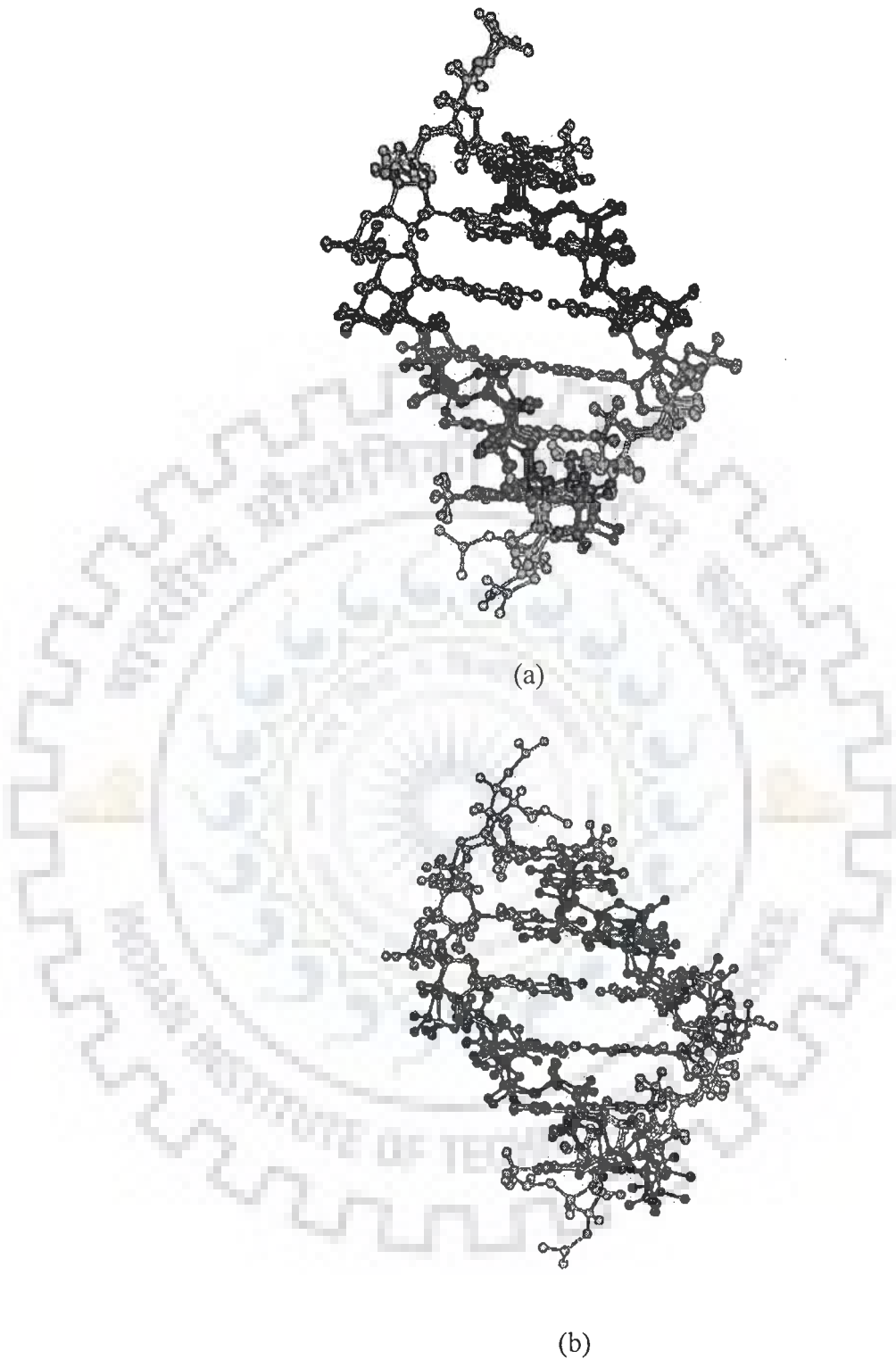


Figure 4.2: Sequential stereo view of the (a) various rMD structures and (b) rMD-B1SA structure of d-TGATCA superimposed with standard B-DNA structure

Further no significant drift in either potential energy or restraint deviations was observed during the final equilibration. It can therefore be concluded that the system reached a minimum energy conformation. A structure obtained without introducing NMR constraints and by following same steps of rMD protocols was found to be quite different. This confirms that the structure is indeed defined by experimental restraints and not the refinement procedure or variables used. The root mean square deviation in any of the rMD structures and either of the starting structures is quite large but among various final structures was very low. This is generally acknowledged as an indication that convergence has been achieved.

Table 4.2 indicates an assessment of refined structures after equilibration (at the end of 25/100 picoseconds) in terms of energetics including restraint violations energies and root mean square derivative of energy with respect to atomic coordinates. The total potential energy of the rMD-B1, rMD-B1SA, rMD-B2, rMD-B2SA and rMD-B1-100 structures lie in the range of 404-428 Kcal mol⁻¹ which is significantly lower than the corresponding energies of initial B-DNA structures (695-709 Kcal mol⁻¹). The forcing potential, which indicates contribution to potential energy due to violations of both experimental distances and torsional angle data, exhibits a decrease from 934-2858 Kcal mol⁻¹ to 198-200 Kcal mol⁻¹ after restrained energy minimization and restrained molecular dynamics. The energy gradient with respect to atomic coordinates lies in the range 0.07 to 0.17 Kcal mol⁻¹ Å⁻¹ in various structures. A summary of experimental restraints and statistical analysis of family of structures generated by restrained molecular dynamics (rMD) is shown in Table 4.3.

4.2.1.1 Conformational Features of rMD Structures

All helical parameters, backbone torsional angles and sugar conformations of the

Table 4.2: Energy terms (Kcal mol⁻¹) and root mean square gradient of energy with respect to atomic coordinates (Kcal mol⁻¹ Å⁻¹) for starting models and rMD structures of d-TGATCA

Structure	Total	Bond	Angle	Dihedral	Vdw	Repulsion	Dispersive	Electrostatic	Restraint ^a	Gradient
B-DNA1	695	74	466	105	343	1607	-1264	-295	934	25.16
rMD-B1	422	75	475	133	14	957	-942	-280	200	0.117
rMD-B1SA	424	75	476	132	15	953	-938	-278	199	0.133
rMD-B1-100	428	75	484	131	11	954	-942	-276	195	0.070
B-DNA2	709	98	451	106	343	1606	-1264	-289	2858	37.74
rMD-B2	414	83	473	132	17	945	-928	-294	198	0.077
rMD-B2SA	404	81	472	128	14	954	-940	-293	199	0.171

^a This contribution has been subtracted from the total energy

^b Root mean square gradient of energy with respect to atomic coordinates (Kcal mol⁻¹ Å⁻¹)

^c Average distance deviation

Table 4.3: Summary of experimental restraints and statistical analysis of family of structures generated by restrained molecular dynamics (rMD)

Parameter		
Distance Restraints		
	Residue	No. of Restraints
Intra residue	T1	17
	G2	13
	A3	19
	T4	15
	C5	15
	A6	16
Inter residue	T1-G2	8
	G2-A3	8
	A3-T4	12
	T4-C5	16
	C5-A6	8
Dihedral restraints		12
Average pairwise RMSD	B-DNA1=0, rMD-B1=0.87 rMD-B1SA=0.97, rMD-B1-100=1.01, B-DNA2=0 rMD-B2=0.85, rMD-B2SA=0.87	
Average residuewise RMSD	T1=2.51, G2=1.28, A3=1.04, T4=1.06, C5=0.92, A6=0.90	

resulting rMD structures were thoroughly analyzed with the program CURVES, version 5.1 (Lavery et al). The structural characteristics of various rMD structures are discussed in the following.

4.2.1.2 Helicoidal Parameters

Plot of various helix axis parameters (global, unless specified otherwise) of d-TGATCA in different structures as a function of residue position in duplex is shown in Fig. 4.3 (a-b) along with that for two classical structures of A-DNA and B-DNA. Base sequence dependent variations in helicoidal parameters are evident. The results on rMD structures are closer to that of B-DNA as compared to that of A-DNA. The helicoidal parameters are classified into three categories: global base pair-axis parameters, intra-base pair or global base-base parameters and the inter-base pair or base pair-step parameters. Among the base pairs-axis parameters, the x-displacement (dx) are ~ -1.0 Å for all residues which is close to a value of -0.7 Å as seen in canonical B-DNA structure. The y-axis displacement (dy) varies from $+0.2$ to -0.2 Å along the sequence. The base pairs are inclined (η) at an angle of -5° to -7° with no significant variation with base sequence. The tip angle (θ) fluctuates from -5° to -7° at 5' end to $\sim +7^\circ$ at 3' end. Such variations have been reported in literature in deoxyoligonucleotides (Mujeeb et al, 1993; Weisz et al, 1994). Among the intra base parameters, the shear (S_x) and stretch (S_y) values do not vary very much from their ideal values. The shear lies within ± 0.2 Å while the stretch lies within the range 0 to -0.2 Å. The stagger (S_z) values lies within the range 0.1-0.4 Å but have large positive values for the two middle base pairs. The buckle varies within ± 0.3 Å. The variations in the propeller twist are significantly large. For the two base pairs in the middle, that

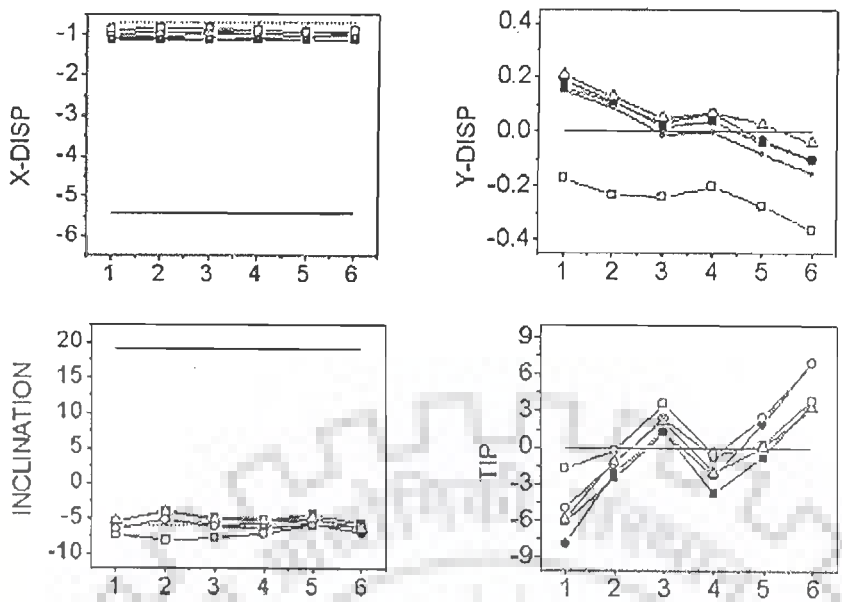


Figure 4.3(a)

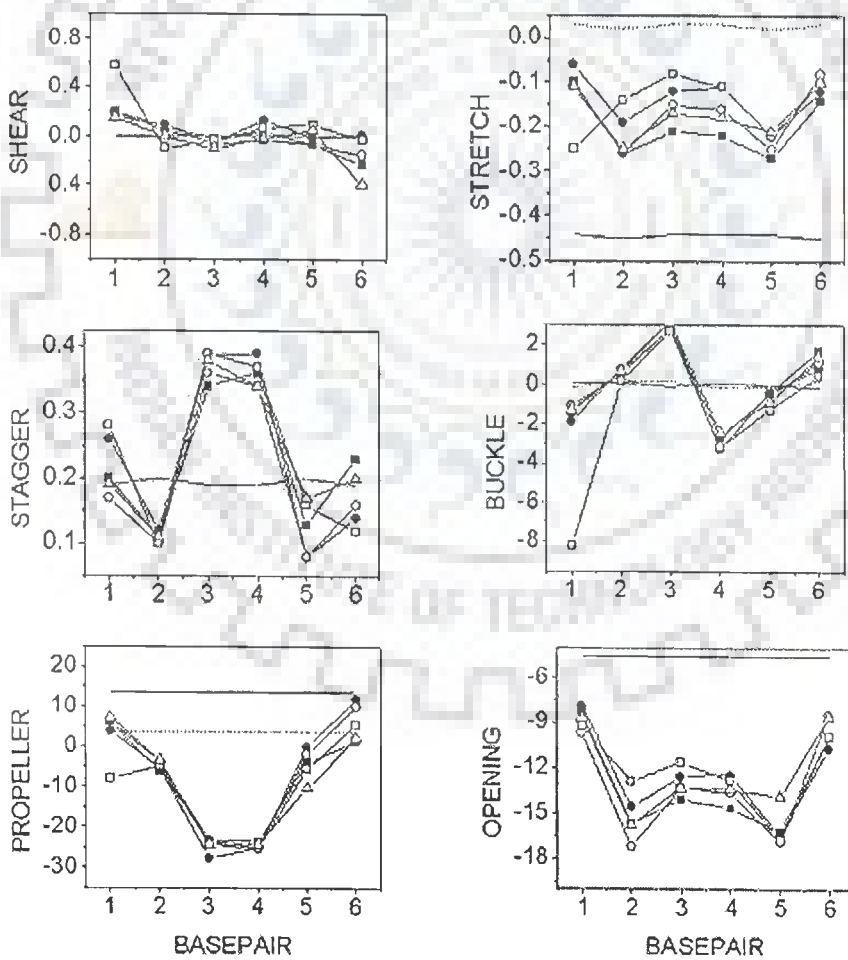
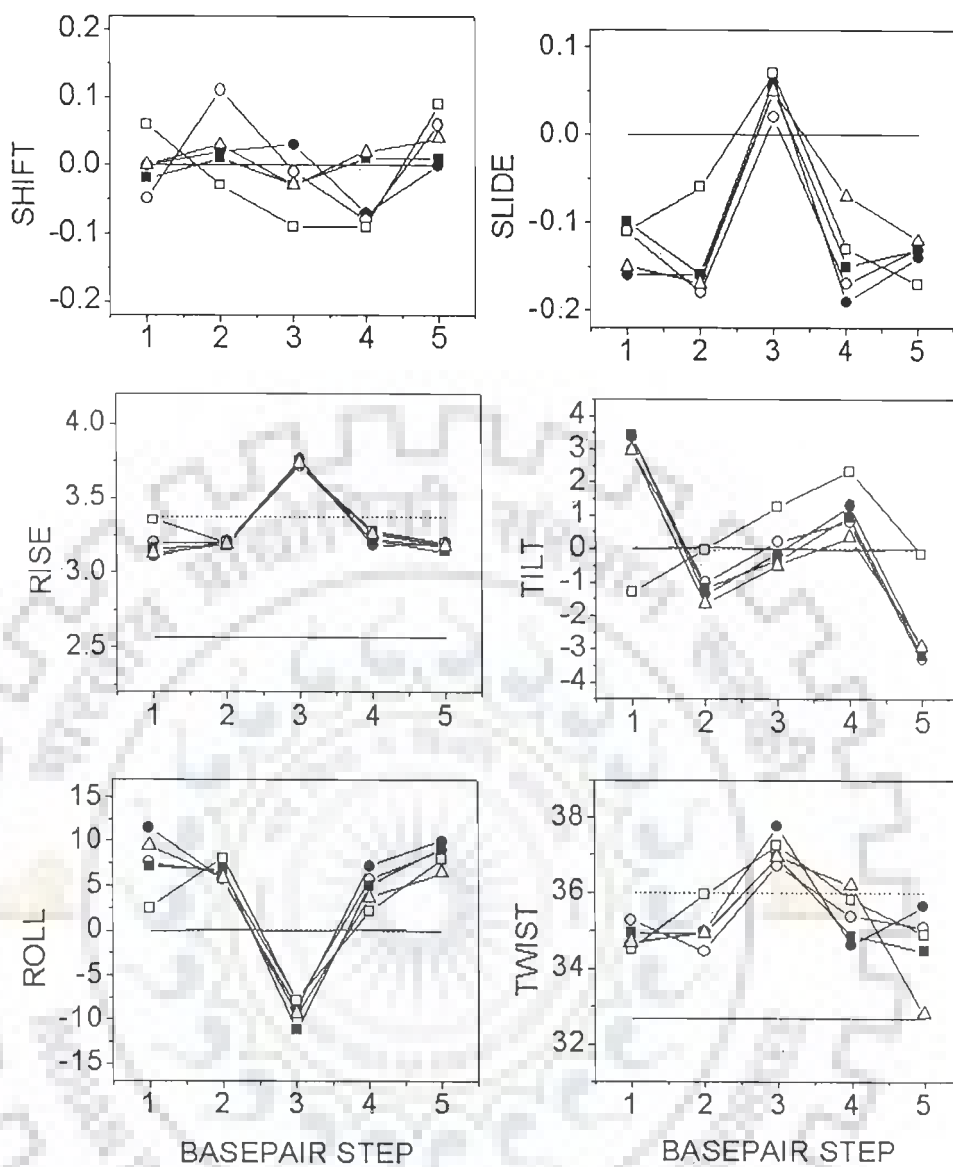


Figure 4.3(b)



(c)

Figure 4.3: Helical (a) base pair axis (b) intra base pair (c) global base base parameters for d-TGATCA calculated for canonical A-DNA (—), B-DNA (----) and different structures obtained by restrained molecular dynamics simulations : rMD-B1 (●) and rMD-B1SA (○) rMD-B2 (■) and rMD-B2SA (□) and rMD-B1-100 (Δ)

is, A3T4 and T4A3, large negative values in the range 23° - 28° are observed. The base pairs at either end show a small positive propeller twist. Large negative values of propeller twist in AT and TA base pairs have been reported in literature (Dornberger et al, 1998; Mujeeb et al, 1993; Weisz et al, 1994) and may possibly occur to avoid steric clashes between the CH_3 group of thymine and 5' neighboring sugar in AX/XT base pairs step (Hunter, 1993). The positive value of propeller twist for terminal basepairs may be attributed to fraying effects at both ends of oligonucleotides. The base pair opening lies between -8° to -17° for all base pairs and is larger in magnitude for non-terminal base pairs.

In regular A-DNA and B-DNA geometries, global values of the inter base pair parameters shift (D_x), slide (D_y), roll (ρ) and tilt (τ) are essentially zero. For different rMD structures, the shift does not show significant variations with the base sequence. The slide is minimum for central base pair step, A3pT4, and about 0.2 Å for all other base pair steps. The rise per residue (D_z) is about ~ 3.2 Å for all base pair steps except A3pT4, for which it is somewhat large, being ~ 3.7 - 3.8 Å. The tilt angle fluctuates within $\pm 4^{\circ}$ and does not appear to be sequence dependent. The roll angle, on the other hand, shows large positive value of $\sim 8^{\circ}$ to 12° at either end of the helix and is -8° to -9° at the central A3pT4 base pair step. A positive roll opens the angle between base pairs towards the minor groove, as a result a wider minor groove and bending towards major groove causing a curvature in helix axis occurs. The large positive roll at T1pG2 steps indicates reduced base stacking and hence demonstrates a flexibility at pyrimidine 3'-5' purine step (Dornberger et al, 1998) which is discussed later in detail. But the negative value of roll angle at the A3pT4 step of helix indicates widening of major groove and narrowing of minor groove at these steps which is

compensated by decrease in propeller twist so as to prevent destacking of bases (Dornberger et al, 1998). The twist angle for all base pairs in different structures lies in the range 34° - 36° except the central base pair in which it is $\sim 37^{\circ}$. The CURVES software reports both the global and local base helical parameters, and a correlation between them is expected (Lavery et al, 1989). The local helical parameters show trends in roll and twist angle similar to that observed in global parameters. The global axis curvature obtained for various rMD structures shows that helix axis bends by an angle of 5° - 6° at each end, which is consistent with the observation of positive roll at these steps. The overall helix bend leading to curvature is $\sim 5^{\circ}$.

4.2.1.3 Groove width

The groove widths of the double helix are defined using the coordinates of the phosphate atoms (Bhattacharya et al., 1992; Mujeeb et al., 1993). In the hexanucleotide only one major and one minor groove exists in the middle of the helix. The width and depth of major groove are 12.2-12.3 Å and 3.8-4.2 Å, respectively. The corresponding values for minor groove are 6.0-6.4 Å and 4.5-4.7 Å, respectively. Thus the major groove is wider by ~ 1.2 Å. This corroborates with the negative value of roll angle at A3pT4 step leading to widening of major groove which is compensated by a large decrease in propeller twist, observed at this step. The width and depth of minor groove, on the other hand increases to a lesser extent.

4.2.1.4 Torsional angles

The variation of torsional angles with base sequence (Fig. 4.4) shows equivalence of strands of duplex. The general features and trends with base sequences for all rMD structures are strikingly identical and a difference in absolute values of torsional angles with different starting structures or different rMD protocols (with and without

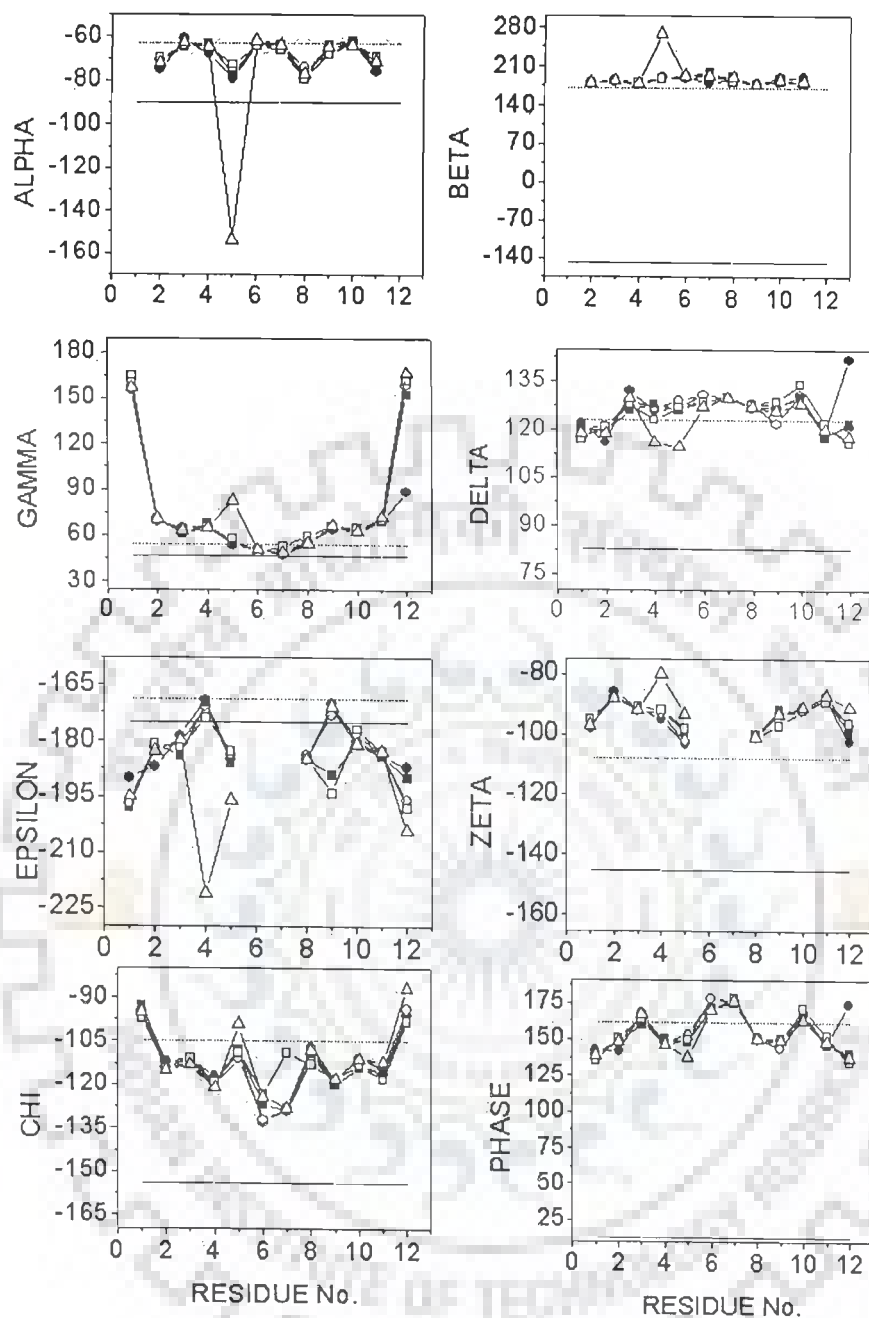


Figure 4.4 : Backbone torsional angles calculated for canonical A-DNA (—), B-DNA (----) and different structures of d-TGATCA obtained by restrained molecular dynamics simulations : rMD-B1 (●) and rMD-B1SA (○) rMD-B2 (■) and rMD-B2SA (□) and rMD-B1-100 (Δ)

simulated annealing) are slightly different for end residues only. This further confirms that all rMD structures are uniquely defined by the restraints obtained by the NMR spectra. The backbone torsional angles (except δ) are not defined directly by NOE distance constraints. We have used a low force constant to permit a smooth search, which is conformationally compatible with other structural features. It is observed that the angles alpha through zeta show variations with base sequence but have values close to that of B-DNA for most residues rather than the corresponding A-DNA structure. The angle α varies in a narrow range -60° to -79° and is largest in magnitude for T4 base in all structures. The angle β does not vary appreciably with base sequence and adopts a trans conformation. The variation of γ is in the range 50° - 70° except that at 5' end it is unusually large; it adopts trans conformation, which is discussed later. The angle δ reflects the deoxyribose puckering and adopts a conformation between that of A-DNA and B-DNA. In most of the rMD structures obtained, it is lowest for T1 residue (119° - 122°) and highest for A6 residue ($\sim 130^\circ$) although the variation is within a small range. The angle ϵ is in trans conformation for all residues while ξ is close to the corresponding value in B-DNA in all rMD structures. The value of P angle in five structures resulting from our restrained rMD simulations is essentially consistent with the results of the NMR data (courtesy Uma Sharma) and shows that it lies in the range 138° - 178° . In most of the rMD structures T1 residue had minimum P value ($\sim 138^\circ$ - 140°) while A6 residue had maximum value ($\sim 178^\circ$). T1 invariably adopted C1'-exo conformation. The average value of pseudo rotation phase angle and hence the sugar puckering differ for the purine and pyrimidine nucleotides; the average value being 164° and 146° , respectively. The

pyrimidine nucleotides thus prefer smaller phase angle as compared to purines (Weisz et al, 1994). Sugar pucker and glycosidic torsional angles are typically the parameters best defined by NMR and define the geometry within a nucleotide. It is observed that glycosidic bond rotation in all structures lies in the range -94° to -133° . At the 5' end of the helix there is tendency for χ to adopt high anti conformation of $\sim -94^\circ$ in all structures, which was also manifested by the lowest base H6-H1' distance as shown in Table 4.1a.

4.3 STRUCTURAL FEATURES OF TpG/CpA BASE PAIR STEP

Structural flexibility of DNA at TpG/CpA base pair step has been reported by NMR (Cheung et al, 1984; Donlan et al, 1992; Dornberger et al, 1998; Weisz et al, 1994), X-ray crystallographic (Gorin et al, 1995; Grzeskowiak et al, 1996) and other techniques (Beutal et al, 1992; Lyubchenko et al, 1993) in literature. A striking feature of X-ray crystallographic structures is a large twist angle of 50° observed at TpG/CpA step (Gorin et al, 1995; Grzeskowiak et al, 1996). As a consequence of high twist and slide values, the inter proton distance, T3H2''-G4H8 and C7H2''-A8H8 at these steps in decanucleotide d-CATGGCCATG were found to be 5.2 Å. Further, the distance between base protons H8/H6 at TpG and CpA base steps is ≥ 6.2 Å (Grzeskowiak et al, 1996). Alternatively two subsets, CA⁺ and CA⁻, with mean twist value of 30.5° and 49° , respectively have been shown to exist in the X-ray crystal structures of DNA samples (Gorin et al, 1995). Our NMR results do not give any evidence of the existence of these structural features (Barthwal et al, 2004). We have examined time dependent fluctuations of several inter proton sequential distances for the TpG/CpA base pair step during 100 ps rMD simulations with different starting geometries. We found that the variation in T1H2''-G2H8 and C5H2''-A6H8 lies

within ± 0.3 Å. The twist angle at TpG/CpA step in several conformers saved at different time intervals in an rMD simulation showed deviation within $\pm 4^\circ$. These are in agreement with those obtained in literature by NMR techniques (Dornberger et al, 1998; Weisz et al, 1994). We have observed NOE cross peaks for sequential NOE connectivities H8-H1', H2' and H2'' at CpA step and H8-H1', H2'' at TpG step even at low mixing times (Barthwal et al, 2004) with distances lying in the range 3.4-4.2 Å (Table 4.4). The twist, roll, and slide values in various rMD structures are $\sim 35^\circ$, 8° - 12° , and -0.13 Å, respectively. These results compare well with those obtained by NMR techniques (Dornberger et al, 1998; Weisz et al, 1994) and a twist angle of $\sim 34^\circ$ reported by electrophoretic techniques (Kabsch et al, 1982).

The NMR conformers have been characterized by a large positive roll angle at TpG step resulting in opening towards a major groove and a concomitant local expansion of minor groove (Weisz et al, 1994). This increases the inter strand distance between A3H2 and C5H1' protons to a value > 4.5 Å compatible with absence of cross peak in the 2D NOESY spectra. We did not observe NOE cross peak for any of the inter strand or intra strand inter proton distances A3H2-C5H1', A6H2-G2H1' and A3H2-T4H1' (Chuprina et al, 1991), the corresponding distance is apparently > 4.2 Å, the resolution in the NOESY spectra. We observed that large positive roll of 9° - 12° at TpG step is accompanied by a tilt of 3° - 4° in our structures, which is consistent with the Tilt-Roll plot relationship at TpG step shown earlier (Dornberger et al, 1998). Large positive roll angle up to $\sim 20^\circ$ were observed in several NMR structures of DNA duplexes at the TpG steps (Dornberger et al, 1998; Mujeeb et al, 1993; Weisz et al, 1994) and were also predicted by Monte Carlo calculations (Zhurkin et al, 1991) emphasizing the unusual conformational behavior and flexibility of this pyrimidine

3'-5' purine step. The preference of positive roll angle in TpG/CpA base pair step to avoid a cross-strand steric clash in minor groove has also been shown (Hunter, 1993). The observed stacking patterns between base pairs at five individual base pair steps viewed along the global helix axis for rMD-B1-100 structure are shown in Fig. 4.5. It is noted that overlap of bases at TpG step is particularly low. The high positive roll at TpG step indicates reduced base stacking interactions which leads to a non-parallelism of the base normal vectors of residues T1 and G2. High flexibility and low stacking interactions have been deduced earlier by gel circularization assays (Lyubchenko et al, 1993), gel-electrophoresis (Beutal et al, 1992) and NMR studies (Cheung et al, 1984; Donlan et al, 1992; Dornberger et al, 1998). These results suggest that the high flexibility at TpG/CpA step in solution can be explained in terms of large positive roll rather than twist based low stacking interaction. The unusually large twist angle (49° - 50°) observed in X-ray crystal structures (Gorin et al, 1995; Grzeskowiak et al, 1996) may be attributed to the crystal packing forces, which disturb the local conformation at TpG step. This conformational behavior at TpG/CpA step has been shown to cause an upfield shift in CH1' resonance of TpG/CpA junction along with a pronounced temperature dependence (Weisz et al., 1994). The C5H1' resonance in our experiments shows a change in chemical shift of 0.33 ppm with temperature which is considerably larger than that observed for H1' protons of other residues (Barthwal et al, 2004). The backbone torsional angles do not vary significantly with the residue and are largely constrained to preferred conformations observed generally in B-DNA. However it was observed that the γ torsional angle about C5'-C4' bond for T1 residue was $\sim 160^{\circ}$ for most rMD structures and $\sim 90^{\circ}$ for few structures (Fig. 4.4), indicating a large deviation from +gauche conformation generally found to exist in B-DNA.

Table 4.4: Comparison of some of the structural features of TpG and CpA base

pair steps

	Present NMR results		NMR (Dornberger et al)		NMR (Weisz et al)		X-ray (Grzeskowiak et al)		X-ray (Gorin et al)	
	TpG	CpA	TpG /CpA		TpG/CpA		TpG/CpA		TpG/CpA	
Twist (°)	34.6	35.3	34.9	34.8	36	40, 37	50		30.5	CA ⁺
									49.0	CA ⁻
Slide, dy (Å)	0.13	± 0.13	0.21	0.24	0.1	-0.1	High		-	
Roll (°)	8-12	9-10	10-15		20	-5, 4	-		-	
B-2'' (Å)	3.6	3.7	3.1	3.4	-		5.2		-	
B-1' (Å)	3.4	3.5	-		-		-		-	
B-2' (Å)	>4.2	4.2	4.6	4.5	-		-		-	
B-B (Å)	^b 5.1	^b 5.3	-		-		≥6.2		-	

B-base proton H8/H6

^b from rMD-B1SA structure

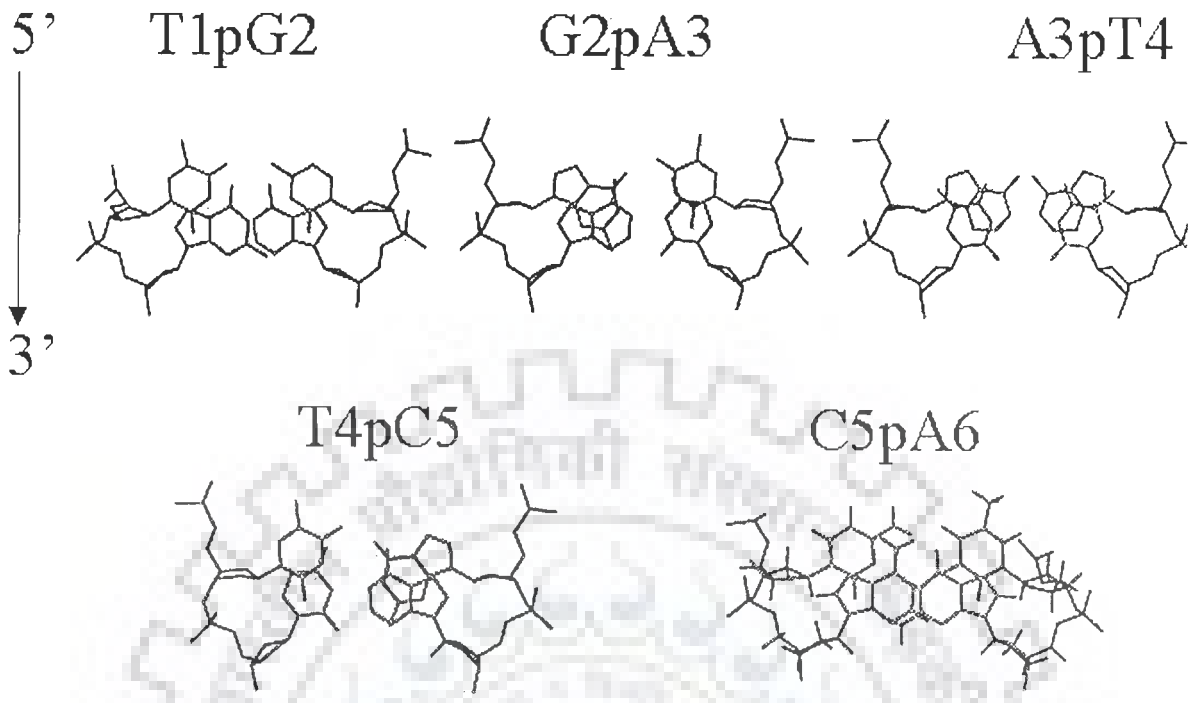


Figure 4.5: Stereo view of five individual base pair steps viewed down the global helix axis showing stacking between adjacent base pairs in d-TGATCA

The corresponding torsional angles β of T1 residue was found to be in trans conformation. In order to examine this aspect, we monitored the variations of all the torsional angles with time in rMD run up to 100 ps. It was found that only three torsional angles, that is, α , β and γ , for T1 and C5 residues showed a significant variation with time (Fig. 4.6 a). The angle γ for T1 residue rapidly flipped between two conformations having torsional angle of 90° and 160° . The corresponding angle β showed fluctuations between two conformational states having torsional angle of -180° and -85° . It is a concerted change from $\beta(t) \gamma(g^+)$ to $\beta(g^-) \gamma(t)$ conformational state. On the other hand, the time dependent fluctuations in C5 residues exhibited an altogether different behavior. The angles α , β , and γ were $-80^\circ(g^-)$, $-170^\circ(t)$, and $+60^\circ(g^+)$, respectively for first 75 ps and then flipped to $-150^\circ(t)$, $-90^\circ(g^-)$, and $+90^\circ(g^+)$, respectively and stabilized at these torsional angles for next 25 ps run. The conformation of backbone thus changed from a state normally found in B-DNA, that is, $\alpha(g^-) \beta(t) \gamma(g^+)$ to another state characterized by $\alpha(t) \beta(g^-) \gamma(g^+)$ for C5 residue. Corresponding to these variations, small shift $\sim 10^\circ$ was observed in δ and ϵ angles after 75 ps. Thus there is a bimodal distribution involving two distinct conformational states (named as 1 and 2 in Table 4.5). It may be noted that a somewhat similar behavior has been reported for G residue in the TpGpC element in a decanucleotide earlier (Weisz et al, 1994). It was found that α and γ undergo a strongly coupled reversible motion during rMD simulations from trans to more common $\alpha(g^-)$ and $\gamma(g^+)$ conformation, respectively while β remained unchanged in trans state for central G residue in TpGpC element. The G6 residue thus shifted from $\alpha(t) \beta(t) \gamma(t)$ to $\alpha(g^-) \beta(t) \gamma(g^+)$ conformation. The effect of backbone perturbations apparently extended to

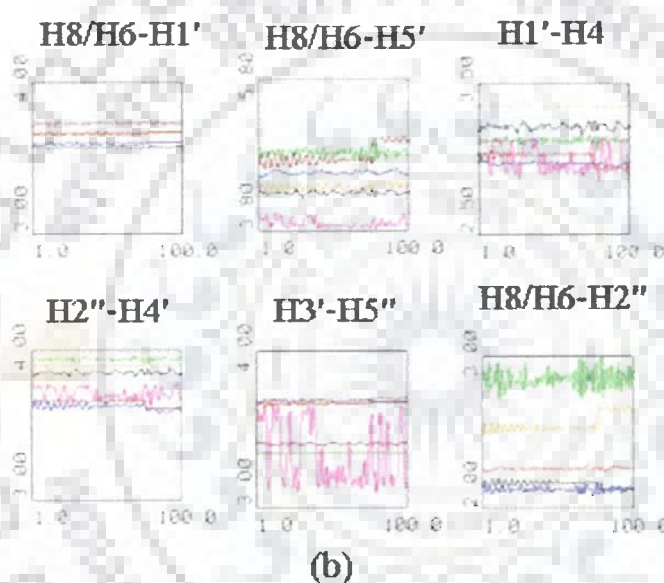
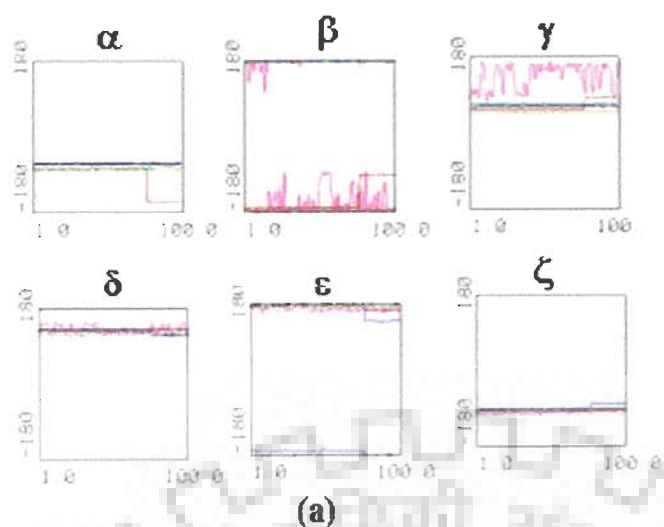


Figure 4.6: Trajectory analysis of 100 ps restrained molecular dynamics simulations in rMD-B1-100 structure of d-TGATCA showing variations in (a) torsional angles α , β , γ , δ , ϵ , ζ in each nucleotide residue : T1-magenta, G2-green, A3-black, T4-blue, C5-red, A6-orange (b) intra nucleotide inter proton distances H8/H6-H1', H8/H6-H5', H1'-H4', H2''-H4', H3'-H5'' as well as inter nucleotide inter proton distance H8/H6-H2'' at different base pair steps : T1pG2-green, G2pA3-blue, A3pT4-red, T4pC5-black, C5pA6-orange

the 3' linked C residue in TpGpC element, which exhibited single conformation but a large standard deviation. Similar trans conformation has been observed in CpG step in a crystal structure of self-complementary A-DNA octamer and its 3' methylene phosphate analogue (Olson et al, 2001). The crystal structure of topoisomerase II poison 9-amino-[N-(2- dimethylamino)ethyl]acridine-4-carboxamide bound to d-CGATCG (Adams et al, 1999) also shows that γ for G2 residue (at the site of intercalation) exists in trans conformational state. The change in torsional angles γ , indicating rotation about C5'-C4' bond, from +gauche to trans state brings H5' and H5'' much closer to the base H8/H6 and H3' protons, respectively (Weisz et al, 1994). In the $\gamma(t)$ state, the substituents H5', H5'' and O5' atoms at the C5' atom position remain staggered and hence are in energetically favorable conformation. The intra nucleotide distances (d) for $\alpha(g^-)$ $\beta(t)$ $\gamma(g^+)$ conformational state occurring normally in B-DNA are : $d(H8/H6-H5') > 4.2 \text{ \AA}$ and $d(H3'-H5'') \sim 3.6 \text{ \AA}$. When γ angle adopts trans conformation the distances are considerably reduced; being $d(H8/H6-H5') \sim 3.4 \text{ \AA}$ and $d(H3'-H5'') < 3.0 \text{ \AA}$. Our experimental results show cross peaks corresponding to H3'-H5'' NOE connectivities for all residues. Some of the distances could not be ascertained accurately due to overlap of peaks but they were found to lie in the range 3.0-3.6 \AA . On the other hand, the NOE cross peak corresponding to base H8/H6-H5' was observed only for T1 residue, the distance being 3.7 \AA (Table 4.1a). This is consistent with the results on rMD simulations which show that γ shifts from g^+ to t state for T1 residue only. For C5 residue it alters by $\sim 30^\circ$ but remains close to g^+ state. Unfortunately there are no direct inter proton distances in our NOESY spectra, which could ascertain the change in conformation due to change in torsional angle α and β . It may thus be concluded that due to conformational flexibility at TpG/CpA

Table 4.5: Two conformational states of T1 ad C5 residues in d-TGATCA observed in 100 ps restrained Molecular Dynamics simulations

Conformer	H1'-H4'	H2''-H4'	H6-H5'	H3'-H5''	^c α	^c β	^c γ	δ	ϵ	χ
	(Å)	(Å)	(Å)	(Å)	(°)	(°)	(°)	(°)	(°)	(°)
^a T1 1	3.1	3.8	4.0	3.6	-	-180 (t)	90 (g ⁺)	140	170	-89.7
2	2.9	3.7	3.9	3.2	-	-85 (g ⁻)	160 (t)	120	160	-86.1
^b C5 1	3.1	3.7	4.8	3.7	-80 (g ⁻)	-170 (t)	60 (g ⁺)	125	178	-105.3
2	2.9	3.6	5.2	3.8	-150 (t)	-90 (g ⁻)	90 (g ⁺)	115	170	-99.0

^aConformers 1 and 2 correspond to conformational states adopted during time intervals 0-40 ps and 41-72 ps, respectively.

^bConformers 1 and 2 correspond to conformational states adopted during time intervals 1-75 ps and 76-100 ps, respectively.

^cThe conformational state occurring normally in B-DNA is $\alpha(g^-) \beta(t) \gamma(g^+)$.

steps, the T1 and C5 residues change from $\beta(t) \gamma(g^+)$ to $\beta(g^-) \gamma(t)$ and $\alpha(g^-) \beta(t) \gamma(g^+)$ to $\alpha(t) \beta(g^-) \gamma(g^+)$ states, respectively. In order to understand the flexibility of backbone in d-TGATCA, we examined the inter proton distances of various intra residue and inter residue base to sugar protons in rMD simulations up to 100 ps. The base H8/H6 to H1' distance within residue depends only upon glycosidic bond rotation, χ . This distance showed negligible variations with time (Fig. 4.6b) and therefore χ does not change appreciably. The base H8/H6 to H2', H2'', H3' distances within a residue are a function of pseudorotation P and χ . They are also found to be very stable with time. The distances H1'-H2', H1'-H2'', H1'-H3', H2'-H3', H2'-H4' do not show any variation with time for any of the residues. The distances H1'-H4' and H2''-H4' show noticeable change for only T1 and C5 residue (Fig. 4.6). For T1 residue, distances H1'-H4' and H2''-H4' fluctuate within the range 3.1-2.9 Å and 3.8-3.7 Å, respectively. As discussed earlier, the distance H1'-H4' is a marker for P_S value and does not vary with mole fraction of N- or S-conformer while distance H2''-H4' decreases significantly with increase in mole fraction of N-conformer. The observed distances, H1'-H4' and H2''-H4', for T1 and C5 residue in two conformational states during rMD simulations (Table 4.5) correspond to a change in P from $162^\circ/180^\circ$ to $\sim 153^\circ$ (also reflected as variation in δ , Fig. 6) and a mixing of 5-10 % of N-conformer to the predominant S-conformation. Thus it may be inferred that P and χ_S are flexible only to a limited extent. The corresponding change in distance H8/H6-H5' and H3'-H5'' during rMD simulations for T1 residue show that torsional angle γ does take up trans conformation as these distances are ~ 3.9 and 3.2 Å at time interval of 41-72 ps. The distance base H8/H6-H5' for C5 residue however is large in both the states during 1-75 ps and 76-100 ps (Table 4.5) and therefore there is no

evidence of existence of trans conformer for angle γ . Further it is noteworthy that the base H8/H6-H2" distance at various base pair steps monitored with time shows corresponding fluctuations/flexibility only at TpG and CpA steps (Fig. 4.6).

The trajectory analysis thus shows that the amplitude and frequency of motions are different at various sites in d-TGATCA. The orientation of base with respect to sugar and the sugar puckers themselves do not show variation through the course of simulation. The relatively large variation in sequential distance and backbone torsional angles α , β , γ at TpG and CpA steps show that backbone is relatively more dynamic. This cannot be attributed to the end effect (due to fraying at either 5' end or 3' end of the helix) as in that case distances and torsional angles corresponding to A6 residue would be expected to show variation with time. The flexibility at TpG and CpA base pair step is corroborated by experimental results obtained by NMR, which correspond to the conformational averaging over different states. The complexities and variability in the motion in DNA contribute to the sequence dependent flexibility and deformability of DNA. The conclusions drawn have important implications in protein-DNA and drug-DNA interactions. Our findings are particularly significant in view of the occurrence of TpG/CpA element in several DNA sequences involved in regulation of gene expression as well as binding to ligands/drugs (Bacolla et al, 1997; Chastain et al, 1998; d'Langlois et al, 1992; Kabsch et al. 1982; Kemler et al, 1989; Leonard et al, 1993; Leonard et al, 1992; Lyubchenko et al, 1993; Nunn et al, 1991; Sarai et al, 1989; Schultz et al, 1991; Trifonov et al, 1986; Weisz et al, 1994). The existence of torsional angle γ in trans state (instead of conventional +gauche state) in a specific drug-DNA complex (Adams et al, 1999) at the ligand binding site only, further demonstrates that studies on sequence dependent variations are directly relevant to recognition of binding sites at DNA.

RESTRAINED MOLECULAR DYNAMICS STUDY ON DRUG-DNA COMPLEX: d(CGATCG)₂ WITH ADRIAMYCIN

Solution structure of adriamycin-d(CGATCG)₂ complex have been analyzed in our laboratory (courtesy Nandana Srivastava). Their NMR data was utilized to obtain the restraint data set, which consists of several intramolecular and intermolecular nuclear Overhauser enhancement cross peaks. The intensities of cross peaks of 2D NOESY spectra at two mixing times, $\tau_m = 150$ and 200 ms, were used to extract the experimental restraints of interproton distances. C1H5-C1H6 peak of cytosine was used as the reference using a distance = 2.46 Å. A range of ± 0.3 Å was provided to distances to account for any errors in integration.

5.1 STRATEGY FOLLOWED

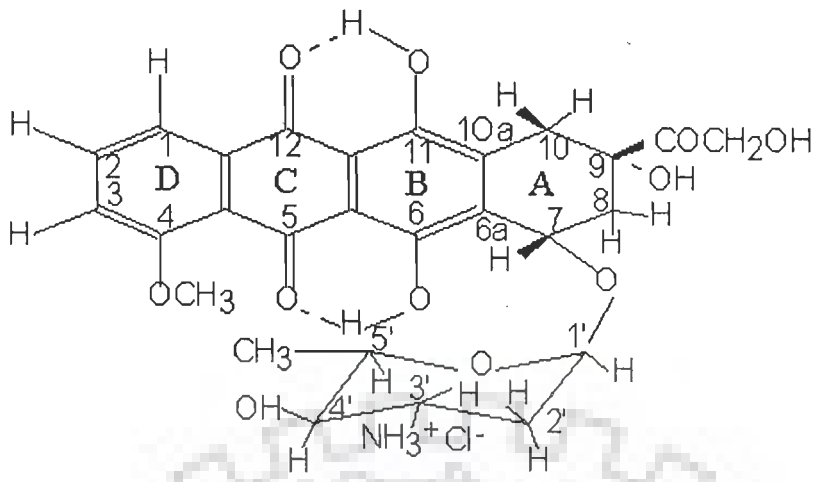
The energy minimization and molecular dynamics calculations were carried out using AMBER 6.0 software (courtesy Prof. Peter Kollman, UCSF, California) on Unix platform using PARAM 10000 super computing facility. Initial model building was carried out using xleap and antechamber modules of AMBER 6.0. Starting structure of 2:1 complex of adriamycin-d(CGATCG)₂ was taken from Brookhaven protein data base (PDB Id: 1D12.pdb). AMBER reads all the atoms of DNA but does not have database for drug molecule. Modification of initial structure was done using INSIGHT II on Silicon Graphics workstation. MOPAC generated the charge while antechamber module of the AMBER prepared the database for the adriamycin molecule. Counterions and hydrogen atom with standard geometry were added to the system by xleap module. This structure was then optimized to remove any bad

van der waal's contacts and to minimize counterions keeping all heavy atoms of the complex fixed. All molecular structures were displayed using the visual molecular dynamics (VMD) software on a Linux workstation. Minimization and restrained molecular dynamics were carried out in vacuum. A distance dependent dielectric constant was used during simulations in vacuum for restrained molecular dynamics (rMD) calculations to mimic the presence of a high dielectric solvent. Pseudoatom corrections were used for methyl and other equivalent protons. The SANDER (simulation annealing with NMR driven energy restraints) module in AMBER 6.0 was used to perform energy minimization and dynamics. To maintain right-handedness and prevent structural artifacts during the simulations, the base pair Watson-Crick hydrogen bonding scheme was also maintained by applying hydrogen bond restraints. A cut off value of 9.0 Å was chosen to calculate all nonbonded interactions in the system. All runs were performed at constant temperature of 300 K. The temperature was regulated by bath coupling using the Berendsen algorithm. Forcefield parm99 of AMBER 6 was used. The energy of the system was minimized using 1000 steps each of steepest descent and conjugate gradient using a total 266 intrasidue and 16 interresidue distance restraints. A typical rMD run consisted of 100 ps simulations with time step of 1 fs. General simulation parameters were kept constant during the complete run of molecular dynamics simulations and structural information was collected after every 4 ps.

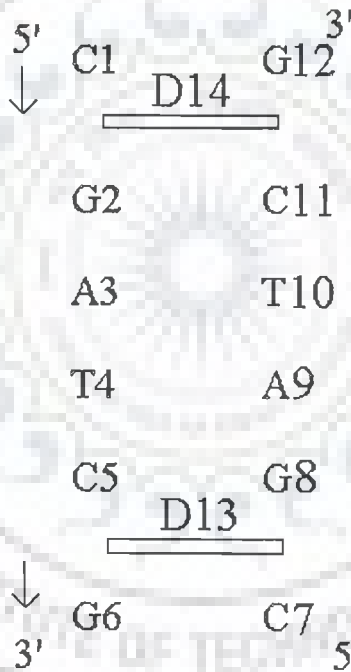
5.2 RESULTS AND DISCUSSION

The nucleotides are labelled from C1 to G6 in the 5' to 3' direction on strand 1 and from C7 to G12 on strand 2 with C1 base paired to G12. The adriamycin molecules are numbered D13 and D14 and the atomic numbering scheme for the molecule is

shown in Fig. 5.1a. The schematic representation of the drug chromophore intercalated between d-C1pG2 and d-C5pG6 sites are shown in Fig. 5.1b. A typical 2D NOESY spectra of complex indicating some of the intermolecular NOEs is shown in Fig. 5.2. Tables 5.1a-c and 5.2 give the interproton distances observed within the DNA hexamer and within the drug protons of the complex, respectively. Table 5.3 lists the interproton distances corresponding to observed intermolecular NOEs between drug and DNA protons. However no sequential NOE connectivity between C1 and G2 or C5 and G6 bases was observed indicating the intercalation of drug chromophore at the two d-CpG steps. The position of anthracycline aglycone as well as daunosamine sugar gets defined by many of these observed NOEs. Best fit refined structure showing all atoms is given in Fig. 5.3. The root mean square deviation between the rMD structure and the starting structure is quite large but among various final structures is very low. This is generally acknowledged as an indication that convergence has been achieved. Table 5.4 indicates an assessment of refined structure in terms of energetics and distance deviation from the target distance. The total potential energy of the final structure is $-768 \text{ Kcal mole}^{-1}$, which is much lower than the initial B-DNA structure. The restraint energy has also reduced from $848 \text{ Kcal mole}^{-1}$ to $202 \text{ Kcal mole}^{-1}$. Table 5.5 shows the pairwise as well as residue wise root mean square deviations (RMSD) of the complex. The starting structure was chosen as reference and the value of target RMSD is chosen to be 0.0. It may be noted that distance deviation reached a minimum of 0.6 \AA from an initial average deviation of 1 \AA .



(a)



(b)

Figure 5.1: (a) Molecular structure of adriamycin and (b) Schematic representation of the 2:1 complex of adriamycin with d-(CGATCG)₂

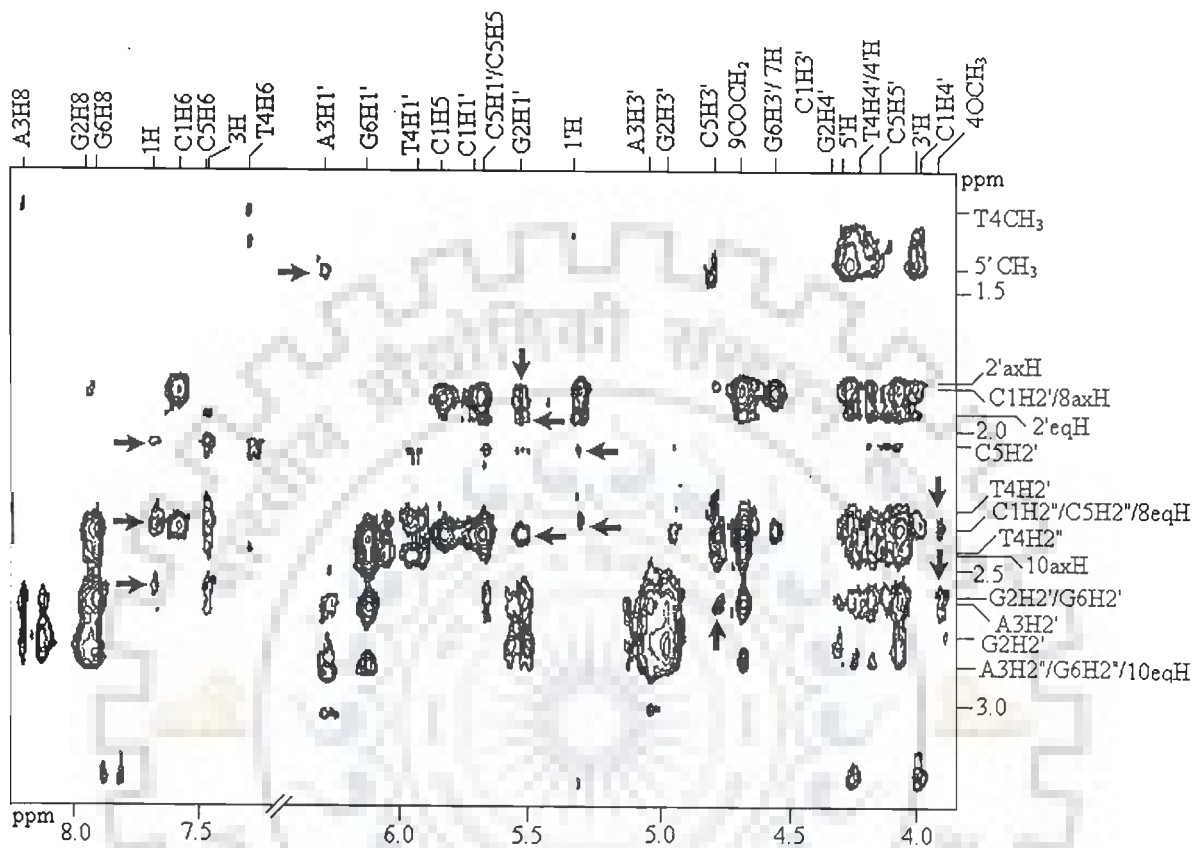


Figure 5.2: NOESY spectrum of 2:1 adriamycin-d-(CGATCG)₂ complex in D₂O at 295K showing some of the intermolecular peaks (→) (Courtesy: Nandana Srivastava)

Table 5.1a: Some of the interproton distances (Å) from inter residue sequential connectivities in hexanucleotide observed in NOESY spectra of the drug-DNA complex at drug to DNA ratio (D/N) = 2.0

A3H8-G2H1'	3.8
A3H8-G2H2'	2.6
A3H8-G2H2''	2.4
A3H5''-G2H1'	3.2
T4H6-A3H1'	3.8
T4H6-A3H2'	4.0
T4H6-A3H2''	2.3
T4CH ₃ -A3H8	3.8
C5H6-T4H1'	3.6
C5H6-T4H2'	3.8
C5H6-T4H2''	2.6
C5H5-T4H1'	3.8

Table 5.1b: Interproton distances (Å) obtained from intranucleotide NOE connectivities (d_i) within sugar protons of hexanucleotide of the drug-DNA complex at drug to DNA ratio (D/N) = 2.0

Protons	C1	G2	A3	T4	C5	G6
H1'-H2'	2.8	2.7	2.9	2.6	2.9	2.7
H1'-H2''	2.2	2.2	2.2	2.2	2.2	2.2
H1'-H3'	3.9	3.6	3.6	3.9	3.9	3.6
H1'-H4'	3.0	3.3	3.0	2.7	3.0	3.1
H1'-H5'	-	-	2.6	-	-	-
H1'-H5''	-	-	-	-	2.9	-
H2'-H3'	2.3	2.3	2.3	-	3.3	2.3
H2''-H3'	2.6	2.5	2.5	-	2.8	2.6
H2'-H4'	2.7	3.0	3.3	2.7	3.0	2.8
H2''-H4'	2.7	2.9	3.3	2.8	2.9	2.6
H2'-H5''	-	-	-	-	-	-
H2'-H2''	2.0	1.8	2.2	1.8	1.8	1.8
H3'-H4'	2.9	2.6	2.5	2.7	2.8	2.6
H3'-H5'	3.1	2.7	-	1.9 ^o	2.1	3.1
H3'-H5''	4.0	3.6	-	-	2.6	-
H4'-H5'	1.8	2.8	2.0	-	-	1.9
H4'-H5''	2.8	3.2	2.0	2.2	2.2	2.2
H5'-H5''	1.9	1.8	1.7	1.8	1.8	1.8

o = overlap of peaks

- absence of cross peaks

Table 5.1c: Interproton distances (Å) obtained from intranucleotide NOE connectivities (d_i) of base to sugar protons of hexanucleotide in the drug-DNA complex at drug to DNA ratio (D/N) = 2.0

Protons	C1	G2	A3	T4	C5	G6
H8/H6-H1'	3.2	-	-	-	2.5 ^o	3.1
H8/H6-H2'	2.4	2.3	2.5 ^o	-	2.5	2.3
H8/H6-H2''	2.7	2.5	3.0	3.0	2.7	2.5
H8/H6-H3'	-	3.8	3.7	-	-	3.1
H8/H6-H4'	-	-	-	-	-	2.7
H8/H6-H5'	3.0	-	-	-	-	-
H8/H6-H5''	3.1	-	-	-	-	-

o = overlap of peaks

- absence of cross peaks

Table 5.2: Interproton distances (Å) obtained from intramolecular NOE connectivities within the drug molecule in the drug-DNA complex at drug to DNA ratio (D/N) = 2.0

J coupled Protons		Within Sugar Protons		Ring A with sugar Protons		Within Ring D Protons		Within Ring A Protons	
1H-2H	2.5	1'H-3'H	3.1	7H-1'H	2.0	1H-4OCH ₃	2.8	10 _{ax} H-8 _{ax} H	3.0
2H-3H	2.5	1'H-4'H	3.2	7H-3'H	2.1	2H-4OCH ₃	2.9	10 _{ax} H-8 _{eq} H	-
1'H-2' _{ax} H	2.6	1'H-5'H	2.9	7H-4'H	2.2	3H-4OCH ₃	2.2	10 _{eq} H-8 _{ax} H	-
1'H-2' _{eq} H	2.6	1'H-5'CH ₃	-	7H-5'H	2.3			10 _{eq} H-8 _{eq} H	2.5
3'H-4'H	2.4	3'H-5'H	o	7H-5CH ₃	-				
4'H-5'H	2.4	3'H-5'CH ₃	-	8 _{ax} H-1'H	o				
3'H-2' _{ax} H	3.0	4'H-2' _{ax} H	o	8 _{ax} H-3'H	2.4				
3'H-2' _{eq} H	2.6	4'H-2' _{eq} H	2.6	8 _{ax} H-4'H	2.6				
2' _{ax} H-2' _{eq} H	o	4'H-5'CH ₃	2.5	8 _{ax} H-5'H	o				
5'H-5'CH ₃	2.1			8 _{ax} H-5'CH ₃	-				
7H-8 _{ax} H	2.2								
7H-8 _{eq} H	2.3								
8 _{ax} H-8 _{eq} H	2.2								
10 _{ax} H-8 _{eq} H	2.2								

o = overlap of peaks

- absence of cross peaks

Table 5.3: Interproton distances (Å) obtained from intermolecular NOE connectivities within the drug molecule in the drug-DNA complex and those obtained from model after rMD simulations

Protons	NMR	Model
C1H5-1H	3.3	3.8
G2H1'-10eqH	3.0	3.2
A3H1'-5'CH ₃	3.2	2.6
C5H6-4OCH ₃	2.2	2.6
C5H6-1H	3.4	6.8
C1H2'' / C5H2''-4OCH ₃	3.3	3.2
C5H5-1H	2.6	5.5
C5H4'-2'eqH	3.6	3.0
C5H1'-2'eqH	2.6	2.6
C5H5-3H	3.5	3.7
C5H4'-2axH	-	3.5
C5H4'-2eqH	-	3.0
G6H5'-1'H	3.0	2.4
G6H5'-2axH	2.5	2.9
G6H5'-2'eqH	2.6	2.8
G6H1'-1'H	3.5	3.8
G6H1'-7H	3.1	3.3
G6H5''-1'H	3.2	3.6
G6H4'-1'H	3.0	2.9

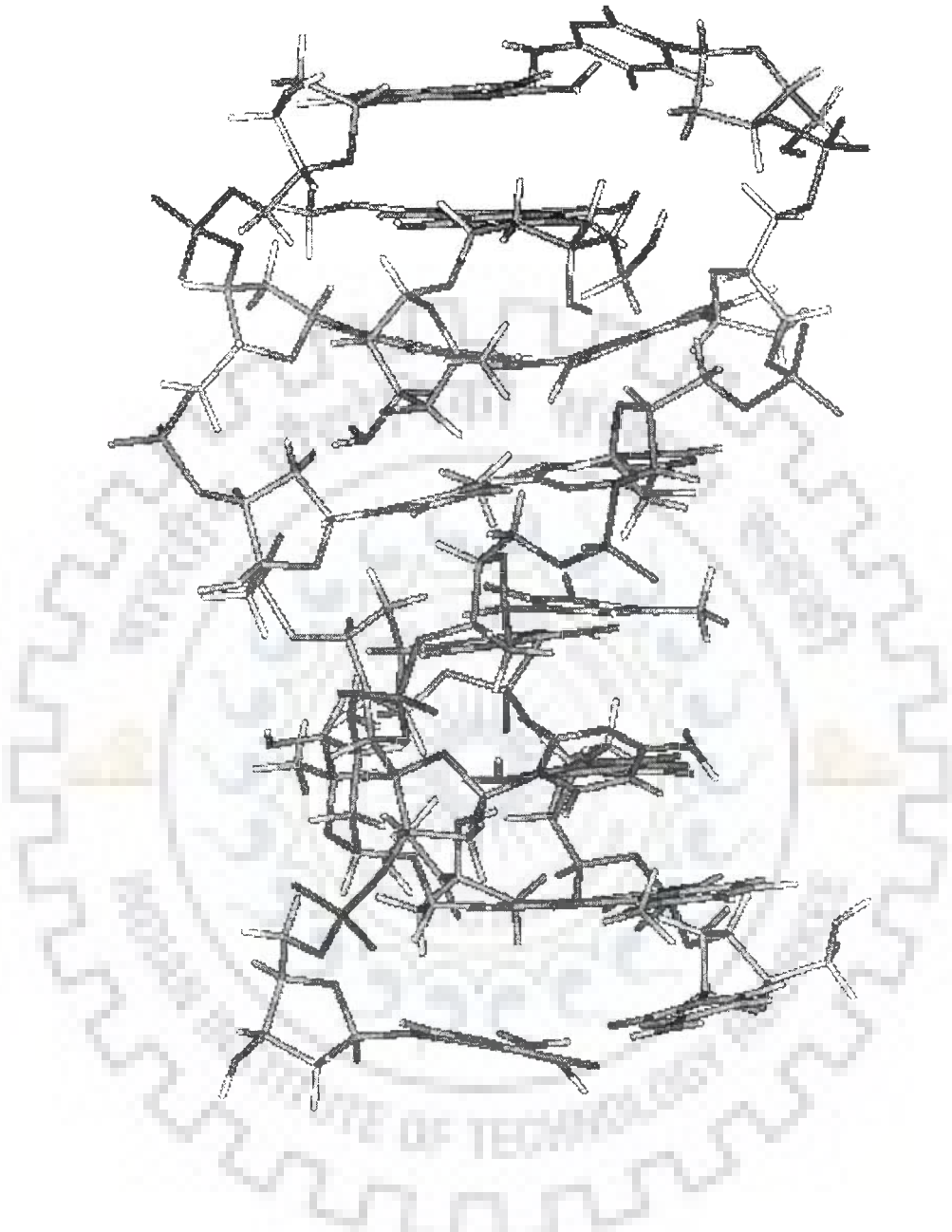


Figure 5.2: Stereo view of the final rMD structure

Table 5.4: Energy terms (Kcal mol⁻¹) for starting model and final rMD structure

Structure	Total	Bond	Angle	Dihedral	Vdw
Initial	915	325	472	222	-176
Final	-768	29	144	254	-161
	Repulsion	Dispersive	Electrostatic	Restraint	Δd^a
Initial	-508	210	-478	848	1.00
Final	-541	152	-846	202	0.60

^aAverage distance deviation

Table 5.5: Summary of experimental restraints and statistical analysis of final structure generated by restrained molecular dynamics (rMD)

Parameter	No. of Distance Restraints
Intra residue	266
Inter residue	34
Average pairwise RMSD	Initial = 0 Final = 0.62
Average residewise RMSD	C1=0.87, G2=1.17, A3=0.62, T4=0.62, C5=0.62, G6=0.62 Adriamycin = 0.77

5.2.1 Conformation of DNA

All helical parameters, backbone torsional angles and sugar conformations of the resulting rMD structures were thoroughly analyzed with the program CURVES, version 5.1 (Lavery and Sklenar, 1989; Lavery and Sklenar, 1996). Plot of some helicoidal parameters (global, unless specified otherwise) as a function of residue position in the duplex is shown in Fig. 5.4 along with that for classical structures of A-DNA and B-DNA. Among the base pair axis parameters, the x-displacement (dx) and y-displacement (dy) are found to vary to a large extent for all base pairs. Large displacements (upto 4 Å) have earlier been observed in intercalated complexes (Frederick et al, 1990; Langlois d' Estaintot et al, 1992; Leonard et al, 1992). The base pairs are inclined at an angle (η) upto 11°, the inclination being larger at 5' end. The tip angle also fluctuates along the base sequence. The variation in shear, stretch, stagger and buckle are fairly large for the CG base pairs at both ends. The propeller twist for the A3.T4 base pair is large and negative (-16°). The positive value of propeller twist at either ends may be due to fraying effects at both ends (Chen and Patel, 1995). Among the interbase parameters, the observed shift (Dx) and slide (Dy) vary in the range -1.3 to +1.9 Å. Large variation upto 1.9 Å have also been observed on formation of intercalated complexes of daunomycin with deoxytetranucleotides (Davies et al, 2000). The rise per residue (Dz) is 3.4 Å at A3pT4 base pair step while that at C1pG2 and C5pG6 base pair step increases upto 8.2 Å to accommodate drug chromophore. The intercalation results in large amount of tilt (ζ) in base pairs. The tilt varies in the range 5° to -19.5°. Large values of tilt, in the range -6° to 12° have been observed as a result of intercalation of daunomycin in CG base pairs (Davies et al, 2000). The roll angle (ρ) varies within $\pm 7^\circ$. Positive roll opens the angle between the

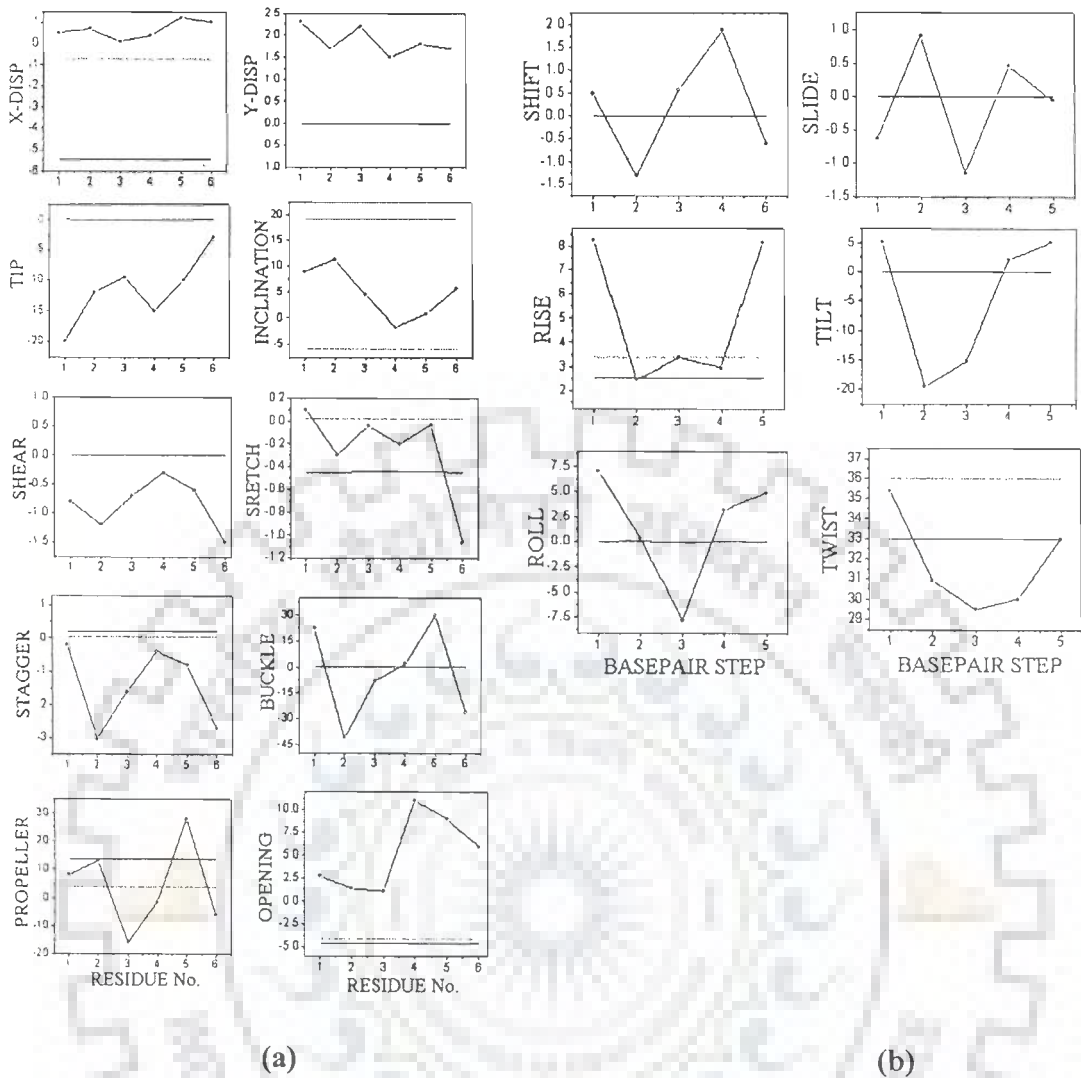


Figure 5.4: Helical parameters (a) base pair axis and base base (b) inter base pair of adriamycin-d-(CGATCG)₂ complex and that calculated for canonical A-DNA (—), B-DNA (---) and of final structure (●) obtained by restrained molecular dynamics simulations

base pairs towards the minor groove; as a result a wider minor groove and bending towards major groove causing a curvature in the helix occurs. The large positive roll at C1pG2 (+7°) and C5pG6 (+5°) steps also indicates reduced base stacking. This may be due to the fact that intercalating anthracycline ring chromophore is oriented approximately perpendicular to the base pair axis in the helix, as found in the crystal structures of the complexes (Frederick et al, 1990; Langlois d' Estaintot et al, 1992; Leonard et al, 1992; Moore et al, 1989; Wang et al, 1987). The large negative value of the roll (-8°) for A3pT4 base pair step is compensated by a decrease in propeller twist to -16° so as to prevent destacking of the bases. The CURVES software reports both global and local helical parameters and therefore a correlation between them is expected. The local inter base parameters also show positive roll angle at both the ends of the helix and negative roll in the centre. The twist (Ω) varies in the range 29.5 to 35.4°. At the intercalation sites C1pG2 and C5pG6, the twist angle is 35.4° and 32.6°, respectively indicating that unwinding of DNA at these steps is upto 3.4°. This is consistent with several observations by viscosity techniques that unwinding angle for daunomycin, adriamycin are upto 6° (Dalgleish et al, 1974; Pachter et al, 1982) while that for some other drugs e.g. actinomycin is about 23° (Sobell and Jain, 1972). The duplex is also found to unwind at sites adjacent to intercalation site upto an angle of 6.5°, as also reported in the case of some other intercalating drugs (Chen and Patel, 1995). The overall helix bend is fairly large (~18°). The groove widths of the double helix are defined using the coordinates of the phosphate atoms. In the hexanucleotide only one major and one minor groove exists in the middle of the helix. In the rMD structure of the complex the width and depth of major groove is 12.3 Å and 2.2 Å while the corresponding values for minor groove are 7.4 Å and 4.0 Å, respectively.

Thus the minor groove is wider perhaps to allow proximity of daunosamine sugar moiety (Trieb et al, 2004). A comparison of observed helical parameters with that found in crystal structure of adriamycin-d-CGATCG complex (Frederick et al, 1990) reveals that inclination of base pair axis and helical twist are nearly same in the two cases. However the roll, propeller twist and the buckle are quite different in solution structure and solid-state structure. Large amount of buckle (upto 36°) at d-CpG site as a result of intercalation has been reported recently (Trieb et al, 2004).

The values of torsional angles along with the values for canonical B-DNA and A-DNA are given in Table 5.6. The torsional angles are not equal in the two strands of the duplex. The difference in absolute values of torsional angles is upto 15° but the general features and trends with base sequence are strikingly identical. The backbone torsional angles are not defined by the restraints obtained from NOESY spectra. We have used a low force constant to permit a smooth search, which is conformationally compatible with other structural features. The torsional angles α , β and γ adopt gauche⁻, trans and gauche⁺ conformations, respectively. The torsional angle ζ however deviates from the normal gauche⁻ conformation and adopts a trans conformation for the G2 and C5 bases. This may be attributed to the opening of base pair at these sites. This is accompanied by a corresponding deviation in torsional angle ϵ for G2 and C5 bases to a lower negative value of -117° and -86°, respectively as compared to a value to -169° found in B-DNA structures. The torsional angle, δ as well as pseudorotation phase angle P, deviates from the normal range around C2' endo conformation to a value of 109-110° for only T4 residue. Further, the glycosyl bond rotation, χ , of the DNA molecule measuring rotation of base around sugar varies

Table 5.6: Glycosyl and backbone torsion angles (°)

RESIDUES	α	β	γ	δ	ϵ	ζ	χ	P
C1	-	-	52	135	-132	-75	-144	144
G2	-79	183	32	149	-117	157	-88	161
A3	-66	138	51	140	176	-91	-111	164
T4	-71	187	50	109	-158	-83	-122	110
C5	-63	170	49	146	-86	171	-76	154
G6	-81	173	37	138	-	-	-94	167
C7	-	-	55	126	-74	-81	-153	153
G8	-72	161	58	138	-98	154	-98	144
A9	-87	155	43	136	171	-88	-116	188
T10	-53	177	49	130	-164	-88	-98	145
C11	-72	166	54	122	-119	-180	-64	150
G12	-69	163	60	147	-	-	-97	185
B-DNA	-63	136	54	123	-169	-108	-105	162

along base sequence. The χ angles are as follows: C1, -144° ; G2, -88° ; A3, -111° ; T4, -122° ; C5, -76° ; G6, -94° . It can thus be seen that the DNA backbone uses a nonsymmetrical mechanism to form complex with adriamycin molecule. On C1pG2 side of the backbone, the 5' deoxycytidine residue changes the glycosyl angle from an anti (-105° to -119° in B-DNA) to a low anti value (-144°). At the same time by adjusting ϵ angle from a near trans (-169° in B-DNA) to a somewhat lower value (-132°), it allows the adjacent bases to separate from 3.4 Å to 7.0 Å.

On the C5pG6 side, both nucleotide units maintain the glycosyl angle at high anti value (-76° , -94°). But, by changing the ϵ value from -169° to a near gauche (-86°) conformation in the C5 residue, it is possible to separate the neighbouring C5 and G6 bases to a distance of ~ 7.0 Å. This can be achieved by coupling it with the rotation of the phosphodiester linkage from a normal gauche-, gauche- conformation to a trans, gauche-, as observed in X-ray crystallography (Wang et al, 1987) and NMR (Mazzini et al, 1998) structures of similar complexes. Although we have not measured phosphorus-31 chemical shifts on complexation, the change in phosphodiester linkage gets reflected in the backbone torsional angles ϵ , ζ , α and β . A correlation between these torsional angles has been found on the basis of a number of B-DNA crystal structures, which have shown that two conformational states are usually observed in B-DNA, namely B_I and B_{II} . The B_I state is characterized by torsional angle α , -62° ; β , 176° ; γ , 48° ; δ , 128° ; ϵ , -176° ; ζ , -95° ; χ , -102° to -119° ; while the B_{II} state is characterized by α , -62° ; β , 176° ; γ , 48° ; δ , 144° ; ϵ , -114° ; ζ , -174° ; χ , -89° . Comparing these values with those obtained in our complex (Table 5.6), it is found that both G2 and C5 residues tend to adopt B_{II} conformation as a result of

intercalation of drug chromophore. The A3 and T4 residues remain in the stabler B_I state except that β in A3 residue shifts from the normal value of 176° to 138° and δ of T4 residue is 109° . It has been reported earlier that the idealized g^-g^- conformation of phosphodiester bond from 5' to 3' direction changes $g^-g^-tg^-g^-g^-g^-g^-tg^-$ (where t stands for trans and g^- stands for gauche-, respectively) in X-ray crystallographic (Wang et al, 1987) and NMR structures (Mazzini et al, 1998) in hexamer sequences d-CGATCG and d-CGTACG on binding to similar drugs. The trans-gauche- conformation in G2pT3 or G2pA3 step in X-ray structure (Frederick et al, 1990; Wang et al, 1987) is associated with change in β angle of T3/A3 residue (adjacent to intercalating bases) to 114° - 138° . Further in these complexes, pseudorotation $P = 105^\circ$ for T3 residue or δ angle of 72° - 92° for A3 and T4 residues have been reported. The corresponding δ or P for T4 residue in our case is 109° - 110° . Thus the conformation of A3.T4 base pair is affected by insertion of drug chromophore between adjacent d-CpG sites.

In order to have insight into the existence of different conformational states, the conformational equilibrium and hence the recognition of the most populated conformation, we analyzed the structures during the course of simulations. We have sampled conformations at an interval of every 4 ps during 100 ps run and obtained torsional angle and interproton distances. Fig. 5.5a-b shows the dynamic variation of the distances H8/H6-H1', H1'-H4' and backbone torsional angles. It is easily seen that the variations are not subject to fluctuations but are stable during all simulations and vary over a small range. The only exception being γ of G2 residue which deviates more from the average value in few structures. This is perhaps indicative of somewhat larger flexibility. Fig. 5.6a-d display results on correlation between some of the

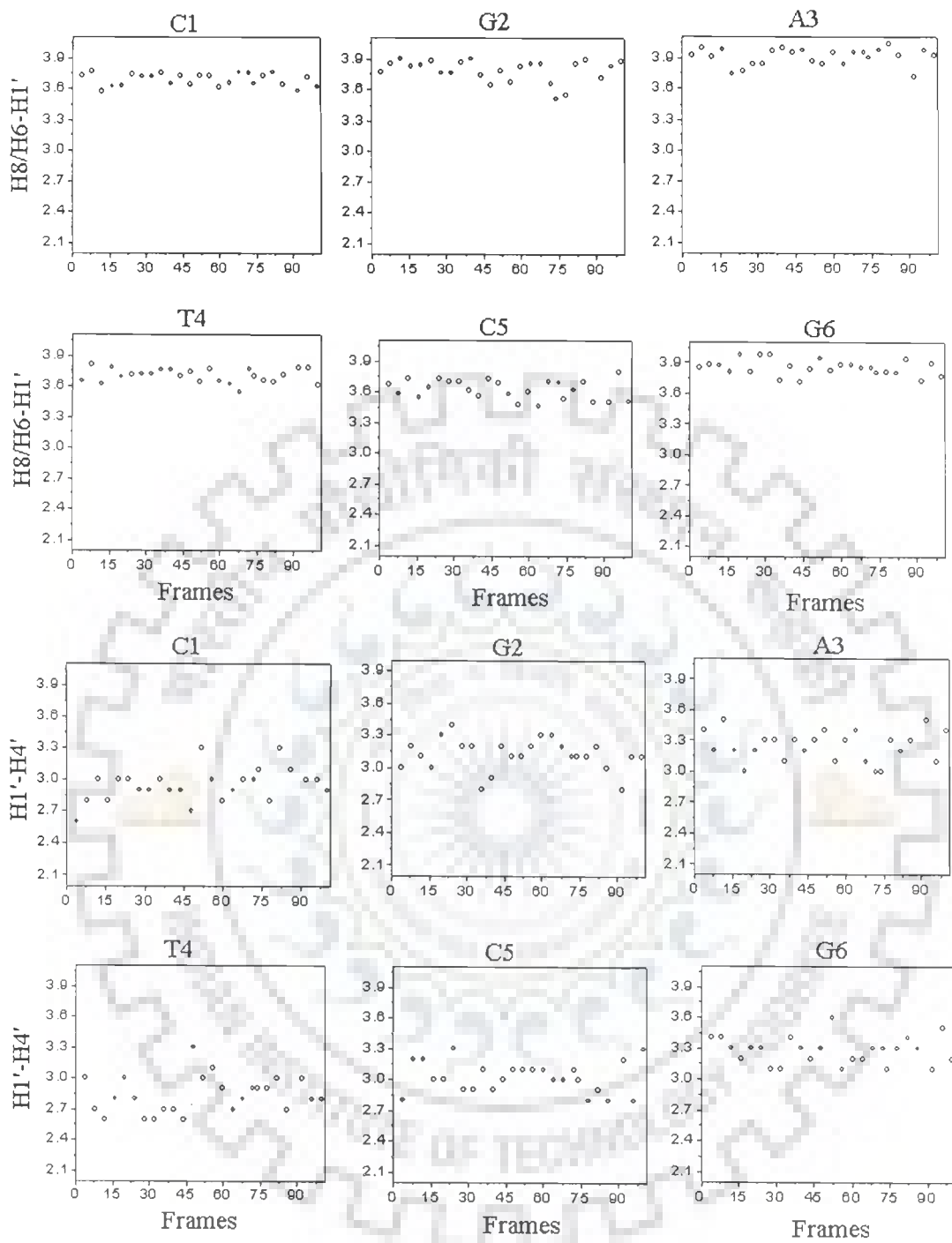
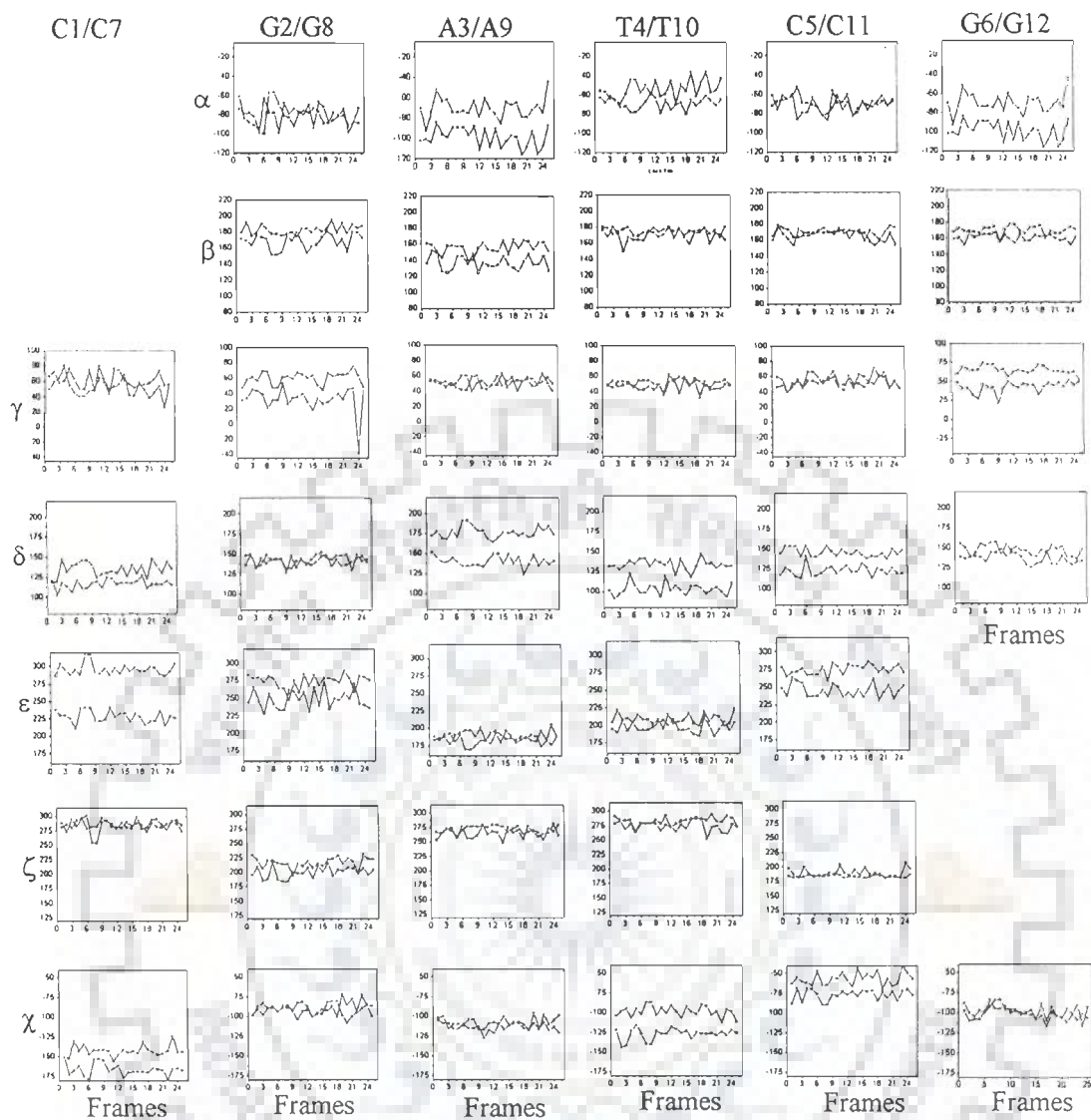


Figure 5.5(a)



(b)

Figure 5.5: Trajectory of 100 ps restrained molecular dynamics simulations showing variations in (a) interproton distances H1'-H4', H8/H6-H1' and (b) backbone torsional angles

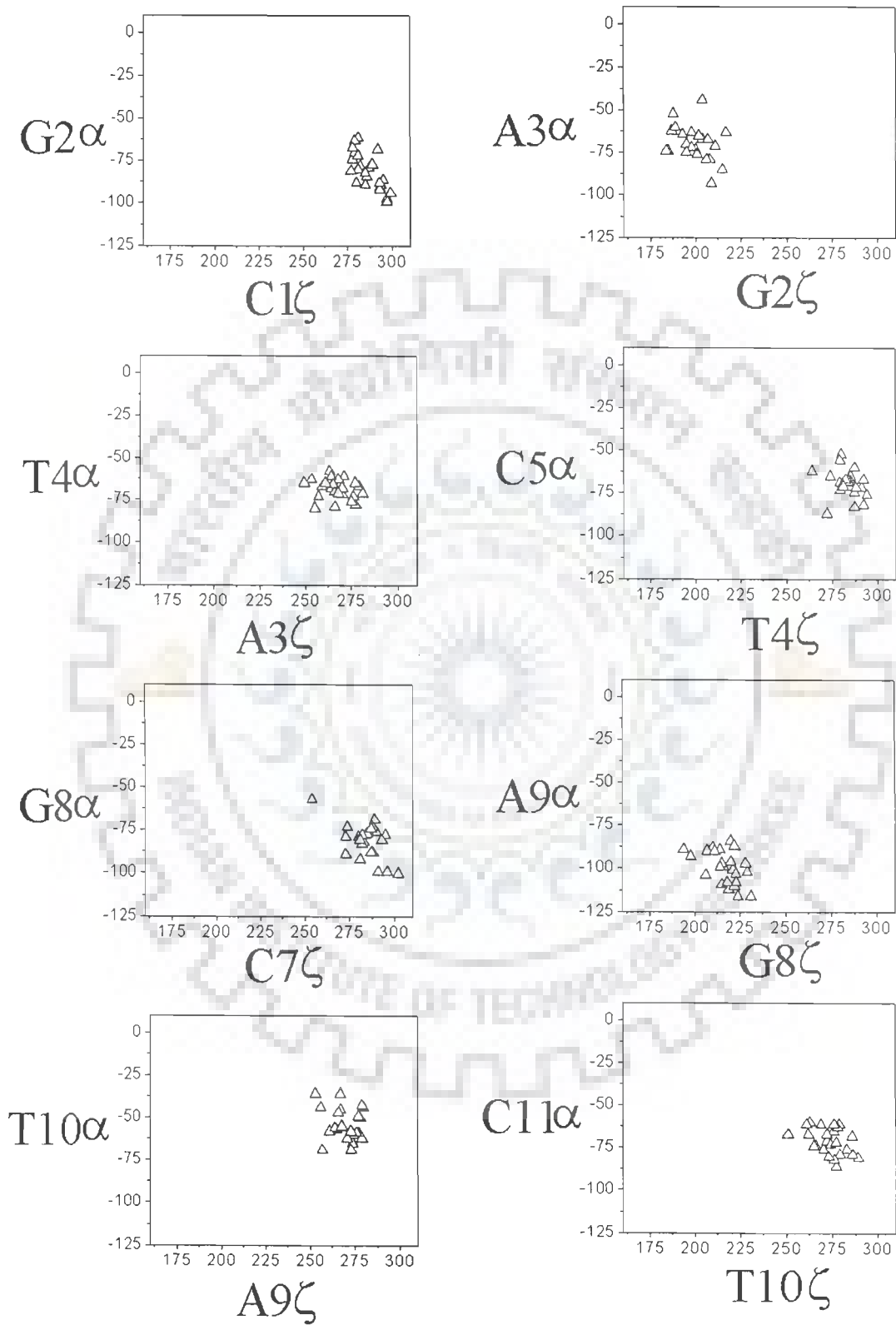


Figure 5.6(a)

torsional angles. The plot of α (of n^{th} residue) and ζ (of $n-1^{\text{th}}$ residue) torsional angles relative to each phosphate shows (Fig. 5.6a) that C1pG2, A3pT4, T4pC5 units are completely in gauche-, gauche- conformation while for G2pA3 and C5pG6 unit, a trans conformation is most stable for ζ angle. The dynamic variation in the backbone torsional angle ζ is also reflected in a change of adjacent angle ε , C4'-C3'-O3'-P.

A correlation between ζ and ε shows (Fig. 5.6b) that the variations in these two angles are coupled. The torsional angle ε deviates from the normal value of -176° to values in the range -80° to -130° whenever ζ angle adopts trans conformation for G2 and C5 residues. Thus the conformational states having torsional angles, δ , 149° ; ε , -117° ; ζ , 157° ; χ , -88° ; and δ , 146° ; ε , -86° ; ζ , 171° ; χ , -76° ; for G2 and C5 residues, respectively (Table 5.6) are indeed the most populated conformations and are close to the characteristic value of δ , 144° ; ε , -114° ; ζ , 174° ; χ , -89° ; for B_{II} conformation of DNA. Further, the β torsional angle of A3 residue deviates from an average value of 176° to lower values (Fig. 5.6c) and γ values of G2 and G6 residues (Fig. 5.6d) tend to adopt lower values in the range $32-37^\circ$ as compared to the average value of 48° . It is interesting to note that distortions at the level of third residue (A3) for angle β and at the level of G2 and C5 for ε , ζ angles have also been observed for some crystal structures (Frederick et al, 1990; Langlois d' Estaintot et al, 1992; Leonard et al, 1992).

NMR solution structure of 2-methoxy-morpholino-doxorubicin with d-CGATCG (Mazzini et al, 1998) shows that trans conformation for ε is significantly more stable for C5 residue although a broad distribution of angles were observed in their structure. There has been evidence in literature that on stretching of DNA, B_{II} conformation of

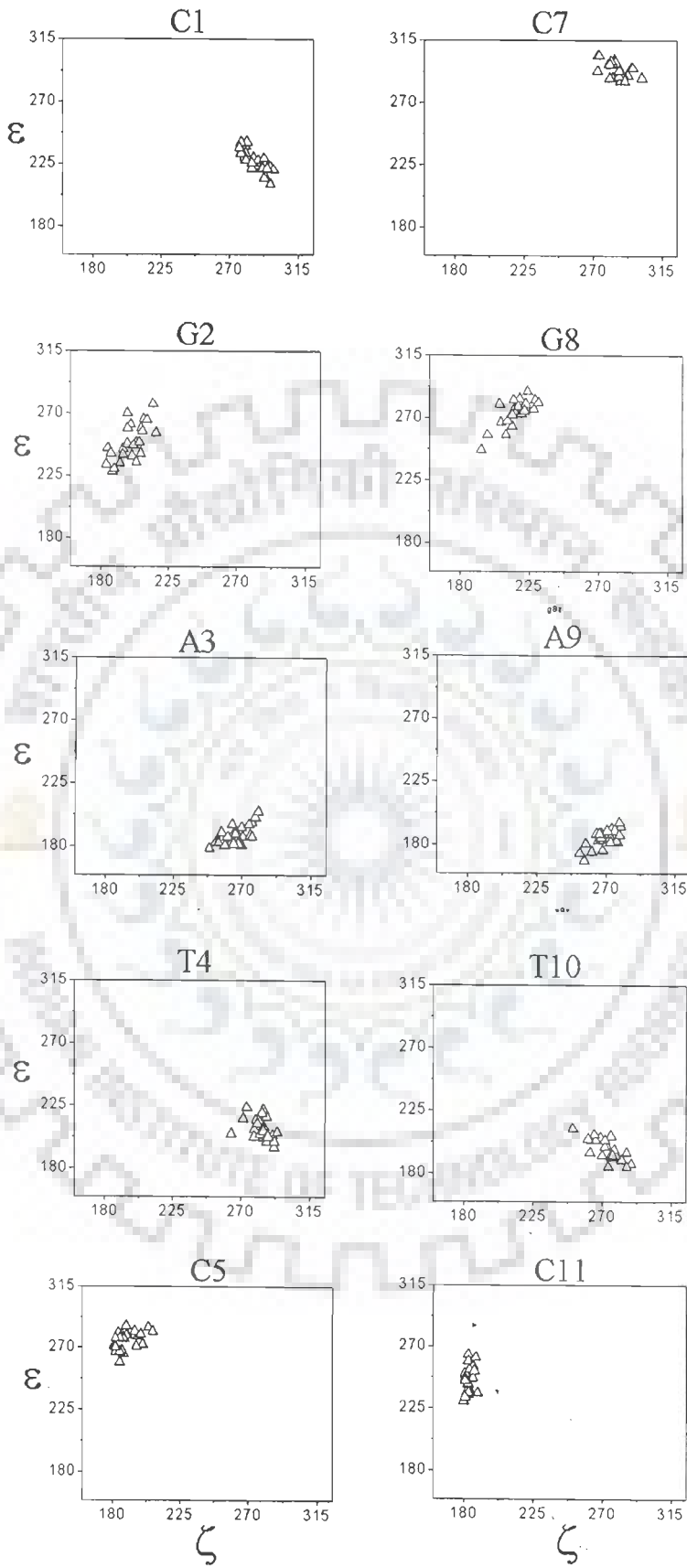


Figure 5.6(b)

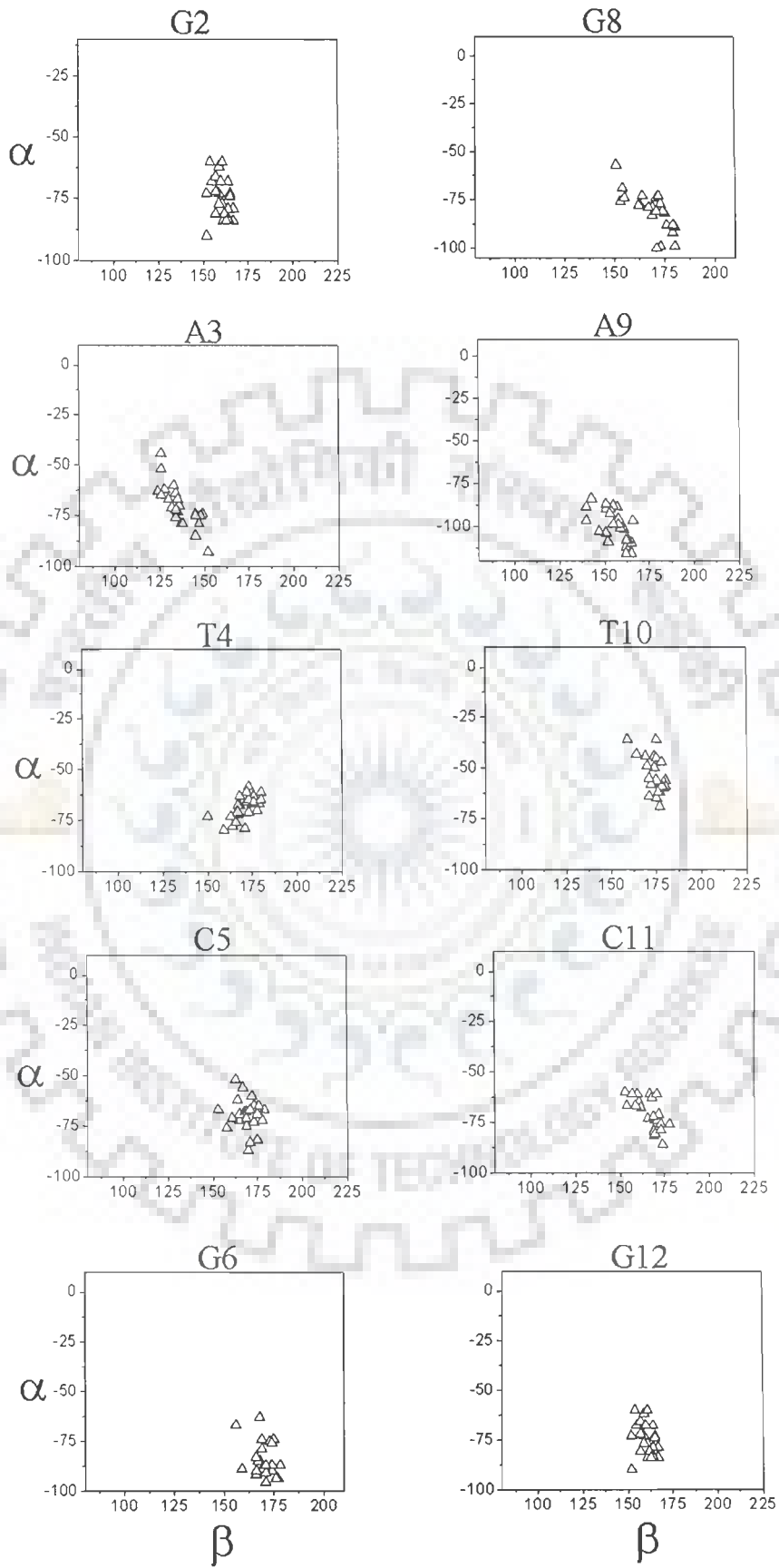
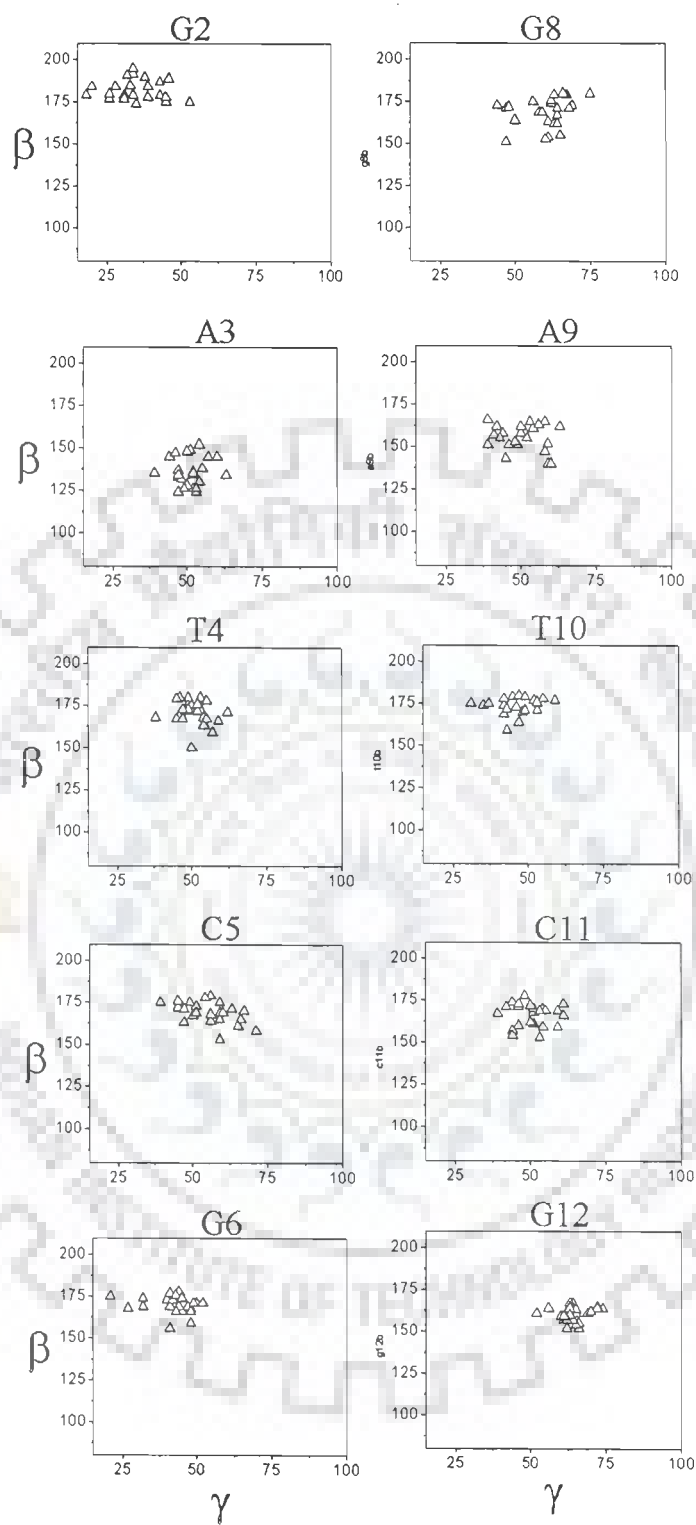


Figure 5.6(c)



(d)

Figure 5.6: Correlation obtained for torsional angles (a) α (of n^{th} residue) and ζ (of $n-1^{\text{th}}$ residue) (b) ε and ζ (c) α and β (d) β and γ

DNA becomes energetically more favourable and more pronounced (Chaires et al, 1997; Wang et al, 1987). The influence of intercalation on the B_I/B_{II} interplay has been investigated by molecular dynamics simulations of intercalation of daunomycin in 14-mer oligodeoxyribonucleotide duplex d-(CGCGCGATCGCGCG)₂ (Treib et al, 2004). It was observed that at the intercalation site C5pG6 the phosphorus is in B_I conformation and the phosphorus directly lying on the opposite strand has B_{II} conformation. Further at the site adjacent to intercalation site, that is, G6pA7 phosphorus is in B_{II} conformation and the corresponding phosphorus in opposite strand is in B_I conformation. Intercalation of daunomycin induces and stabilizes a distinct pattern of phosphates of the DNA backbone. There appears to be a possibility to directly influence the DNA backbone through complexation, hence leads to a redirection of intercalation caused structural changes to the backbone. Our observations that intercalation site C1pG2 is in B_I conformation while adjacent site G2pA3 is in B_{II} conformation and the phosphates on the opposite strands have corresponding opposite B_I/B_{II} conformation corroborate the findings in literature (Treib et al, 2004)

5.2.2 Conformation of Adriamycin

The bond distance and angles in the adriamycin molecule are within the limit of accepted values. In the aglycon part of the molecule, the B and D rings are most aromatic with an averaged C-C distance of 1.39 Å. The distance between O5 and O6 atoms and between O11 and O12 atoms are 2.71 and 2.59 Å, respectively. Thus they presumably form intramolecular hydrogen bonds. The aromatic part of the aglycon is quite planar with rms distance of 0.74 Å for the least squares plane calculated from all the atoms of ring B, C and D without the exocyclic atom. The methyl group in the

4-methoxy side chain is also in plane with a deviation of 0.76 Å. The orientation of methoxy group is such that the methyl group is pointed away from O5 atoms and protrudes into the solvent region.

The torsional angles of the adriamycin molecule in the complex are listed in Table 5.7 along with those of daunomycin derivatives in the free state (Neidle and Taylor, 1977) and in the same/similar bound complexes obtained by X-ray crystallography (Frederick et al, 1990; Moore et al, 1989) techniques. In ring A, the torsional angles around C19-C20 and C20-C7 bonds are negligible ($2-9^\circ$) while that around C8-C9 and C9-C10 bonds are $54^\circ-60^\circ$ in magnitude. Thus practically all atoms except C9 atom are out of the plane containing other atoms and aromatic rings B, C, D. The C9 atom is displaced by 0.85 Å in same direction as the amino sugar relative to the plane of aglycon molecule as a consequence of which 9OH can no longer form intramolecular hydrogen bond with 7H atom.

The torsional angles of ring A are different from that found in the X-ray crystal structure of unbound related drug, daunomycin, (Neidle and Taylor, 1977) but close to that observed in X-ray crystal structure of adriamycin with d-CGATCG (Frederick et al, 1990). The torsional angles in the glycosyl linkage, that is, around C20-C7-O7-C1' and C7-O7-C1'-C2' bond, are lower (-153° , -147°) than the corresponding angles in the pyridine salt of daunomycin molecule (Neidle and Taylor, 1977) in the free state (-114° , 167°). The difference in conformation obtained from that in other similar structures can be seen in Fig. 5.7. The amino sugar is in a chair conformation with all the side chains pointing away from the aglycon. The torsional angle around C1'-C2' bond is -47° , being shorter than the expected ideal gauche value ($\pm 60^\circ$) in the six membered ring.

Table 5.7: Selected torsional angles (°) of the adriamycin in the complex and comparison with literature

ADRIAMYCIN	Present Study CGA+adm	Moore et al CGA + adm	Frederick et al CGA + adm	Neidle et al dnm
RING A				
C20-C7-C8-C9	-39.6	-29.0	-39.9	-48.2
C7-C8-C9-C10	60.4	53.0	60.6	57.9
C8-C9-C10-C19	-54.2	-51.0	-56.0	-38.4
C9-C10-C19-C20	26.0	28.0	26.0	13.8
C10-C19-C20-C7	-1.8	-4.0	-0.8	-4.6
C19-C20-C7-C8	8.9	5.0	8.9	20.4
GLYCOSYL				
C8-C7-O7-C1'	81.6	97.0	68.2	124.9
C20-C7-O7-C1'	-152.6	-137.0	-160.4	-113.8
C7-O7-C1'-O5'	-90.4	-81.0	-74.6	-67.5
C7-O7-C1'-C2'	147.0	149.0	147.9	167.4
AMINO SUGAR				
O5'-C1'-C2'-C3'	-46.8	-58.0	-56.0	-53.8
C1'-C2'-C3'-C4'	51.5	57.0	40.0	55.7
C2'-C3'-C4'-C5'	-53.5	-18.0	-39.0	-61.2
C3'-C4'-C5'-O5'	54.6	-40.0	49.0	61.0
C4'-C5'-O5'-C1'	-55.9	47.0	-55.0	-58.8
C5'-O5'-C1'-C2'	50.2	7.0	60.0	56.5

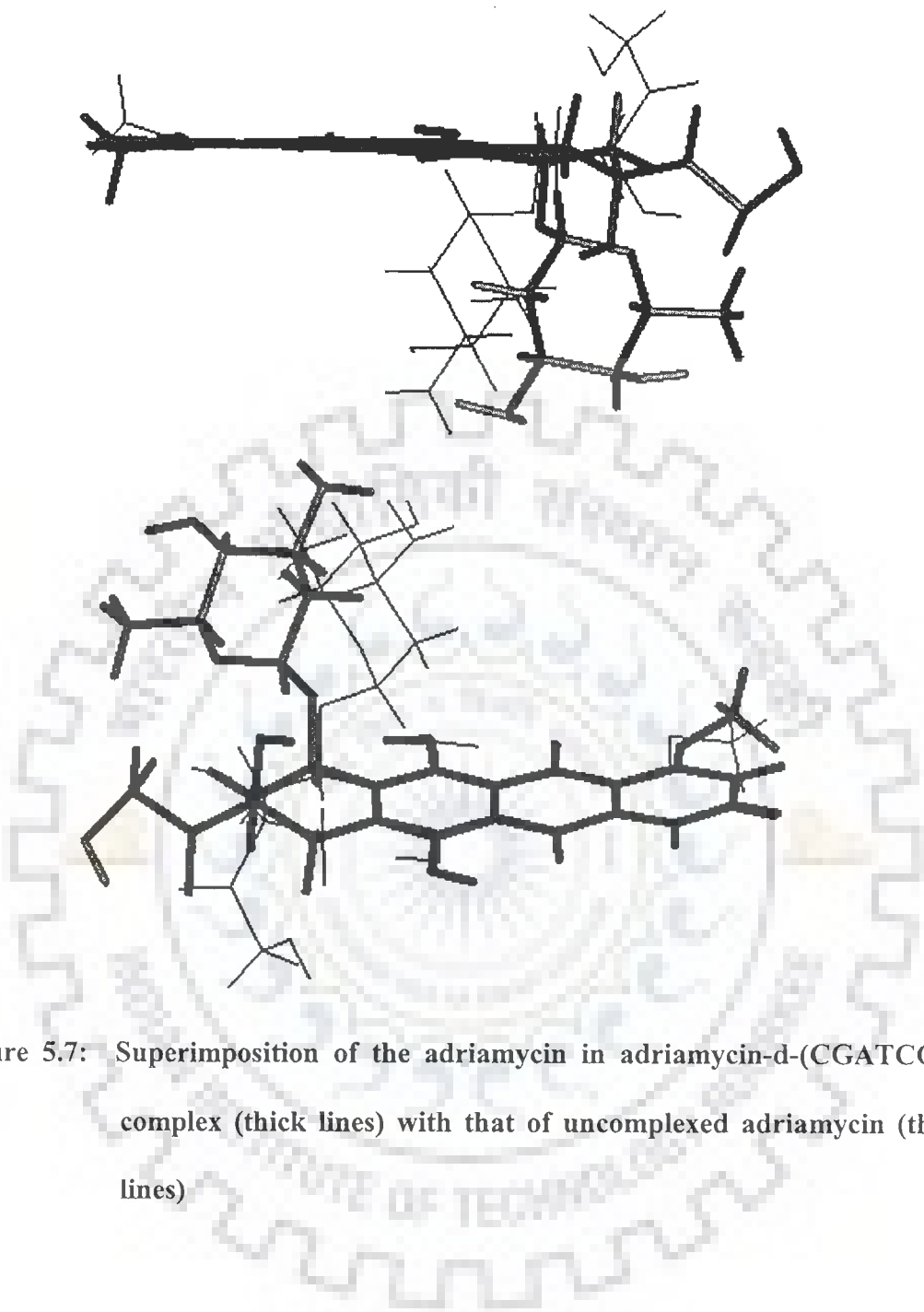


Figure 5.7: Superimposition of the adriamycin in adriamycin-d-(CGATCG)₂ complex (thick lines) with that of uncomplexed adriamycin (thin lines)

5.2.3 DNA-Adriamycin Interactions

Several inter molecular NOEs between drug protons and DNA protons have been observed and are listed in Table 5.8. The NOE cross peaks C5H6-4OCH₃, C1H5-1H, C5H5-1H, C5H5-3H (weak in intensity) clearly show that the aromatic chromophore of drug is stacked with C1 and C5 bases such that ring D of the drug chromophore points towards C1 and C5 bases. These NOE connectivities have earlier been observed by NMR studies of complexes of similar drugs with d-CGATCG or d-CGTACG sequences of DNA (Barthwal et al, 1994; Igarashi and Sunagawa, 1995; Mazzini et al, 1998; Odefey et al, 1992, Robinson et al, 1997). The observed NOEs C5H1'/C1H1'/C5H5-4OCH₃ and C1H2''/C5H2''-4OCH₃ further corroborate that ring D is close to C1 and C5 bases. The observed NOEs of G6H1' with 1'H and 7H protons indicate that ring A is close to G6 residue. Further G2H1' is in close proximity to 8axH, 8eqH and 10eqH. This orientation of aglycon moiety is possible if it is in orthogonal position with respect to C1.G6 and G2.C5 base pairs. The orientation of the amino sugar linked to 7H proton of ring A follows from these results and is further confirmed by NOE contacts such as A3H1'-5'CH₃. Several observed intermolecular NOEs (Table 5.8) define the complete geometry of the complex.

A view showing the stacking interaction of the anthracycline chromophore between the bases, - the stacking of G2.C11 base pair over A3.T10 base pair and A3.T10 base pair over T4.A9 base pair is shown in Fig. 5.8. These are somewhat similar to that existing in canonical B-DNA structures but there are significant deviations from 2-fold symmetry relating the backbone of the B-DNA molecules. The G2.C11 base pair is translated towards minor groove by ~1.3 Å and tilted with respect to A3.T10 base

pair. The A3.T10 base pair is translated along long axis of the base pair by about 1 Å with respect to next base pair along 5'-3' direction. When the chromophore of drug intercalates between the base pairs and amino sugar is in close proximity of DNA, some of the functional groups of adriamycin are involved in specific interactions with atoms of DNA. As a consequence, change in some of the substituent groups at ring A, ring D or daunosamine sugar have moderate or no influence on its biological activity. Fig. 5.9 shows the position of drug with respect to DNA molecule to illustrate some of these close contacts and interactions. It is found that the hydroxyl oxygen atom of 9OH in ring A is within the hydrogen bonding distance of N3 and N2 atoms of guanine base G2. The distance between O9 and G2N3 atom is 2.93 Å and varies in the range 2.6-3.0 Å in 25 structures saved at equal intervals during 100 ps rMD simulations indicating thereby that a strong hydrogen bond exists. The distance of O9 from G2N2 atom is 3.4 Å and varies in the range 3.1 to 3.9 Å suggesting that this hydrogen bond is rather weak. Our results on a complex of daunomycin with d-TGATCA are contrary to these observations. O7 atom of adriamycin which links the chromophore and amino sugar, is close to N2 of G2 residue with the separation of 3.5 Å while O9 is far from O4' of G2 (5.1 Å). The distance of O7 atom from O9 atom of 9OH hydroxyl group in ring A is 4.53 Å so that there is no possibility of intramolecular hydrogen bond between O7 and 9OH in contrast to that found in X-ray crystal structures of daunomycin and its derivatives in uncomplexed form (Anguilli et al, 1971; Courseille et al, 1979; Neidle and Taylor, 1977; von Dreele and Einck, 1977). Apparently in order to have hydrogen bond of O9 with G2N3 the ring conformation is altered in a specific way which moves O7 atom away. (Wang et al, 1987). This hydrogen bonding interaction is likely to be sensitive to conformation of

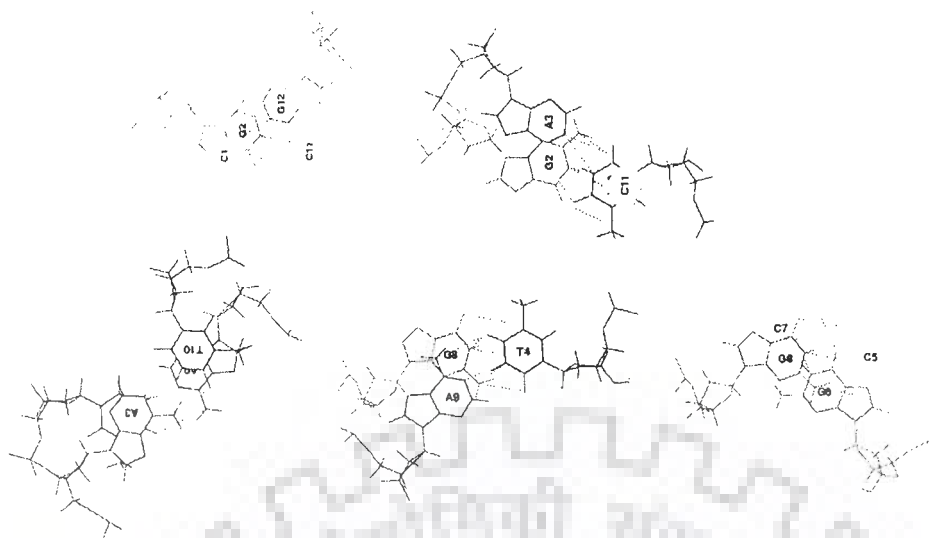
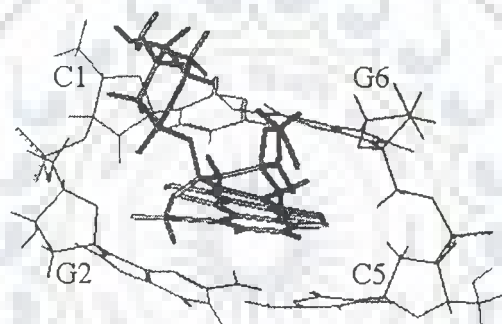
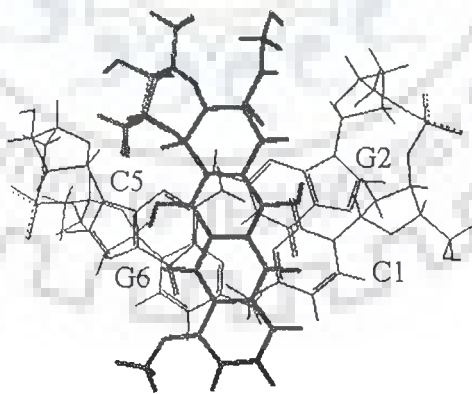


Figure 5.8: Overlap geometry of base pairs at different steps along the sequence



(a)



(b)

Figure 5.9: Drug-DNA stacking interaction in the intercalation site showing the orientation of the adriamycin with respect to base pairs (a) front view (b) top view

ring A. The X-ray crystallography structures of adriamycin and daunomycin with d-CGATCG/other hexamer sequences (Frederick et al, 1990; Moore et al, 1989; Nunn et al, 1991; Wang et al, 1987) show that carbonyl oxygen at C13 position of ring A is bonded to O2 of the cytosine C1/thymine T1 ring through a bridging water molecule while that in daunomycin-d-TGATCA complex shows water molecule hydrogen bonding to O13 without any further interaction (Nunn et al, 1991). The distance between O13 and O2 of C1 in our rMD structure is 6.42 Å so that bridging of O13 to O2 of C1 through water may not be possible. Further the distance between O5 and C5N1 is very large and that between O4 and O-1P of G6 is 7.32 Å. A hydrogen bond involving O4 and O5 atoms with phosphate groups of A6 are possible through two water molecules acting as bridges in between, as reported in X-ray crystal structures (Nunn et al, 1991). The amino group in the daunomycin sugar has been implicated in the electrostatic interactions between the daunomycin and the phosphate group of nucleic acid (Gabbay et al, 1976). In X-ray crystal structure of anthracycline drugs with hexamer sequences (Frederick et al, 1990; Nunn et al, 1991; Wang et al, 1987; Moore et al, 1989) the amino groups form hydrogen bonds via its three hydrogen atoms to oxygen atoms in the neighboring T4 and C5 residue. In adriamycin-d-CGATCG complex (Frederick et al, 1990) the amino hydrogen is within 3.3 Å distance of O2 of C11, O4' of C11 and O2 of T10 forming hydrogen bonds. In our rMD structures these N-H...O distances from C5O2, C5O4' and T4O2 atoms are 3.65, 3.96 and 4.23 Å, respectively.

It has been shown that the ammonium group of the daunosamine sugar ring contributes considerably to the binding (Williams et al, 1990) and due to its different

positioning and flexibility (Lipscomb et al, 1994; Trieb et al, 2004), it is differently stabilized in the minor groove in different anthracycline complexes. We have therefore looked into these hydrogen bonds contacts throughout the course of simulations. It is found that the distance of NH_3^+ from C5O2, C5O4' and T4O2 are in the range 3.2-4.0, 3.7-4.3 and 3.1-3.7 Å, respectively. At the other intercalation site, the distance of NH_3^+ from C11O2, C11O4' and T10O2 are in the range 4.1-5.0, 3.1-3.9, 4.5-5.1, respectively. If we consider 3.3 Å as the cut off distance for hydrogen bond then NH_3^+ moiety is able to make at the most two hydrogen bonds. The distance of NH_3^+ from O4' of T4/T10 and N3 of A3/A9 are in the range 4.9-6.0 and 4.2-4.8 Å, respectively so that there are no contacts through hydrogen bonds between these groups of atoms, as seen in some X-ray crystal structures of daunomycin with d-TGTACA and d-CGTACG sequences (Moore et al, 1989; Wang et al, 1987; Nunn et al, 1991).

An interesting feature of daunomycin/adriamycin is its flexibility of glycosidic bond rotation C7-O7-C1'-C2', which is important for anchoring of the intercalater in minor groove. Throughout the course of simulations, we find that the glycosidic angle C7-O7-C1'-C2' (Fig. 5.10a) remains within a narrow range of angles, 138° to 160°, and stabilizes at 147°. This dihedral angle adopts an angle of 162°-168° in uncomplexed daunomycin and its analogues (Anguilli et al, 1971; Courseille et al, 1979; Neidle and Taylor, 1977; von Dreele and Einck, 1977). In the X-ray crystal structure of adriamycin complexed with d-CGATCG, it is 148° while in some complexes e.g. 4'epiadriamycin complexed with d-TGATCA and daunomycin with d-CGATCG it is 132°-137° (Langlois d' Estaintot et al, 1992; Lipscomb et al, 1994). In most other crystal structures, this glycosidic angle is 145°-161° (Hu et al, 1997; Leonard et al,

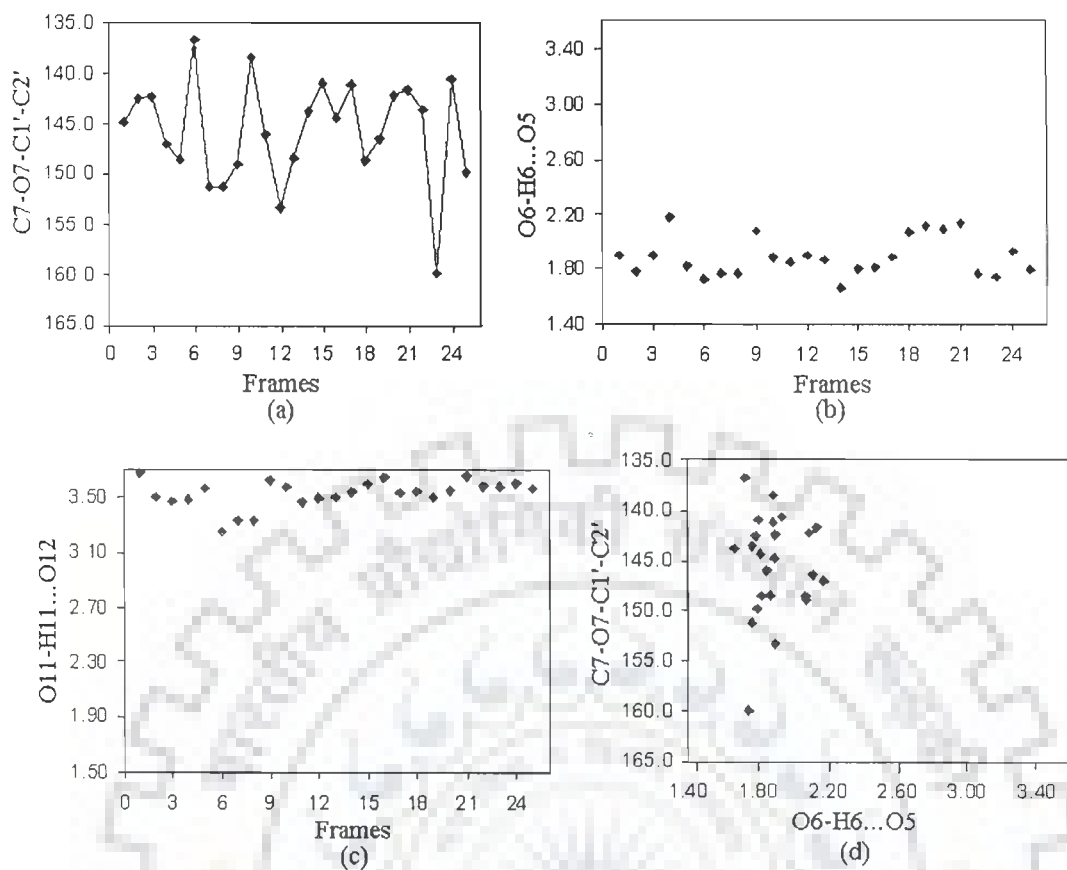


Figure 5.10: Trajectory analysis of 100 ps rMD simulations showing variations of (a) glycosidic dihedral angle $C7-O7-C1'-C2'$ (b) bond length in $O6-H6...O5$ hydrogen bond (c) bond length in $O11-H11...O12$ hydrogen bond. Correlation between glycosidic angle and $O6-H6...O5$ bond is shown in (d)

1992; Moore et al, 1989; Saminadin et al, 2000; William et al; 1990). The molecular dynamics simulations have however shown (Trieb et al, 2004) that besides the two conformations represented in X-ray structures, a third conformation with a much lower dihedral angle is also accessible; thus the first one is 155°-162°, second at 135°-138° and a third shows dihedral angle value of 57°-61°. The energy barrier between 137° and 159° conformations is 0.3 to 0.7 Kcal mole⁻¹ and between 137° and 59° is 1.4 Kcal mole⁻¹. We did not observe the 59° conformation while we observed that the dihedral angle varies in the range 138-160°. Apparently in our case, the first and second substates were kinetically readily accessible. The conformation of glycosidic bond is directly related to flexibility of sugar ring which points towards the minor groove to build stabilizing contacts with DNA through NH₃⁺ moiety. Trieb et al have shown that in the first conformation centered at 159°, the nitrogen of the ammonium group is at a distance of 5.5, 5.1 and 3.2 Å from C5O4', T4O2 and T4O4', respectively. While in the second conformation centered at 137°, the corresponding distances are 3.2, 3.0 and > 6 Å, respectively. In the third conformation having glycosidic dihedral angle centered at 59°, the distance of nitrogen of NH₃⁺ from G6O4' and G6O5' are 3.4 and 3.0 Å, respectively. The observed distance of nitrogen of NH₃⁺ from C5O4'/C11O4', T4O2/T10O2, T4O4'/T10O4' in present studies is in the range 3.1-5.1 Å and that from G2O4' and G2O5' is in the range of 9-12 Å. These findings are consistent with the correlation of glycosidic dihedral bond with stabilization of complex through ammonium group in minor groove, as suggested by Trieb et al. It may be noted that the conformation of glycosidic bond and ring A conformation relates to cleavage of C7-O7 bond and subsequent production of free radicals which are responsible for cell toxicity. During the course of simulations, it

was observed that hydrogen atom of 6OH group of ring B of adriamycin pointed towards O5 atom (and was away from O7 atom) in practically all 25 structures (Fig. 5.10b) while hydrogen of 11OH pointed away from O12 and was facing towards C10 position (Fig. 5.10c). Apparently 6OH...5O hydrogen bond only is stabilized in the drug-DNA complex. This is in sharp contrast to the existence of both hydrogen bonds in the uncomplexed daunomycin, adriamycin and 4'-epiadriamycin investigated by us by molecular dynamics simulations using NMR restraints. The position of H atom of 6OH remains fixed and is not correlated to glycosidic bond rotation C7-O7-C1'-C2' (Fig. 10d) which while varying in the range 137°-160°, positions the daunosamine sugar moiety close to 6OH in different orientations. The stabilization of 6OH...5O hydrogen bond thus ensures a fixed position of hydrogen atom of 6OH which has been found to be close to C5H1' (distance 2.86 Å) of DNA (Table 5.8). Besides this, several other contacts O5-C5H1', O6-C5H1', O5-C5H2', 4OCH₃-C5H2', 6OH-C5H1' have distances within 3 Å. This observation is significant and establishes the involvement of 4OCH₃, O5, O6, 6OH atoms in stabilizing the drug-DNA complex. In addition, there are several non bonded van der waal's interactions (listed in Table 5.8) that may be important in stabilizing the complex. Some of these contacts are: 10axH with C1O2; 10eqH with G2N3; 3'H with G2N2; 2'axH-C5O2, etc. Some of these contacts are similar to those observed in X-ray crystal structure of daunomycin with CGTACG (Wang et al, 1987).

Adriamycin drug differs from daunomycin by a hydroxyl group attached at C14 position, that is, presence of 9COCH₂OH group as compared to 9COCH₃ group in daunomycin. In the rMD structure of the complex, it was observed that the hydroxyl group makes short van der waal's contact with A3H5' (2.94 Å) and A3H4' (3.45 Å).

(Å)

Table 5.8: Close contacts between drug-DNA molecules

S.No	Protons	CGA+Adm ^a	S.No	Protons	CGA+Adm ^a
1.	C1O2-10axH	3.02	26.	A3H2-N3'	3.08
2.	C1H2'-11OH	2.62	27.	A3H2-H1N3'	2.41
3.	G2H1'-CH ₂ OH	5.33	28.	T4O2-4'H	5.0
4.	G2H4'-CH ₂ OH	5.11	29.	T4O2-H2N3'	4.32
5.	G2H5'-CH ₂ OH	5.45	30.	T4O4'-CH ₂ OH	7.6
6.	G2O3'-CH ₂ OH	5.05	31.	T4C5'-H2C14	7.16
7.	G2P-CH ₂ OH	7.87	32.	T4H5'-C14	6.19
8.	G2N3-10eqH	3.03	33.	T4H5'-H2C14	6.04
9.	G2N2-3'H	2.62	34.	C5O2-2axH	2.74
10.	G2O4'-10eqH	2.4	35.	C5O2-H3'	2.52
11.	G2H1N2-O9	4.46	36.	C5C1'-2eqH	4.9
12.	G2H1N2-O7	4.08	37.	C5H1'-O5	3.0
13.	G2H2N2-3'H	2.41	38.	C5H1'-O6	2.42
14.	G2H2N2-NH ₃	4.29	39.	C5H2'-O5	2.50
15.	G2H4'-C14	3.22	40.	C5H1'-6OH	2.86
16.	G2H4'-C13	3.37	41.	C5H1'-2eqH	2.50
17.	G2H4'-O13	3.24	42.	G6N2-10axH	2.47
18.	A3H5'-CH ₂ OH	2.94	43.	G6N3-7H	2.72
19.	A3H5''-CH ₂ OH	4.08	44.	G6O4'-7H	2.64
20.	A3O5'-CH ₂ OH	4.98	45.	G6O4'-H1'	3.59
21.	A3O4'-CH ₂ OH	3.85	46.	G6C4'-H1'	4.06
22.	A3H4'-CH ₂ OH	3.45	47.	G6H5'-C2'	2.99
23.	A3N3-H1N3'	5.18	48.	G6H5'-2eqH	2.77
24.	A3N3-H2N3'	4.07	49.	G6H5'-H1'	2.21
25.	A3C2-H1N3'	3.44	50.	G6H1N2-8axH	5.26

^aCGA+adm = d(CGATCG)₂ + adriamycin

Its distance from G2O3' and G2 phosphorus atom is 5.05 and 7.87 Å (Table 5.8), respectively. This group has been implicated in binding to phosphate through water bridge in X-ray crystal structure of adriamycin with d-CGATCG (Frederick et al, 1990).

Summarizing the results, we find that 4OCH₃, 5O, 6OH, O7 groups are involved in drug-DNA interactions. This may require existence of 6OH...5O hydrogen bond. Involvement of NH₃⁺ group in interaction is perhaps related to conformation of glycosidic bond. The binding to DNA through 9CO13, 9OH, 9CH₂OH groups may depend upon ring A conformation. Presence of 11OH...12O hydrogen bond may not be critical for binding and atoms of position 1, 2, 3, 12, 11 may not be involved in drug-DNA interactions.

5.3 CONCLUSIONS

The restrained molecular dynamics simulations of the complex of adriamycin with d-CGATCG based on intramolecular and intermolecular NOEs have led to a detailed conformational analysis. The intercalation of drug chromophore at d-CpG steps is stabilized by stacking interactions while several other hydrogen bonds and van der waal's interactions stabilize the drug-DNA complex. The O9 atom is involved in hydrogen bond formation with G2N3 and G2N2H while O7 atom has close contact with G2N2 atom. The glycosidic bond C7-O7-C1'-C2' is stabilized around 147°. In the minor groove, hydrogen bonding contacts of NH₃⁺ moiety with C5O2, T4O2 and C5O4' atoms exist. The 6OH...5O hydrogen bond is stabilized and 4O, 4OCH₃, 5O, 6OH atoms show close contacts with several atoms of C5 residue. Further 14OH group of 9COCH₂OH has close van der waal's contacts with A3H5' and A3H4'. The specificity of drug-DNA interactions arises from the conformation of ring A,

glycosidic bond, position of NH_3^+ group in minor groove, the substituent group at position 4, 5, 6, 7, 9 and daunosamine sugar, which conformation have a role in stabilizing the drug-DNA complex.

The right-handed DNA has significant variations both in backbone geometry and sugar puckering associated with the accommodation of a large intercalator molecule with an amino sugar. The intercalating base pairs show considerable buckle and the minor groove is wider. The conformation of G2pA3 and C5pA6 phosphates are altered and are close to B_{II} conformation. Also at both intercalation sites as well as sites adjacent to intercalation sites, the phosphorus on one strand is in B_I state while the one directly lying on opposite strand is in B_{II} state. The β torsional angle of A3 residue and δ (and hence pseudorotation P) of T4 residue have considerably lower values in the complex. Solution structure by NMR thus establishes the molecular basis of action of drug on DNA.

RESTRAINED MOLECULAR DYNAMICS STUDY ON DRUG-DNA COMPLEX: d(TGATCA)₂ WITH DAUNOMYCIN

Solution structure of daunomycin-d(TGATCA)₂ complex have been analyzed in our laboratory (courtesy Uma Sharma). Their NMR data was utilized to obtain the restraint data set, which consists of several intramolecular and intermolecular nuclear Overhauser enhancement cross peaks. The intensities of cross peaks of 2D NOESY spectra at two mixing times, $\tau_m = 150$ and 200 ms, were used to extract the experimental restraints of interproton distances. CH5-CH6 peak of cytosine was used as the reference using a distance = 2.46 Å. A range of ± 0.3 Å was provided to distances to account for any errors in integration.

6.1 STRATEGY FOLLOWED

The energy minimization and molecular dynamics calculations were carried out using AMBER 6.0 software (courtesy Prof. Peter Kollman, UCSF, California) on Unix platform using PARAM 10000 super computing facility. Initial model building was carried out using xleap and antechamber modules of AMBER 6.0. Starting structure of 2:1 complex of daunomycin-d(TGATCA)₂ was taken from nucleic acid database (NDB Id: ddf032). AMBER reads all the atoms of DNA but does not have database for drug molecule. Modification of initial structure was done using INSIGHT II on Silicon Graphics workstation. MOPAC generated the charge while antechamber module of the AMBER prepared the database for the daunomycin molecule. Counterions and hydrogen atom with standard geometry were added to the system by xleap module. This structure was then optimized to remove any bad van der waal's

contacts and to minimize counterions keeping all heavy atoms of the complex fixed. All molecular structures were displayed using the visual molecular dynamics (VMD) software on a Linux workstation. Minimization and restrained molecular dynamics were carried out in vacuum. A distance dependent dielectric constant was used during simulations in vacuum for restrained molecular dynamics (rMD) calculations to mimic the presence of a high dielectric solvent. Pseudoatom corrections were used for methyl and other equivalent protons. The SANDER (simulation annealing with NMR driven energy restraints) module in AMBER 6.0 was used to perform energy minimization and dynamics. To maintain right-handedness and prevent structural artifacts during the simulations, the base pair Watson-Crick hydrogen bonding scheme was also maintained by applying hydrogen bond restraints. A cut off value of 9.0 Å was chosen to calculate all nonbonded interactions in the system. All runs were performed at constant temperature of 300 K. The temperature was regulated by bath coupling using the Berendsen algorithm. Forcefield parm99 of AMBER 6.0 was used. The energy of the system was minimized using 1000 steps each of steepest descent and conjugate gradient using a total 190 intraresidue and 46 interresidue distance restraints (Table 2). A typical rMD run consisted of 100 ps simulations with time step of 1 fs. General simulation parameters were kept constant during the complete run of molecular dynamics simulations and structural information was collected after every 4 ps.

6.2 RESULTS AND DISCUSSION

The nucleotides are labelled from T1 to A6 in the 5' to 3' direction on strand 1 and from T7 to A12 on strand 2 with T1 base paired to A12. The daunomycin molecules are numbered D13 and D14 and the atomic numbering scheme for the molecule is

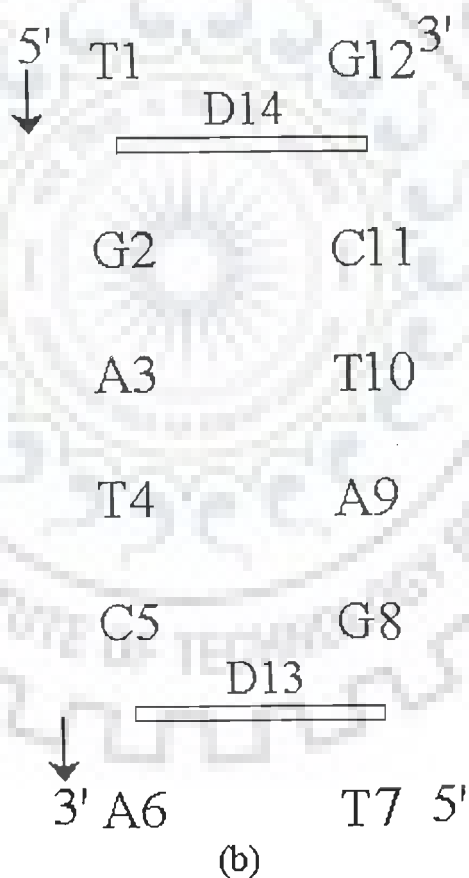
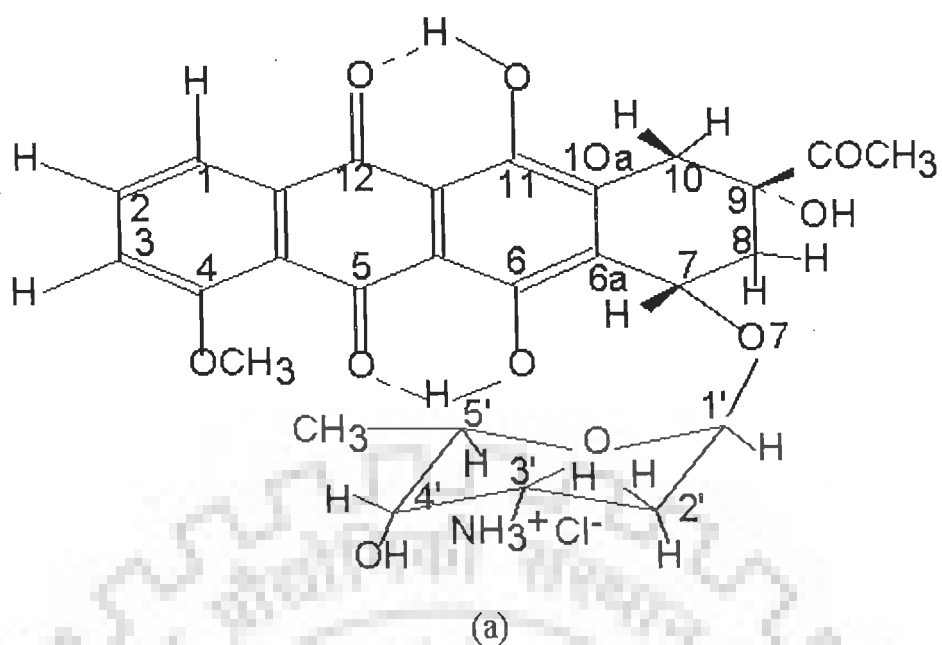


Figure 6.1: (a) Molecular structure of daunomycin (b) Schematic representation of the 2:1 daunomycin-d-(TGATCA)₂ complex

shown in Fig. 6.1. A typical 2D NOESY spectrum of complex indicating some of the intermolecular NOEs is shown in Fig. 6.2. Tables 6.1a-c and 6.2 give the interproton distances observed within the DNA hexamer and within the drug protons of the complex, respectively. Table 6.3 lists the interproton distances corresponding to observed intermolecular NOEs between drug and DNA protons. The DNA protons showed several NOEs with drug protons. Sequential NOE connectivities between T1 and G2 as well as between C5 and A6 bases were not observed. Instead NOE connectivities between T1CH₃ and 1H, 2H, 3H protons as well as between C5H5, C5H6 and 4OCH₃ protons were observed which show that drug chromophore intercalates at T1pG2 and C5pA6 steps. The schematic representation of the drug chromophore intercalated between d-T1pG2 and d-C5pA6 sites is shown in Fig. 6.1b. The best-fit refined structure showing all atoms is given in Fig. 6.3. The root mean square deviation between the rMD structure and the starting structure is quite large but among various final structures is very low. This is generally acknowledged as an indication that convergence has been achieved. Table 6.4 indicates an assessment of refined structure in terms of energetics and distance deviation from the target distance. The total potential energy of the final structure is 430 Kcal mole⁻¹, which is much lower than the initial B-DNA structure. The restraint energy has also reduced from 2043 Kcal mole⁻¹ to 1300 Kcal mole⁻¹. Table 6.5 shows the pairwise as well as residue wise root mean square deviations (RMSD) of the complex. The starting structure was chosen as reference and the value of target RMSD is chosen to be zero. It may be noted that distance deviation reached a minimum of 0.71 Å from an initial average deviation of 0.81 Å.

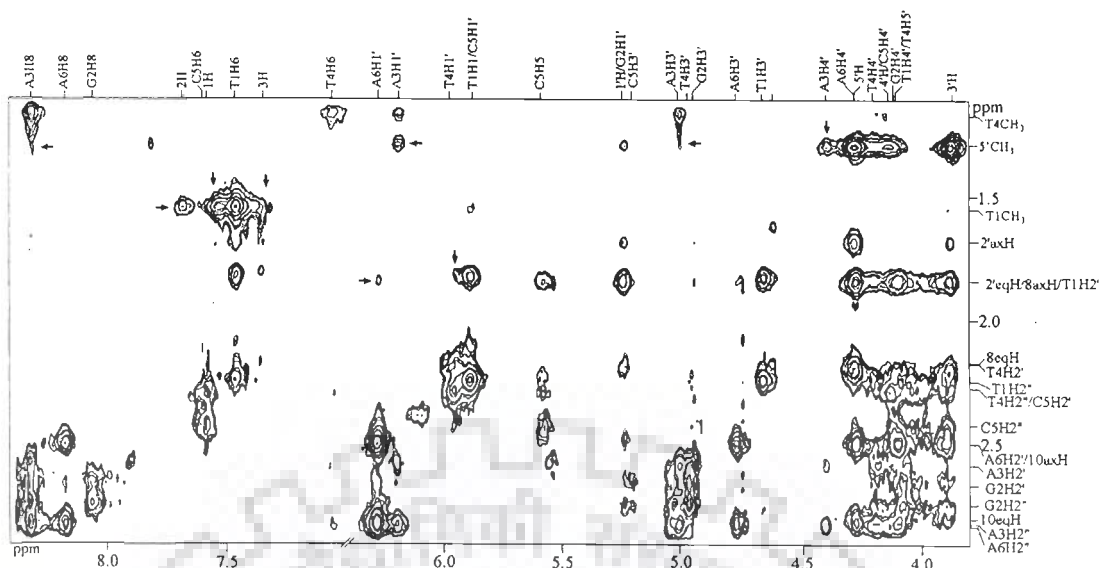


Figure 6.2: NOESY spectrum of 2:1 daunomycin-d-(TGATCA)₂ complex in D₂O showing intermolecular cross peaks (shown by arrow) between drug and DNA at $\tau_m = 350$ ms (courtesy: Uma Sharma)

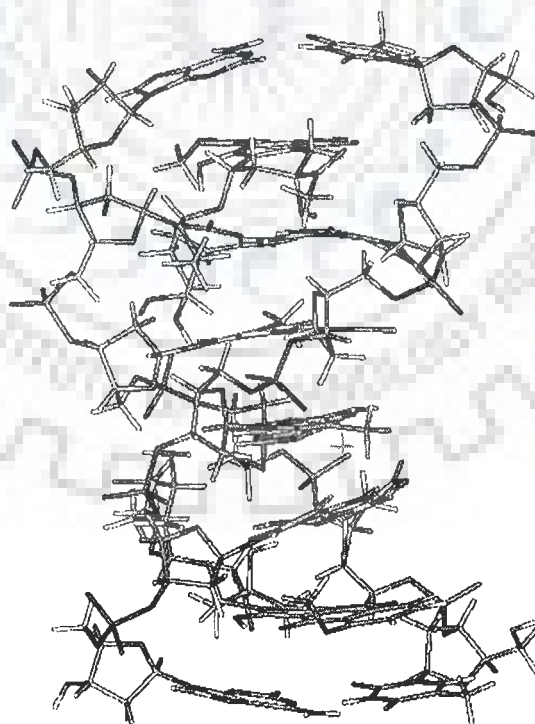


Figure 6.3: Stereoview of the final structure obtained by restrained molecular dynamics simulations

Table 6.1a: Some of the interproton distances (Å) from inter residue sequential connectivities in hexanucleotide observed in NOESY spectra of the drug-DNA complex at drug to DNA ratio (D/N) = 2.0

A3H8-G2H1'	3.4
A3H8-G2H2'	2.5
A3H8-G2H2''	2.5
T4H6-A3H1'	2.6
T4H6-A3H2'	2.8
T4H6-A3H2''	2.7
T4CH ₃ -A3H8	2.6
C5H6-T4H1'	3.0
C5H6-T4H2'	2.5
C5H6-T4H2''	2.5
C5H5-T4H2'	3.5
C5H5-T4H2''	2.5

Table 6.1b: Interproton distances (Å) obtained from intra nucleotide NOE connectivities (d_i) within sugar protons of hexanucleotide of the drug-DNA complex at drug to DNA ratio (D/N) = 2.0

Protons	T1	G2	A3	T4	C5	A6
H1'-H2'	2.7	2.7	2.7	2.7	2.7	2.7
H1'-H2''	2.2	2.2	2.2	2.2	3.8	2.2
H1'-H3'	3.0	-	3.0	-	-	3.1
H1'-H4'	3.1	3.8	3.0	2.9	3.8	2.8
H2'-H3'	2.2	2.2	2.2	3.8	3.8	2.3
H2''-H3'	2.5	2.5	2.5	3.8	3.8	2.6
H2'-H4'	3.8	3.8	3.1	3.8	3.8	3.1
H2''-H4'	3.8	3.8	3.0	3.8	3.8	3.0
H2'-H2''	1.8	1.8	1.8	1.8	1.8	1.8
H3'-H4'	2.6	2.4	2.4	3.8	3.8	2.8
H5'-H5''	1.8	2.0	1.8	1.8	1.8	1.8

- indicates absence of cross peak

Table 6.1c: Interproton distances (\AA) obtained from intra nucleotide NOE connectivities (d_i) of base to sugar protons of hexanucleotide in the drug-DNA complex at drug to DNA ratio (D/N) = 2.0

Protons	T1	G2	A3	T4	C5	A6
H8/H6-H1'	3.0	3.8	3.7	3.2	3.1	2.7
H8/H6-H2'	2.5	2.7	2.5	2.6	2.8	2.4
H8/H6-H2''	2.7	2.6	2.8	2.8	2.6	2.7
H8/H6-H3'	3.2	3.4	3.0	3.5	3.5	3.4
H8/H6-H4'	-	3.8	3.8	3.6	-	3.7
H8/H6-H5'	3.5	3.6	3.6	-	-	3.6
H8/H6-H5''	3.5	3.6	3.8	-	-	3.6

- indicates absence of cross peak

Table 6.2: Interproton distances (Å) obtained from intramolecular NOE connectivities within the drug molecule in the drug-DNA complex at drug to DNA ratio (D/N) = 2.0

J coupled Protons		Within Sugar Protons		Ring A with sugar Protons		Within Ring D Protons		Within Ring A Protons	
1H-2H	2.4	1'H-3'H	3.0	7H-1'H	-	2H-4OCH ₃	2.6	10 _{ax} H-8 _{ax} H	2.7
2H-3H	2.4	1'H-4'H	2.6	7H-3'H	-	1H-4OCH ₃	3.1	10 _{ax} H-8 _{eq} H	2.5
1'H-2' _{ax} H	2.4 ^o	1'H-5'H	2.5	7H-5'H	3.3	3H-4OCH ₃	2.2	10 _{eq} H-8 _{ax} H	2.5
1'H-2' _{eq} H	2.4 ^o	1'H-5CH ₃	3.6	7H-5CH ₃	-			10 _{eq} H-8 _{eq} H	-
3'H-4'H	^o	3'H-5'H	2.2	8 _{ax} H-1'H	2.4 ^o			10 _{eq} H-9COCH ₃	-
4'H-5'H	^o	3'H-5'CH ₃	2.6	8 _{ax} H-3'H	3.0 ^o			10 _{ax} H-9COCH ₃	-
3'H-2' _{ax} H	2.4 ^o	4'H-2' _{ax} H	^o	8 _{ax} H-4'H	3.1			8 _{ax} H-9COCH ₃	-
3'H-2' _{eq} H	2.4 ^o	4'H-2' _{eq} H	3.1	8 _{ax} H-5'H	2.8			8 _{eq} H-9COCH ₃	-
2' _{ax} H-2' _{eq} H	^o	4'H-5'CH ₃	2.4	8 _{ax} H-5'CH ₃	-			8 _{ax} H-5CH ₃	-
5'H-5'CH ₃	2.4								
7H-8 _{ax} H	2.8								
7H-8 _{eq} H	2.9								
8 _{ax} H-8 _{eq} H	^o								
10 _{ax} H-10 _{eq} H	^o								

^o = overlap of peaks

Table 6.3: Interproton distances (Å) obtained from intermolecular NOEs and those obtained from the structure generated by rMD simulations

S. No.	Cross peak	NMR	Model	S.No.	Protons	NMR	Model
1.	T1CH ₃ -1H	2.0	3.3	10.	T4H1'-2eqH	3.2	6.2
2.	T1CH ₃ -2H	2.3	4.6	11.	C5H6-4OCH ₃	2.6	2.5
3.	T1CH ₃ -3H	2.6	6.0	12.	C5H5-4OCH ₃	2.5	2.7
4.	T1CH ₃ -10axH	3.2	8.1	13.	C5H2''-2axH	3.1	5.4
5.	A3H2''-5'CH ₃	2.8	6.2	14.	C5H5-2axH	3.1	6.7
6.	A3H8-5'CH ₃	2.7	7.2	15.	C5H2'-4OCH ₃	2.2	2.7
7.	A3H1'-5'CH ₃	2.5	3.6	16.	A6H1'-2'eqH	3.8	4.8
8.	A3H4'-5'CH ₃	2.4	4.0	17.	A6H1'-1'H	3.7	4.8
9.	A3H3'-5'CH ₃	3.7	5.8	18.	A6H2-8axH	-	3.5

Table 6.4: Energy terms (Kcal mol⁻¹) for starting model and final rMD structure

Structure	Total	Bond	Angle	Dihedral	Vdw
Initial	2.27x10 ³	471	469	224	-241
Final	430	43	148	265	-162
	1-4 Vdw	Electrostatic	1-4 Electrostatic	Restraint	Δdv^a
Initial	198.3	-610	-291	2043	0.81
Final	157	-987	-331	1300	0.71

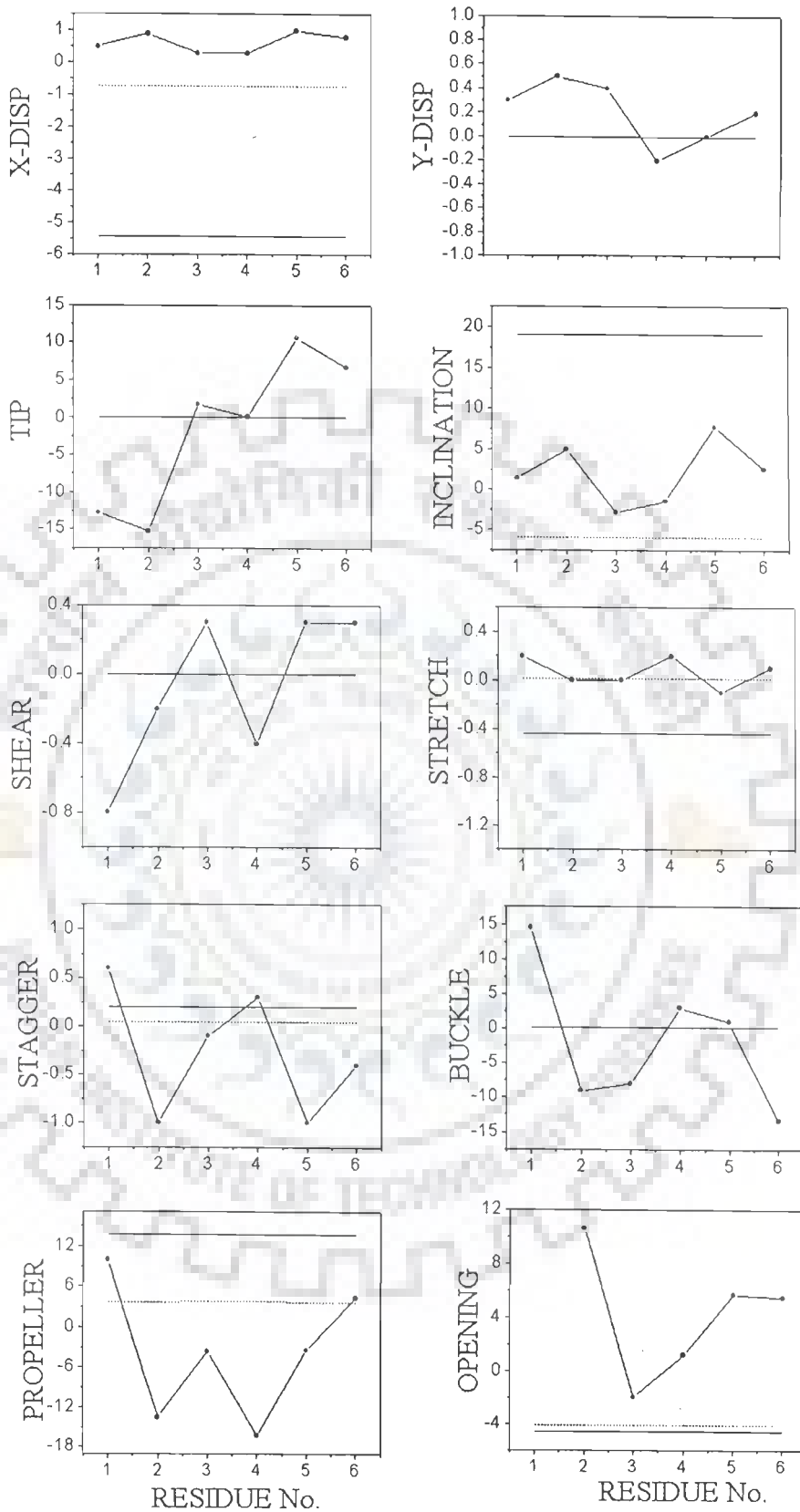
^aAverage distance deviation

Table 6.5: Summary of experimental restraints and statistical analysis of the final structure

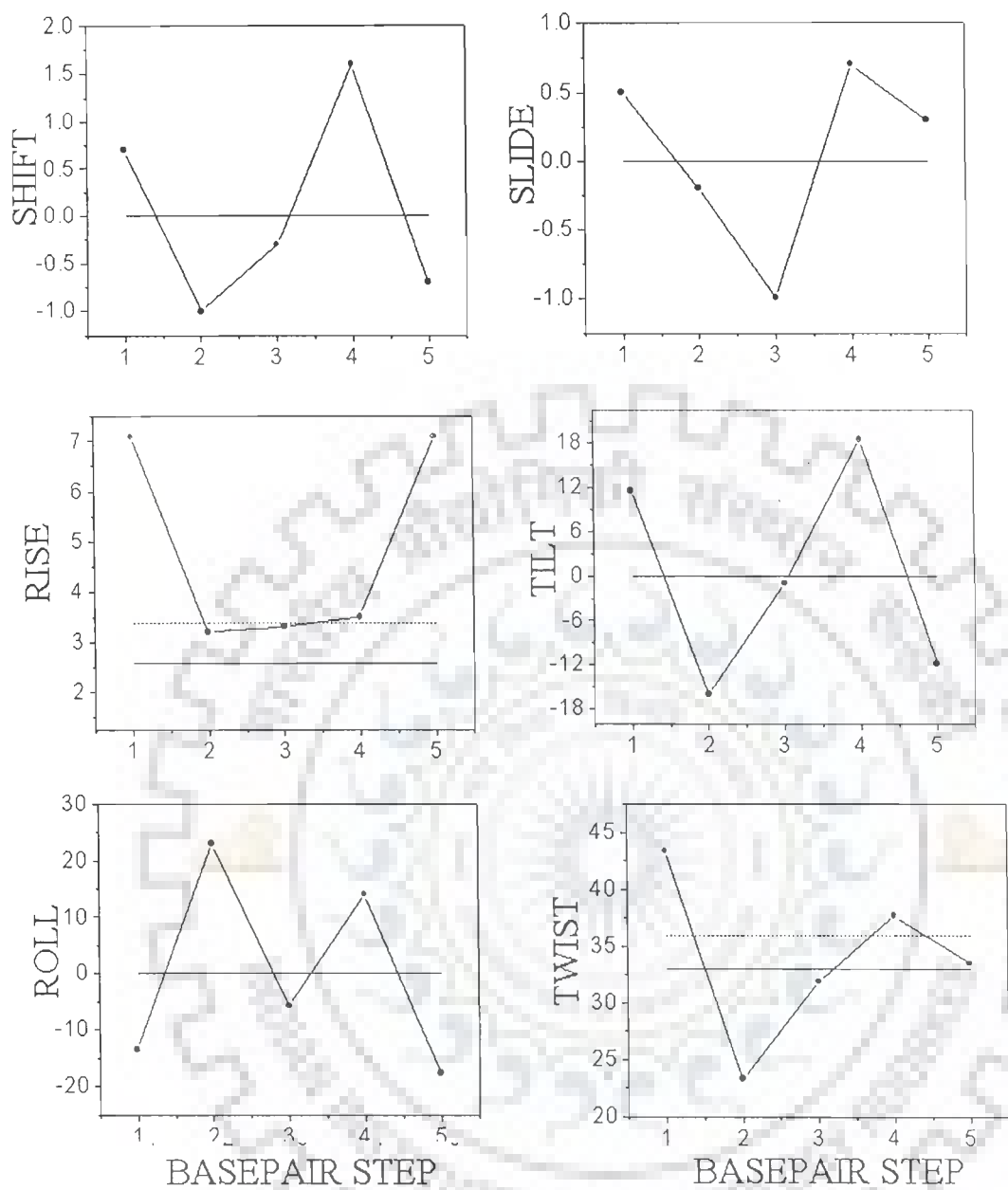
Parameter	
No. of Distance Restraints	
Intra residue	190
Inter residue	46
Average pairwise RMSD	Initial = 0 Final = 0.72
Average residuewise RMSD	T1 = 1.3, G2 = 1.2, A3 = 41.2, T4 = 0.8, C5 = 1.3, A6 = 0.70 Daunomycin = 2.5

6.2.1 Conformation of DNA

All helical parameters, backbone torsional angles and sugar conformations of the resulting rMD structures were thoroughly analysed with the program CURVES, version 5.1 (Lavery and Sklenar, 1989; Lavery and Sklenar, 1996). Plot of some helicoidal parameters (global, unless specified otherwise) as a function of residue position in the duplex is shown in Fig. 6.4 along with that for two classical structures of A-DNA and B-DNA. Among the base pair axis parameters, the x-displacement (dx) and y-displacement (dy) are found to vary to a large extent (~ 1.1 Å) for all base pairs. Large displacements are generally observed in intercalated complexes (Langlois d' Estaintot, 1992; Leonard et al, 1992; Nunn et al, 1991). The base pairs are inclined at an angle of 5° and 8° for the two GC base pairs, that is, G2.C11 and C5.G8. The tip angle fluctuates along the base sequence. The base pairs at both 5' and 3' ends are found to be buckled by $+14^\circ$ and -13° , respectively. The stagger is maximum, ~ 1.2 Å for the two CG base pairs. It is noteworthy that in the X-ray crystal structure of the daunomycin and 4'-epiadriamycin with d-TGATCA (Langlois d' Estaintot, 1992; Leonard et al, 1992; Nunn et al, 1991) also, stagger is found to be maximum for CG base pairs and large values of buckle due to intercalation have been reported. The propeller twist for G2.C11 and T4.A3 base pairs are large and negative. The positive values of propeller twist at either ends may be due to fraying effects at both the ends (Chen and Patel, 1995). Among the inter base pair parameters, the shift (Dx) is maximum at G2pA3 and T4pC5 steps while the slide (Dy) is maximum in the middle of the hexanucleotide, that is, at A3pT4 step. The rise at base pair steps is 3.2-3.5 Å while at TpG and CpA steps it is ~ 7.1 Å to accommodate the drug chromophore. The intercalation results in large amount of tilt (τ) in all base pair steps except that in the



(a)



(b)

Figure 6.4: (a) and (b) Helical parameters for d-TGATCA complexed with daunomycin calculated for structure obtained by restrained molecular dynamics simulations (•) and that for canonical A-DNA (—), B-DNA (----)

middle of the helix, that is, A3pT4 step. Large positive values of the roll angle (ρ) at G2pA3 and T4pC5 steps, result in a wider minor groove and bending towards major groove causing a curvature in the helix. The large positive roll at these base pair steps also indicates reduced base stacking which gets reflected in the change in chemical shift of corresponding base protons. The local inter base parameters also show similar changes in roll angle and tilt. The twist angle (Ω) at T1pG2 and G2pA3 steps is 43° and 23° , respectively. The observed deviation from an average value of 34° found in the B-DNA structures, is more than that observed in the corresponding X-ray crystal structures (Langlois d' Estaintot, 1992; Leonard et al, 1992; Nunn et al, 1991) of daunomycin and 4'-epiadriamycin with d-TGATCA (37° and 30° at T1pG2 and G2pA3 steps, respectively). The unwinding of DNA at the site of intercalation is upto 11° and is consistent with that reported by viscosity techniques (Pachter et al, 1982). The overall axis bend is about 11° . The width of major and minor groove are 13.5 and 7.6 Å, respectively and their depth is lower than that in standard B-DNA structures. The wider minor groove presumably allows proximity of daunosamine sugar moiety. The backbone torsional angles along with the values for canonical B-DNA and A-DNA are given in Table 6.6. The torsional angles are not exactly equal in the two strands of the duplex but the general features and trends with base sequence are same. Since these torsional angles are not defined by the restraints obtained by NOESY spectra, we have used a low force constant to permit a smooth search which is conformationally compatible with other structural features. The angles α , β and γ adopt gauche⁻, trans and gauche⁺ conformations, respectively in practically all residues of both the strands except that β for A3, T4 residues deviates in one strand from 176° (canonical B-DNA) to 123 - 128° . The angle δ as well as pseudorotation

Table 6.6: Backbone torsional angles ($^{\circ}$), pseudorotation phase angle ($^{\circ}$) and glycosidic bond rotation ($^{\circ}$) of the final structure

RESIDUES	α	β	γ	δ	ϵ	ζ	χ	P
T1	-	-	54	137	-138	-75	-152	164
G2	-66	-173	45	139	-164	-147	-69	150
A3	-46	128	54	134	-91	-170	-132	138
T4	-61	123	50	116	162	-87	-122	113
C5	-75	177	49	150	-128	170	-74	153
A6	-69	158	65	147	-	-	-102	174
T7	-	-	52	144	-118	-70	-150	175
G8	-58	-175	25	136	-92	147	-60	143
A9	-81	159	33	156	179	-95	-107	199
T10	-76	178	58	117	-175	-84	-112	112
C11	-62	175	46	137	-131	-175	-83	141
A12	-80	159	73	147	-	-	-106	175
B-DNA	-63	136	54	123	-169	-108	-105	162

phase angle P has a low value of $116-117^\circ$ only for T4 residue in both the strands. The torsional angle ζ however deviates from the normal gauche- conformation and adopts a trans conformation for the G2 ($-147^\circ, +147^\circ$) and C5 residues ($+170^\circ, -175^\circ$). This may be attributed to the opening of base pairs at these sites. This is accompanied by a corresponding deviation in torsional angle ϵ for G2 and C5 residues to a lower negative value of -92° (in one strand) and $-131^\circ, -128^\circ$ (in both strands), respectively as compared to a value of -169° found in canonical B-DNA structures. The glycosyl rotation angle χ measuring the rotation of base around the sugar varies as follows: T1: $-152^\circ, -150^\circ$; G2: $-69^\circ, -60^\circ$; A3: $-132^\circ, -107^\circ$; T4: $-122^\circ, -112^\circ$; C5: $-74^\circ, -83^\circ$ and G6: $-102^\circ, -106^\circ$. Thus it is observed that DNA backbone uses a non-symmetrical mechanism to allow intercalation of drug chromophore between T1pG2 and C5pA6 sites. On the T1pG2 side of the backbone, the 5' deoxythymine residue changes the glycosyl angle from an anti (-105° to -119° in B-DNA) to a low anti value ($-152^\circ, -150^\circ$). At the same time by adjusting ϵ from a near trans (-169° in B-DNA) to a somewhat lower value of ($-138^\circ, -118^\circ$), it allows the adjacent bases to separate from 3.4 \AA to 7.0 \AA . On the C5pA6 site, both nucleotide units (C5 and A6 in both the strands) maintain the glycosyl angles at high anti values ($-74^\circ, -83^\circ, -102^\circ, -106^\circ$). By changing the ϵ value from -169° to a conformation tending towards gauche ($-128^\circ, -131^\circ$) in the C5 residue, it is possible to separate the C5 and A6 bases to a distances of $\sim 7.0 \text{ \AA}$. This is made possible by coupling it with rotations about phosphodiester linkage from a normal gauche- - gauche- conformation to a trans - gauche- as observed in X-ray crystallography structure of similar complexes (Barthwal et al, 1994; Frederick et al, 1990; Wang et al, 1987, Williams et al, 1990).

Such changes get reflected as downfield shift in phosphorus-31 NMR spectra or alternately in backbone torsional angles ϵ , ξ , α and β . X-ray crystallographic analysis of various B-DNA structures have shown that B-DNA can exist in two conformational states, namely B_I and B_{II}, characterized by torsional angles α , -62° ; β , 176° ; γ , 48° ; δ , 128° ; ϵ , -176° ; ξ , -95° ; χ , -102° to -119° and α , -62° ; β , 176° ; γ , 48° ; δ , 144° ; ϵ , -114° ; ξ , -174° ; χ , -89° , respectively. The G2 residue in one strand and C5 residue in both strands adopt B_{II} conformation due to intercalation. The A3 (in one strand) and T4 (in both strands) residues remain in stabler state except that δ of T4 residue and γ of G2, A3 residues shift to lower values of 116° - 117° and 25° - 33° , respectively. It has been shown that in the crystal structure of daunomycin with d-TGATCA (Nunn et al, 1991), γ of A3 residue is 24° ; G2 and C5 residues are close to B_{II} conformations adopting ϵ and ξ angles of -131° , 153° and -98° , 167° , respectively. G2 and C5 residues adopt B_{II} conformation in X-ray crystal structure of 4'-epiadriamycin with d-TGATCA (Langlois d' Estaintot, 1992) also. Further A3 and T4 residues in second strand do not show a reduction in β as observed in corresponding X-ray crystal structure (Nunn et al, 1991). A lower value of β has been observed in X-ray crystal structure (Frederick et al, 1990; Wang et al, 1997) and NMR solution structures (Mazzini et al, 1998) of daunomycin/adriamycin/their analogues with d-CGATCG and d-CGTACG.

Our results show that two strands of DNA are not symmetrical. One strand showed odd combination of torsional angles. The G2 residue shows ϵ , -164° ; ξ , -147° and A3 residue is close to B_{II} conformation having ϵ , -91° ; ξ , -170° . The β angle of both A3 and T4 residues showed lower values, 123 - 128° (Table 6.6). A lower value of β has

been reported in X-ray crystal structure of 4'-epiadriamycin with d-TGATCA (Langlois d' Estaintot, 1992) but not in the complex of daunomycin with d-TGATCA (Nunn et al, 1991). A lower value of β angle has been associated with change in phosphodiester bond from idealized g^-g^- conformation to tg^- observed in some crystal structures (Frederick et al, 1990).

In order to have insight into the conformational equilibrium and recognize the most populated conformation of the DNA molecule in the drug-DNA complex, we looked into the torsional angles, various intra residue and inter residue interproton distances, as well as their correlation in 25 structures saved at an interval of 4 ps during 100 ps molecular dynamics simulations. The interproton distance H8/H6-H1' directly is a measure of glycosidic bond rotation, χ , while the distance H1'-H4' is characteristic of pseudorotation P_5 of the major S-conformer of deoxyribose. Among all residues, χ of G2 residue adopts most high anti conformation while P is lowest for A3 and T4 residues (Table 6.6). The same is reflected in Fig. 6.5a. Further it is clear that the variations are not subject to fluctuations but are stable during all simulations and vary over a small range. The torsional angles α , β of A3 residue and ϵ of G2 residue deviate (Fig. 6.5b) more from the average value in few of the structures and could perhaps be the region of somewhat greater flexibility. Fig. 6.6a-d display results on correlation between some of the torsional angles. It is observed that in most cases various conformations adopted during simulations are clustered to one region in graph. The maximum scatter in data of torsional angles occurs (Fig. 6.6a-c) in α and β angles of A3 residue. The variations in these two angles are indeed coupled to each other (Fig. 6.6a). The plot of α (of n^{th} residue) and ζ (of $n-1^{\text{th}}$ residue) torsional angles relative to each phosphate shows (Fig. 6.6c) that T1pG2, T4pC5 units are

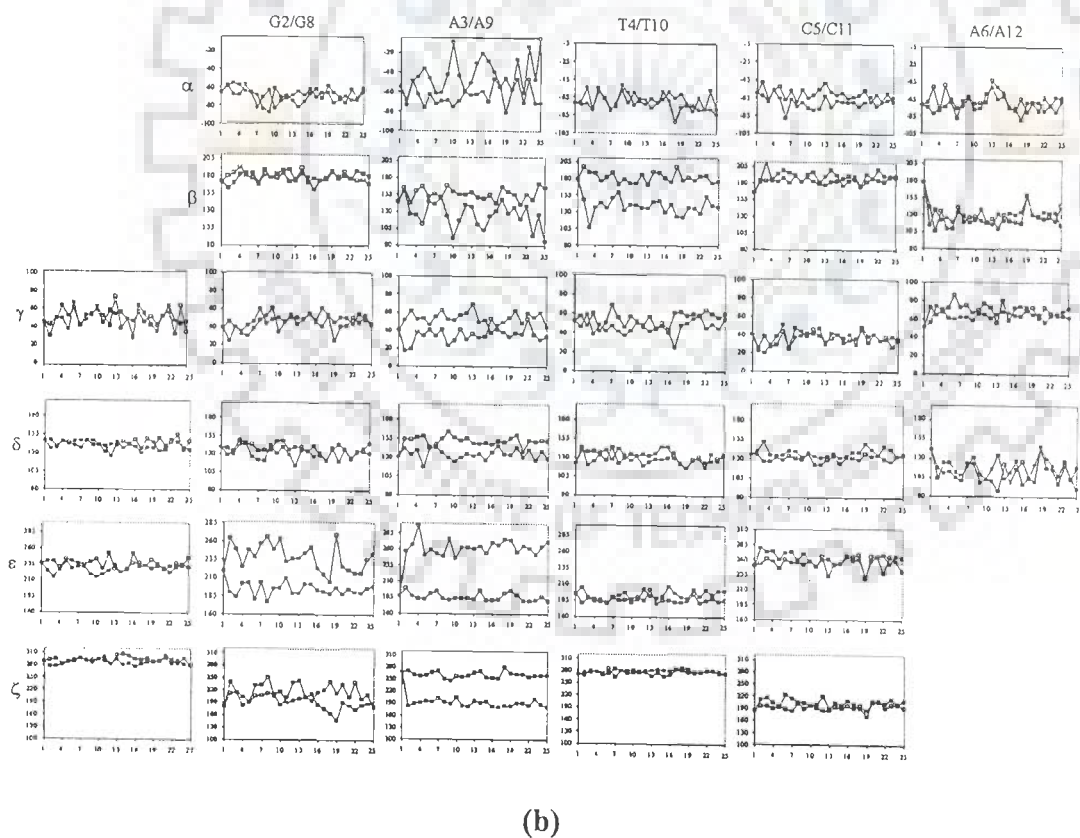
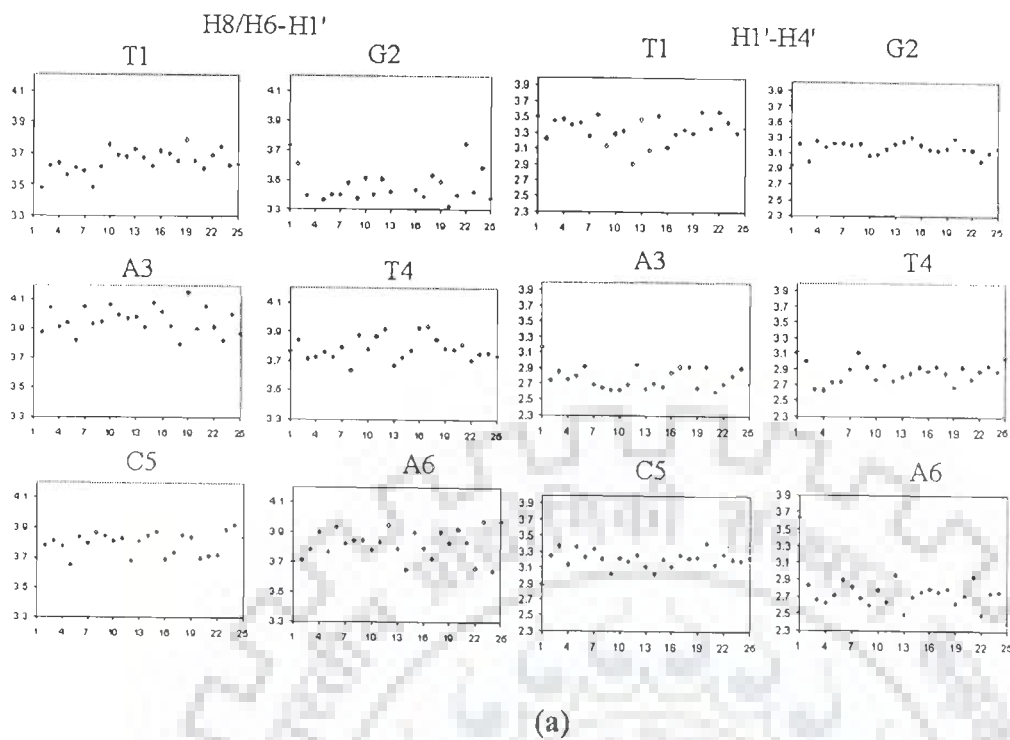
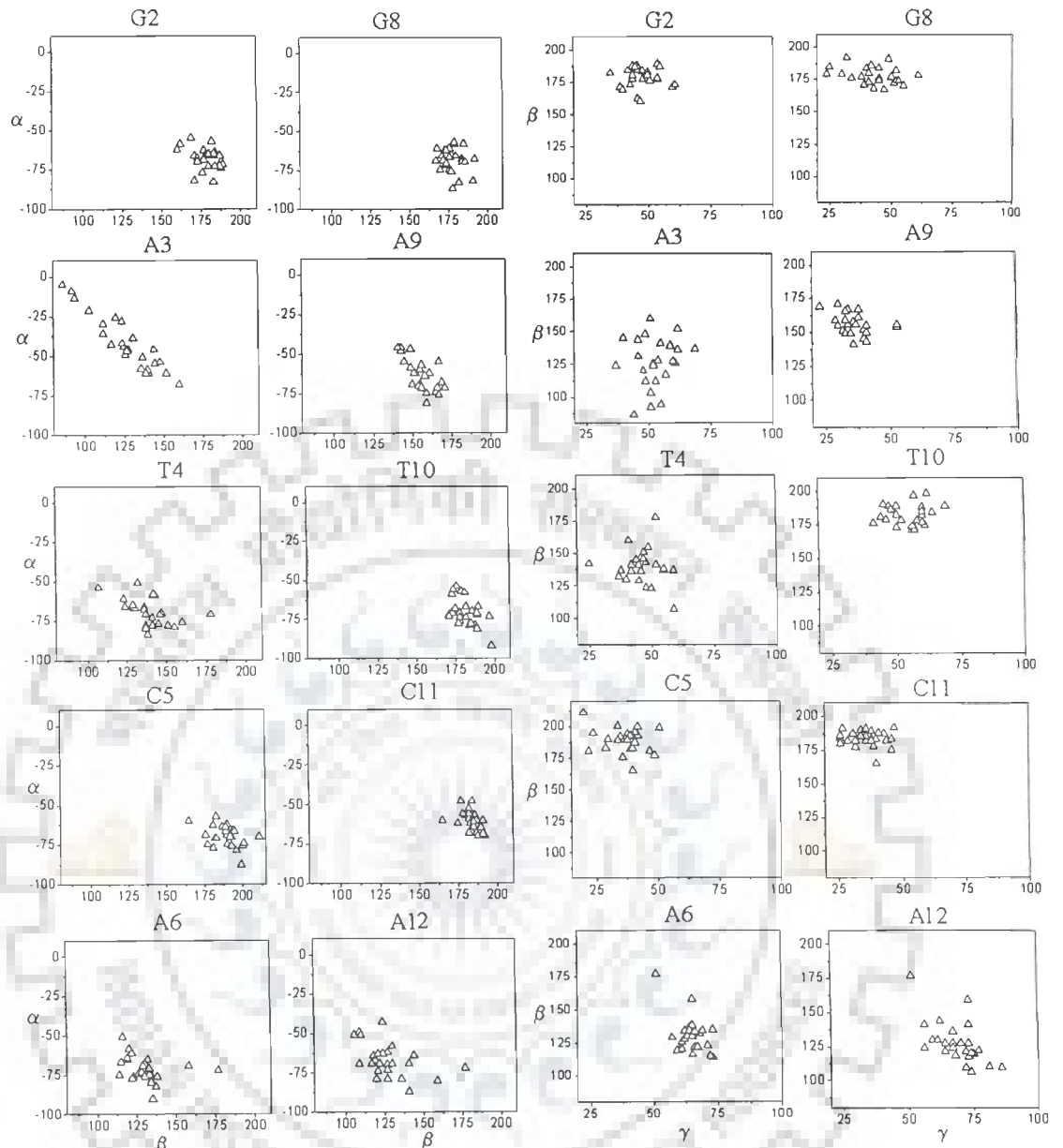


Figure 6.5: Trajectory analysis of 100 ps restrained molecular dynamics simulations showing variations in (a) interproton distances H8/H6-H1' and H1'-H4' (b) backbone torsional angles



(a)

(b)

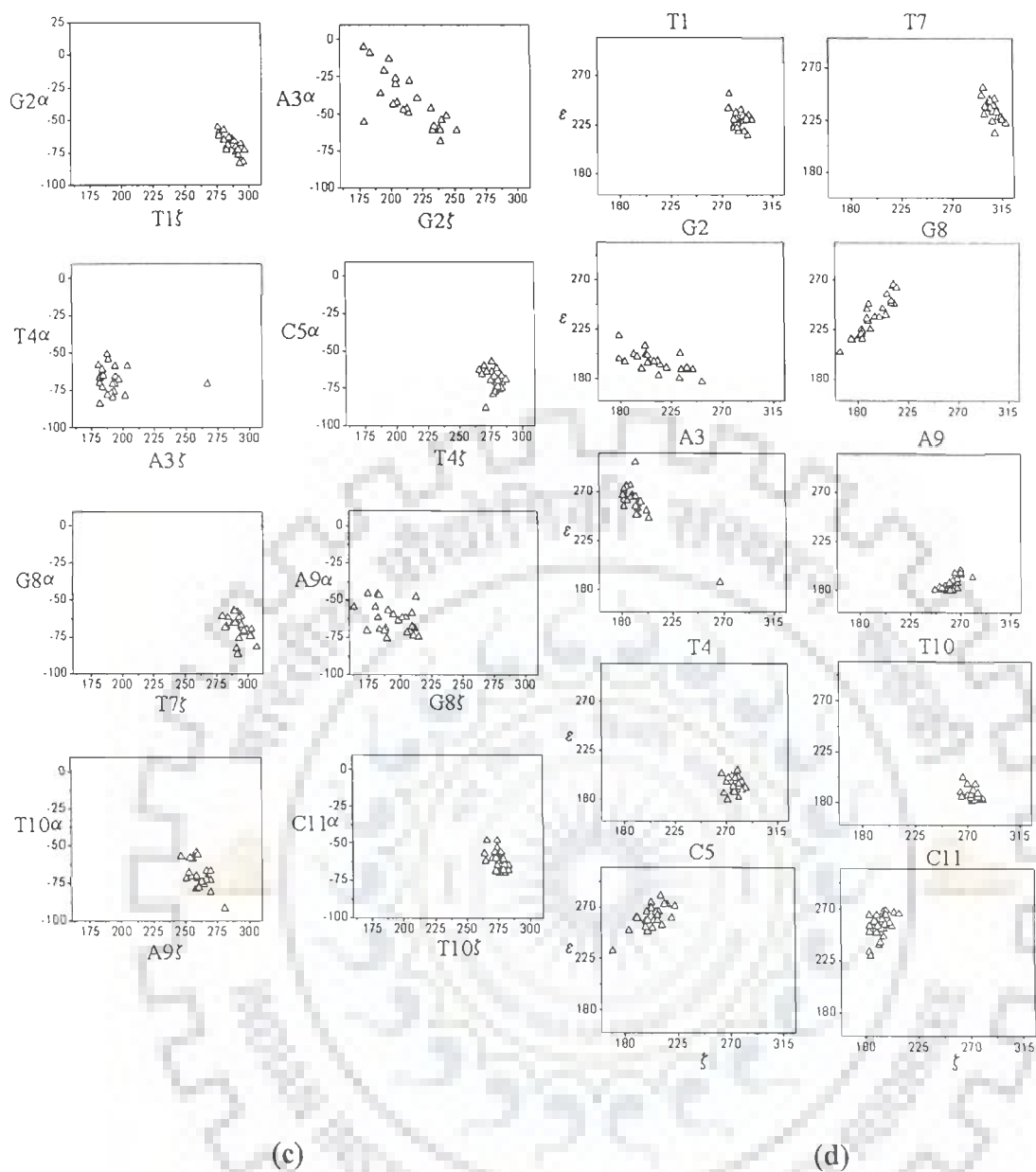


Figure 6.6: Correlation between various torsional angles (a) Correlation between α and β (b) Correlation between β and γ (c) Correlation between $\alpha(n+1)$ and $\zeta(n)$, where n is the residue number (d) Correlation between ϵ and ζ

completely in gauche-, gauche- conformation while for G2pA3, A3pT4 and C5pA6 units, a trans conformation is most stable for ζ angle. The dynamic variation in the backbone torsional angle ζ is also reflected in a change of adjacent dihedral angle ϵ , C4'-C3'-O3'-P. A correlation between ζ and ϵ shows (Fig. 6.6d) that the variations in these two angles are coupled. The torsional angle ϵ deviates from the normal value of -176° to values in the range $\sim 110^\circ$ whenever ζ angle adopts trans conformation, say for example in C5 residue. These values of torsional angles are close to the characteristic value of ϵ , -114° ; ζ , 174° ; χ , -89° ; for B_{II} conformation of DNA and are indeed the most populated conformations. In fact it is found that in first strand T1, T4 are clustered towards B_I conformation while C5 residue is adopting B_{II} conformation. The corresponding residues in second strand adopt practically identical conformations; that is T7, T10 adopt B_I conformation while C11 adopts B_{II} conformation (Fig. 6.6d). In the first strand, A3 adopts B_{II} conformational state in 24 structures while it adopts B_I conformational state in 1 structure. On the contrary, corresponding A9 residue is clustered around B_I conformations in all the 25 structures. The G2 and G8 residues show a large amount of scatter of data in ϵ - ζ correlation (Fig. 6.6d) but a distinct preference for B_{II} conformation is observed. An interesting behaviour of phosphodiester linkage emerges from this data; if the phosphodiester bonds show B_I conformation in one strand, then the corresponding bonds on opposite strand are in B_{II} conformation. For instance, T1pG2 phosphodiester is in B_I conformation state and the base pairing segment on second strand, that is, C11pA12 is in B_{II} conformation or vice versa. Such correlation has recently been observed by Trieb et al on intercalation of daunomycin in $d(\text{CGCGCGATCGCGCG})_2$ by molecular dynamics simulations. It has been suggested that there appears to be a

possibility to directly influence the DNA backbone through complexation and hence lead to a redirection of intercalation caused structural changes to the backbone. Also there has been evidence in literature that on stretching of DNA, B_{II} conformation becomes energetically more favourable and more pronounced (Anguilli et al, 1971; Grzeskowiak et al, 1991; Neidle and Taylor, 1977; von Dreele and Einck, 1977).

6.2.2 Conformation of Daunomycin

Daunomycin consists of three fused aromatic rings B, C and D bound to a cyclohexane ring, ring A, with an amino sugar attached at C7 position. The bond distances and bond angles are generally within the limit of accepted values. The average C-C distance in BCD ring is 1.41 Å. The aromatic part of a glycon is quite planar with rms distance of 1.3 Å for the least squares plane calculated from all the atoms of rings B, C and D without the exocyclic atoms. If all the exocyclic oxygen atoms (O4, O5, O6, O11, O12) as well as C7 and C10 are included in the calculations the rms distance is 1.1 Å. Few deviations greater than 0.1 Å are observed; e.g. C21 lying 0.61 Å on one side of BCD plane.

The orientation of 4OCH₃ group is such that methyl group is pointed away from O5 atom and protrudes into the solvent region. The distance between keto O5 and phenolic O6 and between keto O11 and phenolic O12 are 2.53 Å and 2.51 Å, respectively. Thus they presumably form intramolecular hydrogen bonds. During the course of restrained molecular dynamics simulations, it was observed that O11-H11...O12 had greater tendency to form intramolecular hydrogen bond than O6-H6...O5. Infact out of the 25 structures saved at equal intervals during 100 ps run of dynamics O11-H11...O12 hydrogen bond existed in 23 structures while in 2 structures this distance increased by ~1.6 Å due to H11 pointing in opposite direction towards

C10 atom instead of O12 atom. The corresponding O6-H6...O5 intramolecular hydrogen bond was observed only in 16 structures and the H6 atom faced C7 atom in other 9 structures with no possibility of existence of hydrogen bond.

The torsional angles of the daunomycin molecule in the complex are listed along with those obtained in similar X-ray crystal structures (Langlois d' Estaintot, 1992; Leonard et al, 1992; Nunn et al, 1991) and free daunomycin (Courseille et al, 1979) molecule in Table 6.7. The torsional angles around C19-C20 and C20-C7 bonds are -10° and 12° , respectively. All the atoms except C9 atom are almost in a plane with a maximum deviation of 1.6 Å. The atom C9 is displaced by 0.88 Å in the same direction as the amino sugar relative to the plane of aglycon (Fig. 6.7) and C9-O9 bond is almost orthogonal to the plane of ring A. O7 and O9 atom can no longer form intramolecular hydrogen bond in contrast to that observed in crystal structure of free daunomycin and related anthracycline antibiotics (Courseille et al, 1979; Gabbay et al, 1976; Lipscomb et al, 1994). The torsional angle in the glycosyl linkage is lower than that in the free daunomycin molecule as well as that in corresponding crystal structure of complex of daunomycin with d-TGATCA (Nunn et al, 1991). During simulations, the torsional angle C7-O7-C1'-C2' lies in the range 137° to 154° in 24 structures while it has the value 160° , as in uncomplexed daunomycin, in one of the 25 structures saved. Apparently the change in conformation of glycosyl linkage or presence/absence of intramolecular hydrogen bond is of no great consequence as far as intercalation of drug in DNA base pairs is concerned. The difference in conformation of ring A can be easily visualized on superimposition of the aglycon part in two cases. The amino sugar is in chair conformation with all the side chains pointed away from the aglycon. The torsional angle about C3'-C4' bond is

Table 6.7: Selected torsional angles (°) of the adriamycin in the complex and their comparison with similar structures available in literature

TORSIONAL ANGLES	Present Work TGA+dnm	TGA+ dnm ^a	TGT+ dnm ^b	TGA+ 4'-epi ^c	TGT+ 4'-epi ^d	dnm ^e
RING A						
C20-C7-C8-C9	-37	-56	-40	-45	-50	-48
C7- C8-C9-C10	57	66	55	68	63	58
C8-C9-C10-C19	-54	-35	-44	-60	-42	-38
C9-C10-C19-C20	32	-2	27	33	14	14
C10-C19-C20-C7	-10	10	-11	-8	-1	-5
C19-C20-C7-C8	12	18	14	13	18	20
GLYCOSYL						
C8-C7-O7-C1'	105	129	120	96	95	125
C20-C7-O7-C1'	-130	-115	-125	-139	-142	-114
C7-O7-C1'-O5'	-79	-115	-105	-102	-81	-68
C7-O7-C1'-C2'	157	127	137	132	159	167
AMINO SUGAR						
O5'-C1'-C2'-C3'	-52	-49	-60	-31	-53	-54
C1'-C2'-C3'-C4'	51	50	49	41	52	56
C2'-C3'-C4'-C5'	-49	-20	-17	-53	54	-61
C3'-C4'-C5'-O5'	51	-16	-5	61	57	61
C4'-C5'-O5'-C1'	-56	19	-9	-55	-59	-59
C5'-O5'-C1'-C2'	55	17	42	36	57	57

^a TGATCA + daunomycin (Nunn et al, 1991)

^b TGTACA + daunomycin (Nunn et al, 1991)

^c TGATCA + 4'-epiadriamycin (Langlois d' Estaintot, 1992)

^d TGTACA + 4'-epiadriamycin (Leonard et al, 1992)

^e daunomycin (Courseille et al, 1979)

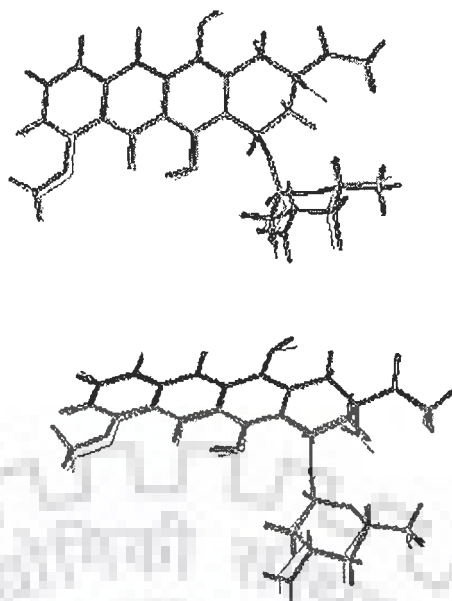


Figure 6.7: Superimposition of the adriamycin in the daunomycin-d-(TGATCA)₂ complex (thick lines) with that of uncomplexed adriamycin (thin lines)

particularly lower (49°) than the expected ideal gauche value (near $\pm 60^\circ$). The C2', C3', C5', O5' atoms are coplanar while the atom C4' is displaced by 0.76 Å away from chromophore while C1' are displaced towards aglycon by the same magnitude.

6.2.3 DNA-daunomycin Interactions

The observed intermolecular NOEs between various drug protons and DNA protons are given in Table 6.3. The NOE connectivities between T1CH₃ and 1H, 2H, 3H protons and between C5H₆, C5H₅ and 4OCH₃ protons are indicative of stacking interactions between protons of drug chromophore and base protons. The 4OCH₃ also gives NOE connectivity with C5H₂' proton. In addition A6H₂ and A6H₁' give NOE connectivities with 8axH of ring A and 1'H of daunosamine sugar, respectively. This shows that the aromatic chromophore of the drug intercalates between T1pG2 and C5pA6 base pair steps such that ring D is positioned near T1 and C5 bases while ring A is close to A6 base. This is possible if the drug chromophore is in an orientation that is perpendicular to the long axis of the base pair with ring D protruding out on major groove side. The observed NOE between A3H₁' and 5'CH₃ protons and several other observed NOE connectivities between daunosamine sugar protons and A3 residue show that the amino sugar of the drug is close to third base pair on its minor groove side. The position of the drug molecule with respect to hexanucleotide and hence the complete geometry of the complex gets defined by several other intermolecular NOEs (Table 6.3) observed in the NOESY spectra. The corresponding interproton distances in the structure obtained by restrained molecular dynamics are close to that calculated from intensities of cross peaks in NOESY spectra and are shown in Table 6.3.

A view showing the stacking interaction of the anthracycline chromophore between the bases is presented in Fig. 6.8a. This clearly shows the manner in which the aglycon chromophore is placed between adjoining base pairs, lying almost orthogonal to the long axis of T1.A12 and G2.C11 base pairs. Figs. 6.8b show the stacking of G2.C11 base pair over A3.T10 base pair and A3.T10 base pair over T4.A9 base pair, respectively. These are somewhat similar to that existing in canonical B-DNA structures but there are significant deviations from the pseudo 2-fold symmetry relating the backbones of the B-DNA molecules. The helix axis also is not in the same position in any two base pairs as would be expected for a perfect B-DNA conformation. The G2.C11 base pair is translated towards the minor groove relative to A3.T10 by about 1.2 Å. It is also tilted with respect to adjacent base pair by about -16° . This represents an alteration in the base stacking at site one removed from the intercalative site. An opposite translation of the axis of G2.C11 base pair by about 0.7 Å relative to T1.A12 is also seen around the intercalator in Fig. 6.8a. The stacking of A3.T10 base pair over the T4.A9 base pair at the center of the molecule (Fig. 6.8b) shows stacking that is typical of purine-pyrimidine sequences in B-DNA except that the two base pairs are translated along the long axis of base pair by about 1 Å. These changes in stacking patterns among adjacent base pairs (including third base pair) get reflected in the changes in chemical shift of base protons in the NMR spectra on binding (courtesy Uma Sharma).

One of the significant features of anthracycline antibiotics is that changing substituent groups at ring A, ring D or daunosamine sugar have moderate or no influence on its biological activity. Some constituent groups are however important for biological function. Fig. 6.9 shows the position of drug with respect to DNA molecule to

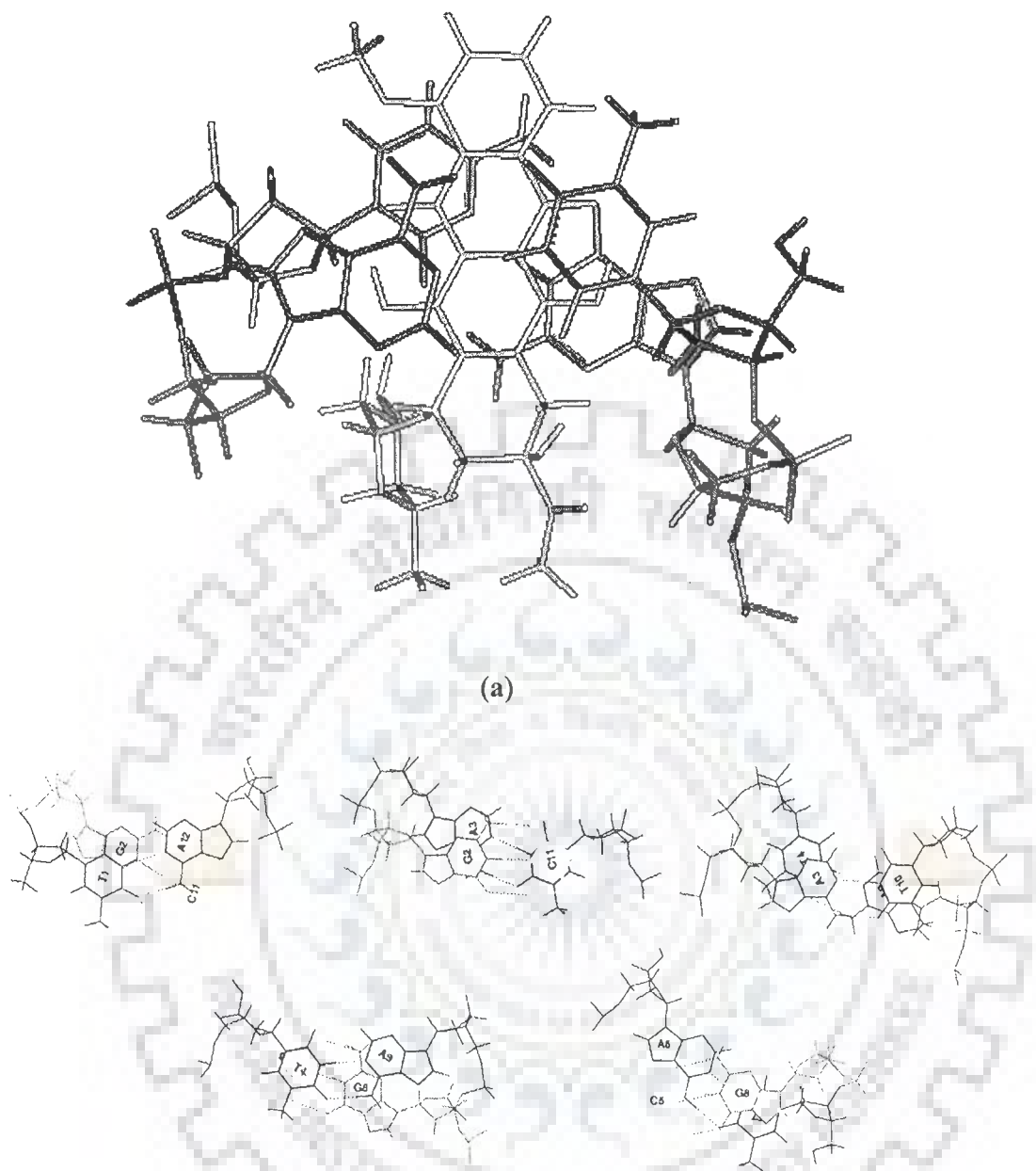


Figure 6.8: (a) stacking interaction of the anthracylene chromophore between the bases (b) Overlap geometry of different base pair steps in complex showing stacking interactions

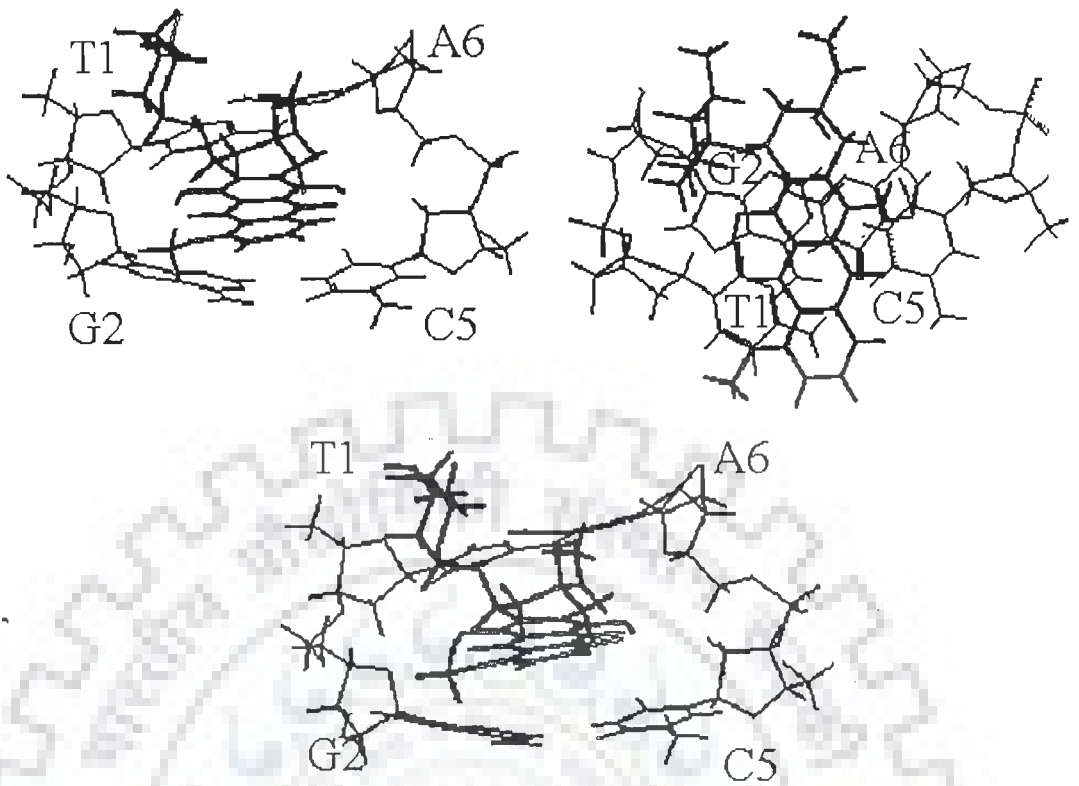


Figure 6.9: Intercalation site showing the orientation of the adriamycin with respect to base pairs (a) front view (b) top view

illustrate some of the hydrogen bonding interactions and close van der waals contacts. It is found that the hydroxyl oxygen atom of 9OH in ring A is within the hydrogen bonding distance of N3 and N2 atoms of guanine base G2. The distance between O9 and G2N3 atom is 2.7 Å and varies in the range 2.65-2.90 Å in the 25 structures saved at equal intervals during 100 ps rMD simulations indicating thereby that a strong hydrogen bond exists. The distance of O9 from G2N2 atom is 2.9 Å and varies in the range 2.76-3.20 Å suggesting the existence of another hydrogen bond. The O9 atom has a van der waal contact of 3.6 Å with O4' atom of G2 residue. O7 atom of drug, which links the chromophore and amino sugar, is close to N2 of G2 residue with a separation of 2.8 Å. The distance of O7 atom from O9 atom of 9OH hydroxyl group in ring A is 4.1 Å so that there is no possibility of intramolecular hydrogen bond between O7 and 9OH in contrast to that found in X-ray crystal structures of daunomycin in its uncomplexed form (Courseille et al, 1979; Gabbay et al, 1976; Lipscomb et al, 1994). During the entire course of simulations, the O7-9OH hydrogen bond was nonexistent. Thus the hydroxyl group on O9 atom, which appears to be important for biological activity, is involved with two hydrogen bonds to a guanine residue adjacent to the chromophore, donating one to N3 and receiving one from N2 atom. Also the 9OH-G2N3 hydrogen bond is shorter than 9O-G2N2H hydrogen bond. In order to have these two hydrogen bonding interactions, O9 and O7 atoms are close to G2 residue in such a way that 9OH is away from O7 atom. This hydrogen bonding interaction is likely to be sensitive to conformation of ring A which is observed to be different from that in uncomplexed daunomycin (Table 6.7).

The X-ray crystallographic structure of daunomycin with d-TGTACA (Nunn et al, 1991) shows that carbonyl oxygen at C13 position of ring A is bonded to O2 of the ring

T1 residue through a bridging water molecule while that in daunomycin-d-TGATCA complex shows water molecule hydrogen bonding to O13 without any further interaction (Nunn et al, 1991). The distance between O13 and O2 of T1 in our rMD structure is 4.7 Å so that possibility of hydrogen bond through bridging water molecule exists. Further the distance between O5 and C5N1 atoms is 3.33 Å, that between O4 and O-1P of residue A6 is 6.6 Å and between 4OCH₃ and O1P of residue A6 is 7.46 Å. This suggests that a hydrogen bond involving O4 and O5 atom with phosphate groups of A6 residue are possible through two water molecules acting as bridges in between. The amino group in the daunosamine sugar has been implicated in the electrostatic interactions between the daunomycin and the phosphate group of the nucleic acid [39]. However, in X-ray crystal structure of daunomycin-d-TGATCA (Nunn et al, 1991) the amino group forms hydrogen bonds via its three hydrogen atoms to oxygen atoms in the neighbouring T4 and C5 residues, that is, C5O2, C5O4' and T4O2 having separation of 2.6, 2.8 and 3.1 Å, respectively. In our rMD structures, these distances N-H...O with C5O2, C5O4' and T4O2 atoms are 3.7, 3.8 and 3.1 Å, respectively so that hydrogen bond between amino group and O2 of T4 residue may only be a strong hydrogen bond. It has been shown that ammonium group of daunosamine sugar contributes significantly to the binding (Frederick et al, 1990; Langlois d' Estaintot, 1992; Leonard et al, 1992; Moore et al, 1989; Nunn et al, 1991; Wang et al, 1987, Williams et al, 1990). It shows considerable positional variability and thermal mobility (Lipscomb et al, 1994; Williams et al, 1992). We have therefore looked into these hydrogen bonding contacts during the course of 100 ps simulations. We find that the distance of nitrogen of NH₃⁺ from C5O2, C5O4' and T4O2 atoms are in the range 3.1-4.8, 3.3-4.7 and 2.8-3.2 Å, respectively. On the other intercalation site, the distance of NH₃⁺ from C11O2, C11O4'

and T10O2 atoms are the range 3.0-4.5, 3.3-4.7 and 2.9-3.5 Å, respectively. If we consider 3.3 Å as the cutoff distance for hydrogen then at least two hydrogen bonds of reasonable good strength exist in the complex. The distance of NH_3^+ from O4' of T4/T10 are in the range 4.2-6.0 Å so that there are no contacts through hydrogen bonds as seen in X-ray crystal structures of daunomycin with d-CGTACG (Wang et al, 1987) and d-TGTACA (Nunn et al, 1992).

An interesting feature of anthracycline complexes is the flexibility of glycosidic bond rotation which has a role in anchoring the intercalator in the minor groove of DNA (Frederick et al, 1990, Treib et al, 2004; Wang et al, 1987; Williams et al, 1990). We find that the glycosidic dihedral angle C7-O7-C1'-C2' varies within a short range of angles, 142°-161° (Fig. 6.10a). This dihedral angle adopts an angle of 162°-168° in uncomplexed daunomycin and its analogues (Courseille et al, 1979; Gabbay et al, 1976; Lipscomb et al, 1994). In the X-ray crystal structure of daunomycin complexed to d-TGATCA (Nunn et al, 1992) it is 127° while in several other structures of similar complexes it lies in the range 132°-163° ((Frederick et al, 1990; Langlois d' Estaintot, 1992; Leonard et al, 1992; Moore at el, 1989; Nunn et al, 1991; Wang et al, 1987, Williams et al, 1990). The molecular dynamics simulations of daunomycin with d-(CGCGCGATCGCGCG)₂ have shown (Bertucat et al, 1998) that three distinct conformational states can exist; the first one is 152°-162°, second at 135°-138° and a third is 57-61°. The energy barrier between 137° and 159° conformations is 0.3 to 0.7 Kcal mole⁻¹ and between 137° and 59° is 1.4 Kcal mole⁻¹. We did not observe the presence of 59° conformation during the course of simulations. Apparently only 137° and 159° conformations were readily accessible kinetically. The flexibility of glycosidic bond permits the daunosamine sugar moiety to point towards the minor groove and build stabilizing contacts with DNA through NH_3^+

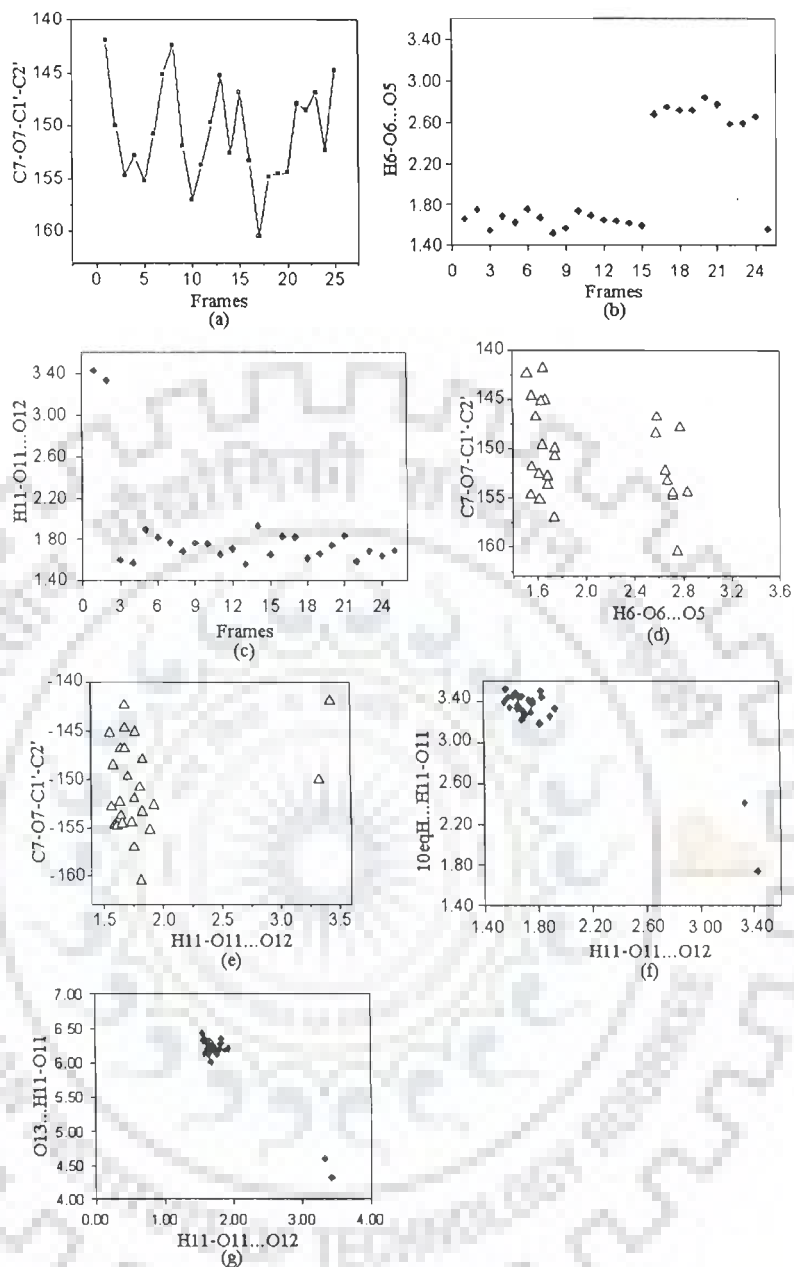


Figure 6.10: Trajectory analysis of 100 ps rMD simulations showing variation in (a) glycosidic dihedral angle $C7-O7-C1'-C2'$ (b) bond length in $O6-H6...O5$ (c) bond length in $O11-H11...O12$. Correlation between glycosidic bond angle and $O6-H6...O5$ (d) glycosidic bond angle and $O11-H11...O12$ (e) $10eqH...H11-O11$ and $O11-H11...O12$ (f) $O6-H6...O5$ and $O11-H11...O12$

moiety. Trieb et al. have shown that in the first conformation centered at 157° , the nitrogen of NH_3^+ moiety is at a distance of 5.5, 5.1 and 3.2 Å from C5O4', T4O2 and T4O4', respectively. In the second conformation centered at 137° , the corresponding distances are 3.2, 3.0 and > 6.0 Å, respectively while in the third conformation centered at 59° , the distances of nitrogen from G6O4' and G6O5' are 3.4 and 3.0 Å, respectively. In our complex, the distance of nitrogen from C5O4'/C11O4', T4O2/T10O2 and T4O4'/T10O4' is in the range 3.1-5.4 Å and that from G2O4' and G2O5' is in the range 9-12 Å. Thus our results are in agreement with the correlation of glycosidic bond with stabilizing hydrogen bonding contacts through NH_3^+ group suggested by Trieb et al. It is important to note that the conformation of glycosidic bond is also related to cleavage of C7-O7 bond and production of free radicals which are responsible for cardiotoxicity. During the course of simulations, it was observed that the hydrogen atom of 6OH group of ring B of daunomycin pointed towards O5 atoms in 16 structures (Fig. 10 b) and was away from O5 atoms but pointed towards O7 atom in 9 structures. The hydrogen of 11OH on the other hand pointed towards O12 in all except 2 structures (Fig. 10c). Thus both the hydrogen bonds, 6OH...5O and 11OH...12, are not stabilized in all the structures. This is in sharp contrast to the existence of both hydrogen bonds in the uncomplexed daunomycin, adriamycin and 4' epiadriamycin investigated by us by molecular dynamics simulations using NMR restraints. In order to see if the stability of these hydrogen bonds is related to glycosidic bond rotation, we looked into their correlation in various structures. Figs. 10d and 10e shows that the presence and absence of hydrogen bonds is not dependent on the glycosidic bond which varies independently in the range 142° - 161° . However on positioning of hydrogen atom of 11OH towards ring A, its distance from 10eqH, 10axH and O13 atoms is considerably decreased, as

Table 6.8: Close contacts between drug and DNA molecule

S.No	Protons	Distance (Å)	S.No	Protons	Distance (Å)
1.	T1O2-10axH	2.76	22.	A3C2-H1N3'	4.20
2.	T1H2'-11OH	2.61	23.	A3H2-N3'	4.30
3.	T1H2'-13O	4.34	24.	A3H2-H1N3'	2.57
4.	T1H2''-13O	5.76	25.	T4O2-4'H	3.49
5.	G2N3-10eqH	2.75	26.	T4O2-H2N3'	4.99
6.	G2N2-3'H	2.67	27.	T4O4'-CH ₂ OH	2.89
7.	G2O4'-10eqH	2.44	28.	C5O2-2axH	2.39
8.	G2H1N2-O9	2.26	29.	C5O2-H3'	3.19
9.	G2H1N2-O7	2.15	30.	C5C1'-2eqH	4.06
10.	G2H2N2-3'H	2.46	31.	C5H1'-O5	2.73
11.	G2H2N2-NH ₃	3.43	32.	C5H1'-O6	2.71
12.	G2H4'-C14	3.27	33.	C5H2'-O5	3.43
13.	G2H4'-C13	3.09	34.	C5H1'-6OH	2.25
14.	G2P-O13	6.00	35.	C5H1'-2eqH	2.56
15.	G2H5'-O13	3.30	36.	A6N3-7H	2.91
16.	G2O4'-O13	3.63	37.	A6O4'-7H	3.21
17.	G2H1'-O13	4.68	38.	A6O4'-H1'	3.81
18.	G2C5'-O13	3.80	39.	A6C4'-H1'	4.53
19.	G2O3'-O13	5.11	40.	G6H5'-C2'	4.07
20.	A3N3-H1N3'	4.31	41.	G6H5'-2eqH	3.32
21.	A3N3-H2N3'	5.00	42.	G6H5'-H1'	3.46

expected. Several other non-bonded van der waals interactions have been observed (Table 6.8) which may be important in stabilizing the complex. The 10eqH is close to G2N3 atom (2.75 Å); 10eqH has close contact with G2O1'atom (2.44 Å); 3'H is close to C5O2 atom (3.19 Å); 2'eqH is closed to C5H1'atom (2.56 Å); 8axH is close to A6H2 atom 3.5 Å; A3H4' is closed to 5'CH₃ group (4.0 Å). Several of these contacts have been observed in X-ray crystal structures of daunomycin with d-CGTACG [27]; for example contact between 8axH and G6H1N2 having a distance of 2.43 Å corresponds to A6H2-8axH contact in our rMD structure. In addition there are contacts involving O5, O6, 6OH atoms which are at a distance of 2.73, 2.71 and 2.25 Å from C5H1' atom, respectively. Further 4OCH₃ is close to C5H2' atom which is 2.7 Å away. These observations are significant and establish the involvement of 4OCH₃, O5, O6, 6OH and ring A protons 2'eqH, 10eqH, 8axH, etc. in stabilizing the drug-DNA complex, Summarizing the interactions, we find that atoms on one side of planar anthracycline ring, that is, 4OCH₃, 5O, O6, 6OH, O7 as well as ring A protons and daunosamine sugar protons are involved in highly specific interactions with DNA and apparently the atoms/groups of atom in position 1, 2, 3, 11, 12 are not critical for binding.

6.3 CONCLUSIONS

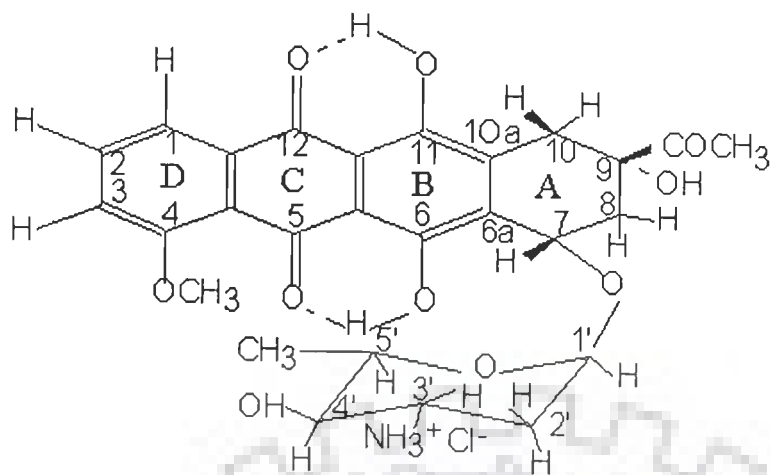
The restrained molecular dynamics simulations of the complex of daunomycin with DNA hexamer sequence d-TGATCA based on intermolecular and intramolecular NOEs have led to a detailed conformational analysis. Stabilization of the drug in the complex is achieved by the intercalation of the aromatic aglycon chromophore of the drug between the base pairs at T1pG2 and C5pG6 sites, which result in π - π stacking and dipole-dipole interactions, the hydrogen bonding interactions and van der waal's interactions. Ring D protrudes out in solution and does not have significant overlap

with adjacent base pairs. The O9 atom is involved in hydrogen bond formation with G2N2 and G2N3 and has close contact with G2O4' atom. The O13 atom of 9COCH₃ group and O7 atom at glycosyl linkage have close contacts with T1O2 and G2N2 atoms, respectively. The conformation of ring A of the drug therefore plays an important role in drug-DNA interactions. In the minor groove, the contact of NH₃ group of daunosamine sugar with T4O2 and C5O2 atoms as well as several other contacts between atoms such as A3H1'-5'CH₃; A3H4'-5'CH₃; C5H2'-4OCH₃; A6H1'-1'H; C5H1'-5O; C5H1'-6OH; etc are involved in highly specific non-bonded interactions. The specificity of drug-DNA interactions arises from conformation of ring A, glycosidic bond, position of NH₃⁺ in minor groove and substituent at position 4, 5, 6, 7, 9 and daunosamine sugar. The third base pair, that is, the one adjacent to intercalating base pair is also involved in drug-DNA interactions. The right handed DNA has significant variations both in backbone geometry and sugar puckering associated with the accommodation of a large intercalator molecule with an amino sugar. Changes in conformation of the right handed double helix are dependent on sequence or the local environment. The intercalating base pairs show considerable buckle and minor groove is wider. The conformation of G2pA3, A3pT4 and C5pA6 are close to B_{II} conformation while the phosphorus directly lying in opposite strand is in B_I state. The β torsional angle of A3 and T4 residue and δ (and hence pseudorotation P) of T4 residue have considerably lower values in complex. The daunosamine molecule also adjusted its conformation in order to fit tightly into the double helix; the ring A conformation has changed to permit 9OH and 9CO to come in close contact with G2 base. On the basis of this conformational analysis based on NMR data, we conclude that it is possible to establish the molecular basis of drug action.

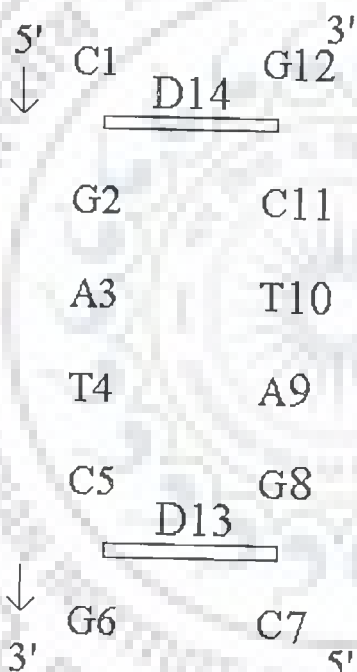
STRUCTURAL INVESTIGATIONS OF HEXAMER d-(CGATCG)₂ COMPLEXED WITH DAUNOMYCIN

The complex of daunomycin with d-(CGATCG)₂ has been characterized on the basis of 1D and 2D NMR techniques. Titration studies are carried out on daunomycin-d(CGATCG)₂ complex by addition of daunomycin (30.2 mM) to 400 μ l of d(CGATCG)₂ (duplex concentration 3.4 mM) in steps of 10 μ l. 90 μ l of daunomycin is added in the final step in order to achieve 2:1 ratio of adriamycin to hexamer duplex concentration (Table 2.1 of chapter 2, Fig. 7.1).

1D Proton NMR spectra at drug to DNA ratio 2:1 is shown in Figure 7.2 (a-c). The phase sensitive double quantum filter COSY (DQF COSY) and TOCSY spectrum was recorded for the 2:1 complex at 12° C and is shown in Fig. 7.3(a-g). Two-dimensional NOESY spectra of 2:1 daunomycin-d(CGATCG)₂ complex were recorded with different mixing times ($\tau_m = 75, 150, 200, 250$ ms) in D₂O and H₂O solvents. NOESY spectra recorded with different mixing time is shown in Fig. 7.4 (a-f). There was a single major DNA conformer, which had the expected patterns of correlation in DQF COSY, TOCSY (Fig. 7.3) and NOESY spectra, (Fig. 7.4). Similarly there was one set of major conformer of the drug bound to DNA thus the dyad symmetry is retained in the the complex. The amount of free DNA or drug, as judged from the chemical shift positions of free DNA (Barthwal et al, 2003) and drug (Barthwal et al, 1996), is negligible. This is expected due to high value of K_{eq} for drug-DNA complex formation compared to the K_{eq} value for drug-dimer or DNA

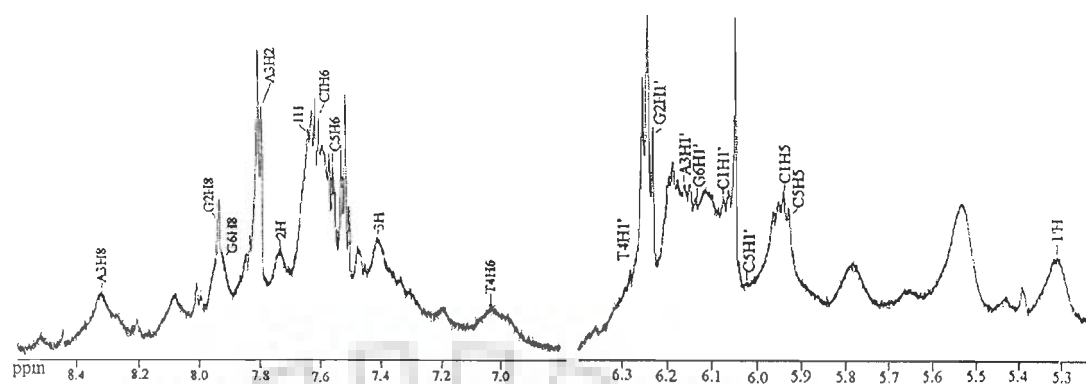


(a)

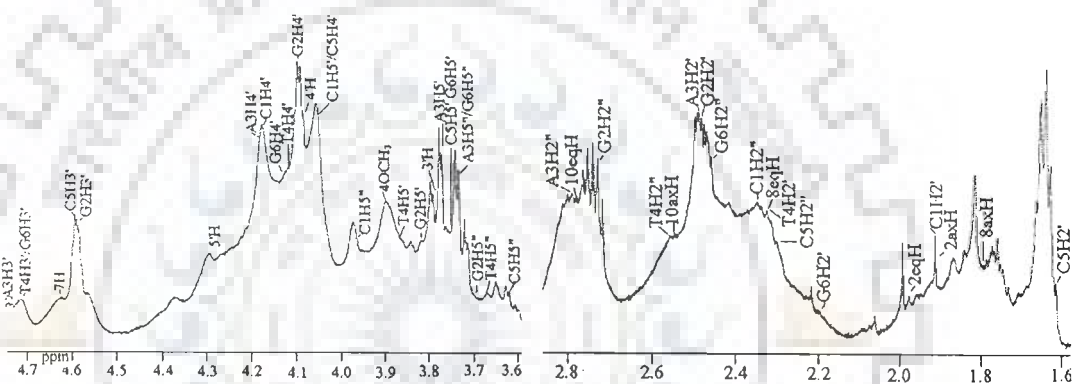


(b)

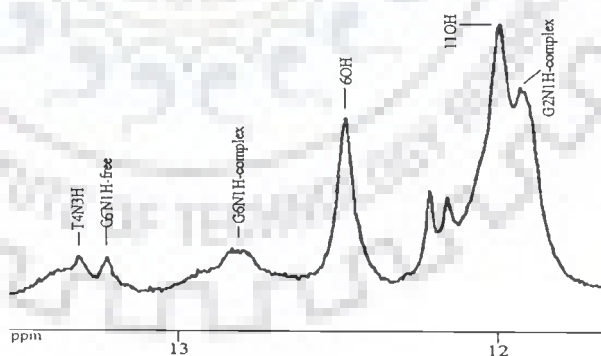
Figure 7.1: (a) Molecular structure of daunomycin and (b) Schematic representation of the 2:1 complex of daunomycin with d-CGATCG₂



(a)



(b)



(c)

Figure 7.2: 1D proton NMR spectra of daunomycin-d-CGATCG at drug to DNA ratio (D/N) = 2.0 (a) base and H1' regions (b) H3', H4', H5'/H5'' and H2'/H2'' regions in D₂O at 295 K (c) imino and amino region in water at 295 K

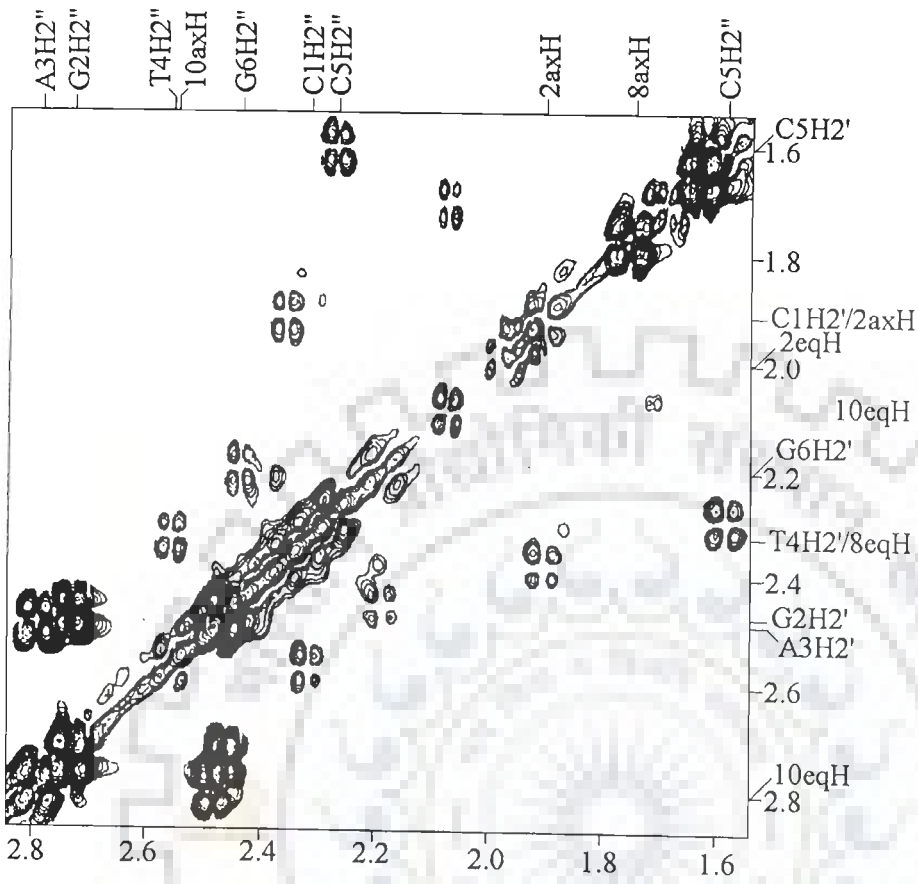


Figure 7.3(a)

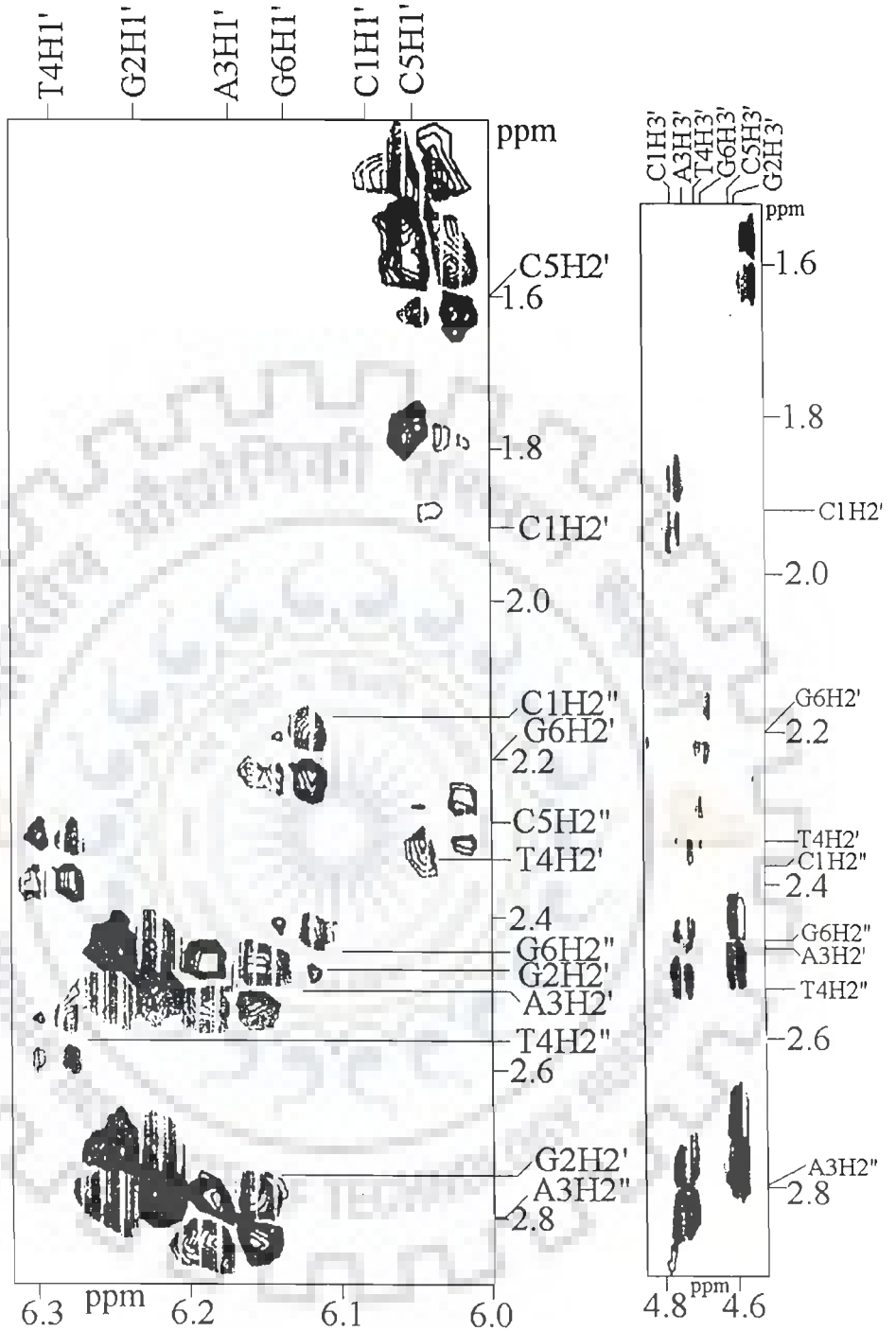


Figure 7.3 (b)

Figure 7.3(c)

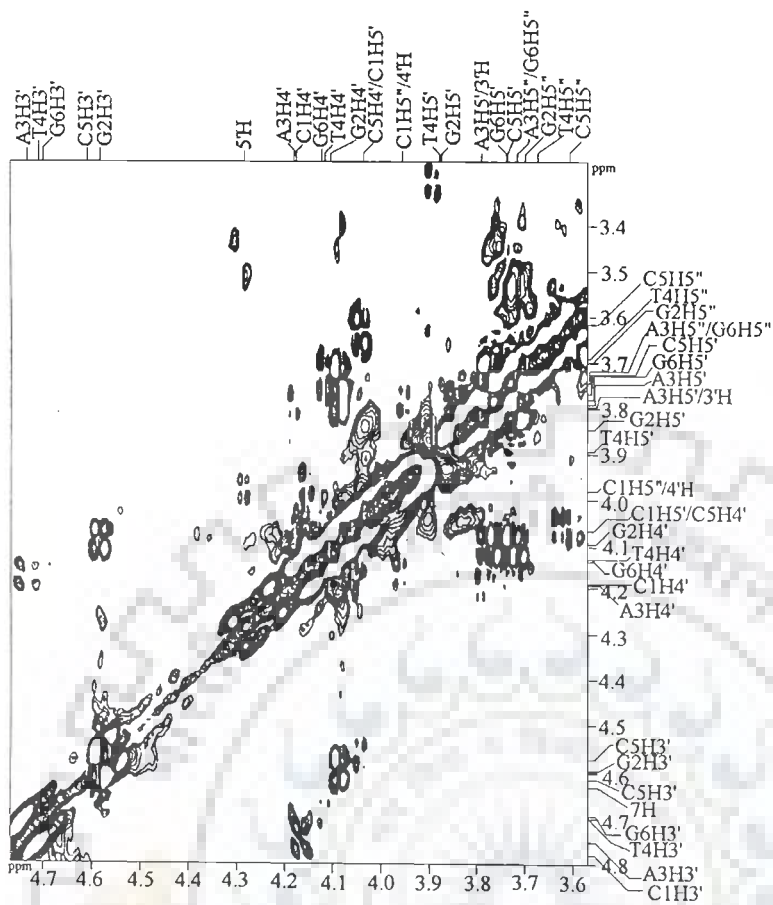


Figure 7.3(d)

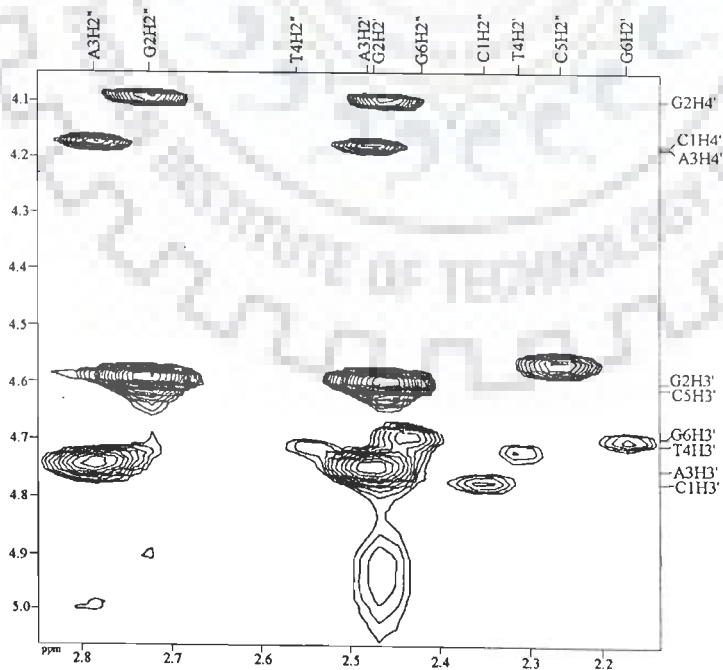
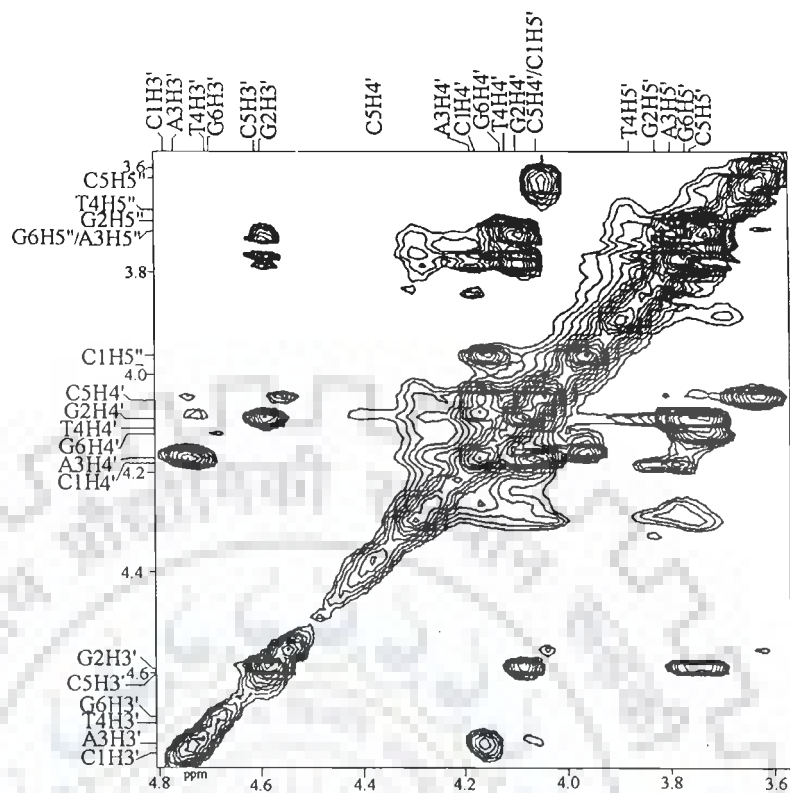
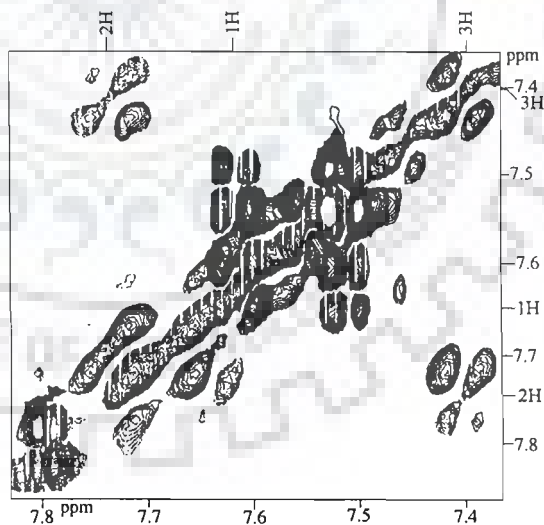


Figure 7.3(e)



(f)



(g)

Figure 7.3: Expanded portion of phase sensitive DQF COSY spectrum (a-d, g) expanded portion of TOCSY spectrum (e, f) of $d(\text{CGATCG})_2 + \text{daunomycin}$ complex

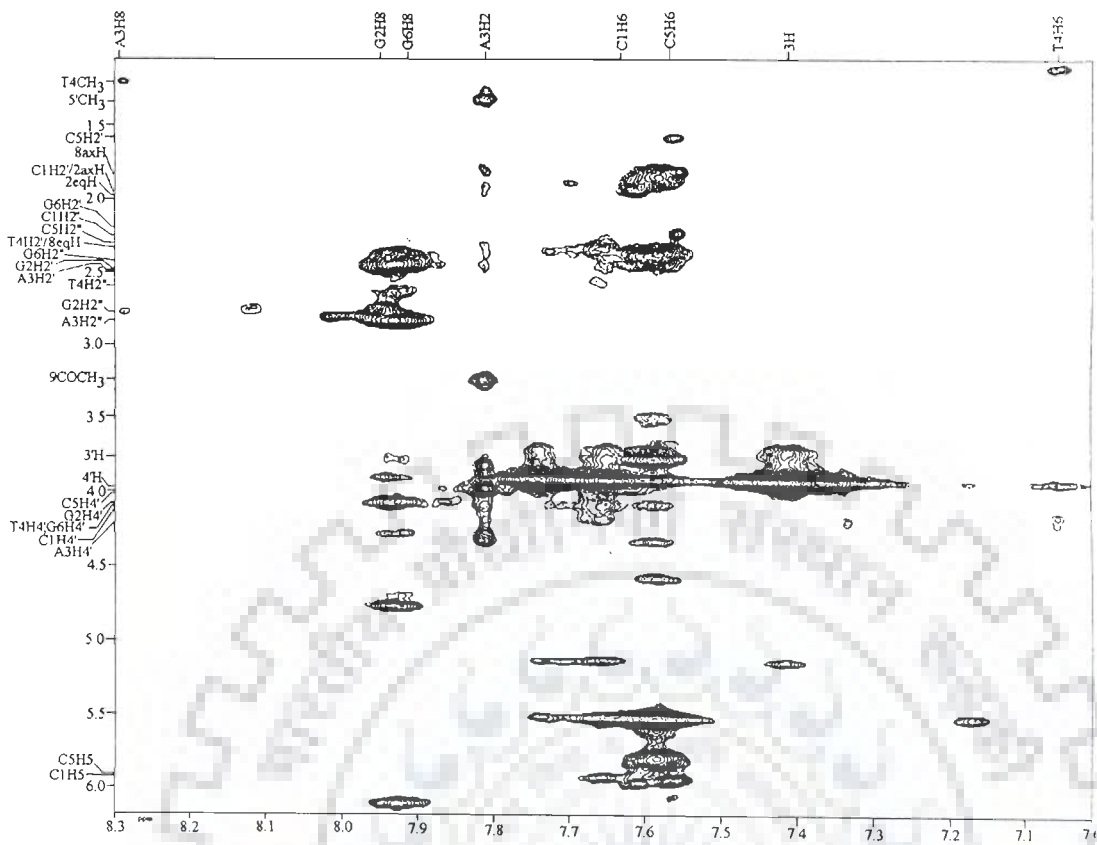


Figure 7.4(a)

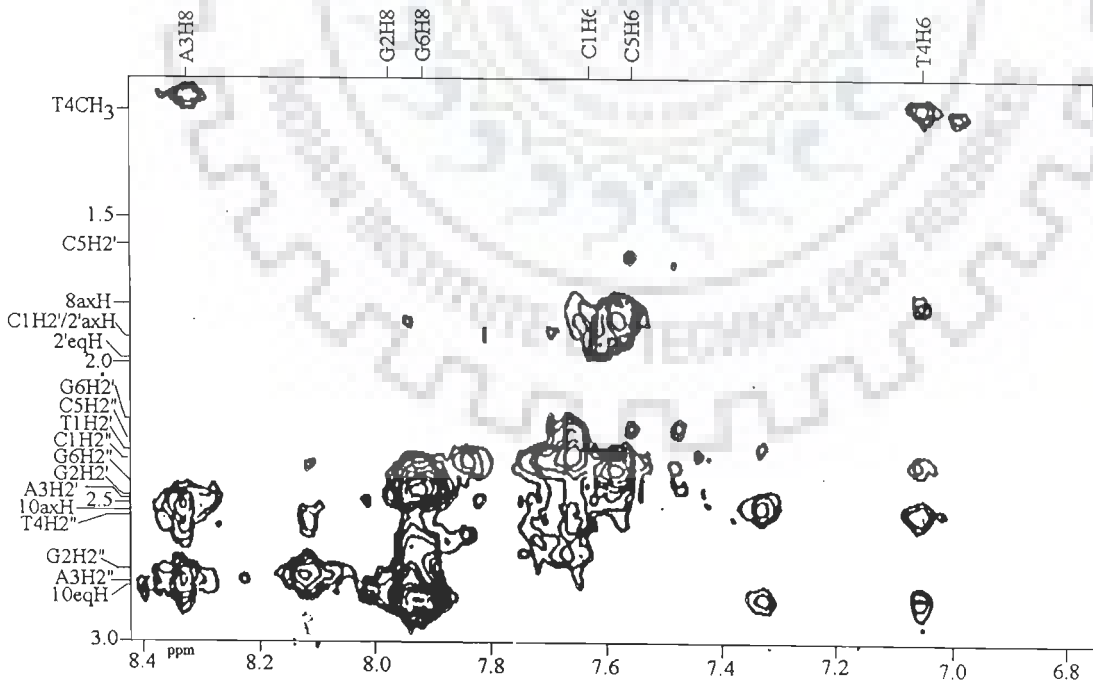


Figure 7.4(b)

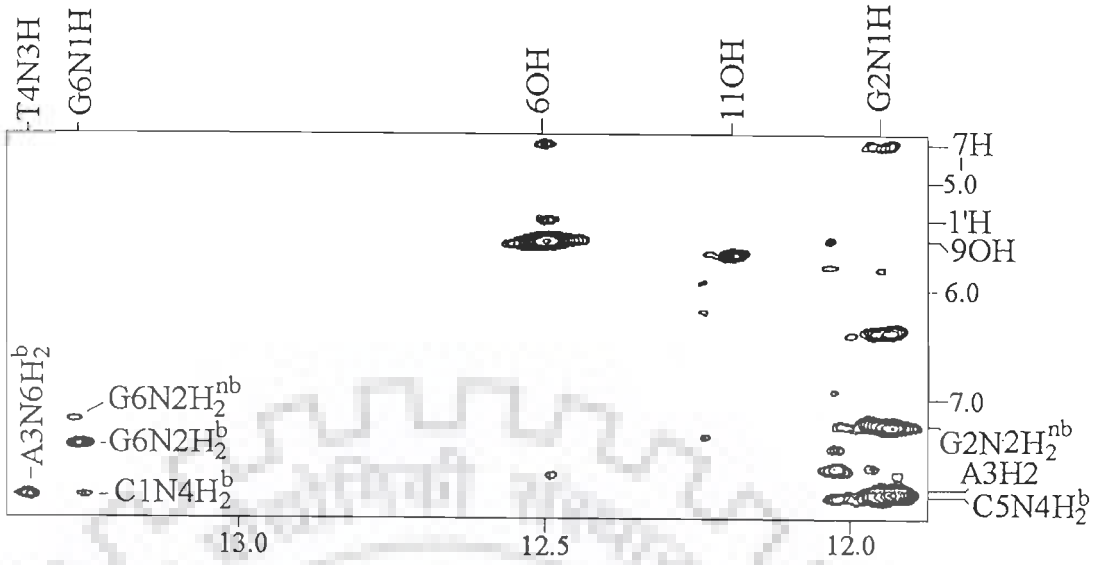


Figure 7.4(c)

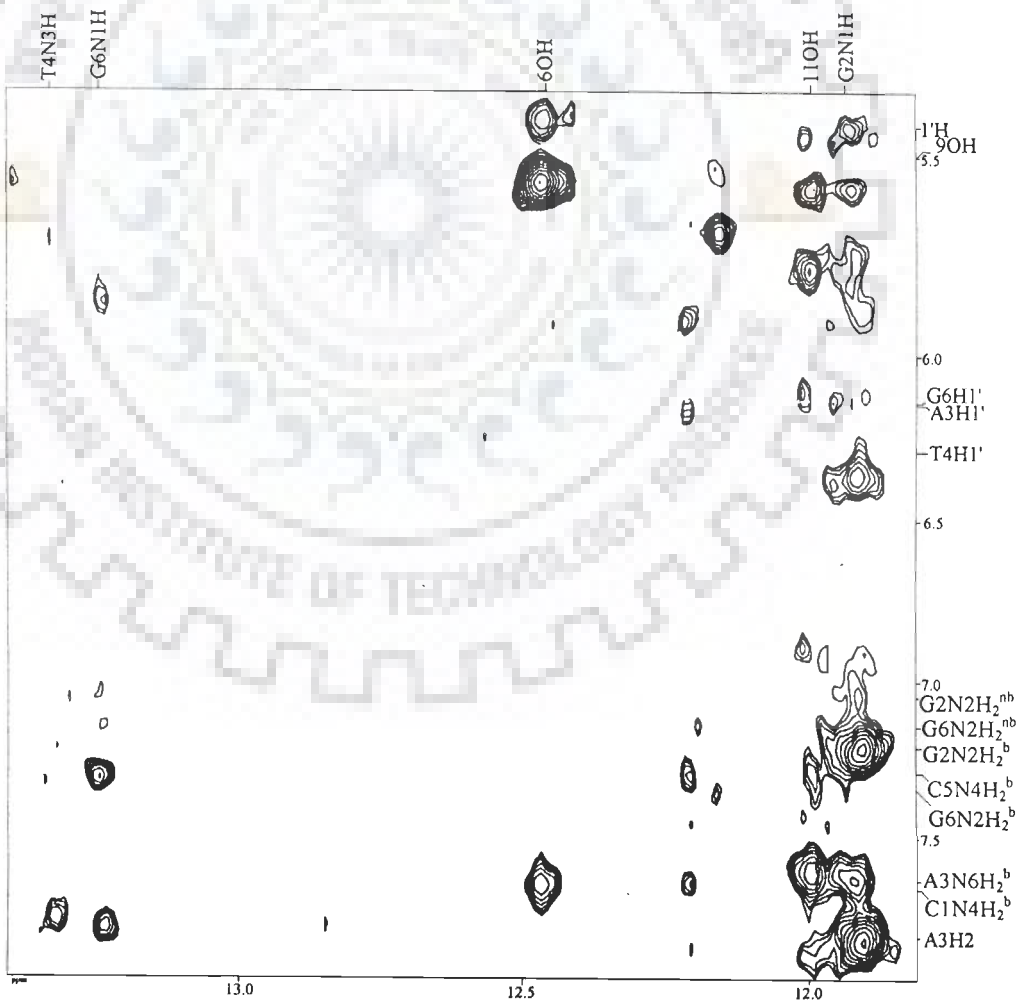


Figure 7.4(d)

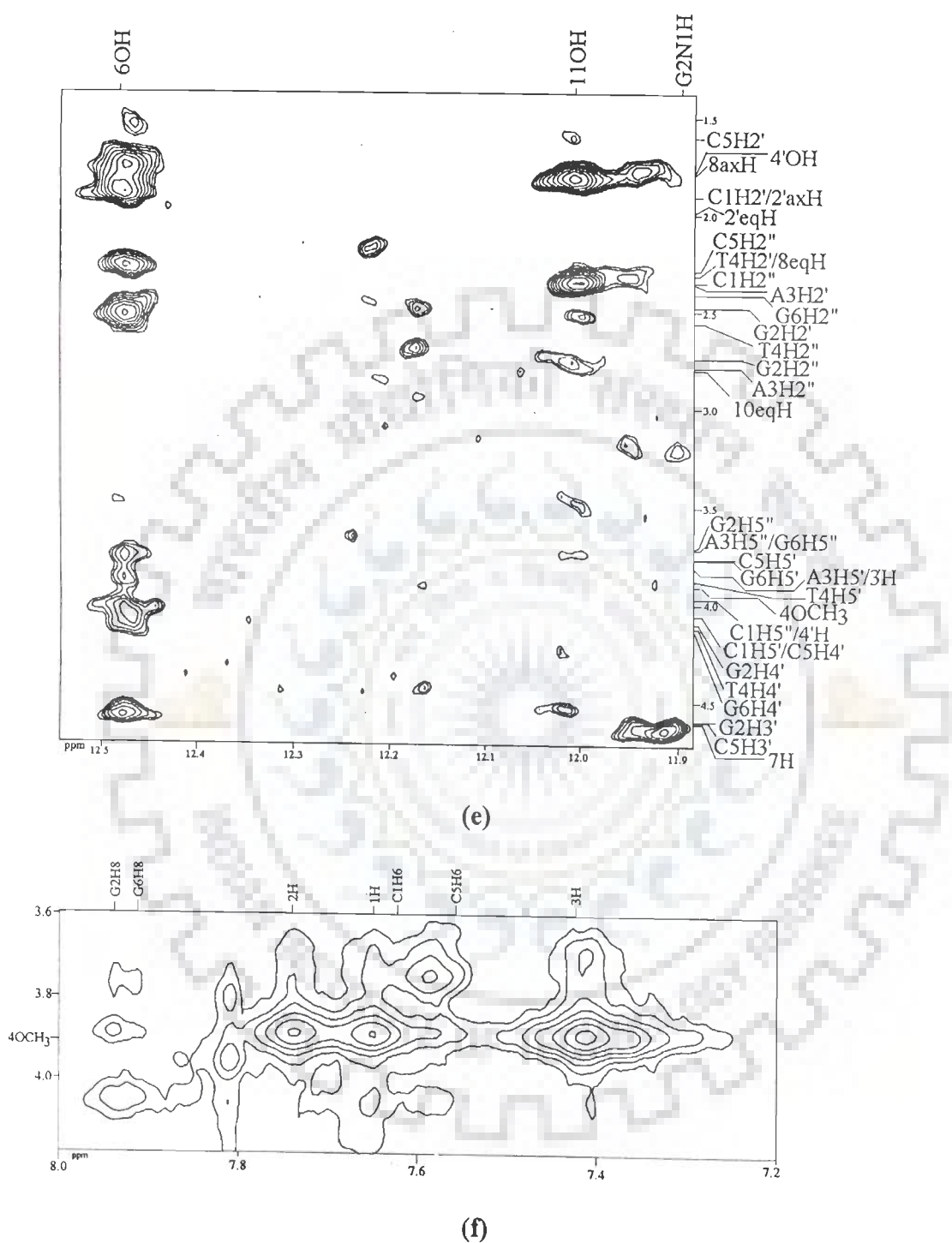


Figure 7.4: Expanded portion of phase sensitive NOESY spectrum of d-(CGATCG)₂ and daunomycin complex (a) $\tau_m = 250$ ms (b) $\tau_m = 200$ ms (c) $\tau_m = 100$ ms (d) $\tau_m = 250$ ms (e) $\tau_m = 100$ ms (f) $\tau_m = 250$ ms

duplex formation (Davies et al, 2000). Same has been established recently by studies on complexation of daunomycin with various tetramer sequences of DNA (Davies et al, 2000) by NMR. The linewidths of all the singlet resonances in the aromatic region (6.0-8.5 ppm) from both drug and nucleotide are relatively large and similar. These are characteristic of a complexed drug molecule in slow exchange on the chemical shift scale. The complex thus formed remained stable indefinitely.

7.1 SEQUENTIAL ASSIGNMENT

The H8, H2 and H6 resonances appear in the region of aromatic protons in the range of 7.05-8.33 ppm. The deoxyribose sugar H1' protons resonate between 6.03-6.29 ppm (Fig. 7.2a) and the sugar H3', H4', H5', H5'', H2' and H2'' resonate between 1.91-4.76 ppm (Fig. 7.2b). The thymine CH₃ protons are observed around ~ 1.08 ppm. The phase sensitive double quantum filter COSY spectrum recorded on this complex gives through bond scalar coupling interactions like H1', H2'/H2'', H3', H4' protons within each of the six sugar ring systems (Fig. 7.3).

7.1.1 ¹H Resonance Assignment of d(CGATCG)₂

The resonance assignment of d(CGATCG)₂ in the complex is carried out by following the standard strategies available in the literature for assignment of B-DNA (Feigon et al, 1982; Frechet et al, 1983; Hare et al, 1983; Hosur et al, 1988; Scheek et al, 1983). Fig. 7.3a shows all the six sets of H2'-H2'' connectivities. These sets of H2'-H2'' connectivities are coupled to their corresponding H1' and H3' protons (Fig 7.3b and 7.3c). The H3' of all residues are coupled to their H4' proton which are further coupled to their respective H5', H5'' protons (Fig 7.3d-f). The base resonances at 7.62 and 7.56 ppm give intense NOE cross peaks with protons resonating at 5.94 and 5.92 ppm, respectively and are therefore assigned to pairs of cytosine H6 and H5 protons

(Fig. 7.4a). The methyl resonance at 1.08 give intense NOE cross peak with base proton at 7.05 ppm which was assigned to T4H6 base proton (Fig. 7.4a).

Six sets of deoxyribose sugar protons thus recognized are assigned to their corresponding residues on the basis of base-H2', H2'' connectivities (Fig 7.4b). Each residue is expected to give two intranucleotide connectivities with H2' and H2'' protons and two internucleotide connectivities with H2' and H2'' protons of the preceding residue in the sequence. It is evident from Fig. 7.4b that one of the cytosine H6 proton resonating at 7.62 ppm gives only two intranucleotide connectivities with H1', H2', H2'' protons and hence is assigned as the terminal residue at 5'-end. Therefore the other H6 proton resonating at 7.56 ppm gets assigned to C5H6 base proton. We observed the internucleotide connectivity of T4H6 base proton with H2'/H2'' protons of A3 residue in the NOESY spectra recorded at $\tau_m = 250$ ms (Fig 7.4b). The adenine base proton, A3H8 in the sequence also gives NOE connectivity with T4CH₃ proton showing their proximity (Fig. 7.4b). Several additional NOEs between pairs of protons H1'-H4', H2''-H4' and base-H1', H3' (Fig. 7.4a) are also observed which are used for further analysis of pseudorotation phase angles(P) and glycosidic bond rotation (χ) of deoxyribose sugars.

7.1.2 Exchangeable Proton Resonances of Hexanucleotide in the Complex

NOSEY at $\tau_m = 250$ ms and 100 ms recorded in water gives interresidue and interstrand cross peaks. A3H2 showed an intense and a less intense cross peak in imino region (11.5-14.0 ppm) which were assigned as T4N3H and G2N1H, respectively. T4N3H is further confirmed by a strong and a weak cross peak in amino region (6.6-9.0 ppm), which were assigned to A3NH₂ and C5N4H₂. Similarly G2N1H is confirmed by two very strong and a fairly strong cross peaks in imino region which

were assigned to C5N4H₂ (bonded), G2N2H₂ (bonded) and G2N2H₂ (non-bonded), respectively (Fig. 7.4c). G6N1H at 13.24 ppm was also assigned on the basis of its strong and weak cross peaks with G6N2H₂ bonded and non-bonded, respectively and a strong interstrand cross peak with C1N4H₂ (Fig. 7.4c-e). The water spectra shows four interstrand (Watson and Crick type) cross peaks, which confirms the existence of hexamer in duplex form after the formation of 2:1 complex. The unambiguous assignment of all protons of d-(CGATCG)₂ in complex was thus made. The change in chemical shift of DNA protons in 2:1 drug to DNA complex with respect to the corresponding chemical shifts in free DNA (Barthwal et al, 2003) are shown in Table 7.1.

7.1.3 Daunomycin Resonance Assignments in the Complex

The complete unambiguous assignment of uncomplexed ¹H NMR of free daunomycin in both D₂O and CDCl₃ (Barthwal et al, 1996) provide the basis for drug resonance assignments in the complex. The non-exchangeable protons of ring D, that is, 1H, 2H and 3H are observed around in the region 7.4-7.8 ppm. These give NOE cross peaks with 4OCH₃ (Fig. 7.4f). The intensity of their cross peaks is expected to be maximum with 3H proton and minimum with 1H proton. Accordingly these have been assigned. (Table 7.2) In ring A 8axH and 8eqH; 10axH and 10eqH are coupled to each other through strong geminal couplings. These pair of protons gives intense cross in DQF COSY spectra (Fig 7.3g). 8axH and 8eqH gives strong cross peak with 7H resonating at 4.62 ppm. The resonance at 3.20 ppm due to three protons is therefore assigned to 9COCH₃ protons of ring A. The proton resonating at 1.33 ppm is assigned to 5'CH₃ protons of daunosamine sugar. This resonance is strongly coupled to 5'H proton

Table 7.1: Chemical shift (ppm) of various DNA protons in free DNA (δ_f), that bound to drug (δ_b) in complex of daunomycin with d-CGATCG at drug to DNA ratio (D/N) = 2.0, and the changes in chemical shift due to binding ($\Delta\delta$)^s

	C1			G2			A3			T4			C5			G6		
	δ_b	δ_f	$\Delta\delta$	δ_b	δ_f	$\Delta\delta$	δ_b	δ_f	$\Delta\delta$	δ_b	δ_f	$\Delta\delta$	δ_b	δ_f	$\Delta\delta$	δ_b	δ_f	$\Delta\delta$
H8/H6	7.62	7.66	0.04	7.94	8.02	0.08	8.33	8.35	0.02	7.05	7.23	-0.18	7.56	7.52	-0.04	7.92	7.97	0.05
H1'	6.08	5.80	0.28	6.23	5.62	-0.61	6.16	6.37	0.21	6.29	6.01	-0.28	6.03	5.81	-0.22	6.13	6.21	0.08
H2'	1.91	1.94	0.03	2.48	2.79	0.31	2.49	2.75	0.26	2.32	2.08	-0.24	1.60	2.04	0.44	2.20	2.67	0.47
H2''	2.35	2.44	0.09	2.74	2.89	0.15	2.79	3.01	0.22	2.56	2.49	-0.07	2.28	2.43	0.15	2.43	2.42	-0.01
H3'	4.76	4.74	-0.02	4.59	5.06	0.47	4.74	5.10	0.36	4.70	4.91	0.21	4.60	4.88	0.28	4.69	4.72	0.03
H4'	4.17	4.11	-0.06	4.09	4.38	0.29	4.18	4.54	0.36	4.11	4.24	0.13	4.05	4.18	0.13	4.12	4.23	0.11
H5'	4.05	3.76	-0.29	3.82	4.12	0.30	3.79	4.30	0.51	3.87	4.13	0.26	3.75	4.10	0.35	3.76	4.12	0.36
H5''	3.96	3.72	-0.24	3.7	4.03	0.33	3.72	4.28	0.56	3.68	4.10	0.42	3.62	4.05	0.43	3.72	4.11	0.39
H5/H2/ CH ₃	5.94	5.93	-0.01	-	-	-	7.81	7.81	-	1.08	1.44	0.36	5.92	5.71	-0.21	-	-	-
NH ₂	7.79 ^b	-	-	7.21 ^b	-	-	7.77 ^b	-	-	-	-	-	7.81 ^b	-	-	7.32 ^b	-	-
				7.05*												7.4*		
NH	-	-	-	11.9	-	-	-	-	-	13.34	-	-	-	-	-	13.24	-	-

^supfield shift indicated as +ve

^b indicates hydrogen involved in hydrogen bonding

* indicates hydrogen not involved in hydrogen bonding

Table 7.2: Chemical shift (ppm) of various drug protons in free form (δ_f), that bound to DNA (δ_b) at 295 K in complex of daunomycin with d-CGATCG at drug to DNA ratio (D/N) = 2.0, and the changes in chemical shift due to binding ($\Delta\delta$)^s

Protons	δ_b	δ_f	$\Delta\delta$	Protons	δ_b	δ_f	$\Delta\delta$
1H	7.65	7.75	0.10	10 _{eq} H	2.80	3.11	0.31
2H	7.74	7.87	0.13	10 _{ax} H	2.53	2.97	0.44
3H	7.41	7.57	0.16	8 _{eq} H	2.32	2.42	0.10
1'H	5.30	5.57	0.27	8 _{ax} H	1.80	2.27	0.47
7H	4.62	5.08	0.46	2 _{ax} H	1.91	2.13	0.22
9COCH ₃	3.20	-	-	2 _{eq} H	1.99	2.13	0.14
5'H	4.28	4.36	0.08	5'CH ₃	1.33	1.43	0.10
4OCH ₃	3.90	4.09	0.19	6OH	12.5	13.85	1.37
4'H	4.08	3.94	-0.02	11OH	12.0	13.17	1.17
3'H	3.79	3.76	-0.03	4'OH	1.78	1.97	0.19
3NH ₃	8.40	8.50	-0.02				

^supfield shift indicated as +ve

s

which is further coupled to 4'H proton (Fig. 7.3d). In the same way the cross peaks of 4'H-3'H, 3'H-2'axH, 3'H-2eqH, 1'H-2axH and 1'H-2eqH assign these resonances. The change in chemical shift of drug protons in 2:1 drug to DNA complex with respect to the corresponding chemical shifts in free drug in monomer form (that is chemical shifts at 355 K, since the drug is known to form stacked dimers at 295 K (Barthwal et al, 1996) are shown in Table 7.2. The resonance at 12.48 ppm is assigned to 6OH proton as it gives NOE cross peaks with 1'H, 7'H protons (Fig. 7.4c). The resonance at 12.0 ppm is assigned to 11OH protons as it gives NOE cross peak with 8axH and 10eqH protons (Fig. 7.4c and 7.4e). 4'OH is assigned (1.78 ppm) on the basis of its cross peak with 6OH proton.

7.2 TITRATION STUDIES

In aromatic protons region the resonances are sharp. However, in H1' region the splitting pattern of all the H1' protons disappear and resonances are broadened. As the drug is added to the DNA hexamer new signals arise while base resonances get broadened. It is noted that several new resonances are found to grow on gradual addition of drug. G2H8 and G6H8 are broadened and C1H6 and C5H6 protons signal also become less intense. In H1' region, all residues are relatively more broadened than the base H8/H6 protons. However, among all residues C5H1' and C1H1' are broadened beyond recognition at D/N (drug/nucleotide) ratio of 2:1 (Fig. 7.2a). Daunomycin proton was clearly seen at the 7.65 ppm while 2H proton appears to emerge as 7.78 ppm as a shoulder of A3H2 resonance (Fig 7.2a). The ring D protons 1H, 2H, 3H and 1'H proton of daunomycin sugar are evident in this complex. 2D NOSEY spectra recorded on this 2:1 (D/N) complex are shown in Fig 7.4 in which all protons have been assigned as discussed earlier.

At 2:1 drug/DNA ratio, all signals were found to be broadened. This could be due to the presence of protons corresponding to multiple complexes. There may be slow exchange between them on NMR time scale, which results in broadening of signals. The base pair protons (H8, H6, H2, H5) and deoxyribose H1' protons (being close to aromatic ring) of the intercalating base pair of DNA are expected to show ring current effect arising from the drug chromophore. However since the base pair at the intercalation step getting destacked from the neighbouring base pair in free DNA (resulting in downfield shift of aromatic protons) and then getting stacked (resulting in upfield shift) with the conjugated aromatic rings ABCD (Fig. 7.1a) of the daunomycin drug, the net change in chemical shift positions is not expected to be large. Among base protons C1H6, G2H8, A3H8, and G6H8 are shifted upfield by 0.04, 0.08, 0.02 and 0.05 ppm, respectively. The maximum upfield shift of 0.18 ppm is observed in T4H6 implying the effect of opening of helix upto the fourth base pair. The C5H6 and C1H5 base pairs show downfield shift of 0.04 and 0.01 ppm, respectively. C5H5 base shows the maximum downfield shift of 0.21 ppm (Table 7.1). The changes in all base protons resonances are attributed to the destacking of the adjacent base pairs in order to permit opening of the DNA helix followed by insertion of daunomycin chromophore between 5'-CpG-3' step of d-(CGATCG)₂.

In deoxyribose sugar, C1H1', G2H1', T4H1' and C5H1' protons are downfield shifted by 0.22-0.61 ppm while A3H1' and G6H1' protons are upfield shifted by 0.21 and 0.08 ppm, respectively (Table 7.1). It is also observed that H1' proton of G2 residue is shifted downfield to a much greater extent than that for G6 residue. This is consistent with the general observation that purines produce large ring current shifts on adjacent nucleotide as compared to pyrimidine due to stacking. Such changes in

chemical shift of DNA protons due to interaction of daunomycin are also reported in literature (Nuss et al, 1980; Patel, 1979; Patel et al, 1981; Phillips and Roberts, 1980). Considering the protons of daunomycin, it is found that ring D protons 1H, 2H and 3H are shifted upfield by 0.10, 0.13 and 0.16 ppm, respectively (Table 7.2). The daunosamine sugar 1'H proton shows upfield shift of 0.27 ppm with respect to its chemical shift position at 355 K (Barthwal et al, 1996). As, several protons in ring A and D of the drug experience large upfield shifts, ~ 0.1 to 0.47 ppm. This is consistent with the results supported by us earlier on binding of daunomycin to d-CpG (Barthwal et al, 1994) and some other oligonucleotides sequences in literature (Nuss et al, 1980; Patel, 1978; Patel, 1979; Patel et al, Phillips and Roberts, 1980; Ragg et al, 1988). These have been attributed to intercalation of drug chromophore between base pairs of DNA, which move apart to a distance of ~ 6.8 Å on binding to drug and are characteristic of stacking interactions between aromatic/conjugated rings (Frederick et al, 1990; Langlois d' Estantot, 1992; Moore et al, 1989; Nunn et al, Wang et al, 1987). The relatively smaller change in 1H and 2H protons of drug, reported earlier also (Patel, 1979; Patel et al, 1981; Phillips and Roberts, 1980), may be due to specific positioning of drug chromophore between base pairs such that the ring A partially protrudes out of base pairs resulting in much lesser overlap with adjacent base pairs and hence experiencing less ring current shifts (Giessner-Prettre and Pullman, 1976). Similar changes in changes in chemical shift of ring D protons have been reported in literature (Nuss et al, 1980; Patel, 1979; Patel et al, 1981; Phillips and Roberts, 1980). The 4OCH₃ protons of ring D of daunomycin also exhibit upfield shift of 0.19 ppm.

The most significant result is the upfield shift of 6OH (12.48 ppm) and 11OH protons

from their position in uncomplexed drug by more than 1 ppm. This is consistent with the stacking of ring BCD within the base pair of DNA. Among ring A protons, 8axH and 10axH show significant upfield shifts of 0.47 and 0.44 ppm, respectively. 7H exhibits upfield shift of 0.46 ppm due to change in conformation of daunomycin on complexation. The changes in chemical shift of daunosamine sugar protons 2'axH, 2'eqH, 4'H, 5'H and 5'CH₃ are in the range of -0.02 to 0.22 ppm which could be due to the conformational adjustment of sugar on binding of daunomycin with d(CGATCG)₂ (Table 7.2).

7.3 CHANGES WITH THE TEMPERATURE

The 1D NMR spectra of 2:1 drug/DNA complex obtained as a result of last titration is monitored as a function of temperature. Fig. 7.5 shows the one-dimensional NMR spectra of complex at different temperature in the range 287-320 K. The chemical shift position of all protons are characteristic of 2:1 drug to DNA complex, at all temperatures, as they were distinctly different from that of drug in monomer or self associated form (Barthwal et al, 1994) or free DNA (Barthwal et al, 2003). It is observed that 3H proton of daunomycin in 2:1 complex resonating at 7.41 ppm at 295 K shifts upfield with increase in temperature with increase in temperature to 7.28 ppm at 320 K. The chemical shift of this proton in self-associated and monomer daunomycin (i.e. chemical shift of daunomycin at 297 and 355 K (Barthwal et al, 1996) are 7.34 ppm and 7.53 ppm, respectively.

It has been shown by Patel, that an increase in temperature results in downfield shift of 1H, 2H, 3H and 4OCH₃ protons due to dissociation of the complex. However our results are contrary to that obtained by Patel since all 1H, 2H and 3H protons shifts

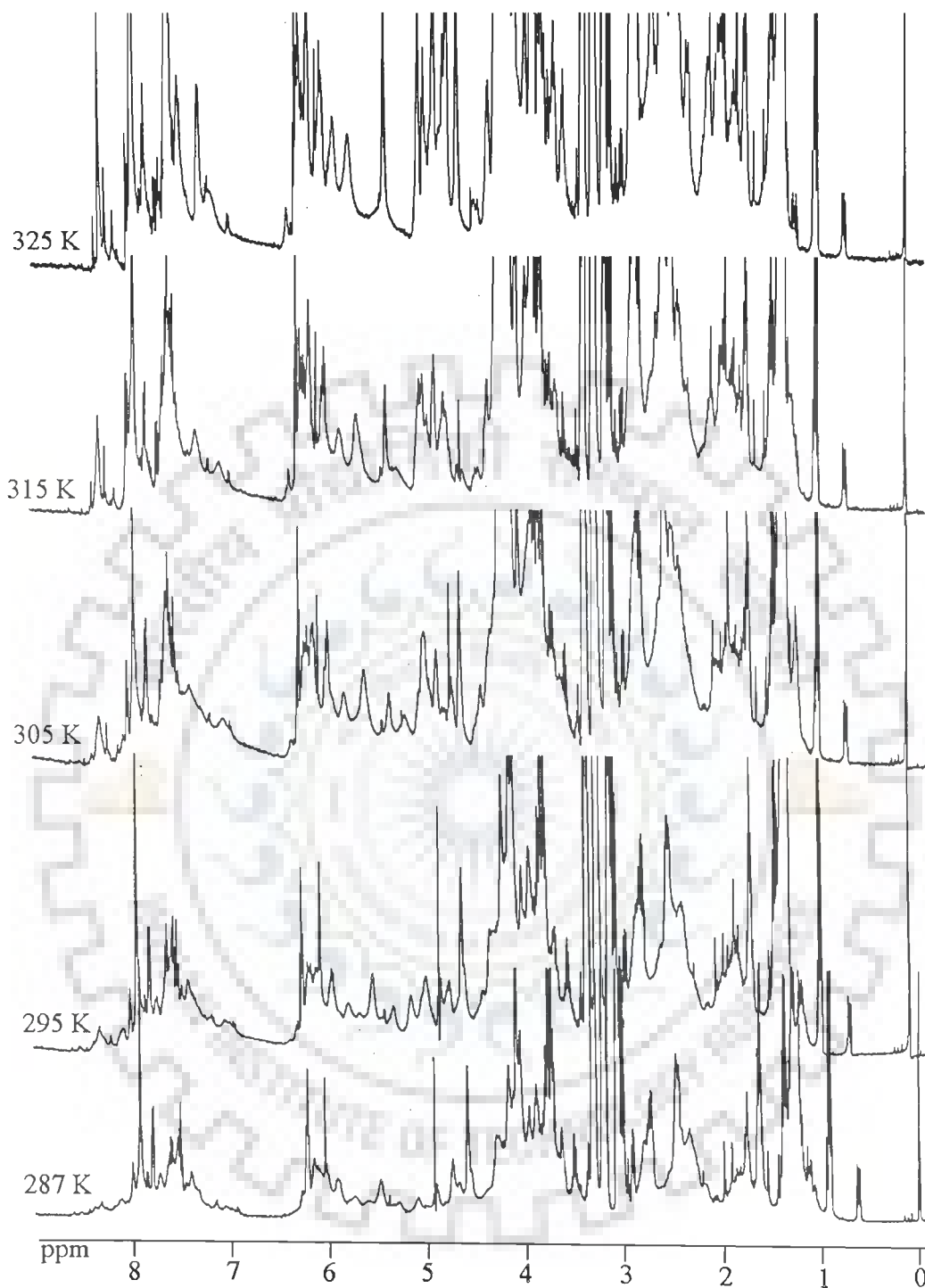


Figure 7.5: Stack plot of 1D proton NMR spectra of d-CGATCG at drug to DNA ratio (D/N) = 2.0 recorded with varying temperatures in the range 277-325 K

upfield with increase in temperature suggesting that our complex form does not dissociate. Further it may be noted that chemical shift of 3H in complex at 295 K is shifted downfield by 0.09 ppm and 0.26 ppm, respectively with respect to the corresponding proton of monomer and self associated form of daunomycin. An upfield shift of 0.05 ppm and downfield shift of 0.02 ppm was observed for 2H and 1H protons of daunomycin with increase in temperature while 1'H of daunosamine sugar shift downfield by only 0.04 ppm due to partial destacking. The base protons and sugar H1' protons of DNA of daunomycin shift downfield with temperature due to partial destacking (Patel, 1979; Phillips and Roberts, 1980).

7.4 STRUCTURAL FEATURES OF DRUG-DNA COMPLEX

The conformational features of drug-DNA complex were investigated primarily on the basis of NMR and restrained molecular dynamics.

7.4.1 Hexamer d-CGATCG

Table 7.3 lists the interproton distances corresponding to observed intermolecular NOEs between drug and DNA protons. Intense NOE cross peaks were observed for several sequential connectivities expected for right handed B-type conformations between the steps, G2pA3, A3pT4 and T4pC5 with the corresponding interproton distances, (base H8/H6)_n-(H1', H2', H2'')_{n-1}, lying in the range, 2.3-4.0 Å. However, a discontinuity in the sequential NOE connectivities at the C1pG2 and C5pG6 step was observed. This may be attributed to the intercalation of anthracycline ring of drug. Thus the drug chromophore intercalates at CpG step, as also reported in X-ray crystallographic studies (Frederick et al, 1990; Langlois d' Estaintot, 1992; Moore et al, 1989; Nunn et al, Wang et al, 1987) and NMR structural analysis of daunomycin complexed with d-CpG in solution (Barthwal et al, 1994). This is also evident from

Table 7.3: Interproton distances (Å) obtained from intermolecular NOE connectivities of hexanucleotide and the drug in the drug–DNA complex at drug to DNA ratio (D/N) = 2.0

Protons	NMR	rMD	Protons	NMR	rMD
C1H5-1H	2.6	3.3	A3H2''-8axH	2.7	5.3
C1H2''-11OH	2.2	2.6	C5H2'-6OH	3.5	4.0
C1H1'-11OH	2.5	3.6	C5H2''-6OH	4.5	5.1
A3H1'-5'CH ₃	3.5	2.3	C5H2'-5' CH ₃		
A3H2-5'CH ₃	3.0	3.5	G6H1'-10eqH	4.0	4.5
A3H1'-5'H	2.9	4.5	G6H1'-7H	3.8	4.1
A3H1'-4'H	3.5	3.5	G6H5''-6OH	3.0	3.2

several intermolecular NOE connectivities seen between drug and DNA protons in the complex (Table 7.3), discussed later in this paper. Several sequential cross peaks i.e. A3H8-T4CH₃, A3H2-G2N1H and T4N3H-A3H2 observed are indicative of good base to base stacking at these base pair steps. These have earlier been observed in the spectra of d-CGATCG (Barthwal et al, 2003] and d-TGATCA (Barthwal et al, 2004). The observed NOEs within DNA molecule and cross peak patterns in COSY spectra give structural information of conformation of oligomer in the complex. Sugar conformation may be determined from J couplings in the COSY spectra or alternatively from the knowledge of inter proton distances within the sugar ring determined from the integrals of cross peaks in NOESY spectra. The deoxyribose sugar protons are broadened at 295 K and hence could not be used to estimate $J(H1'-H2')$, $J(H1'-H2'')$ or, sums of couplings. The limitations are normally due to severe spectral overlap, limited digital resolution and inherent line widths. Several studies on deoxyribonucleotides have shown that the sugar moiety exists in at least two rapidly interconverting conformations (a) a minor N-conformer (mole fraction of χ_N) with pseudorotation phase angle, $P_N = 9^\circ-18^\circ$ and pucker amplitude $\phi_N = 36^\circ$ that is, the same as the same as C3' endo geometry and (b) a dominant S-conformer (mole fraction χ_S) with a pucker amplitude ϕ_S varying in the range $28^\circ-44^\circ$ and pseudorotation phase angle P varying around C2' endo geometry in the range $108^\circ-180^\circ$ (Barthwal et al, 2004; Chaires et al, 1982; Giessner-Prettre, 1976). The DQF COSY spectra shows cross peak patterns for 1'-2', 1'-2'', 2'-3' connectivities for all residues. However 2''-3' and 3'-4' cross peak patterns were observed only for G2 and A3 residues, (Table 7.4a). The spin-spin coupling constants, $J(H2''-H3')$ and $J(H3'-H4')$, for deoxyribose of standard B-DNA are about 0.8 Hz which is close to

Table 7.4a: Presence (marked as +) and absence (marked as -) of intraresidue cross peak patterns as observed in phase-sensitive double quantum filter COSY spectra of the drug–DNA complex at drug to DNA ratio (D/N) = 2.0

Connectivities	C1	G2	A3	T4	C5	G6
H1'-H2'	+	+	+	+	+	+
H1'-H2''	+	+	+	+	+	+
H2'-H3'	+	+	+	+	+	+
H2''-H3'	-	+	+	-	-	-
H3'-H4'	-	+	+	-	-	-

resolution in our DQF COSY spectra. These J values will however increase if N-conformer is present since the corresponding J (H2''-H3') and J(H3'-H4') values are 9.7 Hz and 8.6 Hz, respectively. The observed presence of cross peak patterns for G2 and A3 residue clearly demonstrates the presence of N-conformer (estimated >10 %) while the predominant conformation of deoxyribose is S-conformer. An attempt has been made to estimate the deoxyribose conformation from intrasugar interproton distances. Although H1'-H2', H1'-H2'', H1'-H3', H2'-H3', H2''-H3', H2'-H4' and H3'-H4' distances vary with P_S and χ_S only in a narrow range, the distances H1'-H4' and H2''-H4' may be used as a marker for sugar conformational analysis to obtain P_S and χ_S . The distance H1'-H4' decreases from 3.0 Å to 2.0 Å when P increases from 18° to 99°-108° and then increases again to 3.0 Å at P = 162°. It is therefore not expected to vary with χ . Our results show that this distance increases in the order A3 < G2 < C1, T4, C5, G6 indicating thereby that pseudorotation of A3 residue is least, followed by that in G2 residue (Table 7.4b). It may be estimated that P_S value for C1, T4, C5 and G6 lies in the range 144°-180°, while for A3 residue have $P_S \sim 108^\circ$ -144°. The distance H2''-H4' serves as a marker distance for χ_S as its value is 3.8 Å for P = 162° and decreases with P to 2.3 Å for P = 18°. Its variation with P in the range P = 144°-180° is negligible. NOESY spectra of the complex shows that H2''-H4' distance is least for A3 and G2 residues (Table 7.4b); therefore A3 and G2 residues may be having maximum fraction of N-conformer. The distances H2''-H3' and H3'-H4' increase with decrease in pseudorotation from a value of 2.52 Å by 0.38 Å and 0.29 Å, respectively in the range 162°-18°. On the other hand corresponding distance H1'-H2' decreases by 0.29 Å. The observed distances are consistent with the inference drawn above.

Table 7.4b: The observed relative intensities of NOE connectivities of the drug–DNA complex at drug to DNA ratio (D/N) = 2.0

Residues	H2''-H4'	H1'-H4'	H8/H6-H1'
C1	w	w	-
G2	ss	s	ww
A3	ss	ss	-
T4	w	w	ws
C5	w	w	s
G6	w	w	ss

The glycosidic bond rotation, χ , is readily estimated from intranucleotide base to sugar proton distances. The H6/H8-H1' distance depends on χ only while H6/H8-H2', H6/H8-H2'' and H6/H8-H3' distances depends on both pseudorotation phase angle, P and χ . The observed H6/H8-H1' distance among nucleotide residues decreases in the order C1, A3 > G2 > T4 > C5 > G6 (Table 7.4b). Thus, among pyrimidines C5 is adopting high anti conformation while C1 may be anti. Among purines, A3 is clearly in anti conformation while G6 is towards high anti conformation. The observed results on sugar conformation and glycosidic bond rotation have been compared with those obtained earlier in similar complexes of with hexamer DNA sequences d-CGATCG and d-CGTACG in Table 7.4a and 7.4b.

7.4.2 Intermolecular Interactions

The NOESY spectra of complex show several intermolecular contacts, which are listed in Table 7.3. These observed results have been compared with similar NMR structures obtained by Igarashi et al, 1995; Mazzini et al, 1998; Odefey et al, 1992 and Robinson et al, 1997. The NOESY cross peaks C5H5-1H, C5H6-4OCH₃, G2N1H-4OCH₃, G2H8-4OCH₃, 6OH-C5H6, 6OH-G2H8 and C5H5-4OCH₃ clearly indicate that the drug chromophore intercalates between CG base pairs at both the sites C1pG2 and C5pG6. As a result of stacking interactions, the 7H atom of drug come in close proximity of G2N1H proton while 11OH lies in proximity of C1H1' proton. Since 1H and 4OCH₃ are on opposites side of ring D of drug chromophore (Fig. 7.1a) the orientation of drug chromophore is therefore such that C5H6 is relatively closure to 1H atom than to 3H atom and C5H5 and C5H6 come in close proximity to 4OCH₃ atoms. The daunosamine sugar hangs close to the third base pair so that A3H1'-5'CH₃ NOE connectivity is observable. It may be noted that A3H1'-5'CH₃ NOE has been

Table 7.4a: Comparison of pseudorotation phase angle, P, (°)

	Present Work	CGA+ mor ^a	CGA+ adm ^b	CGA+ dnm ^c	CpG+ dnm ^d
	rMD				
C1	165, 164	120, 143	158	160	153
G2	146, 144	95, 136	141	142	135
A3	140, 146	77, 73	129	131	
T4	154, 152	92, 130	124	122	
C5	148, 143	137, 119	151	141	
G6	207, 192	147, 142	161	165	

^a CGATCG + morpholinodoxorubicin

^b CGATCG + adriamycin

^c CGATCG + daunomycin

^d CpG + daunomycin

Table 7.4b: Comparison of glycosidic bond rotation (°)

	Present Work	CGA+mor ^a	CGA+ adm ^b	CpG+ dnm ^c
	rMD			
C1	-131, -133	-	148	-120
G2	-96, -96	-131, -92	-90	-90
A3	-135, -132	-148, -146	-130	
T4	-109, -109	-141, -123	-113	
C5	-98, -102	-105, -112	-90	
G6	90, -92	-104, -110	-90	

^a CGATCG + morpholinodoxorubicin

^b CGATCG + adriamycin

^c CpG + daunomycin

observed in similar X-ray crystal of these structures (Igarashi et al, 1995; Mazzini et al, 1998; Odefey et al, 1992). Several other observed NOEs (Table 7.3) help in defining the geometry of complex and have been used as restraints for molecular dynamics simulations.

7.5 RESTRAINED MOLECULAR DYNAMICS

The energy minimization and molecular dynamics calculations were carried out using AMBER 6.0 software (courtesy Prof. Peter Kollman, UCSF, California) on unix platform using PARAM 10000 super computing facility. Initial model building was carried out using xleap and antechamber modules of AMBER 6.0. Starting structure of 2:1 complex of daunomycin-d(CGATCG)₂ was taken from protein data bank (PDB Id: 1da0). AMBER reads all the atoms of DNA but does not have database for drug molecule. Modification of initial structure was done using INSIGHT II on Silicon Graphics workstation. MOPAC generated the charge while antechamber module of the AMBER prepared the database for the daunomycin molecule. Counterions and hydrogen atom with standard geometry were added to the system by xleap module. This structure was then optimized to remove any bad van der waals contacts and to minimize counterions keeping all heavy atoms of the complex fixed. All molecular structures were displayed using the visual molecular dynamics (VMD) software on a linux workstation. Minimization and restrained molecular dynamics were carried out in vacuum. A distance dependent dielectric constant was used during in vacuum for restrained molecular dynamics (rMD) calculations to mimic the presence of a high dielectric solvent. Pseudoatom corrections were used for methyl and other equivalent protons. The SANDER (simulation annealing with NMR driven energy restraints) module in AMBER 6.0 was used to perform energy minimization and dynamics. To

maintain right-handedness and prevent structural artifacts during the MD run, the base pair Watson-Crick hydrogen bonding scheme was also maintained by applying hydrogen bond restraints. A cut off value of 9.0 Å was chosen to calculate all nonbonded interactions in the system. All run was performed at constant temperature of 300 K. The temperature is regulated by bath coupling using the Berendsen algorithm. Forcefield parm99 of AMBER 6 was used. The energy of the system was minimized using the 1000 steps each of steepest descent and conjugate gradient using a total 266 intraresidue and 30 interresidue distance restraints. A typical rMD run was consisted of 100 ps simulation with time step of 1 fs. General simulation parameters were kept constant during the complete run of molecular dynamics simulations and structural information collected after every 4 ps. The root mean square deviation between the rMD structure and the starting structures is quite large but among various final structures is very low. This is generally acknowledged as an indication that convergence has been achieved. Table 7.5 shows the pairwise as well as residue wise root mean square deviations (RMSD) of the complex. The starting structure was chosen as reference and the value of target RMSD is chosen to be zero. It is noted that C1 and G6 shows the maximum deviation from the starting structure which indicates the distortion in these two bases is more than internal G2 and C5 bases. It may be noted that distance deviation reached a minimum of 0.71 Å from an initial average deviation of 0.82 Å. Table 7.6 indicates an assessment of refined structure in terms of energetics and distance deviation from the target distance. The total potential energy of the final structure is $-232 \text{ Kcal mole}^{-1}$, which is much lower than the initial B-DNA structure. The restraint energy has also reduced from $1173 \text{ Kcal mole}^{-1}$ to $566 \text{ Kcal mole}^{-1}$. The final structure obtained after rMD simulations is shown in Fig.7.6.

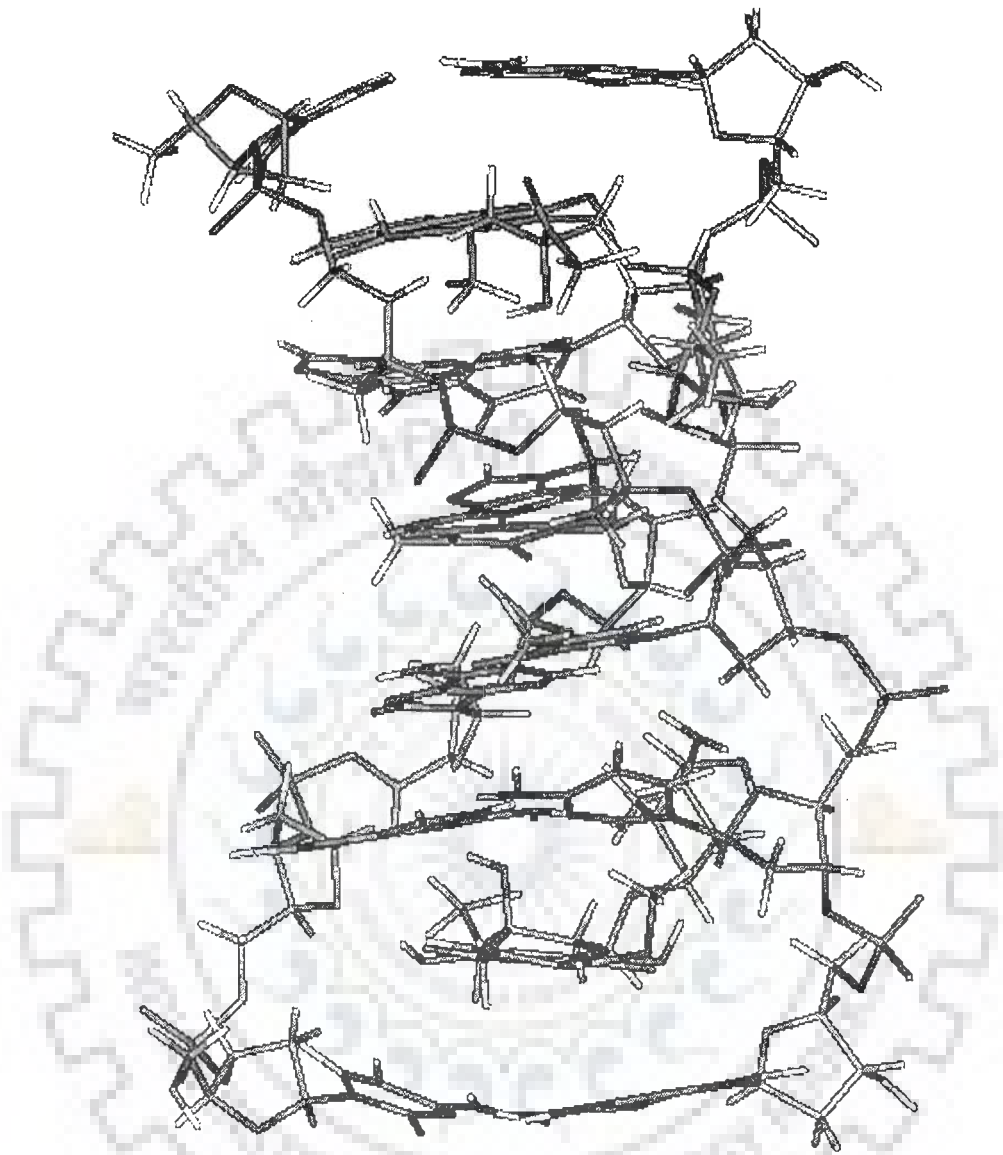


Figure 7.6: Stereoview of the final rMD structure

Table 7.5: Summary of experimental restraints and statistical analysis final structure generated by restrained molecular dynamics (rMD) simulations

Parameter	
No. of Distance Restraints	
Intra residue	100
Inter residue	28
Average pairwise RMSD	Initial = 0 Final = 0.42
Average residuewise RMSD	C1=1.45, G2 = 0.65, A3 = 0.50, T4 = 0.46, C5 = 0.89, G6 = 1.48 Daunomycin = 0.71

Table 7.6: Energy terms (Kcal mol⁻¹) for starting model and final rMD structure generated by restrained molecular dynamics (rMD) simulations

Structure	Total	Bond	Angle	Dihedral	Vdw
Initial	765	203	434	322	-153
Final	-232	50	263	286	-134
	1-4 Vdw	Electrostatic	1-4 Electrostatic	Restraint	Δdv^a
Initial	210	-842	-581	1173	0.82
Final	190	-879	-175	566	0.71

^aAverage distance deviation

7.5.1 Conformation of DNA

The nucleotides are labeled from C1 to G6 in the 5' to 3' direction on strand 1 and from C7 to G12 on strand 2 with C1 base paired to G12. The daunomycin molecule are numbered D13 and D14 and the atomic numbering scheme for the molecule is shown in Fig. 7.1a. The schematic representation of the drug chromophore intercalated between d-C1pG2 and d-C5pG6 is shown in Fig. 7.1b.

All helical parameters, backbone torsional angles and sugar conformations of the resulting rMD structures were thoroughly analysed with the program CURVES, version 5.1 (Lavery and Sklenar, 1996). Plot of some of the helicoidal parameters (global, unless specified otherwise) as a function of residue position in the duplex is shown in Fig. 7.7a-b along with that for two classical structures of A-DNA and B-DNA. Among the base pair axis parameters, the x-displacement (dx) show large variations upto 0.6 Å for G2.C11 and C5.G8 base pairs while y-displacement (dy) are found to vary to in a narrow range (0 to 0.3 Å). The base pairs are inclined upto an angle of $\sim 3^\circ$ for the two GC base pairs. The tip angle fluctuates along the base sequence. Though the variation in stagger is not very large but it is maximum for the G2.C11 and C5.G8 base pairs. The variation in shear and stretch is not very large. At 5'-C1pG2 basepair step the C1 base is buckled by 19° while G2 get buckled by 15° in opposite direction. Same variation is observed at 3'-C5pG6 base pair step. The propeller twist for the A3.T10 and T4.A9 base pairs is negative $\sim -6^\circ$ while it is large for the G2.C11 and C5.G8 ($\sim 26^\circ$) base pairs. Among the inter base pair parameters, the shift (Dx) is maximum at G2pA3 and T4pC5 steps while for C1pG2 and C5pG6 steps it is 0.8 Å. Large variations in shift upto 1.9 Å have also been observed on formation of complex of daunomycin with deoxytetranucleotides (Davies et al, 2000).

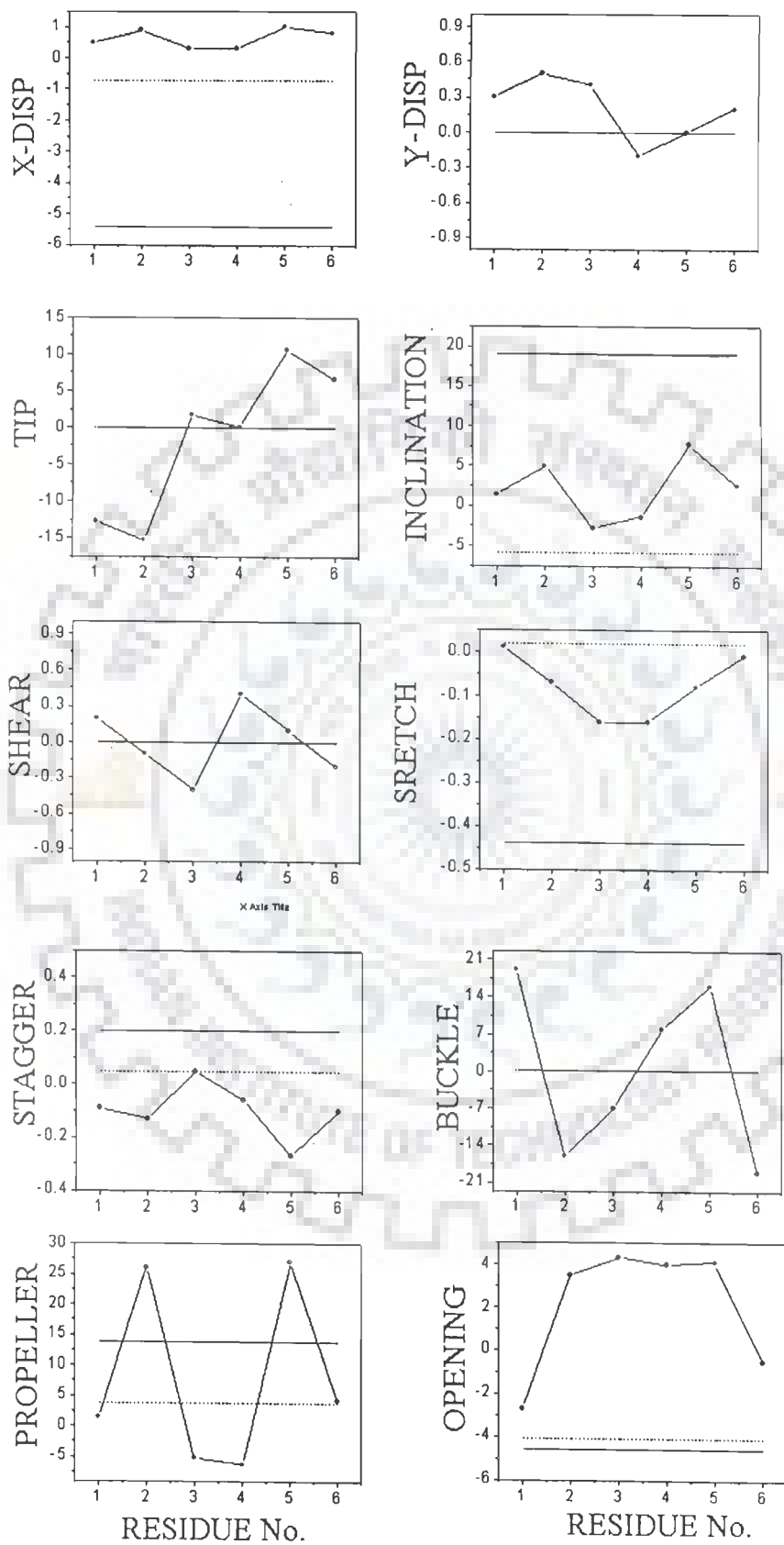
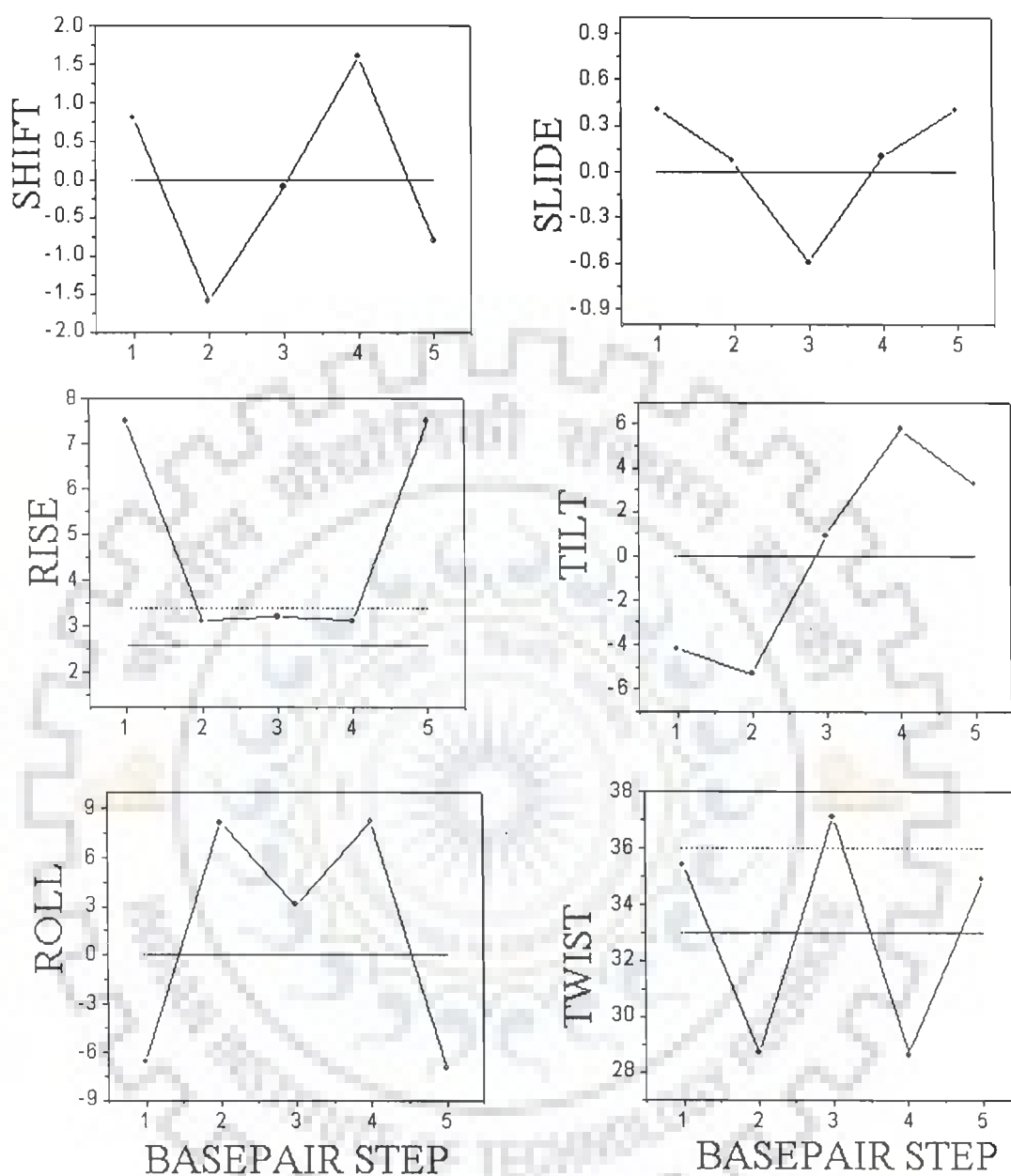


Figure 7.7(a)



(b)

Figure 7.7: (a) and (b) Helical parameters for d-CGATCG complexed with daunomycin calculated for structure obtained by restrained molecular dynamics simulations (•) and that for canonical A-DNA (—), B-DNA (---)

The slide (D_y) is maximum (~ 0.6 Å) in the middle of the hexanucleotide, that is, at A3pT4 step. The rise at base pair steps is 3.0-3.2 Å while at CpG and CpG steps it is ~ 7.5 Å to accommodate the drug chromophore. The intercalation results in large amount of tilt (τ) in the helix, upto $\sim 6^\circ$. Large values of tilt, in the range -6 to 12° have been observed as a result of intercalation of daunomycin in CG base pairs (Davies et al, 2000). Large positive values of the roll angle (ρ), $\sim 8^\circ$ at G2pA3 and T4pC5 steps, results in a wider groove and bending towards major groove causing a curvature in the helix.

The roll is positive for A3pT4 so it forces the propeller twist at this step to become negative in order to prevent the destacking of the bases. The twist (Ω) varies in the range 28° to 37° . At the intercalation sites C1pG2 and C5pG6, the twist angle is 35° indicating that unwinding of DNA at these steps is very small. This is consistent with several observations by viscosity techniques that unwinding angle for daunomycin, adriamycin are upto 6° while that for some other drugs e.g. actinomycin is about 23° (Pachter et al, 1982). The duplex is also found to unwind at sites adjacent to intercalation site upto an angle of 7° , as also reported in the case of some other intercalating drugs (Chen and patel, 1995). The overall helix bend is 3° . The groove widths of the double helix are defined using the coordinates of the phosphate atoms. In the hexanucleotide only one major and one minor groove exists in the middle of the helix. In the rMD structure of the complex the width of major groove is 13.0 Å while the corresponding values for minor groove is 8 Å. Thus the major groove becomes wider. A comparison of observed helical parameters with that found in crystal structure of adriamycin-d-CGATCG complex (Frederick et al, 1990) reveals that tilt and helical twist are nearly same in the two cases. However the roll, propeller twist

and the buckle are quite different in solution structure and solid-state structure.

The values of torsional angles along with the values for canonical B-DNA and A-DNA are given in Table 7.7. The torsional angles are not equal in the two strands of the duplex. The difference in absolute values of torsional angles is upto 8° and the general features and trends with base sequence are strikingly identical. The backbone torsional angles are not defined by the restraints obtained from NOESY spectra. We have used a low force constant to permit a smooth search, which is conformationally compatible with other structural features.

The angles α , β and γ adopt gauche⁻, trans and gauche⁺ conformations, respectively in practically all residues of both the strands except that β for G2 residue deviates from 176° (canonical B-DNA) to 137° . The angles δ as well as pseudorotation phase angle, P , has a low value of 140° - 145° only for G2 and A3 residues in both the strands. The torsional angle ζ however deviates from the normal gauche⁻ conformation and adopts a trans conformation for the G2 and C5 residues (-178° , $+178^\circ$). This may be attributed to the opening of base pairs at these sites. This is accompanied by a corresponding deviation in torsional angle ϵ for G2 and C5 residues to lower negative values of -144° , -99° and -146° , -99° in both strands, respectively as compared to a value of -169° found in the canonical B-DNA structures. The glycosyl rotation angle χ measuring the rotation of base around the sugar varies as follows: C1: -131° -133° ; G2: -96° , -96° ; A3: -135° , -132° ; T4: -109° , -109° ; C5: -98° , -102° and G6: -90° , -92° . Thus it is observed that DNA backbone uses a non-symmetrical mechanism to allow intercalation of drug chromophore between the d-C1pG2 and d-C5pG6 sites. On the C1pG2 side of the backbone, the 5'-deoxycytidine

Table 7.8: Backbone Torsional angles ($^{\circ}$), and Pseudorotation phase angle, ($^{\circ}$) and glycosidic bond rotation of the final structure of generated by restrained molecular dynamics (rMD) simulations

RESIDUES	α	β	γ	δ	ϵ	ζ	χ	P
C1	-	-	50	142	-130	-72	-131	140
G2	-88	179	67	136	-144	-178	-96	149
A3	-58	137	58	118	-175	-83	-135	149
T4	-67	168	52	124	-168	-81	-109	141
C5	-61	179	35	145	-99	-178	-98	148
G6	-68	174	34	145	-	-	-90	183
C7	-	-	52	143	-131	-71	-133	161
G8	-89	178	69	135	-146	-179	-97	145
A9	-58	137	61	122	-179	-84	-132	165
T10	-67	-167	52	123	-161	-78	-109	139
C11	-64	175	38	140	-100	-178	-102	146
G12	-67	177	34	143	-	-	-92	186
B-DNA	-63	136	54	123	-169	-108	-105	162

residue changes the glycosyl angle from an anti (-105° to -119° in B-DNA) to low anti value (-131° , -133°). At the same time by adjusting ϵ from a near trans (-160° to B-DNA) it is somewhat low to B-DNA to a somewhat lower value of (-130° , -131°) it allows the adjacent bases to separate from 3.4 Å to 7.5 Å. On the C5pG6 site, both nucleotide units (C5 and G6 in both the strands) maintain the glycosyl angles at high anti values (-98° , -90° , -102° , -92°). By changing the ϵ value from -169° to a conformation tending toward gauche (-94° , -99°) in the C5 residue, it is possible to separate the C5 and G6 bases to a distances of ~ 7.5 Å. This is made possible by coupling it with rotations about phosphodiester linkage from a normal gauche-, gauche- conformation to the trans, gauche- as observed in X-ray crystallography structure of similar complexes (Frederick et al, 1990; Langlois d' Estaintot, 1992; Moore et al, 1989; Nunn et al, Wang et al, 1987). Such changes get reflected as downfield shift in P-31 NMR spectra or alternately in backbone torsional angles ϵ , ξ , α and β . X-ray crystallographic analysis of various B-DNA structures have shown that they exist in two conformational states, namely B_I and B_{II}, characterized by torsional angles. α , -62° ; β , 176° ; γ , 48° ; δ , 128° ; ϵ , -176° ; ξ , -95° ; χ , -102° to 119° and α , -62° ; β , 176° ; γ , 48° ; δ , 144° ; ϵ , -114° ; ξ , -174° ; χ , -89° , respectively.

Comparing these values, with those obtained in our complex (Table 7.7), it is found that both G2 and C5 residues tend to adopt B_{II} conformation as a result of intercalation of drug chromophore. The A3 and T4 residues remain in the stabler B_I state except that β in G2 residue shifts from a normally observed value of 176° to 137° . It has been reported earlier that the idealized g^-g^- conformation of phosphodiester bond from 5' to 3' direction changes $g^-g^-tg^-g^-tg^-$ (where t stands for trans and g^- stands for gauche-, respectively) in X-ray crystallographic

(Frederick et al, 1990; Langlois d' Estaintot, 1992; Moore et al, 1989; Nunn et al, Wang et al, 1987) and NMR structures (Davies et al, 2000) in hexamer sequences d-CGATCG and d-CGTACG on binding to similar drugs. The trans, gauche-conformation in G2pT3 or G2pA3 step in X-ray structure (Frederick et al, 1990) is associated with change in β angle of T3/A3 residue (adjacent to intercalating bases) to 114° - 138° . Further in these complexes, pseudorotation $P=105^\circ$ for T3 residue or δ angle of 72° - 92° for A3 and T4 residue have been reported. The corresponding δ and P for A3 residue in our case is 118° - 121° and 140° - 145° , respectively. Thus the conformation of A3-T4 base pair is affected by insertion of drug chromophore between adjacent d-CpG sites.

In order to have an insight into the conformational states of the DNA molecule in the drug-DNA complex, we looked into the torsional angle of all structures at an interval of every 4 ps during 100 ps molecular dynamics simulations and there correlation with each other. Fig. 7.8 shows the dynamic variation of the torsional angle ζ is reflected in the change of adjacent angle ϵ . It is observed that ζ angle for G2 and C5 is populated near 186° , a value corresponding to B_{II} conformational stage while all other residues adopt the more stable B_I conformation. Thus it is clearly seen that G2 and C5 adopt B_{II} conformation in the complex. The phosphates lying directly opposite to these are in B_I conformational state. The backbone angle β do not show a significant variation with respect to canonical B-DNA except for the little lower value obtained for G2 residues. It is interesting to note that distortions at the level of third units for angle β and at the level of G2/G8 and C5/C11 for ϵ have also been observed in some crystal structures (Frederick et al, 1990; Moore et al, 1989; Wang et al, 1987).

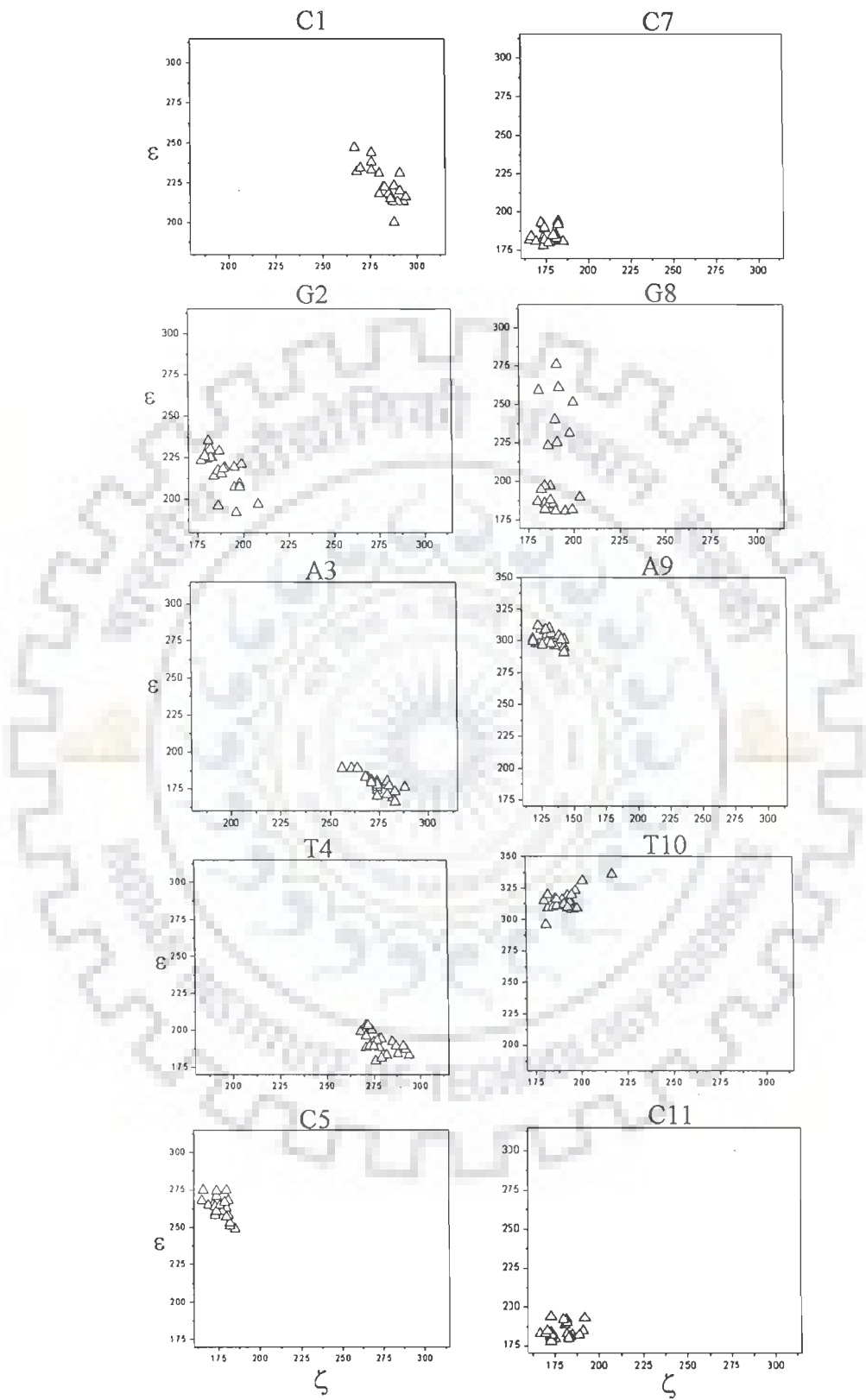


Figure 7.8: Correlation obtained for torsional angles ϵ and ζ

7.5.2 Conformation of Daunomycin

Therefore these distortions appear to be induced by the intercalation of the two anthracycline molecules.

Daunomycin consists of three fused aromatic rings B, C and D bound to a cyclohexane ring, ring A, with an amino sugar attached at C7 position. The bond distances and bond angles are generally within the limit of accepted values. The average C-C distance in BCD ring is 1.42 Å. The aromatic part of a glycon is quite planar with rms deviation of 1.2 Å for the least squares plane calculated from all the atoms of rings B, C and D without the exocyclic atoms. If all the exocyclic oxygen atoms (O4, O5, O6, O11, O12) as well as C7 and C10 are included in the calculations the rms deviation is 0.89 Å.

The orientation of 4OCH₃ group is such that methyl group is pointed away from O5 atom and protrudes into the solvent region. The distance between keto O5 and phenolic O6 and between keto O11 and phenolic O12 are 2.60 Å and 2.62 Å, respectively. Thus they presumably form intramolecular hydrogen bonds. During the course of restrained molecular dynamics simulations, both of these hydrogen bonds remain consistent.

The torsional angles of the daunomycin molecule in the complex are listed along with those obtained in similar X-ray crystal structures (Frederick et al, 1990; Moore et al, 1989) and free daunomycin (Neidle et al, 1977) molecule in Table 7.8. The torsional angles around C19-C20 and C20-C7 are -19.4° and 4° , respectively. All the atoms except C9 atom are almost in a plane with a maximum deviation of 0.4 Å. The atom C9 is displaced by 0.89 Å in the same direction as the amino sugar relative to the plane of aglycon and C9-O9 bond is almost orthogonal to the plane of ring A. O7 and

Table 7.8: Selected torsional angles (°) of the adriamycin in the complex and comparison with literature

ADRIAMYCIN	Present Study CGA+dnm ^a	Moore et al CGA + adm ^b	Frederick et al CGA + adm ^b	Neidle et al dnm ^c
RING A				
C20-C7-C8-C9	-14	-29.0	-39.9	-48.2
C7- C8-C9-C10	34	53.0	60.6	57.9
C8-C9-C10-C19	-48	-51.0	-56.0	-38.4
C9-C10-C19-C20	44	28.0	26.0	13.8
C10-C19-C20-C7	-19	-4.0	-0.8	-4.6
C19-C20-C7-C8	4	5.0	8.9	20.4
GLYCOSYL				
C8-C7-O7-C1'	82	97.0	68.2	124.9
C20-C7-O7-C1'	-154	-137.0	-160.4	-113.8
C7-O7-C1'-O5'	-77	-81.0	-74.6	-67.5
C7-O7-C1'-C2'	162	149.0	147.9	167.4
AMINO SUGAR				
O5'-C1'-C2'-C3'	-54	-58.0	-56.0	-53.8
C1'-C2'-C3'-C4'	61	57.0	40.0	55.7
C2'-C3'-C4'-C5'	-59	-18.0	-39.0	-61.2
C3'-C4'-C5'-O5'	62	-40.0	49.0	61.0
C4'-C5'-O5'-C1'	-56	47.0	-55.0	-58.8
C5'-O5'-C1'-C2'	57	7.0	60.0	56.5

^aCGA+dnm = d(CGATCG)₂+daunomycin

^bCGA+adm = d(CGATCG)₂+adriamycin

^cdnm =daunomycin

O9 atom can no longer form intramolecular hydrogen bond in contrast to that observed in crystal structure of free daunomycin and related anthracycline antibiotics (Anguilli et al, 1971; Courseille et al, 1979; von Dreele and Einck, 1977). During simulations, the torsional angle C7-O7-C1'-O5' lies in the range -64° to -83° in 25 structures which is near to the value (-68°) it has in uncomplexed daunomycin. Apparently the change in conformation of glycosyl linkage or presence/absence of intramolecular hydrogen bond is of no great consequence as far as intercalation of drug in DNA base pairs is concerned. The difference in conformation of ring A can be easily visualized on superimposition of the aglycon part in two cases. The difference in conformation obtained from that in other similar structures can be seen in Fig. 7.9. The amino sugar is in chair conformation with all the side chains pointed away from the aglycon. The torsional angle about C3'-C4' bond is particularly lower (45°) than the expected ideal gauche value (near $\pm 60^\circ$). The C2', C3', C4', O5' atoms are coplanar while the atom C5' is displaced by 0.85 Å away from chromophore while C1' are displaced towards aglycon by the same magnitude.

7.5.3 DNA-Daunomycin Interactions

Sequential NOE connectivities between C1 and G2 as well as between C5 and G6 bases were not observed. Instead NOE connectivities between C5H6 and 6OH, C1H5 and 1H, 2H protons as well as between C5H5, C5H6 and 4OCH₃ protons were observed. In addition G6H1' give NOE connectivities with 7H of ring A and C1H1' gives NOE with 11OH proton. This shows that the aromatic chromophore of the drug intercalates between C1pG2 and C5pG6 base pair steps such that ring D is positioned near C1 and C5 bases while ring A is close to G6 base. This is possible if the drug chromophore is in an orientation that is perpendicular to the long axis of the base pair

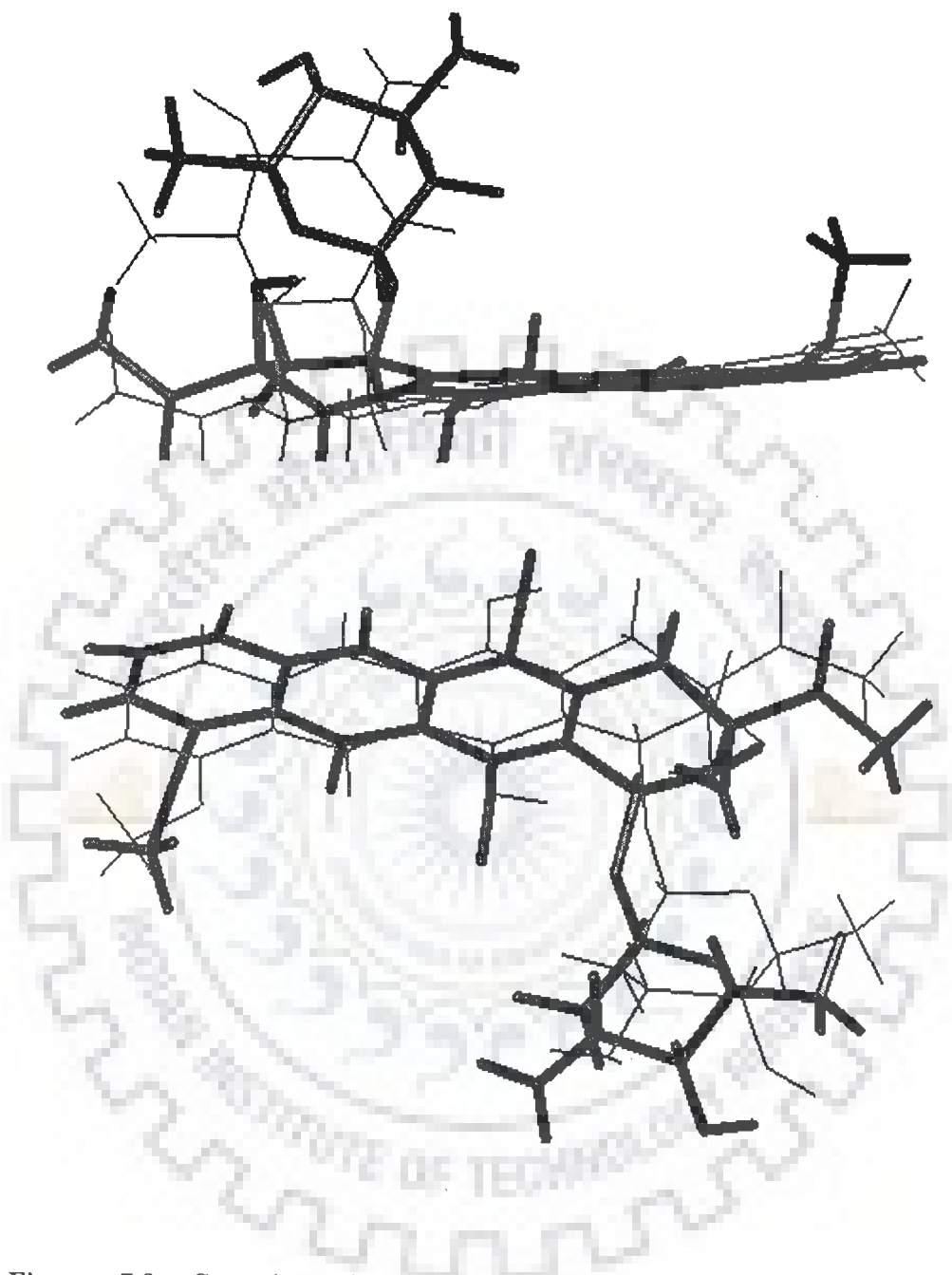


Figure 7.9: Superimposition of the daunomycin in the daunomycin-d-(CGATCG)₂ complex (thick lines) with that of uncomplexed daunomycin (thin lines)

with ring D protruding out on major groove side. The observed NOE between A3H1' and 5'CH₃, 5'H, 4'H protons and several other observed NOE connectivities between daunosamine sugar protons and A3 residue (A3H2-5'CH₃) show that the amino sugar of the drug is close to third base pair on its minor groove side. The position of the drug molecule with respect to hexanucleotide and hence the complete geometry of the complex gets defined by several other intermolecular NOEs (Table 7.3) observed in the NOESY spectra. The corresponding interproton distances in the structure obtained by restrained molecular dynamics are close to that calculated from intensities of cross peaks in NOESY spectra and are shown in Table 7.3.

A view showing the stacking interaction of the anthracycline chromophore between the bases is presented in Fig 7.10. It may be noted that the aglycon chromophore of the drug is placed between C1.G12 and G2.C11 base pair in a position perpendicular to the long axis of base pairs. Fig. 7.10 shows the stacking of G2-C11 base pair are A3.T10 base pair and A3.T10 base pair over T4.A9 base pair respectively. These overlap geometries are somewhat different from that in canonical B-DNA structure. The second base pair step, G2pA3 (Fig. 7.10) there is translation of base pair towards minor groove by about 1.6 Å. In the middle of the duplex, the base pair are shifted along long axis by about 0.6 Å. These translations coupled with a change in twist angle between base pairs upto 6° bring about a change in stacking interactions which manifests itself as change in chemical shift between base protons and H1' protons of deoxyribose.

Fig. 7.11 shows the position of drug with respect to DNA molecule to illustrate some of the hydrogen bonding interactions and close van der waal's contacts. It is found that 9OH group of the daunomycin is within hydrogen bonding distance of N2H and

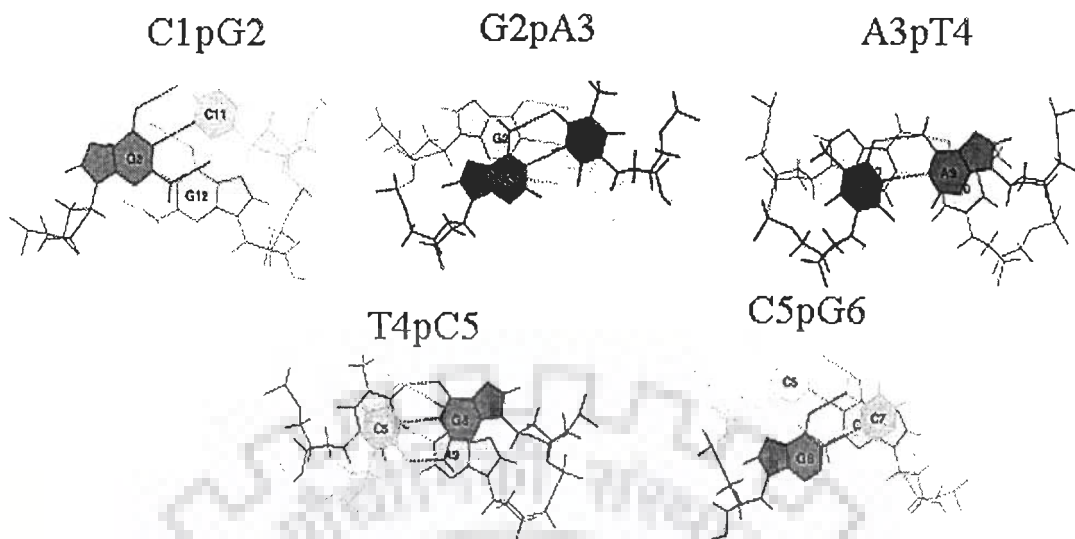


Figure 7.10: Overlap of base pairs at different base pair steps in d-(CGATCG)+daunomycin complex showing stacking interactions

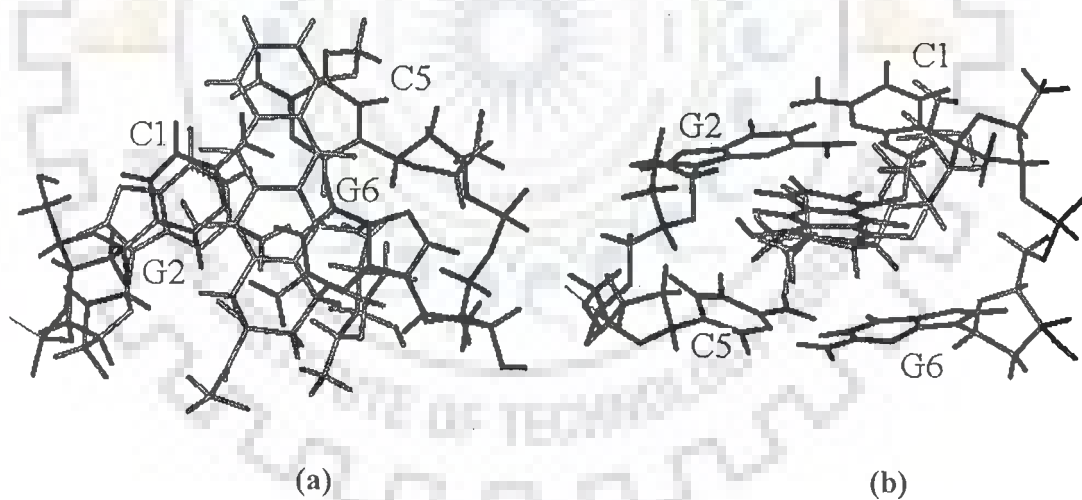


Figure 7.11: Drug-DNA stacking interaction in the intercalation site showing the orientation of the daunomycin with respect to base pairs (a) top view (b) front view

N3 atoms of G2 residue. The distance O9-H9...G2N3 is 2.7 Å and lies in the range 2.6-2.8 Å in the 25 structures saved at every 4 ps during 100 ps rMD simulations. This indicates existence of a strong hydrogen bond. The G2N2H...O9 distance is 3.4 Å and lies in the range 2.9-3.7 Å suggests the existence of another hydrogen bond.

The O7 atom which links ring A with daunosamine sugar is close to G2N2 atoms and is at distance of 2.9-3.3 Å. The O9-H9...O7 distance is large so that there is no possibility of hydrogen bond, as observed in uncomplexed daunomycin (Anguilli and Einck, 1971; Courseille et al, 1979; von Dreele and Einck, 1977).

The distance of carbonyl oxygen at C13 position of ring A is at a distance of 4.6-5.7 Å from O2 of C1 residue so that hydrogen bond through a bridging water molecule may be possible. The distance of O5 from C5 N1, O4 from G6O1P and 4OCH₃ from G6N7 are almost 3.1, 14.7 and 9.1 Å, respectively. Therefore an interaction of O5' with C5N1 through O6-H6 atom only is possible. In X-ray crystal structures the interaction of amino group with oxygen atoms in neighbouring residues have been seen (Frederick et al, 1990; Langlois d' Estaintot et al, 1992; Leonard et al, 1992; Moore et al, 1989; Wang et al, 1987) via its three hydrogen atoms. In our structure these distances N-H...O from C5O4', T4O2 and C5O2 are 3.1, 2.9 and 3.4 Å, respectively. At the other intercalation site, the corresponding N-H...O distances from C11O4', T10O2 and C11O2 are 3.3, 3.3 and 3.2 Å, respectively. Thus all the three hydrogen bonds are possible. This is in contrast to adriamycin-d(CGATCG) complex in which only one strong hydrogen bond was possible. It has been shown that NH₃⁺ group shows considerable variability and thermal mobility (Lipscomb et al, 1994; Trieb et al, 2004). We therefore looked into these distances throughout the simulations. It is found that all N-H...O distances lie in the range 2.9-3.4 Å. Further

the distance of NH_3^+ from T4O4'/T10O4' atom is about 5.8-6.3 Å so that no contact is possible. It has been shown that the glycosidic bond rotation C7-O7-C1'-C2', which is responsible for positioning NH_3^+ and anchoring the drug in the minor groove, exists in three conformational states (Trieb et al, 2004). In the three states, the dihedral angles adopt values in the range of 152°-162°, 135°-138° and 57°-61° and consequently the distance of NH of NH_3^+ moiety from oxygen/nitrogen atoms C5O4', T4O2, T4O4', C5O2, G2O4', G2O5', A3N3 and A9N3 vary. In the present study, it was found that C7-O7-C1'-C2' varied in the range 153-168° so that only one of the substates is stabilized in our complex. The distance N-H...O from C5O2/C11O2, C5O4'/C11O4', T4O2/T10O2 are less than 3.4 Å. The distance NH from T4O4'/T10O4', G2O4', G2O5', A3N3/A9N3 are in the range 4-12 Å so that these contacts do not exist. The results are in conformity with the findings of Trieb et al.

During the course of simulations, it was found that 6OH group of ring B pointed towards O5 atom in only 5 structures (Fig. 7.12a) so that distance of H6 of O6-H6 moiety from O5 atom was within 2.0-2.4Å. It was away from O5 atom in other structures and pointed towards O7 atom with no possibility of hydrogen bond. On the other hand O11-H11...O12 hydrogen bond existed in all the 25 structures (Fig. 7.12b). This is in contrast to the existence of both hydrogen bonds in uncomplexed drugs. It may be noted from Fig. 7.12a and 7.12b that the presence/absence of hydrogen bond is not correlated to the glycosidic angle adopted (that is, whether it is 153° or 168°). Several other non bonded contacts were seen in the structure (shown in Table 7.9), which may help in stabilizing the drug-DNA complex. Many of these contacts involve 4OCH₃, O5, O6, O7, 6OH, ring A and sugar protons in presumably a specific manner.

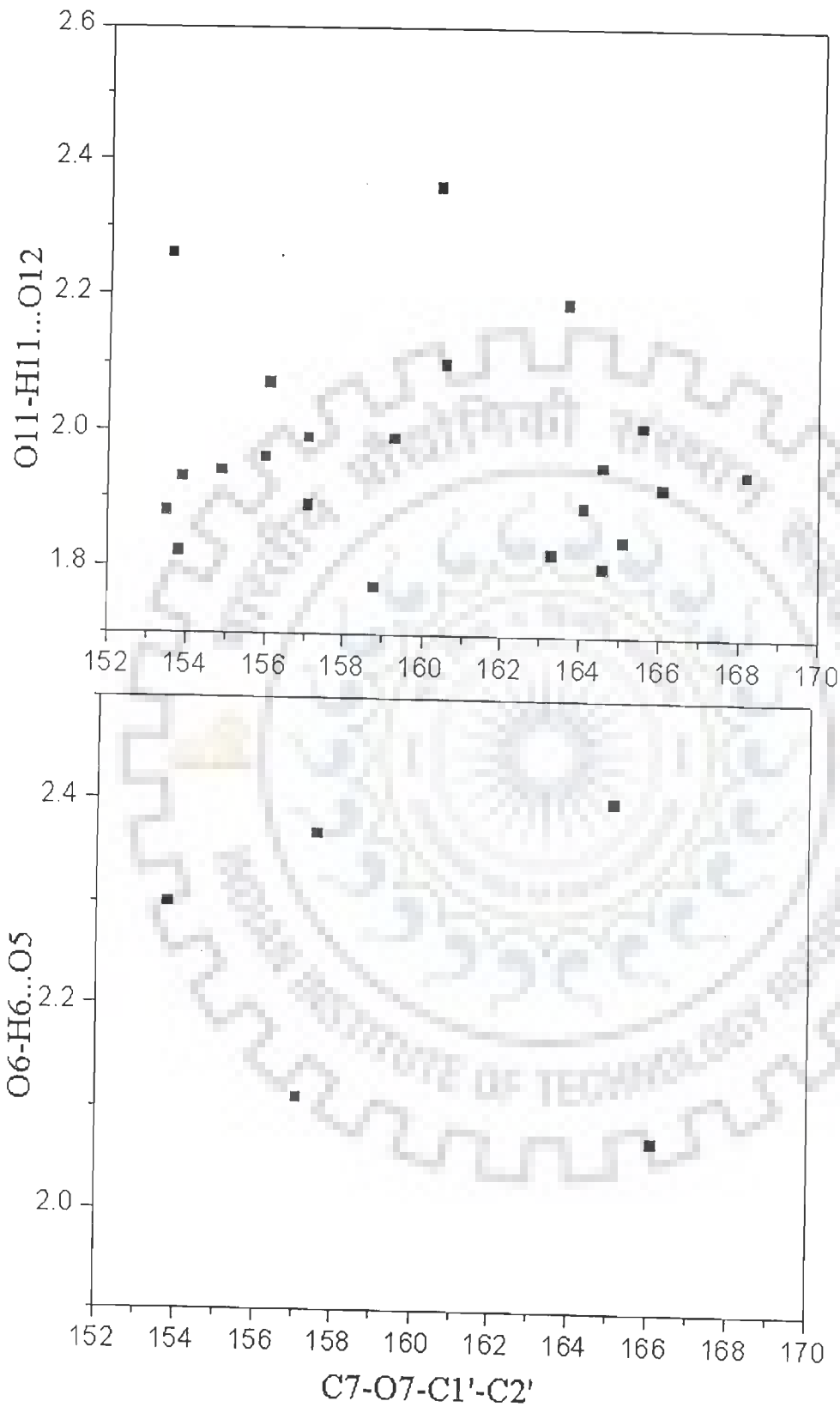


Figure 7.12: (a) Correlation between (a) glycosidic angle and O11-H11...O12 bond (b) glycosidic angle and O6-H6...O5 bond

Table 7.9: Close contacts between drug and DNA molecule

S.No	Protons	CGA+dnm ^a	S.No	Protons	CGA+dnm ^a
1.	C1O2-10axH	4.02	21.	T4H5'-C14	12.21
2.	C1H2'-11OH	2.63	22.	T4H5'-H2C14	11.96
3.	G2N3-10eqH	4.67	23.	C5O2-2axH	2.66
4.	G2N2-3'H	2.50	24.	C5O2-H3'	2.56
5.	G2O4'-10eqH	2.90	25.	C5C1'-2eqH	2.75
6.	G2H1N2-O9	4.84	26.	C5H1'-O5	3.09
7.	G2H1N2-O7	2.95	27.	C5H1'-O6	3.04
8.	G2H2N2-3'H	2.08	28.	C5H2'-O5	2.93
9.	G2H2N2-NH ₃	4.25	29.	C5H1'-HO6	2.16
10.	G2H4'-C14	3.73	30.	C5H1'-2eqH	2.04
11.	G2H4'-C13	3.67	31.	G6N2-10axH	4.14
12.	G2H4'-O13	3.66	32.	G6N3-7H	2.75
13.	A3N3-H1N3'	4.67	33.	G6O4'-7H	2.84
14.	A3N3-H2N3'	4.63	34.	G6O4'-H1'	2.36
15.	A3C2-H1N3'	4.28	35.	G6C4'-H1'	2.89
16.	A3H2-N3'	2.66	36.	G6H5'-C2'	5.95
17.	A3H2-H1N3'	3.24	37.	G6H5'-2eqH	2.41
18.	T4O2-4'H	4.64	38.	G6H5'-H1'	2.16
19.	T4O2-H2N3'	3.31	39.	G6H1N2-8axHH	4.83
20.	T4C5'-H2C14	12.25			

^aCGA+dnm = (CGATCG)₂ + daunomycin

CONCLUSIONS

The drug chromophore intercalates between C1pG2 and C5pG6 steps and is stabilized by π - π stacking. The hydrogen bonds G2N3...H9-O9 and G2N2H...O9 help in further stabilization of complex. O7 and O13 of 9COCH₃ form contacts with nucleotide residues in neighbourhood, NH₃⁺ moiety forms three hydrogen bonds with C5O4', C5O2 and T4O2 atoms. The glycosyl bond adopts one conformational substate having dihedral angle in the range 153-168°. The O6-H6...O5 hydrogen bond is much less stabler than O11-H11...O12 hydrogen bond. Several nonbonded contacts involve ring A and daunosamine atoms and may be responsible for specificity of interaction.

COMPARISON OF STRUCTURES OF THREE COMPLEXES

Table 7.9 shows comparison of structural features in three complexes studied by rMD using interproton distances from NMR spectra as restraints. It is observed that in all cases the chromophore intercalates at first and last base pair steps. The four interactions namely C1H5/T1CH₃-1H; A3H1'-5'CH₃; C5H5/C5H6/C1H2'/C5H2' with 1H/4OCH₃/6OH; G6H1'/A6H1' with 1'H/7H are common to all complexes. The hydrogen bond G2N2H...O9 and G2N3...H9-O9 are common to all complexes. The glycosidic bond angle C7-O7-C1'-C2'; the presence and absence of O6-H6...C5 and O11-H11...O12 hydrogen bond; NH₃⁺ moiety forming hydrogen bonds with O2 of C5, O4' of C5 and O2 of T4 residues; and DNA conformation vary somewhat in the three complexes (Table 7.9). These interactions with ring A atom, daunosamine sugar atom, 4O, 5O atoms of ring D and C bring about specificity in drug-DNA complex giving rise to variation in their biological action. The present study is a significant step towards understanding of molecular basis of action of these drugs enabled by solution studies using nuclear magnetic resonance spectroscopy.

Table 7.9a: Comparison of structural features in three complexes studied by rMD

CGA+adm ^a	NMR (Å)	Model (Å)	TGA+dnm ^b	NMR (Å)	Model (Å)	CGA+dnm ^c	NMR (Å)	Model (Å)
C1H5-1H	3.3	3.8	T1CH ₃ -1H	2.0	3.3	C1H5-1H	2.6	3.3
			T1CH ₃ -2H	2.3	4.6	C1H1'-11OH	2.5	3.6
			T1CH ₃ -3H	2.6	6.0	C1H2''-11OH	2.2	2.6
			T1CH ₃ -10axH	3.2	8.1			
G2H1'-10eqH	3.0	3.2				G2H1'-10eqH	-	3.7
						A3H1'-4'H	3.5	3.4
						A3H1'-5'H	2.9	3.7
A3H1'-5'CH ₃	3.2	2.6	A3H1'-5'CH ₃	2.5	3.6	A3H1'-5'CH ₃	3.5	2.3
			A3H2''-5'CH ₃	2.8	6.2	A3H2''-8axH	2.7	
			A3H8-5'CH ₃	2.7	7.2	A3H2-5'CH ₃	3.0	3.8
			A3H3'-5'CH ₃	3.7	5.8			
			A3H4'-5'CH ₃	2.4	4.0			
			T4H1'-2'eqH	3.2	6.2			

Table 7.9a Continued.....

C5H5-1H	2.6	5.5	C5H5-4OCH ₃	2.5	2.7		
C5H6-4OCH ₃	2.2	2.6	C5H6-4OCH ₃	2.6	2.5		
C5H6-1H	3.4	6.8					
C1H2''/C5- 4OCH ₃	3.3	3.2	C5H2'-4OCH ₃	2.2	2.7		
						C5H2'-6OH	3.5 4.0
						C5H2''-6OH	4.5 5.1
C5H4'-2'eqH	3.6	3.0					
C5H1'-2'eqH	2.6	2.6					
C5H5-3H	3.5	3.7	C5H5-2'axH	3.1	6.7		
C5H4'-2'axH		3.5	C5H2''-2'axH		5.4		
C5H1'-2'eqH		3.0					

Table 7.9a Continued.....

CGA+adm ^a	NMR	Model	TGA+dnm ^b	NMR	Model	CGA+dnm ^c	NMR	Model
						G6H5''-6OH	3.0	3.2
G6H1'-7H	3.1	3.3				G6H1'-7H	3.8	3.3
						G6H1'-10eqH	4.0	4.5
G6H5'-1'H	3.0	2.4						
G6H5'-2'axH	2.5	2.9						
G6H5'-2'eqH	2.6	2.8	A6H1'-2'eqH	3.8	4.8			
G6H1'-1'H	3.5	3.8	A6H1'-1'H	3.7	4.8			
G6H5''-1'H	3.2	3.6	A6H2-8axH		3.5			
G6H4'-1'H	3.0	2.9						

^aCGA+adm = (CGATCG)₂+adriamycin

^bTGA+dnm = (TGATCA)₂+daunomycin

^cCGA+DNM = (CGATCG)₂+daunomycin

Table 7.9b: Comparison of structural features in three complexes studied by rMD

	CGA+adm	TGA+dnm	CGA+dnm
C7-O7-C1'-C2'	137-160°	142-161°	153-168°
NH ₃ ⁺ with T4O2, C5O4', C5O2	Two hydrogen bond stability	Two hydrogen bond stability	Three hydrogen bond stability
O6-H6...O5	Exists in all 25 structures	Seen in 16 out of 25 structures	O6-H6...O5 is not stabilized. Seen in 5 out of 25 structures
O11-H11...O12	Not stabilized.	Seen in 23 out of 25 structures	Exists in all 25 structures
G2N2H...O9	Present	Present	Present
G2N3...O9	Short stable hydrogen bond	Short stable hydrogen bond	Short stable hydrogen bond
B _{II} conformation	Exists at G2pA3 and C5pG6 base pair steps	Exists at G2pA3, A3pT4 and C5pA6 base pair steps	Exists at G2pA3 and C5pG6 base pair steps

REFERENCES

1. Adams A., Guss J.M. and Collyer C.A. Crystal structure of the topoisomerase II poison 9-amino-[N-(2-dimethylamino)ethyl]acridine-4-carboxamide bound to the DNA hexanucleotide d(CGATCG)₂. *Biochemistry*, 1999, 38, 9221.
2. Altona C. and Sundaralignam M. Conformational analysis of the sugar ring in nucleosides and nucleotides. A new description using the concept of pseudorotation. *J. Am. Chem. Soc.*, 1972, 94, 8205.
3. Anguilli R., Foresti E., Rivi di S.L., Isaacs N.W., Kennard O., Mothewell W.D.S., Wampler D.L. and Arcamone F. Structure of daunomycin: X-ray analysis of N-Br-acetyl daunomycin solvate. *Nature (London), New Biol.*, 1971, 234, 78.
4. Arcamone F. and Penco S. In "Anthracyclines and anthracediones based anticancer agents". (Eds. Lown J.W.), Elsevier, New York, 1988.
5. Arcamone F. Doxorubicin: In "Anticancer Antibiotics". Academic Press, New York, 1981.
6. Arora S.K. Molecular structure, absolute stereochemistry, and interactions of nogalamycin, a DNA-binding anthracycline antitumor antibiotic. *J. Amer. Chem. Soc.*, 1983, 105, 1328.
7. Bacolla A., Gellibolian R., Shimizu M., Amirhaeri S., Kang S., Ohshima K., Larson J.E., Harvey S.C., Stollar B.D. and Wells R.D. Flexible DNA: Genetically unstable CTG.CAG and CGG.CCG from human hereditary neuromuscular disease genes. *J. Biol. Chem.*, 1997, 272, 16783.
8. Barthwal R., Awasthi P., Monica., Kaur M., Sharma U., Srivastava N., Barthwal S.K. and Govil G. Structure of DNA sequence d-TGATCA by two-

- dimensional Nuclear Magnetic Resonance Spectroscopy and Restrained Molecular Dynamics. *J. Struct. Biol.*, 2004, 148, 34.
9. Barthwal R.B., Mujeeb A. and Govil G. Interaction of daunomycin with deoxydinucleotide d-CpG by two dimensional proton magnetic resonance techniques. *Arch. Biochem. Biophys.*, 1994, 313, 189.
 10. Bertucat G., Lavery R. and Prévost C.A. A model for parallel triple helix formation by RecA: Single-strand association with a homologous duplex via the minor groove. *J. Biomol. Struct. Dyn.*, 1998, 16, 535.
 11. Beutal B.L. and Gold L. In vitro evolution of intrinsically bent DNA. *J. Mol. Biol.*, 1992, 228, 803.
 12. Bhattacharyya D. and Bansal M. Groove width and depth of B-DNA structures depend on local variations in slide. *J. Biomol. Struct. Dyn.*, 1992, 10, 213.
 13. Bodenhausen G., Freeman R. and Turner D.L. Suppression of artifacts in two-dimensional spectroscopy. *J. Magn. Reson.*, 1977, 27, 511.
 14. Calendi E., Di Marco A., Reggiani M., Scarpinato B. and Valentini L. On physico-chemical interactions between daunomycin and nucleic acids. *Biochem. Biophys. Acta.*, 1965, 103, 25.
 15. Celda V., Widmer H., Leupin W., Chazin W., Denny A. and Wuthrich K. Conformational studies of d-(AAAAATTTT)₂ using constraints from nuclear overhauser effects and from quantitative analysis of the cross peak fine structures in two-dimensional ¹H Nuclear Magnetic Resonance spectra. *Biochemistry*, 1989, 28, 1462.
 16. Chaires J.B. Daunomycin inhibits the B → Z transition in poly d-(G-C). *Nucleic Acids Research*, 1983, 11, 8485.

17. Chaires J.B. Thermodynamics of the daunomycin-DNA interaction: Ionic strength dependence of the enthalpy and entropy. *Biopolymers*, 1985a, 24, 403.
18. Chaires J.B., Dattagupta N. and Crothers D.M. Biochemistry. Self-association of daunomycin. *Biochemistry*, 1982, 21, 3927.
19. Chaires J.B., Dattagupta N. and Crothers D.M. Kinetics of the daunomycin-DNA interaction. *Biochemistry*, 1985, 24, 260.
20. Chaires J.B., Dattagupta N. and Crothers D.M. Studies on interaction of anthracycline antibiotics and deoxyribonucleic acid: Equilibrium binding studies on interaction of daunomycin with deoxyribonucleic acid. *Biochemistry*, 1982a, 21, 3933.
21. Chaires J.B., Fox K.R., Herrera J.E., Britt M. and Waring M.J. Site and sequence specificity of the daunomycin-DNA interaction. *Biochemistry*, 1987, 26, 8227.
22. Chaires J.B., Herrera J.E. and Waring M.J. Preferential binding of daunomycin to 5'A/TCG and 5'A/TGC sequences revealed by footprinting titration experiments. *Biochemistry*, 1990, 29, 6145.
23. Chastain P.D. and Sinden R.R. CTG repeats associated with human genetic disease are inherently flexible. *J. Mol. Biol.*, 1998, 275, 405.
24. Chen C.W., Knop R.H. and Cohen J.S. Adriamycin inhibits the B to Z transition of poly (dGm⁵dC). *Poly (dGm⁵dC)*. *Biochemistry*, 1983, 22, 5468.
25. Chen H. and Patel D.J Solution structure of a quiniomycin bisintercalator DNA complex. *J. Mol. Biol.*, 1995, 246, 164.

26. Chen K.X., Gresh N. and Pullman B. A theoretical investigation on the sequence selective binding of daunomycin to double-stranded polynucleotides. *J. Biomol. Struct. Dyn.*, 1985, 3, 445.
27. Chen K.X., Gresh N. and Pullman B. A theoretical investigation on the sequence selective binding of adriamycin to double-stranded polynucleotides. *Nucleic Acids Research*, 1986, 14, 2251.
28. Cheung S., Arndt K. and Lu P. Correlation of Lac-Operator Imino proton exchange kinetics with its Function. *Proc. Natl. Acad. Sci., U.S.A.*, 1984, 81, 3665.
29. Chuprina V.P., Lipanov A.A., Fedoroff O.Y., Kim S.G., Kintanar A. and Reid B.R. Sequence effects on local DNA topology. *Proc. Natl. Acad. Sci., U.S.A.*, 1991, 88, 9087.
30. Cieplak P., Rao S.N., Grootenhuys P.D.J. and Kollman P.A. Free energy calculation on base specificity of drug-DNA interactions: Application to daunomycin and acridine intercalation into DNA. *Biopolymers*, 1990, 29, 717.
31. Cirilli M., Bachechi F. and Ughetto G. Interactions between morpholinyl anthracyclines and DNA. The crystal structure of a morpholino doxorubicin bound to d-(CGTACG). *J. Mol. Biol.*, 1992, 230, 878.
32. Courseille C., Busetta B., Geoffre S. and Hospital M. Complex daunomycin-butanol. *Acta Cryst.*, 1979, B35, 764.
33. Dalgleish D.G., Fey G. and Kersten W. Circular dichroism studies of complexes of the antibiotics daunomycin, nogalamycin, chromomycin and mithramycin with DNA. *Biopolymers*, 1974, 13, 1757.
34. Davies D.B., Eaton R.J., Baranovsky S.F. and Veselkov A.N. NMR investigation of the complexation of daunomycin with deoxytetranucleotides

- of different base sequence in aqueous solution. *J. Biomol. Struct. Dyn.*, 2000, 17, 887.
35. Derome A.E. In "Modern NMR techniques for chemistry research". Volume 6, Pergamon Press, Oxford U.K. 1987.
36. Di Marco A., Arcamone F. and Zunino F. In "Antibiotics". (Eds. Corcoran J.W. and Hahn I.E.) Springer-Verlag, Berlin, 1974,101.
37. Dickerson R.E., Bansal M., Calladine C.R., Diekmann, S., Hunter W.N., Kennard O., Kitzing von E., Lavery R., Nelson H.C.M., Olson W.K., Saenger W., Shakked Z., Sklenar H., Soumpasis D.M, Tung C.S., Wang A.H.J. and Zhurkin V.B. Definitions and Nomenclature of Nucleic Acid Structure Parameters. *J. Mol. Biol.*, 1989, 208, 787.
38. Donlan M.E. and Lu P. Transcriptional enhancer related DNA sequences: Anomalous ^1H NMR NOE crosspeaks. *Nucleic Acids Research*, 1992, 20, 525.
39. Dornberger U., Flemming J. and Fritzsche H. Structure determination and analysis of helix parameters in the DNA decamer d-(CATGGCCATG)₂ comparison of results from NMR and crystallography. *J. Mol. Biol.*, 1998, 284, 1453.
40. Favier A., Blackledge M., Simorre J.P., Crouzy S., Dabouis V., Gueiffer A., Dominique M. and Debouzy J.C. Solution structure of 2-(pyrido[1,2-e]purin-4-yl)amino-ethanol intercalated in the DNA duplex d-(CGATCG)₂. *Biochemistry*, 2001, 40, 8717.
41. Feigon J., Wright J. M., Leupin W., Denny W.A. and Kearns D.R. Use of two-dimensional NMR in the study of double-stranded decamer. *J. Amer. Soc.*, 1982, 104, 5540.

42. Frechet D., Chen D. M., Kan L.S. and Tso P.O.P. Nuclear overhauser effect as a tool for the complete assignment of non-exchangable proton resonance in short deoxyribonucleic acid helices. *Biochemistry*, 1983, 22, 5194.
43. Frederick C.A., Williams L.D., Ughetto G., Van der Marel G.A., Van Boom J.H., Rich A. and Wang A.H.J. Structural comparison of anticancer drug-DNA complexes: Adriamycin and daunomycin. *Biochemistry*, 1990, 29, 2538.
44. Fritzsche H., Triebel H., Chaires J.B., Dattagupta N. and Crothers D.M. Studies on interaction of anthracycline antibiotics and deoxyribonucleic acid geometry of intercalation of iremycin and daunomycin. *Biochemistry*, 1982, 21, 3940.
45. Gabbay E.J., Grier D., Fingerie R.E., Reimer R., Levy R., Pearce S.W. and Wilson W.D. Interaction specificity of the anthracyclines with deoxyribonucleic acid. *Biochemistry*, 1976, 15, 2062.
46. Gao Y.G. and Wang A.H.J. Crystal structures of four morpholino-doxorubicin anticancer drugs complexed with d-(CGTACG) and d-(CGATCG): Implications in drug-DNA crosslink. *J. Biomol. Struct. Dyn.*, 1995, 13, 103.
47. Giessner-Prettre C. and Pullman B. On the atomic or local contributions to chemical shifts due to the anisotropy the diamagnetic susceptibility of the aromatic side chain of amino acids and of the porphyrin ring. *Biochem. Biophys. Res. Commun.*, 1976, 15, 2277.
48. Gochin M. Zon G. and James. T.L. Two dimensional COSY and two dimensional NOE spectroscopy of d(AC)₄, d(GT)₄: Extraction of structural constraints. *Biochemistry*, 1990, 29, 11161.

49. Goodsell D.S., Kopka M.L., Cascio D. and Dickerson R.E. Crystal structure of CATGGCCATG and its implication for A tract bending models. *Proc. Natl. Acad., Sci., USA.*, 1993, 90, 2930.
50. Gorenstein G. ³¹P NMR of DNA Spectroscopic methods for analysis of DNA. *Methods in Enzymology*, 1992, 211, 254.
51. Gorin A.A., Zhurkin V.B. and Olson W.K. B-DNA twisting correlates with base-pair morphology. *J. Mol. Biol.*, 1995, 247, 34.
52. Graves D.E. and Krugh T.R. Adriamycin and daunorubicin bind in a cooperative manner to deoxyribonucleic acid. *Biochemistry*, 1983, 22, 3941.
53. Gronenborn A. M. and Clore G.M. Investigation of the solution structure of short nucleic acid fragments by means of nuclear overhauser enhancements measurements. *Prog. NMR Spec.*, 1985, 17, 1.
54. Grzeskowiak K. Sequence dependent structural changes in B-DNA. *Chem. Biol.*, 1996, 3, 785.
55. Grzeskowiak K., Yanagi K., Prive G.G. and Dickerson R.E. The structure of B-helical C-G-A-T-C-G-A-T-C-G and comparison with C-C- A-A-C-G-T-T-G-G. The effect of base pair reversals. *J. Biol. Chem.*, 1991, 266, 8861.
56. Gunther U. L., Ludwig C. and Ruterjans H. NMRLAB-Advanced NMR data processing in MATLAB. *J. Magn. Reson.*, 2000, 145, 201.
57. Hare D.H., Wemmer D.E., Chou S.H., Drobny G. and Reid B.R. Assignment of the non-exchangable proton resonances of d-(CGCGAATTCGCG)₂ using two-dimensional methods. *J. Mol. Biol.*, 1983, 171, 319.
58. Holbrook S.R., Wang A.H.J., Rich A. and Kim S.H. Local mobility of nucleic acids as determined from crystallographic data III daunomycin-DNA complex. *J. Mol. Biol.*, 1988, 199, 349.

59. Hosur R.V., Govil G. and Miles H.T. application of two-dimensional NMR spectroscopy in the determination of solution conformations of nucleic acids. *Magn. Reson. Chem.*, 1988, 26, 927.
60. Hosur R.V., Ravikumar M., Roy K.B., Tan-Zu-Kun, Miles H.T. and Govil G. In "Magnetic resonance in biology and medicine". (Eds. Govil G., Khetrupal C.L. and Saran A.) Tata Mcgraw Hill, New Delhi, 1985, 305.
61. Hosur, R.V., Ravikumar M., Chary K.V.R., Sheth A., Govil G., Tan-Zu-Kunn and Miles H.T. solution structure of d-GAATTCGCAATTC by 2D NMR: A new approach to determination of sugar geometries in DNA segments. *FEBS Letts.*, 1986, 205, 71.
62. Hu G.G., Shui X., Leng F., Priebe W., Chaires J.B. and Williams L.D. Structure of DNA-bisdaunomycin complex. *Biochemistry*, 1997, 36, 5940.
63. Hunter C.A. Sequence-dependent DNA Structure: The role of base stacking interactions. *J. Mol. Biol.*, 1993, 230, 1025.
64. Igarashi J. and Sunagawa M. Structural analysis by NMR of antitumor drug-DNA complexes: 9-aminoanthracycline (SM-5887). *Bioorganic & Medicinal Chemistry Letters*, 1995, 5, 2923.
65. Islam S.A., Neidle S., Gandecha B.M., Partridge M., Patterson L.H. and Brown J.R. Comparative computer graphics and solution studies of the DNA interaction of substituted anthraquinones based on doxorubicin and mitoxantrone. *J. Med. Chem.*, 1985, 28, 857.
66. Jeener J. Paper presented at the AMPERE International summer school, Borsko, Polje, Yugoslavia, 1971.
67. Jones M.B., Hollstein U. and Allen F.S. Site specificity of binding of antitumor antibiotics to DNA. *Biopolymers*, 1987, 26, 121.

68. Kabsch W., Sander S. and Trifonov E.N. The helical twist angle of B-DNA. *Nucleic Acids Research*, 1982, 10, 1097.
69. Keeler J. and Neuhaus D. Comparison and evaluation of methods for two-dimensional NMR spectra with absorption mode line shape. *J. Magn. Reson.*, 1985, 63, 454.
70. Kemler I., Schreiber E., Muller M.M., Matthias P. and Schaffner W. Octamer transcription factors bind to two different sequence motifs of the immunoglobulin heavy chain promoter. *EMBOJ.*, 1989, 8, 2001.
71. Kosikov K.M, Gorin A.A., Zhurkin V.B. and Olson W.K. DNA stretching and compression: Large-scale simulations of double helical structures. *J. Mol. Biol.*, 1999, 26, 1301.
72. Kumar R., Hosur R.V., Chary K.V.R., Sheth A., Govil G., Kunn T.Z. and Miles H.T. Solution structure of d-GAATTCGAATTC by 2D NMR: A new approach to determination of sugar geometries in DNA segments. *FEBS Letts.*, 1986, 205, 71.
73. Lam S. L. and Au-Yeung S.C.F. Sequence specific local structural variations in solution structures of d(CGXXCG)₂ and d(CAXXTG)₂ self complementary deoxyribonucleic acids. *J. Mol. Biol.*, 1998, 266, 745.
74. Langlois d'Estaintot B., Gallois B., Brown T. and Hunter W.N. The molecular structure of a 4-epiadriamycin complex with d-(TGATCA) at 1.7 Å resolution: Comparison with the structure of 4'-Epiadriamycin d-(TGTACA) and d-(CGATCG) Complexes. *Nucleic Acids Research*, 1992, 20, 3561.
75. Lavery R. and Sklenar H. CURVES 5.1. Helical analysis of irregular nucleic Acids. Laboratory of Theoretical Biology. CNRS, Paris, 1996.

76. Lavery R. and Sklenar H. The definition of generalized helicoidal parameters and of axis curvature for irregular nucleic acids. *J. Biomol. Struct. Dyn.*, 1988, 6, 63.
77. Lavery R. and Sklenar J. Defining the Structure of Irregular Nucleic Acids: Conventions and Principles. *J. Biomol. Struct. Dyn.*, 1989, 6, 655.
78. Leonard G.A., Brown T., Hunter W.N. Anthracycline binding to DNA. High-resolution structure of d-(TGTACA) complexed with 4'-epiadriamycin, *Eur. J. Biochem.* 1992, 204, 69.
79. Leonard G.A., Hambley T.W., Mc Auley Hecht K., Brown T. and Hunter W.N. Anthracycline-DNA interactions at unfavourable base pair triplet binding sites: Structures of d-(CGGCCG)/daunomycin and d-(TGGCCA)/adriamycin complexes. *Acta Cryst.*, 1993, D49, 458.
80. Lerman L.S. Structural considerations in the interaction of DNA with acridines. *J. Mol. Biol.*, 1961, 3, 18.
81. Lipscomb L.A., Peek M.E., Zhou F.X., Berrand J.A., Van Derveer D. and Williams L. D. Water ring structure at DNA interfaces: Hydration and dynamics of DNA-anthracycline complexes. *Biochemistry*, 1994, 33, 3649.
82. Lown J.W., Sim S.K., Majumdar K.C. and Chang R.Y. Strand scission of DNA by bound adriamycin and daunorubicin in the presence of reducing agents. *Biochem. Biophys. Res. Commun.*, 1977, 76, 705.
83. Lyubchenko Y.L., Shlyakhtenko L., Appella S.E. and Harrington R.E. CA runs increase DNA flexibility in the complex of λ cro protein with the O_{R3} site. *Biochemistry*, 1993, 32, 4121.

84. Manfait M., Alix A.J.P., Jeannesson P., Jardillier J.C. and Heophanides T. Interaction of adriamycin with DNA as studied by resonance Raman spectroscopy. *Nucleic Acids Research*, 1982, 10, 3803.
85. Maple J.R., Thacher T.S., Dinur U. and Hagler A.T. Biosym forcefield research results in new techniques for the extraction of inter and intra molecular forces. *Chemical Design Automation News*, 1990, 5, 5.
86. Maple J.R., Dinur U. And Hagler T. Derivation of force field for molecular mechanics and dynamics from ab-initio energy surfaces. *Proc. Natl. Acad. Sci., U.S.A.*, 1988, 85, 5350.
87. Marion D. and Wuthrich K. Application of phase sensitive two-dimensional correlated spectroscopy (COSY) for measurement of ^1H - ^1H spin coupling constant in proteins. *Biochem. Biophys. Res. Comm.*, 1983, 113, 967.
88. Mazzini S., Mondelli R. and Ragg E. Structure and dynamics of intercalation complexes of anthracyclines with d-(CGATCG)₂. 2D- ^1H and ^{31}P NMR investigations. *J. Chem. Soc., Perkin Trans.*, 1998, 2, 1983.
89. Mc Ateer K. and Kennedy M.A. NMR evidence for base dynamics at all TpA steps in DNA. *J. Biomol. Struct. Dyn.*, 2000, 17, 1001.
90. Messori L., Temperini C., Piccioli F., Animati F., Di Bugno and Orioli P. Solution chemistry and DNA binding properties of MEN 10755, a novel disaccharide analogue of doxorubicin. *Bioorganic & Medicinal Chemistry*, 2001, 9, 1815.
91. Miller K.J. and Newlin D.D. Interactions of molecules with nucleic acids VI. Computer design of chromophoric intercalating agents. *Biopolymers*, 1982, 21, 633.

92. Mondelli R., Ragg E. and Fronza G. Conformational analysis of N-acetyl daunomycin in solution. A transient H nuclear overhauser effect study of the glycosidic linkage geometry. *J. Chem. Soc., Perkin Trans.*, 1987, II, 27.
93. Mondelli R., Ragg E., Fronza G. and Arnone A. Nuclear magnetic resonance conformational study of daunomycin and related antitumor antibiotics in solution. The conformation of ring A. *J. Chem. Soc., Perkin Trans.*, 1987, II, 15.
94. Moore M.H., Hunter W.N., Langlois d'Estaintot B. and Kennard O. DNA-drug interactions. The crystal structure of d-(CGATCG) complexed with daunomycin. *J. Mol. Biol.*, 1989, 206, 693.
95. Mujeeb A., Kerwin S.M., Kenyon G.L. and James T.L. Solution structure of conserved DNA sequence from the HIV-I genome: Restrained molecular dynamics simulation with distance and torsion angle restraints derived from two-dimensional NMR spectra. *Biochemistry*, 1993, 32, 13419.
96. Nakata Y. and Hopfinger A.J. An extended conformational analysis of doxorubicin. *FEBS Letts.*, 1980, 95, 583.
97. Nakata Y. and Hopfinger A.J. Predicted mode of intercalation of doxorubicin with dinucleotide dimers. *Biochem. Biophys. Res. Commun.*, 1980a, 95, 583.
98. Neidle S. and Taylor G.L. Nucleic acid binding drugs. Some conformational properties of the anticancer drug daunomycin and several of its derivatives. *FEBS Letts.*, 1979, 107, 348.
99. Neidle S. and Taylor G.L. Nucleic acid binding drugs: Part IV. The crystal structure of the anti cancer agent daunomycin. *Biochim. Biophys. Acta.*, 1977, 479, 450.

100. Neidle S., Sanderson M.R. and Waring M.J.. In "Molecular aspects of anticancer drug action" . Mac Millan, London, 1983.
101. Neuman J.M., Cavailles J.A., Herve M., Dinh S.T., Langlois d'Estaintot B., Huynh Dinh T. and Igolen J. 500 MHz ¹H NMR study of the interaction of daunomycin with B and Z helices of d-(CGm⁵CGCG). FEBS Letts., 1985, 182, 360.
102. Norwood T., Tillett M. and Lian L.Y. Influence of cross-correlation between the chemical shift anisotropies of pairs of nuclei on multiple-quantum relaxation rates in macromolecules. Chem. Phys. Letts., 1999, 300, 429.
103. Nunn C.M., Meervelt L.V., Zhang S., Moore M.H. and Kennard O. DNA-drug interactions. The crystal structures of d-(TGTACA) and d-(TGATCA) complexed with daunomycin. J. Mol. Biol., 1991, 222, 167.
104. Nuss M.E., James T.L., Apple M.A. and Kollman P.A. A NMR study of the interaction of daunomycin with dinucleotides and dinucleoside phosphates. Biochim. Biophys. Acta., 1980, 609, 136.
105. Nuss M.E., Marsh F.J. and Kollman P.A. Theoretical studies of drug-DNA interactions. Empirical Energy Function calculations on the interaction of ethidium, 9-aminoacridine, and proflavin cations with base-paired dinucleotides GpC and CpG. Biochemistry, 1979, 14, 825.
106. Nuss ME., James T.L., Apple M A and Kollman P.A., Biochem. Biophys. Acta. An NMR study of the interaction of daunomycin with dinucleotides and dinucleosides phosphates. Biochim. Biophys. Acta., 1980, 609, 136.
107. Odefey C., Westendorf J., Diechmann T. and Oschkinat H. Two dimensional nuclear magnetic resonance studies of an intercalation complex between the novel semisynthetic anthracycline 3'-deamino-3'-(2-methoxy-4-morpholinyl)-

- doxorubicin and the hexanucleotide duplex d-(CGTACG). *Chem. Biol. Interact.*, 1992, 85, 117.
108. Olson W.K. and Lu X.J.. 3DNA version 1.4.1, A 3-dimensional Nucleic acid Structure analysis and rebuilding software package. Department of Chemistry, Rutgers University, NJ, 2001.
109. Pachter J.A., Huang C.H., Du Vernay V.H., Prestayko A.W. and Crooke S.T. Viscometric and fluorometric studies of deoxyribonucleic acid interactions of several new anthracyclines. *Biochemistry*, 1982, 21, 1541.
110. Paciucci P.A., Cuttner J., Gottlieb A., Davies R.B., Martelo O. and Molland F. Sequential mitoxantrone, daunorubicin and cytosine arabinoside for patients with newly diagnosed acute myelocytic leukemia. *Am. J. Haematol.*, 1997, 56, 214.
111. Patel D.J. and Canuel L.L. Anthracycline antitumour antibiotics. Nucleic acid interactions. Structural aspects of the daunomycin, poly(dA-dT) complex in solution. *Eur. J. Biochem.*, 1978, 90, 247.
112. Patel D.J. Helix-coil transition of the dG-dC-dG-dC self-complementary duplex and complex formation with daunomycin in solution. *Biopolymers*, 1979, 18, 553.
113. Patel D.J., Kozlowski S.A. and Rice J.A. Hydrogen bonding, overlap geometry, and sequence specificity in anthracycline antitumour antibiotic. DNA complexes in solution. *Proc. Natl. Acad. Sci., U.S.A.*, 1981, 78, 3333.
114. Phillips D.R. and Roberts G.C.K. Proton nuclear magnetic resonance study of the self-complementary hexanucleotide d-(pTpA)₃ and its interaction with daunomycin. *Biochemistry*, 1980, 19, 4795.

115. Piantini U., Sorensen O.W. and Ernst R.R. Multiple quantum filters for elucidating NMR networks. *J. Am. Chem. Soc.*, 1982, 104, 6800.
116. Pigram W.J., Fuller W. and Hamilton L.D. Stereochemistry of intercalation: Interaction of daunomycin with DNA. *Nature New Biol.*, 1972, 235, 17.
117. Pilch D.S., Yu C., Makhey D., Lavoie E.J., Srinivasan A.R., Olson W.K., Saucers R.R., Brealauer K.J., Geacintov N.E. and Liu L.F. Minor groove-directed and intercalative ligand DNA interactions in the poisoning of DNA topoisomerase I by protoberberine analogs. *Biochemistry*, 1997, 36, 12542.
118. Pindur U., Haber M. and Sattler K. Antitumour active drug as intercalators of deoxyribonucleic acid. *Journal of Chemical Education*, 1993, 70, 263.
119. Plumbridge T.W. and Brown J.R. Spectrophotometric and fluorescence polarization studies of the binding of ethidium, daunomycin and mepacrine to DNA and to Poly (I.C). *Biochim. Biophys. Acta.*, 1977, 479, 441.
120. Pohle W., Flemming J. and Bohl M. Adriamycin binding to DNA phosphates as evidenced by spectroscopic and quantum-chemical results. *Studia Biophysica*, 1987, 122, 223.
121. Pohle W., Flemming J., Bohl M. and Bohlig H. Subsidiary hydrogen bonding of intercalated anthraquinonic anticancer drugs to DNA phosphate. *Biophysical Chem.*, 1990, 35, 213.
122. Quigley G.J., Wang A.H. J., Ughetto G., Van der Marel G., Van Boom J.H. and Rich A. Molecular structure of an anticancer drug-DNA complex: Daunomycin plus d-(CpGpTpApCpG). *Proc. Natl. Acad. Sci., USA.*, 1980, 77, 7204.
123. Radha P.K. Madan A Nibedita R. and Hosur R.V. Solution structure of the combined segment of Myb cognate DNA sequence by 2D NMR, spectral

- simulation, restrained energy minimization, and distance geometry calculations. *Biochemistry*, 1995, 34, 5913.
124. Ragg E., Mondelli R., Battistini C., Garbesi A. and Colonna F.P. ^{31}P NMR study of daunorubicin-d-(CGTACG) complex in solution: Evidence of the intercalation sites. *FEBS Letts.*, 1988, 236, 231.
125. Rameta D.P., Mudd C.P., Berger R.L. and Breslauer K.J. Thermodynamics characterization of daunomycin-DNA interactions: Microcalorimetric measurements of daunomycin-DNA binding enthalpies. *Biochemistry*, 1991, 30, 9799.
126. Redfield A.G., Kunj S. and Ralph E.K. Quadrature fourier NMR detection, simple multiplex for dual detection and discussion. *J. Magn. Reson.*, 1975, 19, 116.
127. Reid B.R., Baukes K., Flynn P. and Nerdal W. NMR distance measurement in DNA duplex: Sugar and bases have the same correlation times. *Biochemistry*, 1989, 28, 10001.
128. Roberts G.C.K. Applications of NMR in drug discovery. *Drug Discovery Today*, 2000, 5, 230.
129. Roberts G.C.K. NMR spectroscopy in structure-based drug design. *Curr. Opin. Biotechnol.*, 1999, 10, 42.
130. Robinson H., Priebe W., Chaires J.B. and Wang A.H.J. Binding of two novel bisdaunorubicins to DNA studied by NMR spectroscopy. *Biochemistry*, 1997, 36, 8663.
131. Roche C. J., Berkowitz D., Sulikowski G.A., Danishefsky S.J. and Crothers D.M. Binding affinity and site selectivity of daunomycin analogues. *Biochemistry*, 1994, 33, 936.

132. Rudolf H. W., Liedl K. R., Rüdiger S., Pichler A., Hallbrucker A. and Mayer E. B-DNA's BI \rightarrow BII Conformer substate dynamics is coupled with water migration. *J. Phys. Chem. B.*, 1998, 102, 8934.
133. Saminadin P., Dautant A., Mondon M., d'Estaintot B.L., Courseille C. and Precigoux G. Release of the cyano moiety in the crystal structure of N-cyanomethyl-N-(2-methoxy ethyl)-daunomycin complexed with d-(CGATCG). *Eur. J. Biochem.*, 2000, 267, 457.
134. Sarai A. and Takeda Y. Lambda repressor recognizes the approximately 2-fold symmetric half-operator sequences asymmetrically *Proc. Natl. Acad. Sci., U.S.A.*, 1989, 86, 6513.
135. Scheek R.M., Russo N., Boelens R., Kaptein R. and Van Boom J.H. Sequential resonance assignments in DNA ^1H NMR spectra by two-dimensional NOE spectroscopy. *J. Amer. Chem. Soc.*, 1983, 105, 2914.
136. Schmitz U., Sethson I., Egan, W.M. and James T.L. Solution structure of a DNA octamer containing the pribnov box via restrained molecular dynamics simulations with distance and torsion angles derived from two-dimensional nuclear magnetic resonance spectral fitting. *J. Mol. Biol.*, 1992, 227, 510.
137. Schultz S.C., Shields G.C. and Steitz T.A. Crystal structure of a CAP-DNA complex: the DNA is bent by 90 degree. *Science*, 1991, 253, 1001.
138. Shafer R.H. Spectroscopic studies of the interaction of daunomycin with transfer RNA. *Biochem. Pharmacol.*, 1977, 26, 1729.
139. Skorobogaty A., White R.J., Phillips D.R and Reiss J.A. The 5'-CA DNA-sequence preference of daunomycin. *FEBS Letts.*, 1988, 227, 103.

140. States D.J., Haberkorn R.A. and Reuben D.J. A two-dimensional overhauser experiment with pure absorption phase in four quadrants. *J. Magn. Reson.*, 1982, 48, 286.
141. Sundaralingam M. *Biopolymers*, 1969, 7, 821.
142. Tewey K.M., Rowe T.C., Yang L., Hallingan B.D. and Liu L.F. Adriamycin induced DNA damage mediated by mammalian DNA topoisomerase II. *Science*, 1984, 226, 466.
143. Trieb M., Rauch C., Wellenzohn, B., Wibowo F., Loerting T., Mayer E. and Liedl K. R. Daunomycin intercalation stabilizes distinct backbone conformations of DNA. *J. Biomol. Struct. Dyn.*, 2004, 21, 713.
144. Trifonov E.N. and Brendal V. *GNOMIC—A Dictionary of Genetic Codes*. Vch Verlagsgesellschaft Weinheim, Germany, 1986.
145. Trifonov E.N. Curved DNA. *CRC Crit. Rev. Biochem.*, 1985, 19, 89.
146. Trist H. and Phillips D.R. In vitro transcription analysis of the role of flanking sequence on the DNA sequence specificity of adriamycin. *Nucleic Acids Research*, 1989, 17, 3673.
147. Tsai C.C., Jain S.C. and Sobell H.M. Visualization of drug-nucleic acid interactions at atomic resolution I. Structure of an ethidium/dinucleoside monophosphate crystalline complex, ethidium: 5-iodouridylyl (3-5) adenosine. *J. Mol. Biol.*, 1977, 114, 301.
148. Tsou K.C. and Yip K.F. Effect of deoxyribonuclease on adriamycin-polynucleotide complexes. *Cancer Res.*, 1976, 36, 3367.
149. von Dreele R.B. and Einck J.J. The crystal and molecular structure of carminomycin I hydrochloride monohydrate. *Acta. Cryst.*, B 33, 1977, 3283.

150. Wang A.H.J, Gao Y.G, Liaw Y.C. and Li Y.K. Formaldehyde cross-links daunorubicin and DNA efficiently: HPLC and X-ray diffraction studies. *Biochemistry*, 1991, 30, 3812.
151. Wang A.H.J., Ughetto G., Quigley G.J. and Rich A. Interactions between an anthracycline antibiotic and DNA: Molecular structure of daunomycin complexed to d-(CpGpTpApCpG) at 1.2 Å resolution. *Biochemistry*, 1987, 26, 1152.
152. Waring M. Variation of the supercoils in closed circular DNA by binding of antibiotics and drugs: Evidence for molecular models involving intercalation. *J. Mol. Biol.*, 1970, 54, 247.
153. Williams L.D., Egli M., Ughetto G., van der Maerl G.A., van Boom J.H., Quigley G.J., Wang A.H.J. and Rich A. *J. Mol. Biol.*, 1990, 215, 313.
154. Williams L.D., Frederick C.A., Ughetto G. and Rich A. Ternary interactions of spermine with DNA: 4'-epidriamycin and other DNA: Anthracycline complexes. *Nucleic Acids Research*, 1990, 18, 5533.
155. Wilson W.D. and Jones R.L. *Nucleic Acids Research*, 1982, 10, 1399.
156. Wuthrich K. In "NMR of proteins and nucleic acids". John Wiley, New York, 1986.
157. Xodo L.E., Manzini G., Ruggiero J. and Quadrioglio F. On the interaction of daunomycin with synthetic alternating DNAs: Sequence specificity and polyelectrolytes effects on the intercalation equilibrium. *Biopolymers*, 1988, 27, 1839.
158. Yang X.L., Robinson H., Gao Y.G. and Wang A.H.J. Binding of macrocyclic bisacridine and ametantrone to CGTACG involves similar unusual intercalation platforms. *Biochemistry*, 2000, 39, 10950.

159. Zhurkin V.B., Ulyanov N.B., Gorin A.A. and Jernigan R.L. Static and statistical bending of DNA evaluated by Monte Carlo simulations. *Proc. Natl. Acad. Sci., U.S.A.*, 1991, 88, 7046.
160. Zunino F., Gambetta R. and Di Marco A. Effects of the stereochemical configuration on the interaction of some daunomycin derivatives with DNA. *Biochem. Biophys. Res. Commun.*, 1976, 69, 744.
161. Zunino F., Gambetta R., Di Marco A. and Zaccara A. Interaction of daunomycin and its derivatives with DNA. *Biochim. Biophys. Acta.*, 1972, 277, 489.

